

**Civilian Radioactive Waste Management System
Management & Operating Contractor**

**Chapter 10
Total System Performance Assessment-Viability Assessment (TSPA-VA)
Analyses Technical Basis Document**

Disruptive Events

B00000000-01717-4301-000010 REV 00

August 14, 1998

Prepared for:

U.S. Department of Energy
Yucca Mountain Site Characterization Office
P.O. Box 30307
North Las Vegas, Nevada 89036-0307

Prepared by:

TRW Environmental Safety Systems Inc.
1261 Town Center Drive
Las Vegas, Nevada 89134

INFORMATION COPY

9809180082 980911
PDR WASTE
WM-11

PDR

Under Contract Number
DE-AC08-91RW00134

102.8

- Part 1

**Civilian Radioactive Waste Management System
Management & Operating Contractor**

**Chapter 10
Total System Performance Assessment-Viability Assessment (TSPA-VA)
Analyses Technical Basis Document**

Disruptive Events

B00000000-01717-4301-000010 REV 00

August 14, 1998

Prepared for:

U.S. Department of Energy
Yucca Mountain Site Characterization Office
P.O. Box 30307
North Las Vegas, Nevada 89036-0307

Prepared by:

TRW Environmental Safety Systems Inc.
1261 Town Center Drive
Las Vegas, Nevada 89134

INFORMATION COPY

Under Contract Number
DE-AC08-91RW00134

DISCLAIMER

This report was prepared as an account of work sponsored by an agency of the United States Government. Neither the United States nor any agency thereof, nor any of their employees, makes any warranty, expressed or implied, or assumes any legal liability or responsibility for the accuracy, completeness, or usefulness of any information, apparatus, product, or process disclosed, or represents that its use would not infringe privately owned rights. Reference herein to any specific commercial product, process, or service by trade name, trademark, manufacturer, or otherwise, does not necessarily constitute or imply its endorsement, recommendation, or favoring by the United States Government or any agency thereof. The views and opinions of authors expressed herein do not necessarily state or reflect those of the United States Government or any agency thereof.

**Civilian Radioactive Waste Management System
Management & Operating Contractor**

**Chapter 10
Total System Performance Assessment-Viability Assessment (TSPA-VA)
Analyses Technical Basis Document**

Disruptive Events

B00000000-01717-4301-000010 REV 00

August 14, 1998

Prepared by:



Ralston Barnard
Performance Assessment Operations

Aug. 14, 1998
Date

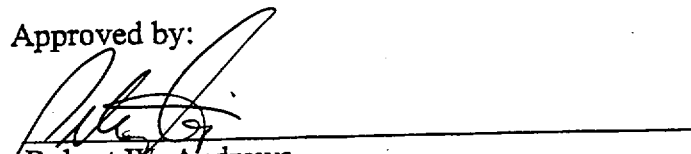
Checked by:



Geoffrey Freeze
Performance Assessment Operations

8/14/98
Date

Approved by:



Robert W. Andrews
Performance Assessment Operations

14 Aug 98
Date

INTENTIONALLY LEFT BLANK

ACKNOWLEDGMENT

The section of this chapter on scenario development (10.2) was contributed by Peter Swift (M&O/SNL). The section on coupled igneous—tectonic processes (10.3) was prepared by Dennis O'Leary (USGS). Richard Aguilar (M&O/SNL) provided information on the dose calculations for the direct-release volcanic scenario. In Section 10.4.3.3, Waste-Package Breach, Michael Itamura (M&O/SNL) performed the calculations to estimate cooling time in a drift from intruding magma. George Barr and Sharon Shannon (both M&O/SNL) performed the analyses of dike and fault activity outside the repository block (Sections 10.4.4 and 10.5.3, respectively). Zekai Ceylan (M&O/FCF) provided calculations of waste-package mechanical degradation (Section 10.4.2.3). Peter Gottlieb and John Massari (both M&O/TRW) contributed documentation and advice for Section 10.6.

Peter Burck (M&O/DE&S) performed the calculations using the ASHPLUME code for Section 10.4.2, including software quality assurance evaluations, and he also provided documentation of this work. Stephen Miller (KTECH Inc.) did the RIP runs for Sections 10.4.3, 10.5, 10.6, and 10.7 and provided documentation of the code modifications and analyses. Isaac Block (M&O/SNL) provided capable graphics support and reference checking. Carol Crawford (M&O/SNL) performed an exhaustive traceability review of the references. Bob Guzowski (SAIC) completed a comprehensive reference review and consistency check of this Chapter.

Kathryn Hansen and Bob Youngs (both Geomatrix, Inc.) provided data, documentation, and interpretations from the Probabilistic Volcanic Hazards Analysis. Greg Valentine and Frank Perry (both LANL) provided considerable expert guidance on parameterizing the volcanic model.

INTENTIONALLY LEFT BLANK

CONTENTS

10.	DISRUPTIVE EVENTS.....	10-1
10.1	INTRODUCTION.....	10-1
10.1.1	Data and Model Quality Assurance.....	10-1
10.2	SCENARIO DEVELOPMENT.....	10-1
10.2.1	The Scenario Development Process.....	10-2
10.2.2	FEP Identification and Screening for the TSPA-VA.....	10-4
10.2.2.1	Selection Process for Disturbed Scenarios for TSPA-VA.....	10-5
10.3	TECTONIC FEATURES OF THE YUCCA MOUNTAIN AREA.....	10-7
10.3.1	Introduction to Coupling of Igneous and Earthquake Processes.....	10-8
10.3.2	Petrology and magmatic origin of the basalts.....	10-10
10.3.3	Duration and recurrence of basaltic activity.....	10-10
10.3.4	The ash event: evidence of coupled processes.....	10-11
10.3.5	Regional associations and tectonic implications.....	10-12
10.3.6	The initiating event and coupled processes.....	10-14
10.3.7	Summary of Tectonic/Volcanic Coupling at Yucca Mountain.....	10-15
10.4	BASALTIC IGNEOUS ACTIVITY.....	10-15
10.4.1	Incorporation of the Probabilistic Volcanic Hazard Analysis.....	10-16
10.4.2	Direct Surface Releases.....	10-17
10.4.2.1	Characteristics of Igneous Activity in the Yucca Mountain Region.....	10-19
10.4.2.2	Number of Waste Packages Hit by a Dike.....	10-25
10.4.2.3	Waste-Package Breach.....	10-27
10.4.2.4	Removal of Waste-Package Contents.....	10-31
10.4.2.5	Incorporation of Waste into Eruptive Flow.....	10-33
10.4.2.6	Xenolith Fraction.....	10-35
10.4.2.7	ASHPLUME Inputs and Analysis.....	10-35
10.4.2.8	Development of Direct-Release Modeling Analysis Parameters.....	10-38
10.4.2.9	Direct-Release Modeling Results.....	10-40
10.4.2.10	Dose Calculations.....	10-41
10.4.2.11	Comparison with Other Analyses.....	10-43
10.4.3	Enhanced Source Term.....	10-44
10.4.3.1	Plumbing of Intrusion.....	10-45
10.4.3.2	Number of Waste Packages Hit.....	10-46

10.4.3.3	Waste-Package Breach.....	10-46
10.4.3.4	Mobilization of Waste-Package Contents.....	10-47
10.4.3.5	Development of Enhanced-Source-Term Modeling Analysis Parameters	10-51
10.4.3.6	Analysis Procedures	10-51
10.4.4	Dike Intrusion Outside Repository Block.....	10-54
10.4.4.1	Reference Saturated-Zone Model.....	10-55
10.4.4.2	Modeling of dikes.....	10-55
10.4.4.3	Interpretation of Modeling Results	10-57
10.5	SEISMIC ACTIVITY.....	10-57
10.5.1	Rockfall.....	10-57
10.5.1.1	Events and Processes that can Cause Rockfall.....	10-58
10.5.1.2	Minimum Size Rock that can Breach a Waste Package.....	10-61
10.5.1.3	Rate of Thinning of Waste-Package Walls	10-62
10.5.1.4	Distribution of Rock Sizes	10-63
10.5.1.5	Damage to Fuel Rods	10-63
10.5.1.6	Development of Rockfall Model Source Term	10-64
10.5.1.7	Results of Rockfall Modeling	10-66
10.5.2	Water-Table Rise	10-67
10.5.3	Fault Altering Saturated Zone Flow	10-68
10.6	NUCLEAR CRITICALITY	10-68
10.6.1	Nuclear Criticality Analysis Methodology.....	10-69
10.6.1.1	Environmental and Degradation Conditions Required for Potential Critical Configurations.....	10-70
10.6.1.2	Neutronics Conditions Required for Critical Configurations.....	10-70
10.6.1.3	Calculation of Fission Output from Criticality Events.....	10-71
10.6.1.4	Performance-Assessment Analyses.....	10-72
10.6.2	Scenarios and Criticality Calculations for Potentially Critical Configurations	10-73
10.6.2.1	In-Package Potentially Critical Configurations.....	10-73
10.6.2.2	External Potentially Critical Configurations.....	10-76
10.6.3	Fission-Output Calculations for Critical Configurations.....	10-78
10.6.3.1	Fission-Output Calculations for In-Package Criticality.....	10-78
10.6.4	PA Consequences of Critical Configurations	10-79
10.6.5	Potential for Autocatalytic Criticality in a Geologic Repository.....	10-81
10.7	HUMAN INTRUSION.....	10-81

10.7.1	Time of Occurrence of Drilling Incident	10-82
10.7.2	Amount of Waste Removed by drilling.....	10-83
10.7.3	Source Term Calculation	10-83
10.7.3.1	Waste-Form Dissolution Rate in Saturated-Zone Waters	10-84
10.7.3.2	Surface-Area Determinations of Spent-Fuel	10-85
10.7.3.3	Amount of water flowing over waste	10-85
10.7.3.4	Mass of contaminants dissolved.....	10-86
10.7.3.5	RIP Analysis.....	10-87
10.7.3.6	Cases Modeled	10-87
10.7.3.7	Results of Human-Intrusion Modeling.....	10-88
10.8	SUMMARY AND RECOMMENDATIONS	10-88
10.8.1	Summary of Source-Term Model Development	10-89
10.8.2	Summary of Modeling Results	10-90
10.8.3	Caveats, Conservatisms, and Modeling Artifacts.....	10-91
10.8.4	Recommendations for License-Application Analyses.....	10-92
10.9	REFERENCES	10-93

FIGURES

Figure 10-1.	Schematic illustration of the FEP screening process.	F10-1
Figure 10-2.	Logic Diagram for the YM TSPA-VA, showing the construction of scenarios using combinations of disruptive FEPs.	F10-2
Figure 10-3a.	Simplified representation of igneous activity scenarios.	F10-3
Figure 10-3b.	Simplified representation of components of direct-release igneous activity scenarios.	F10-4
Figure 10-3c.	Simplified representation of components of direct-release igneous activity scenarios (continued).....	F10-5
Figure 10-4a.	Direct-release branches of the generalized event tree for igneous activity.	F10-6
Figure 10-4b.	Indirect-effects branches of the generalized event tree for igneous activity.	F10-7
Figure 10-5.	Simplified representation of components of enhanced-source-term igneous activity scenario.	F10-8
Figure 10-6.	Simplified representation of components of indirect-effect igneous activity scenario.....	F10-9
Figure 10-7.	Simplified representation of the rockfall scenario.	F10-10
Figure 10-8.	Simplified representation of the seismic indirect-effects scenario.....	F10-11
Figure 10-9.	Simplified representation of the in-package nuclear criticality scenario.....	F10-12
Figure 10-10.	Simplified representation of the out-of-package nuclear criticality scenario.....	F10-13
Figure 10-11.	Simplified representation of the human-intrusion scenario.	F10-14
Figure 10-12.	Location of Plio-Pleistocene volcanic centers in the Yucca Mountain area and outline of the Crater Flat Volcanic Zone (CFVZ).	F10-15
Figure 10-13.	Magma volume vs age of eruption for Pliocene and Quaternary volcanic events in the Yucca Mountain region.....	F10-16
Figure 10-14.	Major faults along Yucca Mountain and locations of trenches that contain basaltic ash. Star symbols show locations of ash remnants from Lathrop Wells cone.	F10-17
Figure 10-15.	Approximate borders of Walker Lane shown by ~~~ pattern. Hatching and strike-slip arrows show location of Amargosa Desert fault system of Schweickert and Lahren (1997).	F10-18
Figure 10-16.	Total crustal strain vs time. Initiating event V culminates in volcanism, a high-strain event. Strain then drops to low level; as horizontal stress decreases, extensional strain increases and different parts of crust fail and slip, culminating in another volcanic event.....	F10-19
Figure 10-17.	Aggregate results for frequency of intersection of an igneous intrusion with the Potential Yucca Mountain repository (after CRWMS M&O 1996a, Figure 4-32a).....	F10-20
Figure 10-18.	Illustration of potential dikes in the Yucca Mountain area (after CRWMS M&O 1996a).	F10-21
Figure 10-19.	Probability density for dike length and orientation inside the repository (after CRWMS M&O 1996a).....	F10-22
Figure 10-20.	PDF for number of vents along a dike inside the repository.....	F10-23

Figure 10-21. PDF for dike width.....	F10-24
Figure 10-22. PDF for conduit diameter.....	F10-25
Figure 10-23. Range of liquid magma ascent velocities as a function of dike width.....	F10-26
Figure 10-24. Range of ascent velocities as a function of conduit diameter (after Wilson and Head 1981, Table 3).....	F10-27
Figure 10-25. Repository outline and modeled configuration (from CRWMS M&O 1997a).....	F10-28
Figure 10-26. Dike intersection with a drift.....	F10-29
Figure 10-27. Intersection of a circular conduit with drifts.....	F10-30
Figure 10-28. Extrapolation of CRM corrosion rates.....	F10-31
Figure 10-29. Waste-package CRM wall stresses as a function of temperature.....	F10-32
Figure 10-30. Waste-package CRM end-cap stresses as a function of temperature.....	F10-33
Figure 10-31. Times for 50% and 70% degradation of CRM.....	F10-34
Figure 10-32. PDFs of ash-particle diameters.....	F10-35
Figure 10-33. PDF for waste-particle sizes (Jarzemba & LaPlante 1996, Figure 4).....	F10-36
Figure 10-34. Distribution of wind direction and speed at Yucca Mountain.....	F10-37
Figure 10-35. Contours for greatest concentration at dose receptor point (Realization 14).....	F10-38
Figure 10-36. Concentration contours for greatest erupted waste amount (Realization 1).....	F10-39
Figure 10-37. Concentration contours for strongest wind blowing away from dose receptor point (Realization 8).....	F10-40
Figure 10-38. Inventory of Se-79 as a function of time.....	F10-41
Figure 10-39. Inventory of Pb-210 as a function of time.....	F10-42
Figure 10-40. Conditional CCDF for mean direct-release volcanic dose rates.....	F10-43
Figure 10-41. CCDFs for peak base-case and direct-volcanic dose rates.....	F10-44
Figure 10-42. Temperature profiles in repository for various amounts of magma filling drift.....	F10-45
Figure 10-43. Profile for base-case drift-wall temperatures with a magmatic intrusion at 10,000 years.....	F10-46
Figure 10-44. Mechanical behavior of alloy 625 as a function of time and temperature.....	F10-47
Figure 10-45. PDF for uranium dioxide particle sizes after interaction with magma.....	F10-48
Figure 10-46. Layout of contaminated basalt in a drift.....	F10-49
Figure 10-47. Times of failure and fractional release rate.....	F10-50
Figure 10-48. Comparison of CCDFs for 100000-year dose rates.....	F10-51
Figure 10-49. Comparison of CCDFs for 1,000,000-year dose rates.....	F10-52
Figure 10-50. Time histories for dose rates over 1,000,000 years.....	F10-53
Figure 10-51. Ratios of doses from enhanced source term with corresponding base-case doses.....	F10-54
Figure 10-52. Examples of new dikes in the saturated flow domain. (a) Dike not attached to existing structure; (b) dike splayed off Solitario Canyon fault....	F10-55
Figure 10-53. SZ reference model: (a) potentiometric surface; (b) representative contaminant concentration contours; (c) representative contaminant breakthrough curve.....	F10-56

Figure 10-54. Dike inserted along Solitario Canyon fault: (a) potentiometric surface; (b) representative contaminant concentration contours; (c) representative contaminant breakthrough curve.	F10-57
Figure 10-55. Dike inserted beneath repository connected to Solitario Canyon fault: (a) potentiometric surface; (b) representative contaminant concentration contours; (c) representative contaminant breakthrough curve.	F10-58
Figure 10-56. Dike inserted southeast of repository: (a) potentiometric surface; (b) representative contaminant concentration contours; (c) representative contaminant breakthrough curve.	F10-59
Figure 10-57. (a) Stress state of drift immediately after excavation. (b) Stress state after 50 years of heating.	F10-60
Figure 10-58. PGV that causes a given damage level for various rock qualities.	F10-61
Figure 10-59. Annual probability of exceedence for horizontal PGV (after CRWMS M&O 1998a, Figure 7-8).	F10-62
Figure 10-60. Critical rock masses for various waste-package wall thickness.	F10-63
Figure 10-61. Time rate of thinning of waste package wall.	F10-64
Figure 10-62. Critical rock masses as function of time.	F10-65
Figure 10-63. Distribution of rock sizes for all units.	F10-66
Figure 10-64. Distribution of rock sizes for the TSw unit.	F10-67
Figure 10-65. Mechanical damage to fuel rods from a circular punch.	F10-68
Figure 10-66. Mechanical damage to fuel rods from a linear punch.	F10-69
Figure 10-67. Distribution of times for breach of waste packages.	F10-70
Figure 10-68. CDF for waste-package failures from rockfall.	F10-71
Figure 10-69. Comparison of waste-package failures for corrosion and rockfall.	F10-72
Figure 10-70. CDFs for waste-package failure from corrosion and rockfall.	F10-73
Figure 10-71. Comparison of patch failure from corrosion and rockfall.	F10-74
Figure 10-72. Dose-rate time histories for rockfall and base case.	F10-75
Figure 10-73. Incremental heat output for 10,000-year criticality (data from Section 3 of this document).	F10-76
Figure 10-74. Radionuclide inventory differences for 10,000-year criticality (after CRWMS M&O 1996c, Section 7.2.1).	F10-77
Figure 10-75. Dose rate time history for 10,000-year criticality starting at 15,000 years after emplacement.	F10-78
Figure 10-76. Difference in dose rates for criticality vs base case.	F10-79
Figure 10-77. Dose rate time histories for the three largest contributors to dose.	F10-80
Figure 10-78. Dose-rate increases from criticality from individual radionuclides.	F10-81
Figure 10-79. Range of waste-form dissolution rates in saturated-zone waters.	F10-82
Figure 10-80. Range of waste-form fractional dissolution rates.	F10-83
Figure 10-81. Dose-rate time histories for individual radionuclides.	F10-84
Figure 10-82. Dose-rate time histories for human intrusion.	F10-85
Figure 10-83. Sensitivities of dose rates to model parameters.	F10-86

TABLES

Table 10-1.	Models Used in Disruptive-Events Analyses.....	T10-1
Table 10-2.	Computer Codes Used in Disruptive-Events Analyses.....	T10-1
Table 10-3.	Summary of Codes, Input/Output Files, and DTNs Associated With Technical Figures.	T10-2
Table 10-4.	Summary of TSPA-VA Screening for Selected NEA FEP Categories.....	T10-13
Table 10-5.	Summary of PVHA Model Input Parameters (after CRWMS M&O 1996a).....	T10-18
Table 10-6.	Eruptive Parameters for Analog Volcanoes.....	T10-20
Table 10-7.	Magma Rise Velocity as a Function of Dike Width (after Wilson and Head 1981, Table 5).	T10-21
Table 10-8.	Ascent Velocity as a Function of Conduit Diameter (adapted from Wilson and Head 1981, Table 3).....	T10-21
Table 10-9.	Number of Waste Packages for each Waste Type (after CRWMS M&O 1997b, Key 04 Table 3-10).	T10-21
Table 10-10.	Number of Waste Packages Hit for Circular Conduits.	T10-22
Table 10-11.	Waste Package Internal Pressure.....	T10-22
Table 10-12.	Fractional Velocities For Agglomerated Pyroclast-Waste Particles.	T10-22
Table 10-13.	Settling Velocities (cm/s) For Waste Particles in Magma.	T10-23
Table 10-14.	Settling Velocities (cm/s) For Agglomerated Waste-Magma Particles.	T10-23
Table 10-15.	Sample ashplume.In File.	T10-24
Table 10-16a.	Selected Examples of Dike Intrusions.	T10-25
Table 10-16b.	Selected Examples of Dike Intrusions.	T10-26
Table 10-16c.	Numbers of Packages Hit By Liquid-Magma Intrusions.	T10-27
Table 10-16d.	Numbers of Packages Hit by Ash Intrusions.	T10-27
Table 10-16e.	Waste-Package Breach Simulations.....	T10-28
Table 10-16f.	Waste-Removal Simulations.....	T10-28
Table 10-16g.	Waste-Entrainment Simulations.....	T10-29
Table 10-16h.	Amount of Waste in Eruptive Source.	T10-29
Table 10-16i.	Parameters for ASHPLUME Simulations.....	T10-30
Table 10-17.	Contributions of Intermediate Processes to Final Source Term.....	T10-30
Table 10-18.	Waste Concentrations at Dose Receptor Point.....	T10-31
Table 10-19.	Comparison of Dose Rates for TSPA-VA and Prior Analyses.....	T10-31
Table 10-20.	Dissolution Rates of Uranium-Bearing Minerals.....	T10-32
Table 10-21.	Waste Elements Susceptible to Mobilization at Magmatic Temperatures.....	T10-33
Table 10-22a.	Selected Examples of Dike Intrusions.	T10-34
Table 10-22b.	Calculation of Total Number of Waste Packages Breached by Magma Intrusion.	T10-34
Table 10-22c.	Calculation of UO ₂ Dissolution.....	T10-35
Table 10-22d.	Calculation of Basalt Dissolution.....	T10-35
Table 10-23.	Rock Quality Ranges.....	T10-35
Table 10-24.	Thermal Spalling at Various Times After Closure.....	T10-36
Table 10-25.	Initial-Condition Factors for DL Calculation.....	T10-36

Table 10-26.	PGV Values for Various IC and DL Values.	T10-36
Table 10-27.	Frequencies of Occurrence for Various PGV Values Over Different Time Periods.	T10-36
Table 10-28.	DL Values for Various Rock Qualities.	T10-37
Table 10-29.	Calculated Waste-Package Damages from Rockfall as a Function of Wall Thickness.....	T10-37
Table 10-30a.	Calculation of Damage Levels at Various Times.....	T10-37
Table 10-30b.	Calculation of Amounts of Waste-Package Degradation.....	T10-38
Table 10-30c.	Association of DL Values with Rock-Size Data.....	T10-38
Table 10-30d.	Falling Rock Masses Resulting from Seismic Events.....	T10-39
Table 10-31.	Summary of Rockfall Grouped by Time Period.	T10-39
Table 10-32.	Summary of In-Package Critical Configurations.	T10-40
Table 10-33.	Summary of Near-Field Critical Configurations.....	T10-42
Table 10-34.	Summary of Far-Field Critical Configurations.	T10-43
Table 10-35.	Contaminant Masses Available in Saturated Zone.	T10-44
Table 10-36.	Human-Intrusion Source Term for Disruption of 2.7 Metric Tons of Spent Fuel.	T10-44
Table 10-37.	Human-Intrusion Source Term for Disruption of 0.55 Metric Tons of Spent Fuel.	T10-45

ACRONYMS

ASHPLUME	computer code for calculating volcanic ash disposal
BDCF	biosphere dose conversion factor
BWR	boiling-water reactor
CAM	corrosion-allowance material
CDB	Characteristics Database System
CCDF	complementary cumulative distribution function
CDF	cumulative distribution function
CFVZ	Crater Flat volcanic zone
CRM	corrosion-resistant materials
CSNF	commercial spent nuclear fuel
DFEP	disruptive features, events, or processes
DHLW	defense high-level waste
DOE	Department of Energy
EFEP	expected features, events, or processes
FEP	features, events, or processes
GENII	computer code for calculating radioactive doses
ka	thousand years ago
kyears	one thousand years
K-Ar	Potassium-argon dating method
Ma	million years ago
M&O	management and operating contracts
MCNP	computer code for calculating criticality potential
MTU	metric tons of uranium

Myears	one million years
NRC	U.S. Nuclear Regulatory Commission
ORIGEN2	computer code for calculating radionuclide inventories
PA	performance assessment
PDF	probability distribution function
PSHA	Probabilistic Seismic Hazard Analysis
PVHA	Probabilistic Volcanic Hazard Analysis
PWR	pressurized-water reactor
RIP	Computer Code for Total System Performance Assessments
TSPA-VA	Total System Performance Assessment-Viability Assessment
WAPDEG	Computer Code for Waste Package Degradation
YMP	Yucca Mountain Project

10. DISRUPTIVE EVENTS

10.1 INTRODUCTION

As part of the effort to demonstrate that performance-assessment analyses have appropriately considered a broad range of representative credible scenarios, disturbances to nominal repository conditions are discussed in this chapter. The effort here is twofold: to demonstrate that a reasonably complete set of features, events and processes that describe the repository behavior have been identified, and to provide analyses that show the response of the repository system to disturbances to nominal conditions. The disturbed-condition analyses are incorporated into the Total System Performance Assessment for the Viability Assessment (TSPA-VA) analyses as sensitivity studies to show the departure of the response of the repository from the base-case conditions. Disturbances to be considered are:

- Basaltic igneous activity
- Seismicity
- Nuclear criticality
- Inadvertent human intrusion.

In addition, this chapter contains a discussion of scenario-development methods. Such methods are necessary to demonstrate that analyses of repository behavior are reasonably complete in their inclusion of features, events, and processes that can affect long-term performance.

Disruptive events are considered to have probabilities less than 1 (that is, their chances of occurring are less than 100%), in contrast to the expected events and processes (for example, waste-package corrosion, thermal effects, groundwater flow and transport). Generally, disruptive events (like volcanoes or earthquakes) are rare and have identifiable starting and ending times, in contrast to continuous processes like corrosion.

As prior analysis have, shown, disruptive events are of low probability, or low consequence, or both, and therefore have limited impact on overall repository performance. Thus, the Yucca Mountain Project has decided to expend limited resources on disturbed-scenario analysis in TSPA-VA. The analyses presented here have used available information and Project expertise, but have not incorporated extensive additional research efforts.

10.1.1 Data and Model Quality Assurance

The following tables identify the traceability information for the models, codes, and input data for these analyses. Table 10-1 lists models and data tracking numbers (DTNs). Table 10-2 gives the computer codes used in the disturbed-event analyses. Table 10-3 links the parameters and distributions used in the analyses with technical data information form numbers and DTNs.

10.2 SCENARIO DEVELOPMENT

Extensive work conducted as part of the characterization of the Yucca Mountain site and during preliminary TSPAs has identified the potentially disruptive events most relevant to long-term

performance of the repository (DOE 1988, Section 8.3.5.13; Barnard et al. 1992, Chapters 6 and 7; Wilson et al. 1994, Chapters 16 and 17). Treatment in the TSPA-VA of these events, which are basaltic volcanism, seismic activity, nuclear criticality, and inadvertent human intrusion, is discussed in detail later in this chapter. Seismicity and nuclear criticality have not been analyzed in previous TSPAs, but the scenarios have been developed (Barr et al. 1996; CRWMS M&O 1997f). This section describes the process the U.S. Department of Energy (DOE) proposes to use to demonstrate, in the license application, that these are, indeed, the most relevant disruptive events. In addition, the application must also demonstrate that no other significant features, events, or processes (FEPs) have been omitted from the analysis and that all significant combinations of relevant FEPs have been considered.

In previous TSPAs, the DOE has chosen to use generalized event trees (in previous work, these have been variously called FEP trees and FEP diagrams) to guide construction of disruptive scenarios (Barnard et al. 1992, Chapter 2; Wilson et al. 1994, Chapter 3). This approach has led to a detailed understanding of the relationships among processes that could contribute to increased radionuclide releases following a disruptive event, and has proven valuable in the design of the specific analyses described later in this chapter. The approach taken in past TSPAs, however, has not documented that these analyses constitute a comprehensive consideration of disruptive scenarios that may affect the repository. Therefore, the DOE has chosen for the TSPA-VA to begin implementing a formal scenario-development methodology that will document the treatment of all FEPs in the analysis (a description of the methodology is given in Section 10.2.1). Implementation of the scenario-development methodology is incomplete for the VA, in part because the process must remain open to consider new information as it becomes available. DOE does not anticipate having final documentation of the formal scenario-development methodology complete before preparation of the license application. Important disruptive scenarios are expected to be identified and analyzed by that time, however.

The ultimate criterion for inclusion of disruptive scenarios in TSPA analyses is whether these events are likely to have a significant impact on performance of the repository system during the period of regulatory concern. The criteria for considering inclusion of disturbed scenarios in TSPA analyses are:

- Probability—Is the probability of the event occurring large enough that it could reasonably occur given the long geologic time under consideration?
- Consequence—Are the potential consequences of the disturbance of sufficient magnitude that repository performance could be adversely impacted?
- Regulatory—Do regulatory requirements mandate consideration of certain types of disturbances (or specifically exclude certain disturbances)?

10.2.1 The Scenario Development Process

As described in Chapter 1, DOE is implementing a scenario development procedure based on the methodology developed by Cranwell et al. (1990, Chapter 2) for the NRC. The approach is consistent with that outlined by DOE in the 1988 Site Characterization Plan for the YMP (DOE

1988, Section 8.3.5.13), and is fundamentally the same as that used in many performance assessments, including the most recent analysis of the Yucca Mountain repository by the NRC (NRC 1995, Chapter 3). The approach has also been used by DOE for the Waste Isolation Pilot Plant (WIPP) (DOE 1996, Section 6.2) and the Greater Confinement Disposal Facility at the Nevada Test Site (Guzowski and Newman 1993), by the Nuclear Energy Agency (NEA) of the Organization for Economic Co-operation and Development (OECD), and by other radioactive waste programs internationally (e.g., Andersson and Eng 1990, pp. 397-404; Stephens and Goodwin 1990, pp. 405-415; Skagius and Wingefors 1992, Chapter 3).

There are five principal steps to the scenario development process.

1. Identify and classify features, events, and processes (FEPs) potentially relevant to the long-term performance of the disposal system.
2. Screen the FEPs using well-defined criteria to distinguish between those FEPs that can be excluded from the TSPA and those that should be included in the analysis.
3. Use the retained FEPs to construct scenarios.
4. Screen the scenarios using the same criteria applied to the FEPs to identify any scenarios that can be excluded from the TSPA.
5. Specify the implementation of the scenarios in the computational modeling for the TSPA, and document the treatment of included FEPs.

These five steps differ slightly from those identified by Cranwell et al. (1990, p. 3), in that FEP classification, which was the second step in their procedure, has been included with the first step, and the final step has been modified to clarify the linkage between scenario development and the TSPA analyses. Each of the five steps is described briefly below.

Step 1: *The initial FEP list.* The initial set of FEPs has been created by combining lists of FEPs previously identified as relevant to the YMP with a draft FEP list compiled by an NEA working group and others (Goodwin et al. 1994; Miller and Chapman 1993; Andersson 1989; NEA 1992; Chapman et al. 1995; DOE 1996). The NEA list is the most comprehensive list available internationally, and currently contains 1261 entries from Canadian, Swiss, and Swedish spent-fuel programs, intermediate and low-level waste programs of the UK, and the US WIPP program. The YMP initial FEP list is organized using the same classification scheme adopted by the NEA working group in their draft list.

Step 2: *Screening the FEP list.* FEPs are first screened for relevance to the YMP, and for redundancy with other entries on the list. Thus, FEPs clearly irrelevant to Yucca Mountain, such as those that are specific only to salt repositories, are identified and set aside. Screening arguments for redundant FEPs identified by multiple programs are mapped to a single entry. Each FEP is then screened for inclusion or exclusion in the TSPA based on regulatory requirements, the probability of the FEP, and its consequence. The screening process is shown schematically in Figure 10-1.

Relevant FEPs are excluded from the TSPA only if their occurrence can be shown to have no significant effect on the overall performance of the system (such as producing a dose less than some regulatory criterion), if they can be shown to have a probability of occurrence of less than $10^{-8}/\text{yr}$ (a probability adopted by DOE as the level of concern for preliminary TSPAs [NRC 1995 1995, page 3-5]), or if they are ruled out by regulation (e.g., deliberate human disruption of the site). Because final regulations are not available for the Yucca Mountain repository, these criteria are preliminary and will be revised for the license application as needed.

Step 3: Constructing scenarios. FEPs retained from Step 2 are identified as either expected FEPs (EFEPs) or disruptive FEPs (DFEPs). Expected FEPs are those that can be assumed, for the purposes of the TSPA, to have a probability of occurrence equal to 1.0 (although they may have uncertain consequences). DFEPs are those that have a probability less than 1.0 and have a significant effect on overall performance. All EFEPs are included in the nominal scenario, which is simulated by the base-case model described in Chapters 2 through 8 of this document. Disruptive scenarios are constructed from all EFEPs and combinations of DFEPs, with the probability of each disruptive scenario calculated as the product of the probabilities of the included DFEPs. Scenario construction can be displayed graphically using logic diagrams (Figure 10-2).

Step 4. Screening scenarios. Scenarios constructed in Step 3 are screened using the same regulatory, probability, and consequence criteria defined in Step 2. For example, the probability criterion may be used to exclude scenarios that include combinations of low probability FEPs for which the product of their probabilities is less than $10^{-8}/\text{year}$.

Step 5. Specifying scenarios for TSPA analysis. All FEPs retained in Step 2 must be included in TSPA analyses either in the nominal scenario or in disruptive scenarios. As shown in Figure 10-1, retained FEPs may be included in the nominal scenario either through explicit modeling or through the selection of parameter values. (Explicit modeling is done by including an approximation of the relevant process in the TSPA analysis; parameter-value selection is done to incorporate uncertainty about the effects of the FEP.) EFEPs are included through both modeling and parameter selection, while DFEPs are included explicitly in modeling of disruptive scenarios.

10.2.2 FEP Identification and Screening for the TSPA-VA

Formal screening arguments for the FEPs contained in the current YMP FEP list have not been completed for the TSPA. The complete FEP list, without screening branches, is still in preparation. FEPs in this list are organized using the NEA's sequential numbering system of the *x.x.x* format, with four major first-order categories identical to those selected by the NEA. These four categories are described briefly in the following paragraphs.

0. *Assessment Basis FEPs*, including factors related to the purpose and scope of the analysis. This category is important primarily for programs in countries with less well-defined regulatory requirements than those of the United States. Most FEPs in this category are likely to be irrelevant for the YMP because they will be superseded by regulatory requirements. However, the category is maintained in the YMP FEP list for completeness.

1. *External FEPs*, including natural or human factors that operate on a global or regional scale outside the domain of the disposal system. FEPs related to decisions concerning repository design are included here also, on the grounds that they operate outside the temporal bounds of the period of performance. Subcategories include repository issues, geological processes, climatic processes, and future human actions.
2. Disposal System Domain: *Environment FEPs*, including environmental factors that operate within the domain of the disposal system. Subcategories include waste forms and engineered features, subsurface geological environment, surface environment, and human behavior.
3. Disposal System Domain: *Radionuclide/Contaminant FEPs*, including factors that affect either the release and migration of radionuclides in the disposal system environment or the resulting doses to humans. Subcategories include contaminant characteristics, release/migration factors, and exposure factors.

Table 10-4 lists selected NEA FEP subcategories from the external factors and disposal system domain categories, together with the screening decisions for the TSPA-VA and a brief comment on the current treatment of the FEP category. Table 10-4 is not intended to provide a comprehensive listing of FEPs, nor does it provide a detailed basis for screening decisions. Many of the FEP categories represent a lumping of multiple FEPs included in the complete list, and the discussion given here is limited to a summary level. The table is included to demonstrate the approach taken, and to provide documentation of many of the FEPs considered in past performance assessments of the Yucca Mountain repository. Complete documentation of all FEPs is expected to be provided in the license application.

10.2.2.1 Selection Process for Disturbed Scenarios for TSPA-VA

To date, basaltic igneous activity, seismic activity, human intrusion, and nuclear criticality have been identified as the disruptive events to be used in scenario construction. These FEPs have been combined into scenarios based on evaluations using the generalized event trees (Barr et al. 1993; Barr et al. 1996; CRWMS M&O 1997f). Only a limited number of scenarios are analyzed for TSPA-VA. They are representative of the much larger number of possible scenarios, but are expected to bound the consequences of the scenario classes. Human intrusion scenarios have also been investigated, but the method of inclusion in the TSPA for the potential licensing analyses is uncertain, pending clarification of regulatory requirements.

Generalized event trees used to develop a detailed list of the factors and issues associated with disturbances differ from "classical" event trees (see McCormick 1981, Chapter 9, for a discussion of classical event trees). Event trees for analysis of reactor accidents or safeguards generally identify sequences of systems that either succeed or fail in protecting the reactor or other site. Because this type of tree tracks success or failure, it is generally binary. Furthermore, each node of the tree can usually be assigned a probability of success, so the overall probability of success or failure of a branch can be estimated. In contrast, the generalized event tree includes not only events, but also processes and features important to defining the factors and issues associated with the disturbance.

Branches of generalized event trees may not be exclusive; at different times in the history of the disturbance, different components of the tree may be dominant. For example, during an active volcanic eruption, waste packages may come in contact with flowing magma, and the direct-release branch of the generalized event tree is invoked. At other times, the waste packages may be engulfed in solidified magma, so the enhanced-source-term branch is applicable. Generalized event trees attempt to provide a reasonably complete listing of important features, events, and processes, compiled as a sequence of branch points. The termination of branches in generalized event trees for disturbances indicates that the performance-assessment (PA) consequences of that scenario are to be evaluated. Frequently, disturbed scenarios do not lead directly to measurable performance assessment (PA) consequences, but are instead alterations of some aspect of the base case. For example, many disturbed scenarios result in a modified radionuclide source term whose impact on total-system PA is determined by using the source term in a base-case, ground-water flow and transport analysis and calculating the change in dose rate at the dose-receptor point.

As an illustration of the selection process for disturbed scenarios, igneous activity is analyzed here in detail. Analogous processes for seismic activity, nuclear criticality, and human intrusion have been done.

A simplified presentation of the three basaltic, igneous-activity scenarios analyzed in TSPA-VA is illustrated in Figure 10-3. The illustrations in the figures are simplifications of the generalized event tree used to develop the scenarios, which is shown in Figure 10-4. Figures 10-3a, b, c show a sequence of branch points. In Figure 10-3a, the first branch point is whether basaltic igneous activity happens at all. This is implicitly indicated in the top box (shown in light green) in the complete event tree, Figure 10-4 (if there is no igneous activity, there are no igneous-interaction consequences). The next branch point in Figure 10-3a is whether the intrusion goes through the repository or not. This is represented by the second row of boxes in the generalized event tree (shown in light blue in Figure 10-3a); these subdivide the tree into the two main branches—direct interactions of repository waste with the intrusion (on the left) and indirect interactions (on the right).

Figure 10-3a continues along the direct-interaction scenarios path. The next branch point is whether the dike contacts the waste packages or misses them in its ascent towards the surface. Figure 10-3a combines several boxes on the tree (all shown in dark gold). As is discussed in Section 10.4, intrusions can be either single events or a sequence of eruptions. An example of the latter is shown in the event tree (Figure 10-4a) by the box entitled "Dike Forms—hydrovolcanic initiation followed by Hawaiian/Strombolian eruption." The next level of branches (still within the dark gold boxes) considers the depth of the fragmentation surface of the magma. As is discussed in detail in Section 10.4, the depth of the fragmentation surface is an important parameter in the analyses. The direct-interaction branch of the tree forms two sub-branches here. Each of the sub-branches bifurcates again to include branches for vertical ascension of the dike or lateral flow of the intrusion down drifts. Implicit in the diagram is that the magmatic intrusion has made contact with the waste packages. If not, there are no further branches or consequences to consider along this branch. (Note the convention in the generalized event tree (Figure 10-4a and b) that a branch that is duplicated elsewhere in the tree is indicated by a circle with a letter in it; the locations of duplicated branches are indicated by triangles with the same letter.)

Figure 10-3b shows the branch point where waste packages are breached by the intrusion. The boxes describing this branch point are shown in light gold in Figure 10-4a. If the packages are breached, Figure 10-3b next indicates whether the waste is removed from the waste packages or is encapsulated and interacts with the magma. Scenarios where the waste is ejected are part of the direct-surface-release scenario and are shown in dark blue in Figure 10-4a.

The last part of the direct-surface-release scenario is shown in Figure 10-3c. The first branch point concerns entrainment of the waste in the ascending intrusive flow. The boxes describing this in Figure 10-4a are shown in red. If the ascending flow does not entrain the waste, consequences are included as part of the enhanced-source-term scenario (discussed next). Finally, Figure 10-3c shows the cases where contaminated ash is dispersed in an ash plume or remains a localized eruption. The boxes describing these options are shown in dark green in Figure 10-4a. Figure 10-3c ends by describing the performance-assessment consequences of ash dispersal; this is shown by the diamonds at the bottom of the direct-release section of Figure 10-4a.

The enhanced-source-term scenario is a subset of the direct-interaction scenario covering the instances when waste may be directly contacted by the magmatic intrusion, but does not reach the surface. Figure 10-5 shows the simplified illustration of this scenario. The corresponding boxes in the event tree, (Figure 10-4a) are shown in pink. The first branch point in Figure 10-5 shows the possible ways that magma and waste can interact. These are shown in the diagram by yellow boxes. Figure 10-5 ends by describing the performance-assessment consequences of groundwater transport of potentially increased amounts of radionuclides; this is shown by the diamond at the bottom of the enhanced-source-term portion of Figure 10-4a.

The last igneous-activity scenario, indirect interactions, is illustrated in Figure 10-6. The branch points here are whether the dike alters groundwater flow in the saturated zone by redirecting the flow path or by being more transmissive than the surrounding rock. In Figure 10-4b, these boxes are shown in purple. The event tree includes several alternatives for dike location and hydrologic characteristics. As is discussed above, the PA consequences of any of the scenarios are indicated by the diamonds at the bottom of the branches.

Figures 10-7 through 10-11 show simplified illustrations for the seismic, criticality, and human-intrusion scenarios, respectively. The illustrations were developed from generalized event trees for tectonism (Barr et al. 1996) and nuclear criticality (CRWMS M&O 1997f). The illustrations for the human-intrusion scenario were developed from guidance provided by the National Academy of Sciences (NAS/NRC 1995, Chapter 4).

10.3 TECTONIC FEATURES OF THE YUCCA MOUNTAIN AREA

The following section describes current thinking of Yucca Mountain Project personnel on the nature and likelihood of any coupling between basaltic igneous activity and tectonic (seismic)

processes (CRWMS M&O 1998c, Sections 3.9.3.6 ff.). The material included here is an abstraction of a more technically comprehensive work¹.

10.3.1 Introduction to Coupling of Igneous and Earthquake Processes

Igneous/tectonic features that postdate the formation of Yucca Mountain are interpreted as analogs for future disruptive events at the Yucca Mountain repository site. The igneous features are chiefly of volcanic origin. They consist chiefly of basaltic dikes, fissure fills, volcanic cones, agglutinated spatter mounds, and lava flows. The igneous features comprise eruptive centers that have similar structural associations.

Only one basalt intrusion is known to be associated with Yucca Mountain structure, and that is a small dike intruded into the Solitario Canyon fault. The basalt is approximately 10 Ma (million years old) (Carr and Parrish 1985, pp. 37-39), appreciably older than the more widely distributed Plio-Pleistocene volcanic basalts found elsewhere in the region, and described below.

The following is a list of the volcanic features in the Yucca Mountain area. See also CRWMS M&O (1998c, Section 3.9.3.2). The largest volume ($\leq 3 \text{ km}^3$), and the oldest (4.6 Ma, Minor et al. 1993) of the Plio-Pleistocene basalts near Yucca Mountain is the basalt of Thirsty Mesa. This is a large ($\sim 22 \text{ km}^2$) lava flow complex that caps a mesa formed on the Thirsty Canyon Tuff (Figure 10-12 shows the Yucca Mountain region and several of the features described here). A group of eroded scoria mounds aligned north-south along the apex of the complex most likely represents the buried source fissure of the lava flows (Crowe et al. 1995, pp. 2-16, 3-27).

The oldest basalt center in Crater Flat is a group of north-trending lenticular dikes and fissure vents, scoria cones and associated lava flows aligned *en echelon* to the northwest. This is the most areally extensive assemblage of lavas, forming thin flows 3 to 5 m thick. The flows are offset more than one meter down to the west along north-south striking faults. The basalt is dated at about 4.3 to 3.7 Ma (Crowe et al. 1995, p. 2-20, Figure 3.10).

The next younger eruptive group in Crater Flat comprises a northeast-trending arcuate alignment of scoria cones (Figure 10-12) named, from the southwest: Little Cones, Red Cone, Black Cone, and (informally) "Makani Cone" (Crowe et al. 1995, p. 2-21). The closest cones to Yucca Mountain are Black Cone and Makani Cone, both located between 8 and 9 km west of the repository block. The cone alignment spans a distance of about 12 km. A single feeder dike of this length seems unlikely (Crowe et al. 1983b). However, Champion (1991, p. 65, col. 1, paragraph 1) inferred, on the basis of paleomagnetic data, that a single intrusive pulse generated the cones, each of which formed during a brief eruptive "cycle." Variation among the

¹ O'Leary, D. W. "Plio-Pleistocene Basaltic Volcanism And Its Relation To Extension In The Crater Flat, Nevada, Tectonic Domain", OFR- in press, US Geological Survey, Denver CO.

*The stress-relieving temperature of Alloy 625 is 870°C, and the anneal temperature is 980°C (ASM 1981, Table 5). Holding the waste package at these temperatures should cause $P_m + P_b$ to decrease. Therefore, it is a conservative assumption to maintain the same stress values for all temperatures.

radiometric dates of the basalts is too great to resolve this point. K-Ar ages of basalt range from about 1.15 Ma to 785 ka (thousand years old) (Crowe et al. 1995, Table 2.2, p. 2-32; Vaniman et al. 1982, Table 1; Smith et al. 1990, p. 84; CRWMS M&O 1998c, Section 3.9.3.1 and Figure 3.9-4).

Two small basaltic eruption centers similar to those of Crater Flat are located at Sleeping Butte, about 47 km northwest of Yucca Mountain (Figure 10-12). The Sleeping Butte centers consist of scoria and spatter cones, and blocky *aa* (a Hawaiian term for lava flows typified by rough, jagged, spinose, clinkery surface) flows extruded from the bases of the cones. The two centers are aligned in a north-northeast direction, along with lenticular feeder dikes. Ages range from about 350 ka (Minor et al. 1993) to 280 ka (Champion 1991, p. 65). Crowe et al. (1995, p. 2-2) gives the age range as 380 ka to 320 ka.

Lathrop Wells cone, located at the southern end of Yucca Mountain, (about 20 km from the repository block) is associated with the smallest and most recent of the Plio-Pleistocene volcanic centers in Crater Flat. It consists of a large scoria cone and 3 to 4 sets of fissures associated with bombs, spatter, and small blocky *aa* flows. Most of the vents and fissures are aligned or elongated to the northwest, parallel to local northwest-striking faults. A range of radiometric ages has been determined for the Lathrop Wells cone basalts (e.g., ; Turrin et al. 1991, Table 1; Champion 1991, p. 66, col. 1, paragraph 3), but the most widely accepted dates for the scoria cone cluster around 80-70 ka (Perry et al. 1998; CRWMS M&O 1998c, Section 3.9.3.1).

Apart from the volcanic center associated with Lathrop Wells, the relationship of local structure to intrusion is obscure. The largest volume basalt extrusions are located west of Yucca Mountain in Crater Flat, implying a genetic association between sites of intrusion and basin substructure. Intriguingly, the largest and most deeply penetrating fault here, the Bare Mountain fault, appears not to have an influence on the location of basaltic intrusions in Crater Flat basin (Crowe et al. 1995, p. 3-28).

The Plio-Pleistocene basaltic volcanic centers form a northwest-oriented alignment termed the Crater Flat volcanic zone (CFVZ), indicated in Figure 10-12 (after Crowe et al. 1995, Figure 3.10). Correlation of cone locations and eruption volumes along a best-fit regression line within the zone implies that intrusion of basaltic magma was controlled by a northwest-trending structure or structures. However, the north-to-northeast orientation of feeder dikes at the volcanic centers seems to reflect the local influence of the regional stress field, as the dikes are nearly parallel to the greatest horizontal compressive stress (Crowe et al. 1995, p. 3-41). The northwest trend of the CFVZ, combined with the north-northeast orientations of dikes within it, suggests the influence of a broad dextral shear couple of crustal dimensions. Crowe and Perry (1990, p. 327) noted that there are no systematic time-space patterns to the distribution of volcanic centers within the CFVZ.

One Pliocene (about 2.8 Ma) volcanic center lies outside the CFVZ at Buckboard Mesa at the northeast side of the Timber Mountain caldera (shown in Figure 10-12). Intrusion here appears to have been controlled by caldera rim fractures. The intruded rock is more felsic than the basalts of the CFVZ. Therefore it likely has a different tectonic association and petrogenetic origin than the basalts of the CFVZ.

The Plio-Pleistocene basalts in Crater Flat total a relatively small volume of rock, (about 1 km³), and the contributions to this volume have decreased over time. The volume of magma per eruptive event has decreased by more than a factor of 30 since Pliocene time (Figure 10-13; Crowe et al. 1995, p. 7-3 and Figure 4.2).

10.3.2 Petrology and magmatic origin of the basalts

The Plio-Pleistocene volcanic rocks of the CFVZ are all alkaline olivine basalts. Their mineralogical and geochemical characteristics indicate derivation from magma generated in the lithospheric mantle, at depths of 45 to 60 km or more (Crowe et al. 1995, Chapter 4-Section II, Chapter 5-Section III). Ascent of the magma through the crust must be rapid, perhaps on the order of days; otherwise, the small batches observed in the Yucca Mountain region would freeze in transit. Crowe et al. (1995, p. 5-9) emphasize the role of buoyancy in magma ascension, but buoyancy could not provide the velocities involved nor account for the pathways. An alternative explanation is that magma rises by means of fluid-assisted fracture propagation. Seismic evidence indicates that magma-assisted fracturing can occur to depths as great as 55 km (Aki and Koyanagi 1981). For the small volume basaltic magmas to ascend the crust and erupt at the surface, they must take advantage of dilatant (tectonic) pathways.

The essential point in this mechanism is volatile content. Clearly, the basalt magmas arrive at the surface having sufficient volatile content (chiefly water) to generate explosive eruptions and *aa* flows (e.g., Crowe et al. 1995, p. 2-31). Once the magma is degassed, it freezes and eruption ceases. A small amount of water (a few weight percent) lowers the temperature at which a given volume of melt can coexist with the host rock, and it lowers the viscosity, but a relatively high partial pressure of water is required to keep the melt mobile within the upper crust.

10.3.3 Duration and recurrence of basaltic activity

The basaltic extrusions described above are clustered in time and space. A tectonic association could be demonstrated if it were possible to associate the clusters with distinct periods and places of crustal disruption. By establishing a genetic linkage among the volcanic features we can gain insights as to cause and process, and can relate these to present-day and projected rates of extensional deformation. In this respect, we consider two kinds of events, tectonic events and volcanic events. A volcanic event is a relatively simple component of a tectonic event; it involves accumulation of a batch of magma in the lower crust or upper mantle, its passage through the crust, and eruption at the surface.

A volcanic event creates intrusive and extrusive features as well as local dynamic disruption, including faulting, fissuring, and earthquakes. The formation of a cinder cone and associated lava flows is typically abrupt and short-lived. For example, Parícutín, in Mexico, was formed in about a decade, then died as abruptly as it was born. It is unlikely that a cone-forming event, complete with satellite mounds and fissure or basal lava flows, would be active for more than several decades. It should be noted that two experts who contributed to the Probabilistic Volcanic Hazard Analysis (PVHA), G. Thompson and W. Hackett, consider typical durations of activity in the range of hundreds of years (CRWMS M&O 1996a, pp. GT-2 and WH-2, respectively).

A tectonic event is complex and, unlike volcanism, is not easily circumscribed in space or time. The process of crustal disruption, involving faulting and fracturing, may occur during an episode that spans centuries or millennia, over distances or areas of tens of kilometers. Such a tectonic episode may be punctuated by several discrete volcanic events. It is necessary, therefore, to think of volcanic events as *cluster events*, that is, a series or group of eruptions spread over time and space, but related genetically within an episode of crustal disruption.

The concept of a volcanic event as an eruptive episode is well expressed by M. Sheridan (CRWMS M&O 1996a, p. MS-2): an *eruptive episode* (or *eruptive cycle*) is defined as a series of active periods of eruption separated by quiescent periods. An active period itself includes short pauses and may operate for several years to thousands of years. Thus, the lifespan of an eruptive episode, such as a cone or cone complex, probably spans decades to a century or more, but the lifespan of a volcanic center probably approximates that of the coeval tectonic event, which could range up to 100 kyear.

Genetically related eruptive features form a volcanic center. Crowe et al. (1995, p. 3-24) associate a volcanic center with an individual period of eruption, but they discriminate *center events* from *cluster events*. Crowe et al. (1995, Chapter 2-Section IV, Chapter 4-Section VI) point out that once a volcanic center is established, it tends to be a site of recurrent activity for perhaps as long as 10^5 years. Thus, the apparently extended history of Lathrop Wells volcanic center suggests that it is the most likely site for an eruption within the next 10^4 years (Crowe et al. 1995, p. 4-18). Such a likelihood therefore decreases the probability that magma will intrude the potential repository site in the event of the most likely site erupting.

Unfortunately, this assessment is somewhat vitiated by the statement: "*Examination of the sequence of the location of past volcanic events shows that there is no consistent pattern in the location of individual volcanic events relative to the location of the immediately preceding volcanic event*" (Crowe et al. 1995, pp. 7-70). Too, there is no way of physically determining when the terminating eruption of a cluster center has occurred; perhaps the most recent activity at the LaThrop Wells Cone center marks the end of volcanogenic tectonism there.

10.3.4 The ash event: evidence of coupled processes

A concern about volcanic activity at Yucca Mountain is whether a volcanic event could include substantial faulting at the mountain. There is considerable evidence, in the form of basaltic ash in fault fissures, that basaltic eruption and faulting have been concomitant events, perhaps reflecting coupled processes.

Trench T8 on the Solitario Canyon fault (indicated in Figure 10-14) exposes a 60- to 70-cm-wide subvertical fissure that formed during the largest known late Quaternary surface rupture. The bottom meter of the exposed fissure contains nearly pure basaltic ash mixed with carbonate clasts derived from the fissure walls. The angularity of the fine sand-size ash grains and the lack of other material of similar grain size indicates deposition primarily directly from an ash cloud shortly after the fissure opened (a certain amount of ash-free pebble silt—possibly tumble fill—was apparently deposited before the ash; Ramelli et al. 1996, pp. 4.7-14 ff.).

Soils in the fissure above the ash, and overlying the fissure itself, provide age dates in the range of 40 to 100 ka, a range that implies that the ash was derived from the Lathrop Wells volcanic center (Ramelli et al. 1996, Section 4.7.3.1.1.4). The geometry of the fissure suggests that about a meter of vertical displacement occurred with formation of the fissure. The ash-filling event accounts for most of the mid-to-late-Quaternary vertical offset which, at about a meter, is at least twice as large as any other displacement on the Solitario Canyon fault. Earlier fissuring in the fault, not associated with volcanism, is indicated by older, gravel-filled and cemented fissures that contain no ash. The ash event was succeeded by faulting of as much as 20 cm vertical displacement around 16 ka or earlier (Ramelli et al. 1996, Section 4.7.4.1.1). The maximum 100-kyear time period for the activity is consistent with the definition given above for a single volcanic/tectonic event.

10.3.5 Regional associations and tectonic implications

The alignment of the CFVZ along the northwesterly orientation of dextral shear in the Walker Lane (Figure 10-15), and the alignment of individual volcanoes and feeder dikes in a generally north-to-north-northeast orientation suggests both regional and local structural control on the emplacement of basaltic magma (Carr 1990, p. 299 ff.; Crowe and Perry 1990, pp. 327-328; Crowe et al. 1995, Chapter 3-Section II; CRWMS M&O 1996a, pp. MK-2, 3). The association implies that dextral shear applied along the axis of the CFVZ created local north-to-north-northeast-striking, transtensional fractures that became sites of dike intrusion and volcanic eruption. The northwesterly alignment of volcanic centers in the CFVZ has been cited as evidence of a large strike-slip fault zone (Schweickert and Lahren 1997; Figure 4). However, no mappable trace of a through-going fault zone has been found. The Pahrump-Stewart Valley fault, shown in Figure 10-15, is the only likely candidate for such a fault, but it does not coincide with the CFVZ. The CFVZ is aligned along the irregular western rim zone of an assemblage of basins, the deepest of which is Crater Flat Basin.

The basaltic volcanic centers in Crater Flat basin show some correspondence with the local fault framework, but the association is perhaps from another source, as the faults probably do not project through the middle crust. The intrusion of basaltic magma is related to deep fracturing in the central and southern parts of the basin. The 3.7 Ma basalt center and its feeder dikes are broadly coincident with the inferred trace of the intersection of the Bare Mountain and the Paintbrush Canyon faults. The distribution of Pleistocene cones and dikes generally conforms to the strike of local Yucca Mountain faults. The distribution of the 1-Ma, basalt center is independent of the Bare Mountain fault and its intersection with any Yucca Mountain fault.

Fracture conduits for basaltic magma must extend from magma source depths in the lithospheric mantle to the surface. Such fundamental fractures must be largely independent of fault mechanics in the upper crust. However, deep fractures must be of local extent and constrained by the form of the basin, as the distribution of volcanic centers is not systematically aligned along the projection of a given fracture or fracture zone. If deep fractures can be propagated to the surface by basaltic intrusion, the dikes cannot exceed the dimensions of basin-confined faults at Yucca Mountain; therefore, the maximum length is probably about 20 km (cf. CRWMS M&O 1996a, Figure 3-62), and the strike probably centers around N30°E (cf. CRWMS M&O 1996a, Figure 3-62). Furthermore, through-the-crust fracturing must be relatively rapid, since magma ascent is thought to occur on a time scale of hours or days (Crowe et al. 1982, p. 11).

We infer that dextral shear applied to Crater Flat basin is sufficient to create transcrustal strain leading to the fracturing.

Recurrent basaltic volcanism in Crater Flat depends on two major tectonic features: small (perhaps segregated) volumes of resident basaltic magma in the upper mantle, and an extending basin that focuses transtensional fractures through the crust to tap the resident magma. Fractures beneath Crater Flat basin may disrupt the mantle, facilitating the accumulation of magma into relatively large volumes in which some differentiation could occur, and it may influence the transfer of heat and water, which would be conducive to increased local melting at depth.

The tectonic model believed to be most likely, that of an extending rhombochasm, or half-graben, provides for a structural and dynamic linkage between volcanism and its distribution in Crater Flat (and in the CFVZ in general). Models based on detachment faulting and transcurrent strike-slip faulting offer no explanation for the nature of basaltic volcanism and its distribution. Mid-to-upper crustal detachment faults dissociate observable structural relations with any deformation that occurs in the deep crust below the detachment; this model affords no predictive value, and it restricts our understanding of coupled processes to chance. The notion that basaltic volcanism in Crater Flat is evidence for a transcurrent strike-slip fault (Schweickert and Lahren 1997, Section 6) begs the question. The fact remains: basaltic volcanism is associated with Crater Flat basin, whether a strike-slip fault cuts the basin or not. Unless basaltic volcanism could be associated with strike-slip faulting apart from the CFVZ, the presence of strike-slip displacement is, in relation to volcanism, a tectonic accident in this setting.

Although the volume and petrology of the basalt volcanic centers vary with time, the locations of the centers show no similar variation. This implies that magma genesis does not control where and when eruption occurs. Magma evolution is not directly related to local tectonics, and the magma itself cannot precipitate fracturing under hydraulic pressure. The magma source zone is uniform over a wide area (the "Amargosa Valley Isotopic Province", CRWMS M&O 1996a, p. 3-28) even though it may consist of locally fractionated magma pods. Hence, it is possible to define a large, cogenetic event distribution — the kettle is always simmering.

Tectonic strain-release varies from place to place. Therefore, even though Crater Flat and Sleeping Butte have the same kind of basalt, eruptions occurred under different local structural conditions. Tectonics are local, and the domainal nature of the Yucca Mountain region has a significant control on what happens where. Crater Flat basin can be considered a tear in the crust, or a crustal flaw where deeply penetrating transtensional fractures are concentrated and recurrent. They are capable of tapping the deep, remaining magma sources in the cooling and stiffening lithospheric mantle. There is a limited amount of lithospheric melt available, and it is decreasing as volatiles are depleted. The main reason there is any melt available and that it gets to the surface to form scoria cones is the presence of water. When local strain thresholds are exceeded, volatile-charged magma ascends in dilatant pathways.

What happens to allow distributed local melt bodies to coalesce to volumes capable of exerting buoyancy effects, and to ascend to the surface without crustal contamination or significant loss of heat? The answer must be a release of compressive stress resulting from crustal failure and generation of fracture pathways for rapid melt ascension. In other words, a tectonic mechanism, extension, must pass some strain-related threshold that allows a combination of critical events to

occur in some cascading sequence: increase in magma volume, coalescence of melt batches over a relatively short period of time, and rapid ascent to ground surface. This implies a coupled process of extension and eruption.

10.3.6 The initiating event and coupled processes

The initiating event—brittle failure or fracture of the middle to lower crust—leads to two tectonic processes: intrusion of basaltic magma into the crust and perhaps to ground surface, and fault slip in the upper crust. Insofar as these processes are linked to the initiating event, they can be considered coupled processes. Coupled processes can also be linked as cause to effect. For example, basaltic volcanism is often preceded or accompanied by earthquakes, because the destabilizing effect of ascending magma causes small fault displacements near the magma conduit. Most such earthquakes are at background magnitudes ($M_L \leq 5.8 \pm 0.4$) and are located within about a 3-km radius of the vent center. The maximum magnitude for a volcanic earthquake in Crater Flat is based on Smith et al. (1996, p. 6284 ff.) and a study of volcanic-related earthquakes worldwide. It seems clear, given the spatial distribution of basaltic volcanism during the past 4 Myears, that this local fault slip and seismicity would have little or no effect on the repository block. Coupled processes that are related to a common, fundamental mechanism, crustal extension, are relevant to faulting at Yucca Mountain, as implied by the “ash event” described above.

The coupled-processes model is built on the concept that continuing tectonic extension triggers a succession of faulting and fracturing events that culminate in intrusion of basaltic magma into high levels of the crust. The width of the basalt dike compensates, in part, for a width of crust that would ordinarily be extended by normal faulting. This is because inflation of the dike exerts a stress that increases the normal stress, thereby reducing the shear stress acting on local faults. Thus, if extension in Crater Flat is proceeding at a rate of 0.01 mm/yr, intrusion of a dike 1 m thick should suppress significant faulting for a period of about 100 kyear within the part of the basin influenced by the dike.

Eventually, however, progressive extension overcomes the stabilizing effect of the dike. The earliest post-intrusive strain effects are manifested by slip on weak, steeply dipping faults in the upper crust, accompanied by small earthquakes. With time, the deeper, stronger faults of the middle crust slip (cf. Bruhn and Schultz 1996, pp. 3404 ff.). Finally, creep in the lower crust/upper mantle is terminated by fracturing, which reaches a critical point of failure with intrusion of magma. Basaltic magma accumulates in lengthening fractures that coalesce into a few major dike conduits. Fracturing decreases local pore pressure, which causes the magma to devolatilize thereby increasing water and other volatile concentrations at the crack tips and precipitating anhydrous silicates in the melt while extending the fractures.

Figure 10-16 illustrates this model of periodic stress relief punctuated by volcanism. The process itself may be cyclical and regular, but the conditions under which it occurs are changing with time. First, the driving mechanism—extension—is not necessarily constant. The rate and direction of extension may vary with time. The dates of volcanism may be a reflection of periods of sporadic extension, within time spans of approximately 200 kyear. Second, it is likely that the crust in the Yucca Mountain region is cooling, strengthening, and dehydrating in the

aftermath of mid-Miocene crustal magmatism. Petrologic data imply that younger basalts came from deeper sources; either sufficient volumes of basalt magma are no longer available in the lower crust/uppermost mantle, or insufficient water is present to facilitate melting and maintain significant melt volumes in the uppermost mantle. In effect, the source region is "running out of gas," and effective stress is increasing over time, making initiating events more unlikely. A third factor is the possibility that magma intrusion has, in fact, happened and can happen again more frequently than is indicated by the basalt volcanic centers. Magma intrusion need not invariably result in eruption. However, at present there is no geophysical evidence to indicate the presence of any large number of scattered dikes, as much as 2 meters thick, within a few to several km of the surface of Crater Flat. If undetected dikes are present in Crater Flat they are most likely at depths greater than about 2 km. R. V. Fisher (CRWMS M&O 1996a, p. RF-9) speculates that there may be ten times as many dikes 2.5 km to 5 km deep as there are at the surface, and M. F. Sheridan (CRWMS M&O 1996a, p. MS-10) estimates that there could have been ten undetected events—roughly one event every 100 kyears.

10.3.7 Summary of Tectonic/Volcanic Coupling at Yucca Mountain

Tectonic extension in the Yucca Mountain area is part of the regional deformation that allows the evolution of the structure of the southern Great Basin to continue. The principal effects of extension are sporadically recurrent faulting and earthquakes, and local basaltic volcanism. In a tectonic sense, Yucca Mountain represents the exposed and eroded part of a slab of volcanic rock that has been faulted by extension and has partly subsided into Crater Flat basin. Crater Flat basin has been a site of tectonic activity for at least 12 Myears and is the center of most recent extension, as indicated by the basaltic volcanoes and the alluvial fill that hides the bedrock structure. Yucca Mountain and Bare Mountain are both peripheral to this activity. However, the rate and variability of extension is uncertain. The only intrusion at Yucca Mountain proper occurred between 9 and 10 Ma, along part of the Solitario Canyon fault. If we consider this history as a long-term trend, we can reasonably conclude that future volcanism will be restricted to Crater Flat and will not occur within the repository block. At times, extension in the basin proceeds to the point where basaltic magma sources at subcrustal depths are tapped, and magma ascends through basin-restricted fractures to eruption. Such volcanism is coupled to local faulting at Yucca Mountain. Intrusion of basalt counteracts local extension for some unknown period of time. This phenomenon and the unknown rates of extension in the basin make prediction of future volcanism impossible. Geologic history provides us with three reasonable conclusions, however: volcanism appears to be decreasing in volume with time; future volcanism likely will be restricted to Crater Flat basin or its southwestern margin; and Yucca Mountain may experience faulting associated with volcanism, but may not experience intrusion.

10.4 BASALTIC IGNEOUS ACTIVITY

Three scenarios for possible igneous activity are being analyzed for this TSPA: occurrence of direct releases to the surface from an eruption; enhancement of the groundwater-transport, radionuclide source term resulting from interaction with a nearby magmatic intrusion; and alteration of saturated-zone flow and transport as a result of igneous intrusive (or seismic) disturbance. These represent only three of the branches of the generalized event tree for igneous

activity (see Figures 10-15a and 10-15b); however, they are representative of several classes of scenarios.

The direct surface release scenario (discussed in Section 10.4.2) assumes that an eruptive center (i.e., a volcanic vent) is able to transport waste to the surface. Otherwise, the waste will be directly or indirectly affected by the dike and the igneous environment, but will remain in the repository. The latter condition is represented by the enhanced source-term-scenario (discussed in Section 10.4.3).

10.4.1 Incorporation of the Probabilistic Volcanic Hazard Analysis

Consequences of igneous activity are discussed here. The annual frequencies of occurrence for each of the three scenarios are taken from the PVHA (CRWMS M&O 1996a). The PVHA for the Yucca Mountain, Nevada, project was conducted to assess the annual frequency of disruption by a volcanic event of the potential repository at Yucca Mountain and to quantify the uncertainties associated with this assessment. In this context, disruption means the physical intersection of magma with the repository volume. The annual frequency provided in the PVHA are applicable to both direct-interaction scenarios—direct surface releases and enhanced source term.

The evaluations of members of a ten-person expert panel were elicited to ensure that a wide range of approaches was considered for the hazard analysis. The results of the individual elicitations were combined to develop an integrated assessment of the volcanic hazard that reflects the diversity of alternative scientific interpretations. The assessment, which focused on the volcanic *hazard* at the site, expressed as the annual frequency of disruption of the potential repository, provides input to an assessment of volcanic *risk*, which expresses the probability of radionuclide release as a result of volcanic disruption.

The PVHA provides the basis for estimates of the annual frequency of occurrence for intersection of the repository site by a volcanic event that reaches the surface during the next 10,000 years. (The experts also considered the changes that might occur in frequency estimates over longer time periods. However, no formal assessments for 1,000,000 years were made [CRWMS M&O 1996a, pp. 1-1 ff.]. As a TSPA-VA abstraction, we use the same frequency estimates for all time periods considered.) The generalized model used in the PVHA includes: (1) an assessment of the spatial and temporal frequency of volcanic events, and (2) an assessment of the spatial extent of an event, given that it occurs (CRWMS M&O 1996a, Section 3.1). Specifically, the PVHA provides a description of volcanic source areas and the future spatial distribution of volcanic events within these areas, spatially varying (i.e., spatially smoothed) distribution of volcanic events (i.e., points), which are associated with volcanic dikes of certain dimensions, distributions of dike lengths and orientations, and assessments of the type of volcanic event that will occur. Individual PVHA expert assessments are summarized in Table 10-5 (after CRWMS M&O 1996a, Section 3.2.2).

The results of the PVHA analysis are that the aggregate expected annual frequency of intersection of the repository footprint by a volcanic event is 1.5×10^{-8} , with a 90-percent confidence interval (5th to 95th percentiles of the distribution) of 5.4×10^{-10} to 4.9×10^{-8} (CRWMS M&O 1996a, Section 4.3). The major contributions to the uncertainty in the

frequency of intersection are the statistical uncertainty in estimating the rate of volcanic events from small data sets and the uncertainty in modeling the spatial distribution of future events. Although there are significant differences among the interpretations of the ten experts, most of the uncertainty in the computed frequency of intersection is because there was an average uncertainty expressed by individual experts in developing the appropriate PVHA model (CRWMS M&O 1996a, Section 4). Figure 10-17 shows the distribution for expected annual frequency of intersection from the PVHA.

Using the annual frequencies of occurrence from the PVHA for intersection of a dike with the repository footprint, an estimate can be made of the probability of an igneous event occurring in the entire Yucca Mountain region. This probability is necessary for the indirect, igneous-effects scenarios. As is discussed in detail in Section 10.4.4, dikes can occur along existing faults or at other locations not associated with existing structures. To first approximation, the probability of dike intrusion in the larger area around the repository is proportional to the increased area (R. Youngs, Geomatrix Corporation, personal communication). Because the current and expected future volcanic centers are to the west of the Yucca Mountain repository block, the probability estimate applies only to any larger area that does not extend to the west of the repository block.

The possible volcanic hazard to the proposed repository is magma feeding a dike or surface eruption, which could ascend directly through the repository or erupt or intrude nearby, compromising the integrity of the waste-isolation system. The basic elements that need to be assessed to define the hazard are the spatial distribution and recurrence rates of future volcanic events in the region. Spatial models represent the future locations of volcanic activity. The most common spatial models used by the expert panel members are those that consider the future occurrence of volcanoes to be homogeneous within particular defined regions or "source zones," defined based on criteria that include spatial distribution of observed basaltic volcanic centers, structurally controlled provinces, and geochemical affinities within a region (CRWMS M&O 1996a, Section 3.2.2, as summarized in Table 10-5 of this document). Parametric spatial distributions and spatial smoothing models were also used by some experts. Temporal models define the frequency of occurrence of volcanic activity and, hence, the probability of occurrence. Many of the experts used homogenous Poisson models to define the temporal occurrence of volcanic events. Nonhomogeneous models were used by some experts to consider the possibility that volcanic events are clustered in time and/or to describe the possible waning or waxing of volcanic activity in the region during the recent volcanic past (CRWMS M&O 1996a, Section 3.2.2, as summarized in Table 10-5 of this document). Results of the study indicate that spatial issues are more important than temporal issues.

10.4.2 Direct Surface Releases

The PA consequences of direct surface releases are primarily the dispersal of contaminated, volcanic ash in the vicinity of an eruption. Several models for ash dispersal exist (e.g., Jarzempa and LaPlante 1996; Searcy et al. 1998). The Center for Nuclear Waste Regulatory Analysis (an NRC contractor) has developed a model for dispersal of radionuclides from an ash plume thought to be typical of volcanic eruptions in the Yucca Mountain region (Jarzempa et al. 1997). The model is embodied in the ASHPLUME code (Jarzempa et al. 1997). This dispersal mechanism represents a suitable illustrative model for direct-surface releases. The radionuclide source term used in the Yucca Mountain example (Jarzempa & LaPlante 1996, p. 10) does not

describe any physical models for waste-package breach and waste entrainment. The source term appears to be based on the entire contents of one waste package being entrained for each eruption modeled. The TSPA-VA analysis applies the ASHPLUME dispersal model to a source term for the entrained radionuclides from the waste that incorporates the physical processes thought to occur.

The source term consists of five components:

- *Plumbing of the intrusion.* This describes the volume of magma available to interact with the waste, and the eruption characteristics.
- *Number of waste packages hit.* This is used to determine the number of waste packages intersected by a basaltic igneous intrusion.
- *Breach of waste package.* This is the mechanism for exposure of the waste to the magma.
- *Removal of contents of waste-package.* This is the mechanism for mobilizing waste from the container.
- *Incorporation of waste into magma.* This describes the mechanism for transporting the mobilized waste in the magmatic flow.

The following processes are postulated for the components of the source term. In some cases, sources for the parameters describing the models are identified. Although not every process has been evaluated, a model for the direct-release source term can be developed from the components. Note, however, that the mechanisms by which a dike that is ascending through rock propagates across an opening (such as the repository drifts) or in a stress-relieved zone surrounding the drifts has not yet been resolved. If analyses show that dikes are unable or unlikely to propagate beyond an opening, then the direct-release scenario changes considerably.

Plumbing of Intrusion

- Intrusion dimensions (orientation, width, length)
- Nature of intrusion (vertical dike, lateral sill)
- Number of eruptive vents
- Fragmentation depth.

Number of Waste Packages Hit

- Layout of emplacement drifts (waste-package orientation, pitch)
- Eruptive vent diameter.

Breach of Waste Package

- Corrosion/Oxidation

- Hostile magmatic components present
- Thinning rate as function of temperature
- Corrosion reactions with waste-package materials
- Variable initial thickness of waste package.
- Slump/Collapse
 - Plastic deformation of waste-package wall
 - Variable initial thickness of waste package
 - Additional static loads
 - Internal pressurization
 - Freezing of magma on waste package/insulation.
- Melting/Dissolution
 - Iron solubility in magma
 - Temperature of magma/melting points of waste-package materials.
- Abrasion
 - Abrasion rate as function of temperature, flow
 - Mechanical properties of pyroclastics/ash
 - Variable initial thickness of waste package.

Removal of Contents of Waste Package

- Particulate Mobilization
 - Liquid mobilization/venturi
 - Gas mobilization/venturi.
- Dissolution
 - Solubility of UO_2 in magma
 - Solubility of other radionuclides in magma.

Incorporation of Waste into Magma

- Advection
 - Rheological properties
 - Newtonian fluid
 - Bingham fluid
 - Density, velocity of fluid (ash-particle size)
 - Waste-particle size, density.
- Adhesion
 - Waste-particle size, charge.
- Dissolution
 - Solubility of waste constituents in magma.

10.4.2.1 Characteristics of Igneous Activity in the Yucca Mountain Region

Igneous activity in the Yucca Mountain area includes both intrusive and extrusive events. Intrusion "plumbing" provides information on the characteristics of dikes (length, width,

orientation, etc.), on their mode of formation (whether they are formed by monogenetic or polycyclic eruptions) and their duration.

From the PVHA report, the following relevant information is available.

- Locations of volcanic source areas and a description of the future spatial distribution of volcanic events within these areas (CRWMS M&O 1996a, Figure 1-1).
- Spatially varying distribution of volcanic events that are associated with dikes of given dimensions (CRWMS M&O 1996a, Section 3.1.4).
- Distributions of dike lengths and orientations relative to the volcanic source points and their potential intersection with the repository (CRWMS M&O 1996a, Section 3.1.6).
- Assessment of annual frequency of occurrence of hydromagmatic eruptions (CRWMS M&O 1996a, Section 3.2.2, as summarized in Table 10-5).

This information is used to update the models used in prior TSPA analyses [TSPA-91 (Barnard et al. 1992, Chapter 7); TSPA-93 (Wilson et al. 1994, Chapter 17)]. The availability of expert assessments (provided as noted below by G. Valentine and F. Perry, Los Alamos National Laboratory) in support of existing data provides additional credibility.

10.4.2.1.1 Types of eruptions

As discussed in Section 10.3, the expected type of future eruption that may occur in the repository region is similar to that exhibited by the Pliocene and Quaternary volcanic centers. These are generally small-volume basaltic eruption, probably a mixed, strombolian-type event (monogenetic basaltic dikes, cinder cones, and lava flows). Given the negligible to very low probabilities provided by the experts to the possibility of hydromagmatic or silicic events in the Yucca Mountain region (G. Valentine and F. Perry, LANL, Minutes of Meeting on volcanic disturbed scenarios, March 1998. Accession number MOL.19980715.0398), these types of events are not included in the igneous-intrusion models. For the direct-release scenario, the nature of the event is assumed to be a single eruptive vent (cone) or multiple eruptive vents (cones) associated with a vertical basaltic dike.

Larger sub-horizontal sheet intrusions (sills) are not included in the scenario models. Sills have not been observed in the Yucca Mountain region, and thus are considered a very low probability event (on the order of 10^{-1} to 10^{-2} probability given a volcanic event). Larger-volume ($\sim 1 \text{ km}^3$) sills are observed in the Paiute Ridge area, an analog site in southern Nevada, (G. Valentine and F. Perry, LANL, Minutes of Meeting on volcanic disturbed scenarios, March 1998. Accession number MOL.19980715.0398) which branch off from some dikes within 300 m of the paleo-surface. These sills occur consistently in hanging-wall blocks adjacent to faults along which dikes are intruded. Generally, these sills are found in the tertiary tuffs near the boundary between the tertiary and Paleozoic rocks. The geometries and spatial distributions of these localized sills suggest that the emplacement of these intrusions was controlled by local near-surface phenomena such as contrasting rock properties on different sides of the faults, the relative material strength of Paleozoic and Tertiary rocks, and/or local stress variations resulting

from paleo-topographic effects (Valentine et al. 1998). The contact between the Tertiary tuffs and Paleozoic bedrock at the potential repository site lies at a minimum depth of approximately 700 m below the repository level. As a TSPA-VA abstraction, for the direct-surface-release scenario, the nature of the intrusion is assumed to be a vertical dike, but for the enhanced-source-term scenario, lateral flow at depth is considered.

10.4.2.1.2 Eruption volumes

The expected total ash mass that would be ejected during a future eruption is based on the total magmatic volume measured during historical eruptions at volcanoes that are considered possible analogs for the types of eruptions that have occurred most recently in the Yucca Mountain region. Based on their research of possible analog events, the Center for Nuclear Waste Regulatory Analysis (CNWRA) (Jarzemba et al. 1997, Table 4-3) has compiled data as summarized in Table 10-6 for the total magmatic volume at these analog sites, and the duration and column height for specific ash-producing eruptions.

10.4.2.1.3 Orientation and Length of Dike

The PVHA provided the annual frequency of occurrence of a dike intersecting the repository. From the PVHA studies, we can calculate the conditional probability that a dike will intersect the repository for any future volcanic center in the Yucca Mountain region. An illustration of potential dikes in relation to the repository location is shown in Figure 10-18. Dike locations and orientations have been calculated for this illustration using the random-location method of placement on a point event (CRWMS M&O 1996a, Section 3.1.6, and Figure 3-11). Parameters for this calculation are event azimuth, event length, and the relative location of the dike on the event.

For those dikes that do intersect the repository, we can calculate the joint probability for the length and orientation of that portion of the dike within the repository boundary. Note that the balance of the dike length may be outside the repository. The joint probability-density surface for dike length and orientation inside the repository is shown in Figure 10-19. The length origin is any point on the western boundary of the repository where a dike crosses the boundary. The distribution of orientations is strongly trending north-south. As expected, the dike orientations are roughly perpendicular to the least principal stress in the region.

10.4.2.1.4 Number of Eruptive Centers

Based on observations at the Yucca Mountain site, the number of eruptive centers (vents) occurring along a dike is expected to be small (G. Valentine and F. Perry, LANL, Minutes of Meeting on volcanic disturbed scenarios, March 1998. Accession number MOL.19980715.0398). The PVHA experts have provided assessments relating the number of events that may occur to the number of eruptive cones that would form during those events. The most likely number of vents along an entire dike length is considered to be one, with a maximum of five (G. Valentine and F. Perry, LANL, Minutes of Meeting on volcanic disturbed scenarios, March 1998. Accession number MOL.19980715.0398). Because not all the dike length is contained within the repository boundary, some vents occur outside the repository. The probability density function (PDF) for the number of vents along the length of the dike inside the

repository reflects this, by showing the most likely number of vents as zero, and a maximum of four. The PDF is shown in Figure 10-20. Although the PDF is shown as a continuous line, only integer numbers of vents are used. Also note that plots of PDFs are presented in this chapter without ordinate scales because they are intended to show the shape only. For calculational purposes, the cumulative distribution functions (CDFs) derived from them have been used (see Section 10.4.2.8).

10.4.2.1.5 Fragmentation depth

The nature of the interaction between a magmatic intrusion and waste packages depends on the physical form of the magma—liquid magma or ash and pyroclasts. Flow velocity, conduit diameter, and bulk density are some of the characteristics that change rapidly at the fragmentation depth. The formation of an ash flow from a liquid-magma flow occurs at the fragmentation depth in the eruption conduit. If fragmentation occurs below the repository depth, any waste packages in the eruptive conduit are subjected to a high-velocity ash and pyroclast bombardment. If fragmentation occurs above the repository depth, the interaction is between liquid magma and waste; subsequently, magma contaminated with radionuclides forms an eruptive ash flow.

The fragmentation depth is primarily a function of the amount of water dissolved in the magma. At some depth, the confining pressure of the rock is reduced sufficiently that the water separates from the magma as a gas, forming bubbles. At the fragmentation depth, the magma changes from liquid rock containing gas bubbles to a gas containing liquid and solid rock fragments and ash. The transition from liquid to ash is fairly abrupt—occurring over a distance of less than 50 m. Because we have no other information, a uniform distribution ranging from 100 m to a maximum depth of 400 m is used to model the fragmentation depth.

Parameter	Minimum	Maximum	Distribution Type
Fragmentation Depth	100 m	400 m	uniform

(Note: throughout this Chapter, those parameters and PDFs that would be presented as single-entry tables are indicated by the box structure shown above. Because they contain a limited number of entries, they are not considered tables, but they are important inputs to the models and the boxes indicate this.)

This distribution is based on consideration of the estimated range of initial water content of the source magma, and the expected depth at which 70 to 80 percent of the volatile fraction would be exsolved as indicated by solubility curves for basalt and water as a function of temperature and pressure. A depth of 400 m is the approximate fragmentation depth for a basalt containing about 2.5% water (Wilson and Head 1981, equation 30, assuming lithostatic pressure). Although Yucca Mountain basalts could have somewhat higher water contents (and therefore deeper fragmentation depth), we limit the depth at 400 m for conservatism. The upper limit of 100 m is consistent with a fragmentation depth for basalt with 1% water (G. Valentine and F. Perry, LANL, Minutes of Meeting on volcanic disturbed scenarios, March 1998. Accession number MOL.19980715.0398). Experimentally determined water content for alkali basalts at mantle

pressures suggest that an upper limit for water content for basalts is 3 percent by weight. The initial water content of Yucca Mountain region basalts is assumed to be relatively high (ranging from 1 to 3 wt. %) for several reasons: (1) the basalts probably are derived from an hydrous mantle source; (2) they are small-volume eruptions that suggest lower degrees of melting, and (3) amphibole phenocrysts have been reported in Crater Flat basalts (G. Valentine and F. Perry, LANL, Minutes of Meeting on volcanic disturbed scenarios, March 1998. Accession number MOL.19980715.0398).

10.4.2.1.6 Dike width and conduit diameter

The PDF for dike width is shown in Figure 10-21. It is based on the assessments of some of the PVHA experts (see Table 10-5), with elaboration from the YMP principal investigators (PIs) investigating volcanism (G. Valentine and F. Perry, LANL, Minutes of Meeting on volcanic disturbed scenarios, March 1998. Accession number MOL.19980715.0398). The consensus is that the dike widths range from 0.5 to 4.5 m. Widths are log-normally distributed, with a mean of 1.5 m and a standard deviation of 1.95. The 4.5-m point represents the 95 percentile of the PDF.

Parameter	Mean	Standard Deviation	Distribution Type
Dike Width	1.5 m	1.95 m	log-normal

A PDF for the diameter of an eruptive conduit has been supplied by the YMP PIs (G. Valentine and F. Perry, LANL, Minutes of Meeting on volcanic disturbed scenarios, March 1998. Accession number MOL.19980715.0398). The size of the conduit is given by a PDF that ranges from typical of dike widths (2-5 m) up to values associated with significant erosion of the country rock (120 m), and is log-normal in shape. The mean is 50 m and the standard deviation is 1.5. The 95th percentile conduit diameter is 120 m. The PDF shape is shown in Figure 10-22.

Parameter	Mean	Standard Deviation	Distribution Type
Conduit Diameter	50 m	1.5 m	log-normal

10.4.2.1.7 Magma Ascent Velocity

The velocity of ascent of magma differs, depending on whether it is a liquid flow or an ash flow. Below the fragmentation depth, we assume the magma is flowing in a dike (planar) configuration. Magma ascent is related to dike width, with the rise velocity proportional to (fissure width)² for low velocity, laminar flow in a narrow fissure and proportional to (fissure width)^{1/2} for high-velocity, turbulent flow (Wilson and Head 1981, p. 2972). Xenolith studies suggest velocities up to a few m/s for magma below the fragmentation surface (Wilson and Head 1981, p. 2980 and Figure 3). Wilson and Head (1981 Table 5) provide values for ascent velocity given dike width for a basalt with viscosity 300 Pa-s and density 2800 kg/m³. These are shown in Table 10-7.

The range of ascent velocities of liquid magma as a function of dike width based on these data is shown in Figure 10-23. These data are fit well by a log-log regression; the regression formula (and goodness-of-fit measure r^2) for magma velocity used in the simulations is

$$\ln(v) = 1.859 \ln(W) - 0.608, r^2 = 0.999; v \text{ in m/s, and } W \text{ in m.} \quad (10-1)$$

For magma flows in circular conduits, Wilson and Head (1981, Table 3) provide values for ascent velocity as a function of conduit radius. These are shown in Table 10-8 and Figure 10-24, expressed as a function of conduit diameter.

The range of ascent velocities of ash and pyroclasts based on the data in Table 10-8 is shown in Figure 10-24. This curve could not be fit with a linearized relationship, so a series of interpolations and extrapolations has been done to provide velocities for the conduit diameters used in the realizations.

Ash-flow velocity increases as the column approaches the earth's surface. As lithostatic pressure decreases approaching the surface, gas pressure within the ascending magma can accelerate it. The velocity is considered to increase uniformly from the value determined from conduit size at depth to its maximum value at the surface. The maximum velocity at the surface for basaltic eruptions in the Yucca Mountain area is considered by the YMP volcanism PIs to be approximately 200 m/s (G. Valentine and F. Perry, LANL, Minutes of Meeting on volcanic disturbed scenarios, March 1998. Accession number MOL.19980715.0398). This is consistent with the maximum eruption velocity reported in Wilson and Head (1981, Figure 3) for magma with a density of 2800 kg/m^3 , viscosity of 10^3 Pa-s , and water content of 1%. As a TSPA-VA abstraction, a velocity gradient of 0.3 m/s per m has been used. Thus, for an average conduit size of 50 m at the maximum fragmentation depth of 400 m, the velocity at depth is 70 m/s (from Figure 10-24, above). A velocity gradient of 0.3 m/s per meter gives a velocity at the surface of about 200 m/s.

The discussion above indicates that there may be correlations among several of the variables. These are recognized in the development of the stochastic realizations. For example, an extremely large conduit diameter (at the 95th percentile or larger) may be inconsistent with a very small eruption volume. The conduit diameter is therefore sampled in a range consistent with the sampling that led to the eruption volume.

10.4.2.1.8 Magma temperature

Magma temperatures range from approximately $1,000^\circ\text{C}$ to $1,200^\circ\text{C}$ (MacDonald 1972, Table 4.2). Lacking further information for intrusions in the Yucca Mountain region, for this analysis, temperatures are assumed to be uniformly distributed.

Parameter	Minimum	Maximum	Distribution Type
Intrusion Temperature	$1,000^\circ\text{C}$	$1,200^\circ\text{C}$	uniform

10.4.2.2 Number of Waste Packages Hit by a Dike

This calculation uses geometric relationships to calculate the number of drifts crossed by an intruding dike and the number of packages directly affected. For there to be direct surface releases, we assume that a volcanic conduit must be in close proximity to the waste packages. The conduit must either directly intersect the waste package or be within one dike-width of the end of the package. This is because the following analysis uses kinematic arguments for the mechanism for removal of waste from the waste package. Waste packages not directly in the path of a magma conduit may be rapidly degraded, but do not contribute any waste to the entrainment to the surface.

10.4.2.2.1 Number of drifts crossed by a Dike

Given information on the characteristics of magmatic intrusions, we use information on spacing of drifts in the repository to determine the number of waste packages hit. Layout of the repository is available from Management and Operations (M&O) design documentation (CRWMS M&O 1997a). This provides drift orientation, drift spacing, drift dimensions, and waste-package spacing. Figure 10-25 shows the design layout and the layout used for the model, adapted from the design document. The model simplifies the actual layout by eliminating those sections where waste is currently not scheduled to be emplaced. The active repository is represented by a rectangular area oriented east-west and north-south, with the emplacement drifts running east-west.

The TSPA base-case thermo-hydrology model (see Chapter 3) represents the repository as having approximately 100 emplacement drifts, each 1,292 m long and spaced 28.6 m apart. The number of drifts crossed by a dike is determined by the northing value of the point of intersection of the dike with the west repository boundary and the northing value of the dike endpoint. The number of waste packages directly impacted by the intrusion depends on the number of vents located inside the repository, and on the nature of the intrusion at repository depth (i.e., either a liquid-magma or an ash/pyroclast flow).

10.4.2.2.2 Number of waste packages per drift hit by a Dike

As is tabulated in Tables 3.5-14 and 3.5-15 in Chapter 3 of this document, the 70,000 MTU of waste is contained in 10,213 packages, according to the schedule given in Table 10-9.

Assuming uniform placement, there are approximately 89 waste packages emplaced per drift. Although the different types of waste package have different dimensions, the average length is 5.5 m (Table 3.5-18 of Chapter 3). The containers thus would have an effective spacing of 14.2 m (including both the 5.5-m waste package and the gap between adjacent packages; Table 3.5-14 of Chapter 3).

Considering first liquid-magma dikes, the eruptive conduit is assumed to be cylindrical with a diameter equal to the dike width. For direct releases we assume the conduit must either directly intersect the waste package, or must come within one dike width of doing so. We further assume that a conduit that directly intersects a waste package has the potential to entrain waste from that

package only. Using trigonometric relationships, the length of intersection of a dike of width DW and orientation α along a drift of diameter 5.3 m is given by the effective dike width, EDW.

$$EDW = DW / \cos(\alpha) + 5.3 \tan(\alpha) \quad (10-2)$$

The probability of a conduit intersecting a waste package and being able to cause direct releases is $(5.5+EDW)/SP$, where SP is the 14.2-m package spacing. Figure 10-26 illustrates this.

The total number of waste packages hit by a dike is thus the number of dike-drift intersections times the above probability (rounded to a whole number of packages). The total number of packages hit provides the radionuclides available to be dispersed by an eruption. The dispersion mechanism for this scenario assumes that all the mobilized radionuclides erupt in an ash cloud through the number of vents determined by the PDF given in Figure 10-20. We conservatively assume that all the waste entrained from breached waste packages by the liquid magma at repository depth is funneled to the eruptive conduit(s) that forms at the fragmentation depth above the repository. If the sampling of number of eruptive vents inside the repository gives zero, then there is no eruptive release; if the sampling gives more than one vent, the total mobilized radionuclides are assumed to be partitioned among the vents located inside the repository. The ASHPLUME code then is used to calculate dispersion of the contaminated ash.

Larger conduit sizes are assumed to occur from ash/pyroclast flows. As the conduit size PDF shows (Figure 10-22), some values of conduit size are larger than the inter-drift spacing. The number of waste packages intersected by the conduit is determined by calculating the lengths of chords (i.e., the drifts) intersected by a circle (i.e., the conduit). Figure 10-27 illustrates this.

To calculate the number of packages hit, first select a value from a uniform random variate $[0,14.3]$ (half the drift spacing—symmetry takes care of the other half) for the conduit center. This is value x_1 in Figure 10-27. x_2 is $28.6-x_1$. If the radius is large enough, x_3 is $28.6+x_1$. The length of a chord (e.g., $2l_1$) defined by a circle of radius, r , and the perpendicular distance to the center (e.g., x_1) is $2r \sin(\cos^{-1}(x_1/r))$. The number of packages hit along the chord is $2l/14.2$. For a maximum conduit diameter of 120 m ($r = 60$ m) up to three drifts can be intersected. Each will have a different chord length, as calculated above. Table 10-10 illustrates some examples of the numbers of waste packages hit for various conduit radii and locations, using randomly generated locations and diameters for the conduits.

The first line of Table 10-10 shows a 13.4-m conduit (radius of 6.7 m) located 4.4 m from a drift. Because the distance between drifts is 28.6 m, the conduit touches only one drift, so x_2 and x_3 are zero. The conduit extends along the drift by about 10 m, which would intersect one package-spacing unit. The second entry illustrates a 4.8-m conduit that is located 14 m away from the drifts. This conduit does not intersect any drifts, so no packages would contribute to direct releases. The third example shows a conduit with radius 58.9 m centered 14.2 m from one drift. Its size allows it to intersect three drifts and hit a total of 22 packages. Lastly, a conduit with radius 20.5 m centered 11.4 m from a drift will intersect two drifts; two packages in each drift are hit, for a total of four.

If the sampling of number of eruptive vents inside the repository gives zero, then there is no eruption of contaminated ash. If there is more than one vent occurring inside the repository, we conservatively assume that both vents are of the same size and that the same number of packages are hit at each conduit. The total amount of radionuclides is the sum of the number of packages from each conduit.

10.4.2.3 Waste-Package Breach

The hostile environment arising from a magmatic intrusion can accelerate the degradation of waste packages. Depending on the time at which the intrusion occurs, the packages will be in various states of degradation. Several mechanisms for waste-package breach are possible: corrosion and oxidation, mechanical disruption, melting/dissolution, and abrasion/ablation. Of these, the most information exists for the first three mechanisms.

10.4.2.3.1 Corrosion

Typical composition of basaltic magmas is roughly as follows: 49 – 53% SiO₂, 14 – 17% Al₂O₃, 10–11% FeO, 8–11% CaO, balance TiO₂, MgO, Na₂O, and other oxides (Westrich 1982, Table 1; Douglass and Healey 1979, Table II; Valentine et al. (1998), Table 5-3). Important gaseous constituents of basaltic magmas are in the range 70%–95% H₂O, 1.5%–2.5% H₂, 2%–10% SO₂, 0.5%–1.5% H₂S, and 1%–20% CO₂. Also present in the 0.1%–0.2% range are HCl and HF (Symonds et al. 1994, Table 4; Gerlach 1980, Table 1).

Numerous investigations on the corrosion processes in hostile environments have been conducted for the oil industry (e.g., Burke 1984; Rhodes et al. 1983). In general, the findings are that low-alloy steels similar to the corrosion-allowance material (CAM) are quite susceptible to corrosion in the presence of CO₂, Cl, and/or H₂S. In particular, iron and nickel undergo extensive sulfidation (Douglass and Healey 1979, Section D); the sulfide reaction products severely compromise the integrity of the metals. Sulfides form highly porous corrosion products that offer no protection as a barrier to further attack, and sulfides generally have low melting temperatures. Furthermore, iron and nickel form low-melting eutectics (melting points in the range 637°–988°C) (Ehrlich and Douglass 1982, Table 1). Additionally, sulfidation rates are orders of magnitude higher than oxidation rates. Consequently, at the much higher temperatures and with the gases associated with an igneous intrusion, we assume that the CAM is so rapidly corroded that it is not a factor in waste-package performance.

For the TSPA-VA waste-package degradation modeling, general corrosion rates for the corrosion-resistant materials (CRM) have been determined. Under dripping environments at 100°C, the median corrosion rate is 6×10^{-6} mm/yr; under non-dripping conditions at 100°C the median rate is 3×10^{-6} mm/yr (Section 3.4). These rates have been extrapolated to volcanic temperatures, as shown in Figure 10-28 below. The nickel-based alloy ASTM B 575 (UNS N06022) (hereinafter called alloy 22) has been chosen as the CRM because of its corrosion resistance at elevated temperatures. Wang and Douglass (1983, p. 112), report that the addition of chromium to nickel-based alloys significantly reduces corrosion rates (particularly sulfidation) at 800°C. Ehrlich and Douglass (1982, Section 6) report that the addition of chromium and

molybdenum to nickel alloys provides a synergistic effect that results in superior corrosion resistance at 1,150°C in a basaltic lava and simulated magmatic gas environment. They report that the Cr and Mo form stable oxides that prevent the formation of liquid Fe and Ni sulfides. In the above work, the oxygen fugacity was reported to be 10^{-20} – 10^{-10} atmosphere; although this is many orders of magnitude less than oxygen available in the atmosphere, it is still sufficient to permit the formation of the stable oxides.

In TSPA-93 (Wilson et al. 1994, Table 17-4), an acceleration of the corrosion in magmatic environments of 10^4 was used for alloy ASTM B 443 (UNS N06625) (hereinafter called alloy 625), based on the work of Ehrlich and Douglass (1982, p. 5). Wang and Douglass (1983, Figure 3) report that, at 800°C in simulated magmatic gases, a Ni-30% Cr alloy experienced a weight gain over 3 hours of ranging from 0.2 to 1.5 mg/cm². This has been converted to an effective general corrosion rate of approximately 4 – 10 mm/yr. (The determination of equivalent corrosion rate for the Wang and Douglass data has been done by assuming a density of approximately 4 for corrosion products of the Ni-Cr alloy. The increase in weight is considered to be made up of nickel and chromium oxides and sulfur compounds.) At 800°C, this corrosion rate is between three and four orders of magnitude greater than an extrapolation of the TSPA-VA base-case CRM corrosion rates. Using an acceleration factor of 10^4 for alloy 22 (because of its enhanced corrosion resistance) is therefore consistent with the Wang and Douglass data. Figure 10-28 illustrates the CRM corrosion rates for temperatures from the base case extrapolated to the magmatic-intrusion regime. The gray band at volcanic temperatures represents the increase applied to reflect the hostile environment. The Wang and Douglass data range between the "X's" shown on the plot. In a drift, the amount of magmatic gas that can reach a waste package may be limited by pneumatic or chemical factors; however, for this analysis we assume that the conditions of the Wang and Douglass experiment apply.

Thus, as a TSPA-VA abstraction, we use CRM corrosion rates in the presence of magma and magmatic gases that are 10^4 times as great as corrosion modeled for the TSPA-VA base case.

10.4.2.3.2 Mechanical Disruption

Mechanical disruption can take several forms. Considered for TSPA-VA are: plastic deformation that could result in collapse of the waste-package walls; and internal pressurization, which could lead to a rupture of the walls.

10.4.2.3.2.1 Mechanical Collapse

When superalloys such as alloy 625 or alloy 22 are overheated, their mechanical properties can degrade because the strengthening phases can dissolve in the alloy matrix, or they can undergo incipient melting (Morral 1984, Appendix I, p. 31 ff.). The degraded mechanical properties can cause the waste package to undergo plastic deformation. At elevated temperatures, the weight of the waste-package wall itself may be sufficient to result in plastic deformation and stress rupture of the container. The M&O Waste-Package Design organization has done calculations to estimate the waste-package wall stresses as a function of temperature and wall thickness. The calculations to determine membrane stress and bending stress ($P_m + P_b$) as a function of waste-package wall thickness at 20°C are reported in CRWMS M&O (1996b, Figure 7-8) for alloy 625

(values for alloy 22 are expected to be similar). The critical design stress intensity, S_m , that can cause a crack through the waste-package wall are taken from the ASME Boiler and Pressure-Vessel Code (ASME 1995, Table 2B), as is the temperature dependence for S_m . The Waste-Package Design organization used as their criterion for wall failure that P_m+P_b exceed $1.5*S_m$. This criterion is appropriate for determining when air and moisture can reach the waste form, but a crack is insufficient to allow waste to be mechanically removed from the waste package. Using data from the ASME Boiler and Pressure-Vessel Code Table 2B, the temperature dependence of S_m from 20° to 430°C is extrapolated to magmatic temperatures (1,000°C and above) and to the solidus temperature for alloy 625 (1,290°C). The extrapolation of critical stress has an inflection point where the ultimate tensile strength decreases rapidly (approximately 800°C). Note that we assume the critical stress limit for the material goes to zero at the solidus temperature. The P_m+P_b values for various CRM wall thicknesses are then compared against the $1.5*S_m$ values as a function of temperature. (P_m+P_b values are not expected to change significantly with increasing temperature*). Figure 10-29 shows the critical design stress (shown as 1.5 times the value of S_m listed in the in ASME Boiler and Pressure-Vessel Code Table 2B), in relation to wall stresses for four amounts of wall degradation. Waste packages that have more than 70% CRM wall-thickness reduction as a result of corrosion are assumed to crack at all temperatures. Those that have wall thicknesses of 50% of original can be expected to crack at temperatures above approximately 900°C. The full-thickness waste package wall may crack only at temperatures above 1,200°C.

A better measure of the stresses necessary to rupture a waste package (in contrast to only causing it to crack) is the ultimate tensile strength. This is also shown in Figure 10-29 for various temperatures (data from Morral, 1984, Table 9, p. 29 ff.). These data have also been extrapolated to the solidus temperature of the alloy 625.

For zero CRM wall-thickness reduction, the waste-package wall membrane and bending stresses are sufficiently below the ultimate tensile strength at temperatures below 1,200°C that failure from this mechanism is unlikely. At 50% wall thinning, the ultimate tensile strength, and P_m+P_b are approximately equal above about 1,000°C, so the waste package is likely to rupture. For 70% and greater wall thickness reduction, the waste-package wall stresses are near or above the ultimate tensile strength of the alloy at magmatic temperatures, so rupture is assumed.

As a TSPA-VA abstraction, we assume that, for temperatures above approximately 800°C and CRM wall thickness reduced by 50% or more, the wall stresses exceed the ultimate tensile strength and the waste package will deform sufficiently to rupture.

10.4.2.3.2.2 Internal Pressurization of Waste Packages

Intact waste packages are filled with helium gas at atmospheric pressure (at room temperature). Reactor fuel rods are pressurized with inert gases; as a result of operation in a reactor, fission

* The stress-relieving temperature of Alloy 625 is 870°C, and the annealing temperature is 980°C (ASM 1981, Table 5). Holding the waste package at these temperatures should cause $P_m + P_b$ to decrease. Therefore, it is a conservative assumption to maintain the same stress values for all temperatures.

product gases can also accumulate inside the rods. During exposure to an igneous environment, if the waste package remains intact, the waste-package internal pressure can increase because of the elevated temperatures. The temperatures at which fuel rods burst have been measured (Lorenz et al. 1980). Above approximately 900°C, most fuel rods burst, releasing over 75% of the contained gas into the waste package (Lorenz et al. 1980, Table 49). If a sufficient number of fuel rods vent their gases, the internal pressure in the waste package can increase substantially. Calculations have been made of the internal pressure in a waste package as a function of the number of fuel rods that burst (CRWMS M&O 1997j, Section 7.2.2.7). Table 10-11 gives the pressures (adapted from Table 7.2.2.7-1).

Table 10-11 gives pressures for both 21 PWR and 44 BWR fuel assemblies. Waste packages with PWR fuel generate higher internal pressures, as the table above shows, because they have more fuel rods in each assembly. The right-hand column of Table 10-11 attempts to account for the additional pressure contributed by the fission products inside fuel rods that have undergone high burnup (in the range 54 GWd/MTU). Although the contribution from fission-product gases is not known, a 50% increase in pressure is considered to be bounding (CRWMS M&O 1997j, Section 7.2.2.7). Calculations for Table 10-11 assume ideal gas behavior, meaning that the pressure is treated as being directly proportional to the temperature at constant volume. Using this relationship, the following pressures are calculated for the 21 PWR fuel assemblies with 100% of the rods burst.

Temperature (°C)	100% Rods Burst	100% Rods Burst *1.5
800	0.93 MPa	1.39 MPa
1,000	1.10	1.65
1,100	1.19	1.78

The stress on the waste package from internal pressurization is calculated using standard engineering formulas (e.g., Roark & Young 1975). For the cylindrical body of the waste package, the circumferential and longitudinal stresses are given by the formula (Roark & Young 1975, Table 29, case 1c)

$$\sigma_{circumf} = Pr/t; \quad \sigma_{long} = Pr/2t \quad (10-3)$$

where $\sigma_{circumf}$ is the circumferential stress, σ_{long} is the longitudinal stress, P is the internal pressure, r is the radius of the cylinder, and t is its thickness. For a waste-package inner radius of 0.712 m and a wall thickness of 0.020 m, a characteristic internal pressure of 1 MPa gives a circumferential stress of approximately 36 MPa and a longitudinal stress of 18 MPa. At 1.78 MPa, the circumferential stress is approximately 63 MPa. All these stresses are well below the ultimate tensile strength of the CRM at temperatures less than 1,200°C (see Figure 10-29). If the waste package wall thickness is reduced by half, however, the circumferential stresses double, and approach the ultimate tensile stress at higher temperatures.

The part of the waste package most likely to fail as a result of internal pressurization are the end caps, because they are flat plates fixed at the circumference. The stress on the end caps as a function of internal pressure is calculated using standard engineering formulas (Roark & Young

1975, Table 24, case 10b). The bending moment at the center of a circular plate fixed at the circumference is given by the formula

$$M_c = Pr^2(1 + \nu)/16 \quad (10-4)$$

where M_c is the moment at the center of the plate and ν is Poisson's ratio (equal to 0.278 for alloy 625 or alloy 22). The stress is given by

$$\sigma = 6M_c/t^2 \quad (10-5)$$

For an internal pressure of 1 MPa and an end-cap thickness of 0.025 m, the stress is approximately 392 MPa on each end cap. This is above the ultimate tensile strength of the CRM at temperatures above approximately 850°C. Figure 10-30 shows the end-cap stresses and the ultimate tensile strengths as a function of temperature.

Furthermore, stresses are higher at the circumference of the end-cap where it is welded to the cylindrical waste package. It is likely that the end caps would fail by cracking at temperatures of 800°C and rupture at the higher magmatic temperatures. If the end-cap wall thickness is reduced by corrosion, the stresses increase as the square of the reduction in thickness; at 800°C, an end cap thickness of 0.0125 m results in a stress of over 1,400 MPa. Rupture is assured.

Because of the significant corrosion resistance of the waste-package inner barrier, the walls of the waste package decrease in thickness very slowly. Only late-time intrusion events are expected to cause waste-package rupture necessary to expose the waste to magma or pyroclasts. Based on simulations done for the TSPA-VA base-case analyses, the time for degradation of the inner barrier to a 50% thickness reduction because of low-temperature, aqueous, general-corrosion ranges from about 160,000 years to 995,000 years. For 70% thickness reduction, the times range between 306,000 years and 960,000 years. (Because these results are based on stochastic simulations, the maximum time for the 50% degradation is slightly greater than that for 70% reduction; this is not significant). Figure 10-31 shows the distribution of times to reach these two levels of corrosion. As a conservative estimate, we use the tenth percentile times for 50% and 70% degradation to determine the extent of CRM corrosion at the time the intrusion occurs. We assume that all waste packages are at the same degree of degradation at the time the intrusion occurs.

10.4.2.4 Removal of Waste-Package Contents

There are two potential processes that are being considered as being able to remove waste from a waste package and incorporate it into the eruptive flow — dissolution of waste in liquid magma, and mobilization of particles by an ash/pyroclast stream. Whether the model for incorporation of waste into the eruptive flow is dissolution in liquid magma or suspension in an ash flow can be selected by the fragmentation depth. Uranium dioxide and zirconium dioxide are soluble in silicate melts (i.e., basalt) at temperatures in the range 1,200°C to 1,550°C (Westrich 1982, Figure 3). At 1,200°C, the UO_2 solubility is approximately 20%, increasing to 38% at 1,550°. Experiments done by Westrich (1982, p. 325) show that it requires about 30 minutes for UO_2 to

reach equilibrium solubility. A flowing magma stream of sufficient volume could eventually dissolve all the UO₂ exposed in the stream. This analysis ignores cooling of the magma or ash by contact with the waste packages or drift walls. Any crust or skin of basalt on the waste package could block further contact by the eruptive stream.

An ash flow past a ruptured waste package could possibly entrain loose waste particles and thus incorporate them into the flow. Such a process would depend on the flow velocity, ash size and density, and the waste-particle size and density. Liquid magma flowing through a waste package can dissolve the UO₂ waste. The smallest waste particles (0.01 cm) can be expected to dissolve the most readily. Thus, it is expected that the very smallest waste particles will not retain their identity in an eruptive column.

10.4.2.4.1 Ash-particle size

Ash-particle size varies over several orders of magnitude. Jarzempa & LaPlante (1996, p. 6 ff.) treat the size distribution as log-normal. Jarzempa et al. (1997, Section 4.1) use for their modeling mean that ranges between 0.01 cm and 10 cm, a mode of 1 cm, and a standard deviation ranging between 0.1 and 1.0. Figure 10-32 illustrates particle-size PDFs for two values of mean and sigma.

Ash fragments larger than about 10 cm are not effectively dispersed by wind from an ash column because of their large size, so this value is used as a cutoff for the ASHPLUME analysis.

10.4.2.4.2 Waste-particle size

Uranium dioxide reactor-fuel pellets are originally about 1 cm in diameter. After irradiation and handling, they can crack into smaller pieces. Jarzempa & LaPlante (1996, Figure 4) use a log-triangular distribution for waste-particle size, as shown in Figure 10-33. For their modeling they use a mean particle size of approximately 0.1 cm, with a range of 0.01 cm to 1 cm. Ayer et al. (1988, Figures 4.12 and 4.13), and Robertson (1969, Figure 3.2) have studied characteristics of irradiated fuel and show particle sizes consistent with those used in the model.

10.4.2.4.3 Elastic-particle interactions

Waste particles have an average density of approximately 11 g/cm³ (Jarzempa & LaPlante 1996, p. 10), and ash particles have a density range of 0.8 to 2.5 g/cm³ (Jarzempa et al. 1997, Section 4.1), with a mean of 1.5 g/cm³. If the ash flow is composed of solids, then an elastic collision between an ash particle and a waste particle can accelerate the waste to the speed of the ash flow if certain size relationships between the ash and waste obtain.

We invoke conservation of momentum: $M_p V_p = M_w V_w$, where the subscripts p and w are for the ash and waste particles, respectively. Initially, V_w is zero; after the collision, V_p is assumed to be zero. If we assume $V_p \approx V_w$, then $M_p \approx M_w$. Assuming spherical particles, the mass is given by $\frac{4}{3} \pi r^3 \rho$. Thus, $r_w = \sqrt[3]{\frac{\rho_p}{\rho_w}} r_p$. Using the mean value for the ash density, we get $r_w = 0.515 r_p$.

Thus, all waste particles smaller than approximately one-half the size of the impacting ash can be accelerated from the waste package by elastic collisions.

10.4.2.4.4 Inelastic-particle interactions

Alternatively, if the ash flow contains liquid or pyroclastic material, then the waste particle could undergo an inelastic collision and adhere to the moving material, and thus be removed from the waste package. When the waste particle sticks to an ash particle, the combined particle is heavier, and conservation of momentum requires that it move more slowly than the magma flow. At some point the velocity of the combined particle will be sufficiently slower than the magma flow velocity so that the particles will not be removed from the package.

In this case, $M_p V_p = (M_p + M_w) V_{(p+w)}$. Now, $V_{(p+w)} < V_p$, with the decrease in velocity given by the ratio of ash particle mass to combined mass. If we invoke simple particle kinematics, we can calculate the minimum velocity of the combined particle below which it will not travel beyond the radius of the waste package (0.83 m) when traveling at an initial 45° trajectory (the angle that results in maximum horizontal range). This velocity is 200 cm/sec vertically. Table 10-12 provides the fractional horizontal or vertical velocities of agglomerated particles consisting of ash of densities 1.5 or 2.65 g/cm³ and a waste particle of density 11 g/cm³. Fractional velocities are the fraction of the velocity of the incident particle that is transferred to the agglomerated particle.

For waste particles much smaller than the ash particles to which they adhere, the velocity of the agglomerated particles is essentially unchanged. If the waste particle is ten times the size of the ash, the agglomerated particles move at about 10^{-4} the speed of the ash flow; there are no ascent velocities assumed in this analysis that are high enough to allow this particle combination to escape the waste package (see Section 10.4.2.1.7). For magma velocities greater than about 10 m/s, waste particles of size ranging from half to the same size as the magma particle size will escape the waste package as agglomerated particles.

As an abstraction for TSPA-VA, we use the PDFs for particle sizes and ash velocities to determine the fractions of particles that can be ejected from waste packages by the two types of collisions. It is required that the waste particle be no larger than half the diameter of the ash particle to be ejected from the waste package by elastic collisions, and no larger than the diameter of the magma particle for inelastic collisions.

10.4.2.5 Incorporation of Waste into Eruptive Flow

Uranium dioxide is soluble in liquid basalt (Westrich 1982, p. 324 and Figure 3). At equilibrium, between 20 and 40 wt. % UO₂ can be incorporated into the magma. (It should be noted that experiments have been done only with liquid basalt – not true magma; the latter contains gases that could increase the reactivity of the magma, and thus the solubility of the UO₂. (Because of our lack of knowledge, we ignore the potential enhanced UO₂ solubility.) As a simplifying assumption for the TSPA-VA analyses, we assume that other radionuclides congruently dissolve in the magma. UO₂ is the major component of spent-fuel waste, so its

behavior determines most of the incorporation of waste into the magma. Dissolved waste will be rheologically indistinguishable from the balance of the flowing magma. Only if waste particles are transported in the eruptive flow will their potentially different rheological behavior become important.

10.4.2.5.1 Settling velocities

Carmichael et al. (1977, eq. 58) provide a discussion of the settling velocity of xenolithic materials in ascending liquid magmas. The settling velocity, v_s , is given by

$$v_s = \sqrt{\frac{4D_w(\rho_w - \rho_L)g}{3C_d\rho_L}} \quad (10-6)$$

where D_w is the diameter of the waste particle, ρ_w and ρ_L are the densities of the waste and magma, respectively; g is the acceleration of gravity; and C_d is a drag coefficient, given by the Reynolds number, R_e : $C_d = 18.0R_e^{-0.6}$. Although the Reynolds number for this problem is not known, v_s is not particularly sensitive to its value. A value of 15 was used, based on the density and viscosity of an alkali basalt (MacDonald 1949).

Using their formulas, a spherical waste particle of density 11 g/cm³ in an ascending magma flow will have the following settling velocities, as shown in Table 10-13.

If the settling velocity is less than the velocity of the ascending magma, the particle will be carried in the magma flow to the surface. It can be seen from the table that for waste particles less than 5 cm in diameter, the settling velocities are no greater than 1 m/s. Therefore, these particles would be advected by rising magma moving at least 1 m/s. The 10-cm particles and larger would require faster magma velocities to keep from settling. The magma density of 2.65 g/cm³ represents liquid magma, while the 1.5 g/cm³ density is used for ash flows. The above table indicates that almost all waste particles can be advected by magma flows with velocity ranges of 1–10 m/s.

Using densities of 11 g/cm³ for waste and 1.5 g/cm³ – 2.65 g/cm³ for ash, an agglomerated particle that formed a prolate spheroid from two equal-diameter particles would have a density ranging from 6.2 g/cm³ to 6.8 g/cm³. Using the formula discussed above, agglomerated particles with these densities would have settling velocities shown in Table 10-14.

It can be seen from the table that, for agglomerated particles whose total size is less than 5 cm in diameter, the settling velocities are much less than 1 m/s. Therefore, these particles would be advected by rising ash flows moving at least 1 m/s. The 10-cm and larger particles would require faster ascent velocities to keep from settling. Because ash-ascent velocities are much greater than 10 m/s, essentially all agglomerated particles can be advected by ash flows.

As an abstraction for TSPA-VA, we assume that, for the fraction of waste particles ejected from a waste package by elastic or inelastic collisions, if the ascent velocity exceeds 10 m/s, those particles will be entrained.

10.4.2.6 Xenolith Fraction

As a check, we can compare the amount of waste entrained in an eruption with observed xenolith fraction data from analog volcanic sites. Xenoliths are rock fragments from the magma conduit that have been carried to the surface with the ascending magma. They can be identified as coming from specific strata along the path of the flow. Valentine et al. (1998, p. 5-9) has provided volume fractions of xenoliths for various formations at the Lucero volcanic fields. Volume fractions per meter of formation depth range from 3×10^{-7} to 2×10^{-4} . To further convert these numbers to values relevant to entrainment of a single waste package, we must include the fraction of dike length represented by a waste package. Valentine et al. (1998, p. 5-12) indicates that dikes at the Lucero field are about 2 km long, so a single waste package has a length about 0.001 of the dike length. The xenolith volume fraction attributable to a single waste package (3×10^{-10} to 2×10^{-7}) can be applied to the total erupted volume assumed for the direct-release analyses to compare against the amount of waste calculated from the above four processes (i.e., number of packages hit, package breach, waste ejection, and waste entrainment).

10.4.2.7 ASHPLUME Inputs and Analysis

The ASHPLUME code uses as input eruption characteristics, such as event duration, column height, initial eruption velocity, eruption power, and mass of erupted material (Jarzemba et al. 1997, Section 4.1). It also requires parameters to model dispersion, such as wind speed, wind direction, air density and viscosity, ash-particle shape factor, and eddy-diffusivity constant. Additionally, it requires the amount of waste incorporated in the eruption, ash-particle size characteristics, waste-particle size characteristics, the incorporation ratio for waste into the ash flow, and maximum ash particle size that can be transported. The program can be run either deterministically or stochastically; in the latter case, the inputs are ranges or PDFs, and the program samples from these for each calculation. For these analyses, the program was run deterministically, because as the radionuclide source term was calculated according to the methods described here, the other ASHPLUME parameters were also stochastically chosen.

Examination of analog data for eruptive-center parameters indicates some correlations among the eruptive volume, the eruption duration, and the plume height (Section 10.4.2.1.2). From these data an approach has been developed for defining the characteristics of possible future eruptions in the Yucca Mountain region. The very limited analog data (9 events, Table 10-6) show no statistical correlation between height of plume, H , and duration, T , or between H and volume, V . There is a nearly statistically significant correlation between $\ln(T)$ and $\ln(V)$, as one might expect (the larger the volume, the longer the time required to erupt the ash). There is a statistically significant correlation between $\ln(H)$ and the volume rate, $\ln(V/T)$, (analogous to H related to mass flux, \dot{Q} —Equation 4-3 in ASHPLUME).

In the TSPA-VA scenarios, total volume (the amount of melt ascending from the mantle) is treated as an independent variable. The historically active analog volcanoes summarized in Table 10-6 are comparable in scale to the Quaternary basaltic volcanoes in the Yucca Mountain region (Jarzemba et al. 1997, Section 4.2.1.1). Based on the analog data summarized in the table above, we use a log-uniform distribution ranging from ~ 0.01 to 1.0 km^3 with a median volume

of 0.1 km³. The median value is comparable to the total magmatic volume estimated for the Lathrop Wells center, which is estimated to be 0.08 km³ (G. Valentine and F. Perry, LANL, Minutes of Meeting on volcanic disturbed scenarios, March 1998. Accession number MOL.19980715.0398). This distribution encompasses the estimates of the total magmatic volume for Quaternary Yucca Mountain Region volcanoes, which, after correcting for erosion, range from 0.001 km³ (Northern Cone) to 0.2 km³ (Quaternary Crater Flat) (Jarzempa et al. 1997, Section 4.2.1.1), and also allows for multi-cone events that were included in the PVHA models. The parameters shown below are expressed as log-10 values of volume.

Parameter	Minimum	Maximum	Distribution Type
Eruption Volume	-2 km ³	0 km ³	log-uniform

As a TSPA-VA abstraction, we assume conservatively that the total erupted magma volume is in tephra blankets. For strombolian events, the ratio of tephra blanket to cone volumes can range from 0 to 13:1 (Self 1976, Section 3). The magmatic volume is converted to total ash mass using an average density of 1.1 gm/cm³ for tephra (Jarzempa et al. 1997, Section 4.1).

As noted above, a weak correlation exists between total ash volume and duration. We use this correlation and its uncertainty to select a duration:

$$\ln(T) = 15.29 + 0.527 \ln(V), \sigma_{\ln(T)} = 1.34, V \text{ in km}^3, T \text{ in seconds.} \quad (10-7)$$

This relationship gives eruption durations ranging from 1.5×10^6 to 4.4×10^6 seconds (17 to 50 days). Then, H is given by the expression:

$$\ln(H) = 7.83 + 0.394 \ln(V/T), H \text{ in km.} \quad (10-8)$$

The eruption power is also an input to ASHPLUME. The eruptive power is sampled from a log-uniform distribution.

Parameter	Minimum	Maximum	Distribution Type
Eruption Power	9.41 W	11.55 W	log-uniform

Distributions for wind speed and direction have been compiled by Jarzempa et al. (1997, Table 4-2) from site observations. Data for wind characteristics at Yucca Mountain are shown in Figure 10-34.

10.4.2.7.1 Modifications to the ASHPLUME code

The ASHPLUME code has the capability of performing both deterministic and stochastic calculations (Jarzempa et al. 1997, Section 2.3). For the latter calculations, several of the parameters discussed above are randomly selected for each stochastic run. Because the radionuclide source term for dispersal by ASHPLUME was calculated stochastically, the code

was modified to allow parameters normally selected stochastically by the code to be entered in deterministic runs. These modifications maintained the correlations required by the stochastic treatment of the source term.

Parameters are supplied to ASHPLUME through the file *ashplume.in*. In deterministic ASHPLUME simulations, the code prompts the user to enter most parameters directly via the keyboard, and the code obtains the remaining parameters from the *ashplume.in* file. Some of the parameters in the *ashplume.in* file are not needed in deterministic simulations and are therefore ignored. The *ashplume.in* file is required for both stochastic and deterministic simulations, but it plays a much more important role in stochastic simulations. A sample file is shown in Table 10-15. The actual file has been annotated with line numbers to the left and indicators to the right of each line to show how the information is used.

The annotation "S" indicates that the value is used in both stochastic and deterministic simulations. Parameters with a "D" are overridden by keyboard input for deterministic runs. Where minima and maxima are indicated for the parameters, the stochastic process samples from the range provided. The notation "D" indicates that the value read from *ashplume.in* is overridden by keyboard entry for deterministic runs. The notation "M" indicates that the use of the parameter by the code has been modified from the original version (Version 1.0).

The first line identifies the simulation and the date on which it was performed. The next four lines (lines 2 through 5) provide the code with the information needed to establish the grid for the simulation. The grid determines where the code will calculate ash and contaminant results. Lines 2-5 include minimum and maximum x and y locations in kilometers and the total number of evenly-spaced points between the minimum and maximum locations on both axes. The minimum and maximum locations are included in the total number of points. This setup for the grid means that the code does not have a great deal of flexibility in the grid used, or in allowing more detail in a desired area such as around the vent. To obtain "irregular" grid coverage or more detail in a particular area, multiple simulations must be performed (changing only the grid and leaving all other input parameters the same). Note that the code does not calculate results at the vent (location $x = 0$ km, $y = 0$ km).

In ASHPLUME Version 1.0, line 6 is designed to accept minimum and maximum values of the eruption duration in seconds. In the version of the code used for these analyses (Version 1.3), the code has been modified to accept the minimum and maximum values of eruption volume in km^3 . As is discussed in Section 10.4.2.7, eruption volume is used as the variable determining other eruption parameters (in place of time used in Version 1.0). This information is entered manually in deterministic runs.

Lines 7 through 12 are used in stochastic runs and are entered manually in deterministic simulations. Line 7 provides the minimum and maximum values for eruption power. Line 8 is used for the minimum and maximum values of log beta, a constant controlling ash dispersion. Line 9 gives the minimum, mean, and maximum values of the log diameter of ash particles. Line 10 provides the minimum and maximum values of the standard deviation of the ash particle diameter. Line 11 is for minimum and maximum ash density values. Line 12 gives the minimum and maximum values of log diameter of ash particles for density calculations.

Lines 13 through 19 are used in both deterministic and stochastic runs. Line 13 contains the value of the particle shape factor, *fshape*. For elliptically shaped particles with principal axes *a*, *b*, and *c*, the shape factor is given by $(b+c)/2a$ with axis *a* the major axis. Line 14 gives air density in g/cm^3 and air viscosity in $g/cm\cdot s$. Line 15 is a constant relating eddy diffusivity to particle fall time. Line 16 is the maximum particle diameter for transport. Line 17 gives the minimum, mean, and maximum fuel-particle log-diameters. Line 18 gives the minimum height of the eruption column considered during transport (in km). Line 19 is the threshold limit on ash accumulation. Ash accumulations lower than this limit are truncated to zero. Parameters on lines 20 and 21 are provided from the keyboard in deterministic simulations. Line 20 is the incorporation ratio, RHOCUT. Line 21 is the total mass of contaminant included in the eruption.

10.4.2.8 Development of Direct-Release Modeling Analysis Parameters

As has been developed in the previous sections, in order for there to be a surface release of radionuclides, the following events must all occur

- A dike must intrude the repository
- A vent on the dike must be located within the repository
- The waste package must be breached
- Waste must be removed from the waste package
- Waste must be entrained in the eruption to the surface.

If all the above criteria are met, we have simulated a radionuclide source term for which the ASHPLUME code can model the dispersion.

Parameters were randomly sampled from the CDFs; stratified sampling was not used. Correlations among parameters were maintained. A total of 300 realizations were calculated. Of those, 17 produced surface releases whose dispersal was simulated using the ASHPLUME code. Tables 10-16a through 10-16i list some of the realizations to illustrate the development of radionuclide source terms for the direct-release scenario. Table 10-16a illustrates simulations of dike intrusions. Given a dike orientation and length inside the repository (drawn from CDFs shown in Figure 10-18, a point along the western repository boundary as the origin of the dike was randomly selected. Because drifts run east-west, the number of drifts crossed by the dike is determined from the north-south component of the dike length. There is a small probability that the dike trends to the northwest; in this case it does not intersect the repository, so the number of drifts crossed is zero. In realization 33, the dike length inside the repository is zero, so no drifts are crossed in this case either. Number of eruptive vents occurring inside the repository boundary was sampled from the PDF shown in Figure 10-20. Realizations 9, 10, 34, 57, 58, and 59 do not have any vents inside the repository in this example, cannot contribute to an eruptive source term, and are not considered further. They can, however, contribute to the enhanced source term for groundwater flow. Realization 33 has zero length inside the repository, so no drifts are crossed. However the vent is modeled as occurring right at the repository boundary, so it is counted as being inside the repository.

Fragmentation depth was drawn from the distribution given in Section 10.4.2.1.5. The location of the fragmentation depth relative to the repository depth determines whether the intrusion is considered to be liquid magma or ash/pyroclasts. A cutoff depth of 300 m was used, because this is the approximate distance of the repository below the surface. Table 10-16b shows these parameters for selected realizations.

The formulas given in Section 10.4.2.2 are used to calculate the numbers of packages hit by dike or ash intrusions. Table 10-16c illustrates the calculations.

For realization 13, the angle of the dike (62.5°) and its width result in its hitting two packages per drift. Mostly, because of the relatively narrow dike widths, only one package is hit per drift. Total Packages Hit is the number per drift times the number of drifts crossed.

Table 10-16d shows the same information for ash intrusions interacting with drifts.

Total packages hit in Table 10-16d is calculated from the conduit diameter and its random location relative to the drifts. The Release Source is the total number of packages contributing, and is the product of Total Packages Hit and the number of vents in the repository. In realizations 8, 14, and 60, two vents occur inside the repository, so the Release Sources are double the number of packages hit in each instance. In realization 80, the conduit diameter is quite small, and it did not intersect a drift. Thus, no packages were hit, and the Release Source is zero.

To simulate waste-package breach, an eruption time between approximately 2,600 years and 1,000,000 years was randomly selected. The early time is the shortest period for which TSPA-VA base-case simulations of CRM corrosion showed that there was no waste-package wall thinning. From Section 10.4.2.3.1, we know that the corrosion rate of the CRM is so slow that attack for only the duration of an eruption is insufficient to breach the waste package. It requires sufficiently long times, during which the CRM is corroding under ambient conditions, before the magmatic environment can thin the waste-package wall to less than 50% of its original thickness. As Figure 10-17 shows, the waste package will collapse at magmatic temperatures for walls thinned by 50% or more. Table 10-16e illustrates several examples of this aspect of the simulation.

The eruption durations in the above examples range from less than 17 days to about 50 days. During that time, the CRM corrosion attributable to the volcanic environment is about 0.001 to 0.002 of the wall thickness. The relatively early times of occurrence of the igneous intrusions for realizations 14 and 27 do not permit significant CRM corrosion to occur. Consequently, there is no waste-package breach and these realizations cannot contribute to the source term.

Removal of waste from the containers requires the proper size relationship between waste and magmatic particles and sufficient ascent velocity. The ascent velocity of liquid magma, as modeled here, is insufficient to remove any waste; only ash flows will do so. Ash particle-sizes were selected from a size distribution bounded by the PDFs shown in Figure 10-32. Waste-particle sizes were selected from the PDF given in Figure 10-33. Ash density was randomly selected from the range $[0.8, 2.5 \text{ g/cm}^3]$. If the selected waste particle is less than half the size of the ash particle, elastic removal of the waste is assumed, and RHOCUT is set to 0.3 for the

ASHPLUME modeling. If the sizes are equal, inelastic collisions are assumed, and RHOCUT is set to 0.0. For waste larger than the corresponding ash particle, no ejection occurs. Table 10-16f illustrates this portion of the simulation.

Realizations 3 and 11 are for liquid-magma dikes, and the slow ascent velocity of the magma results in no particles being ejected from the waste package. In realization 26, the waste particle is larger than the ash particle, so ejection also does not occur. In the remaining examples, roughly half experience inelastic collisions. The simulations show that roughly half the time the ash/waste particle-size relationship is correct for particles to be ejected.

Entrainment occurs if the ascending magma or ash is moving fast enough to overcome the settling of the dense waste particles in the upward flow. As Section 10.4.2.4 discusses, waste particles are removed by elastic collisions if they are less than half the diameter of the impinging ash particle. They are removed by inelastic collisions (agglomeration of waste and ash or magma) if the waste is no bigger than the impinging particle. Figure 10-33 shows that the most likely waste-particle size is about 0.1 cm, while the most likely ash particle size ranges from 0.01 to 1 cm. Table 10-16g illustrates this portion of the simulation.

In realizations 35 through 67, the agglomerated particle density is less than the ash density, so the settling velocity for these cases is considered zero.

The amount of radionuclides available to be dispersed is given by the amount of waste entrained from a single waste package times the number of waste packages hit. Some examples are given in Table 10-16h.

One commercial spent nuclear fuel (CSNF) waste package contains about 8.2×10^6 g of radionuclides, so the amounts of waste released in these realizations range from about 1/2 waste-packages' worth to over 13.

Simulation of parameters for the ASHPLUME code is shown in Table 10-16i. These are calculated from the relationships discussed in Section 10.4.2.7. The eruption volume is randomly selected from the log-uniform distribution, and the eruption duration and column height are then calculated according to the relationships provided. Dispersion of ash is controlled by wind speed and direction. Wind speed is randomly sampled from an exponential distribution based on an average wind speed (Jarzemba et al. 1997, eq. 4-1). Wind speed and direction have been sampled and included in Table 10-16i.

Realizations 35 and 84 should have minimal impact on dose receptors located in the Amargosa Valley to the south of the potential repository. Clearly, if dose receptors are considered elsewhere, such as Jackass Flats, then contamination blowing in directions other than south become important.

10.4.2.9 Direct-Release Modeling Results

Three hundred simulations of igneous intrusions were run. As discussed above, seventeen realizations resulted in eruptive releases of waste. A summary of how each stage of the

modeling affected the source term is given in Table 10-17. The table reports the percentage of realizations that were eliminated by the processes considered.

The final percentage of realizations remaining (5%) in Table 10-17 is consistent with the 5.7% of the simulations that were calculated. The features/processes that contribute the most to source-term reduction are the number of vents that occur inside the repository (60% of the time it is zero), and the waste-particle removal and entrainment processes. If we assume that all waste packages are breached when they come in contact with magma or pyroclasts (i.e., the percent eliminated by the "Waste-Package Breach/insufficient time" entry above is zero), then the final percentage that fail in the above table increases from 5% to 6%. Because some packages would fail earlier than has been modeled in this analysis, the doses may increase more than the increase in failed packages because of higher radionuclide inventories.

The seventeen realizations used in the ASHPLUME simulations and the areal waste concentrations at a dose receptor point 20 km due south of the eruption are given in Table 10-18. This point, located in the Amargosa Valley, has been chosen so as to describe the reference individual for dose determinations. Details are provided in the TSPA-VA document, Section 3.8. In cases where the wind is not blowing toward the south, concentrations are very small at the dose receptor point. The largest waste concentration (4.914×10^{-11} g/cm²) occurs for a wind blowing due south and an eruption that entrains 23 waste packages. The importance of wind direction and velocity on concentration at a specific point can be seen from the tiny concentrations for winds blowing away from the receptor point (e.g., compass headings N, NE, NNE).

Example concentration maps are shown in Figures 10-35 through 10-37. Figure 10-35 shows the realization that produced the highest areal concentration at the dose receptor point. Figure 10-36 shows the realization that had the greatest mass of waste erupted, and Figure 10-37 shows the realization where the wind blew most strongly away from the dose receptor point. Figure 10-36 shows that instances where we have low concentrations at the dose receptor point we also have relatively low concentrations elsewhere in the Yucca Mountain region.

10.4.2.10 Dose Calculations

Doses are calculated by using the ORIGEN2 database (DOE 1992) to determine the radionuclide inventory for the 39 radionuclides of interest at the time of the eruption. Biosphere dose-conversion factors (BDCFs) are then applied to the concentrations of each radionuclide present at the dose-receptor point and summed to give the total dose. Biosphere Volcanic Scenario 2, the dose exposure resulting from agricultural use of land contaminated with radioactive ash, is used for the analyses. This scenario is discussed in Section 9.5.5 of this document.

10.4.2.10.1 Inventory Calculations

The radionuclide inventory is estimated using the Characteristics Database (CDB) System LWR PC Database (DOE 1992). This program contains information generated by ORIGEN2 on the radiological characteristics of spent nuclear fuel from commercial light-water reactors. This information includes radioactive totals, elemental compositions, and individual isotopes for

different burnups, initial enrichments, and decay times. The CDB can provide this information for many burnup values in PWR or BWR reactors for 23 decay times, ranging from 1 year to 1,000,000 years.

The CDB is used to calculate the quantity (in grams) of each of the 39 radionuclides of interest at the decay times most closely corresponding to the times of occurrence of the eruptions using PWR fuel with 33,000 MWd/MTU burnup and standard initial enrichment of 3.3%. To estimate the quantity of each of the 39 radionuclides present at the times of the 17 realizations (which range from 387,644 years to 875,269 years), inventories for each of the 23 decay times were calculated. The inventories were then fit using a regression formula. In some cases, the curve fit is an exponential that approximates simple radioactive decay. Figure 10-38 illustrates this for Se-79.

The data points in Figure 10-38 show the inventory values from the CDB, and the curve is the regression fit to the data. The fitting equation is then used to estimate the inventory of Se-79 at the time of each realization.

Other radionuclides exhibit more complicated behavior as a result of ingrowth from radiological parent nuclei. Figure 10-39 illustrates this for Pb-210, whose parents are Po-210 and Tl-210. The inventory of Pb-210 increases for about 200,000 years as the parent nuclei decay away. After that, its inventory decreases. Because the times of the 17 realizations are all greater than 200,000 years, this part of the curve is fit with an exponential that permits estimation of the inventory at specific times.

Once the quantities of the 39 radionuclides are found, the areal concentrations of each nuclide at the receptor point are calculated from the ASHPLUME output. These concentrations allow a calculation of dose through the application of BDCFs.

The BDCFs incorporate both the biological effects of radiation and the pathways through which the radiation reaches the receptor. Pathways include inhalation, ingestion, resuspension, submersion, and groundshine. BDCF values are developed using the GENII-S computer code (Leigh et al. 1993). GENII-S is a stochastic version of the code GENII (Napier et al. 1988); for a discussion of the two codes, see Section 9.2.2.1. The same stochastic modeling approach used for the other modeling components of the TSPA is adopted for the biosphere modeling. The specific representations of the GENII-S input parameters are provided with discussion, in Section 9.2.3 of this document. Many of the parameters required in order to model the volcanic scenario for the biosphere are represented by variables. The expected distributions of the BDCF are generated by randomly sampling from these distributions (using a Latin Hypercube approach to improve computational efficiency) and running multiple realizations of the predictive code.

The information needed to specify the required BDCF distribution is provided by data generated through 125 realizations of the GENII-S code. The mean value and standard deviation are calculated for each distribution along with the 5th, 50th, and 95th percentiles of the distribution. As described in volcanic dose scenario 2 (Section 9.5.5), the receptor is assumed to be exposed to radionuclides in the environment for a 1-year period and the BDCFs represent the 50-year committed doses resulting from this exposure. The 95th percentile BDCF represents the

maximally exposed individual. The BDCFs used for this analysis are given in Table 9-22 of this document.

10.4.2.10.2 Million-Year dose results

Figure 10-40 shows the conditional complementary cumulative distribution function (CCDF) for peak individual dose rates over 1,000,000 years. In calculating the conditional probability, the CCDF includes the simulations where there were no eruptive releases.

Figure 10-41 compares the peak individual dose rates from volcanic eruptions over 1,000,000 years with the peak dose rates from the TSPA-VA base case (see Chapter 11 of this document for a discussion of the base-case dose calculations). As is shown in Figure 10-17, the probability of occurrence of igneous activity in the Yucca Mountain area is estimated in the PVHA document as a range with a mean value of 1.5×10^{-8} and a maximum value of approximately 10^{-7} per year. For the peak dose rate from volcanic eruptions, we use the maximum probability of occurrence over 10^6 years, which gives a factor of 10^{-1} to be applied to the conditional CCDF. Using the mean probability, the factor is 0.015. The results are shown in Figure 10-41.

10.4.2.11 Comparison with Other Analyses

The ASHPLUME code has been used by Jarzempa and LaPlante to model radionuclide releases and doses at the Yucca Mountain area (Jarzempa and LaPlante 1997). Their application of the ASHPLUME code is substantially the same as has been done in the TSPA-VA analyses although the intent of their analysis could be interpreted as being different from that for the TSPA-VA.

- Jarzempa and LaPlante considered only the consequences of volcanic eruptions. They modeled 1,000 releases and developed dose-rate statistics. The TSPA-VA analysis incorporated the probabilities of volcanic activity and the entrainment mechanisms. The difference is that the TSPA-VA work produced many fewer releases.
- Jarzempa and LaPlante assumed that the entire contents of one waste package (10^7 grams) were entrained in the ash plume for each eruption modeled (Jarzempa and LaPlante 1997, Section 2.7). This work used a variable amount of waste entrained—ranging from 4×10^6 to 1.7×10^8 g.
- Jarzempa and LaPlante assumed that entrainment could occur at any time in the history of the repository. Many of their eruptions occur at relatively early times when radionuclide inventories are larger than at later times. Modeling assumptions for this work cause eruptions to occur at later times (after approximately 385,000 years).
- The dose conversion factors (DCFs) used by Jarzempa and LaPlante (1997, Table 7) for the greatest contributors to dose rates range between two and four times larger than the BDCFs used in the TSPA-VA analysis.

Considering all the differences between the modeling approaches, it would require approximately 2,000,000 realizations using the TSPA-VA approach to produce the 1,000 results of Jarzempa and LaPlante.

The 17 releases from the TSPA-VA work give the descriptive statistics shown in Table 10-19. The arithmetic mean of the 17 samples is selected as the best measure of central tendency and as a way of discounting the very low values of dubious physical meaning. Calculated skewness of the seventeen samples is positive suggesting that the distribution of dose rates is skewed right.

Because of the positive skew, the fact that dose rate must be greater than or equal to zero, and the fact that dose rate can obtain a value much higher than any of the simulated values, it is not unreasonable to believe that the distribution of dose rates may be log-normal. The log-normal distribution is defined by two parameters, the expected value or mean, and the standard deviation. With the limited information available, it is not unreasonable to believe that the central tendency of the distribution is on the order of the sample mean and the standard deviation is on the order of the sample standard deviation.

A log-normal distribution of dose rates can be simulated using the sample mean and standard deviation. Simulating 10,000 releases, the probability that the total dose rate is greater than 1.4×10^{-2} mrem/year is 0.1 percent. Although precise statistics for the comparable Jarzempa and LaPlante results are not available, it is estimated that their work shows an approximate 9 percent probability of having dose rates exceed the 1.4×10^{-2} mrem/year value (Jarzempa and LaPlante 1997, Figure A-8).

10.4.3 Enhanced Source Term

An igneous intrusion that passes near waste packages can accelerate their degradation even if it does not make direct contact. Higher temperatures and hostile volatiles from the nearby intrusion can result in premature failure of the waste package. Alternatively, if lateral flow at the repository horizon, the waste packages can come in direct contact with magma that does not continue to the surface. After the waste packages are breached, the contents could mix with magma or pyroclasts, or become mobilized by the elevated temperature. This could result in radionuclides being more accessible to any groundwater that eventually flows through the repository drifts. The PVHA study can be used to provide likelihoods that a dike ascends to a shallow depth without reaching the surface.

Many of the processes discussed in the previous section can be generalized to describe the enhanced source term. The main difference from the direct-surface-release case is that waste does not need to be physically removed from the container to become available for groundwater transport. The processes to consider are:

Plumbing of Intrusion

- Intrusion dimensions
 - Orientation, width, length.
- Nature of intrusion (relative likelihoods)
 - Dike, sill

- Layout of emplacement drifts
- Waste package orientation, pitch.

Waste-Package Breach

- Corrosion/Oxidation
 - Hostile magmatic components present
 - Thinning rate as function of temperature
 - Corrosion reactions with waste-package materials
 - Variable initial thickness of waste package
- Slump/Collapse
 - Plastic deformation of waste-package wall
 - Variable initial thickness of waste package
 - Additional static loads
 - Internal pressurization
 - Freezing of magma on waste package/insulation.
- Melting/Dissolution
 - Iron solubility in magma
 - Temperature of magma/melting points of waste-package materials.
- Abrasion
 - Abrasion rate as function of temperature, flow
 - Mechanical properties of pyroclastics/ash
 - Variable initial thickness of waste package.

Mobilization of Contents

- Thermal Effects
 - Volatilization.
- Dissolution
 - Solubility of UO_2 in magma
 - Solubility of other radionuclides in magma.

10.4.3.1 Plumbing of Intrusion

We consider those packages within the range of effects of the elevated temperature and the hostile volatiles from an intruding dike. In addition to those packages damaged by a dike but not entrained, lateral flow along a drift could affect many waste packages. One of the products of the PVHA studies is the assessment of the likelihood of a dike ascending to shallow depths but not extending to the surface (CRWMS M&O 1996a, Section 3.2.1, as summarized in Table 10-5 of this TSPA-VA Technical Basis Document). Such a dike could flow laterally in the repository works.

As an abstraction for TSPA-VA, we assume that the greatest impact occurs if magma flows laterally into an emplacement drift. This is evaluated by determining the numbers of packages that could be contacted by magma for various dike-drift intersections.

10.4.3.2 Number of Waste Packages Hit

The extent of lateral flow by an intrusion along an emplacement drift is a random distance that can be affected by many variables, such as the speed of chilling of the dike, magma temperature, magma viscosity, or mechanical barriers in the drift, and is not estimated here. Lacking further knowledge regarding the extent of lateral flow, as a TSPA-VA abstraction we assume that the two packages adjacent to the intrusion are contacted by the magma.

10.4.3.3 Waste-Package Breach

The same analysis discussed in Section 10.4.2.3 for waste-package breach applies for this scenario. Waste packages can undergo accelerated corrosion and plastic deformation leading to breach. Additionally, magma can form a skin around a portion of the packages that may "heat soak" them. The time that waste packages would be exposed to a heat soak can be estimated from an analytical thermal-conductivity calculation (Carslaw & Jaeger 1986, p. 258, eq. 1) for the decay of heat from a thermal pulse. Assuming a one-dimensional, semi-infinite medium, the temperatures at points corresponding to the waste-package wall and the drift rock wall have been calculated for thermal pulses that represent the drift being filled 25%, 50% and 75% with magma. Although the igneous intrusion is at quite high temperatures relative to the surrounding rock, it does not have a great amount of thermal mass. Thus, it cools fairly quickly, as illustrated in Figure 10-42. The figure shows the temperatures at the waste package (Figure 10-42a) and drift (Figure 10-42b) walls attributable to an 800°C magmatic intrusion. For all amounts of magma filling the drift, the rock wall has essentially returned to ambient temperature after ten years, and the waste package cools to ambient soon thereafter. The temperatures at the waste package are about 30% hotter than corresponding drift-wall temperatures.

Figure 10-43 puts the temperature excursion from an intrusion into the context of the normal drift-temperature profile. The plot assumes that the drift fills with magma to 50% depth at 10,000 years. The ten-year temperature spike does not significantly alter the long-term temperature profile. Data are for the waste-package wall under long-term-average climate conditions.

Waste packages exposed to several years of high temperatures with the loads imposed by being engulfed in magma would quite likely fail as a result of wall collapse or end-cap blowout. Figure 10-44 shows the stress-rupture and ultimate tensile-strength behavior of alloy 625 (the alloy used as a surrogate for alloy 22) as a function of temperature and time.

The data in Figure 10-44 are for 100-hour and 1,000-hour exposures at temperatures ranging from 650 to 870 °C Morral (1984, Table 10, p. 33). Ultimate tensile strength data are from Morral (1984, Table 9), and the critical stresses are from CRWMS M&O (1996b, Figure 7-8). Figure 10-42a shows that the waste-package wall temperature after 0.1 year (approximately 875 hours) has decreased from the magmatic-temperature region (700° to 900°, recognizing the cooling of the magma caused by the heat capacity of the waste package) to approximately 200°C. As a TSPA-VA abstraction, we assume that the time at high temperature is sufficient to cause stress rupture and collapse of the inner barrier of the waste package.

Gases that evolved from the magma as it entered the drifts can be captured by the rock in the drift and the drift walls. These gases can later react with groundwater when it enters the drift, creating a chemical environment considerably different from the ambient. The persistent elevated temperature and associated aggressive gases can further enhance waste-package degradation compared with that modeled in Section 10.4.2.3.2. As a TSPA-VA abstraction, one assumes the accelerated corrosion and deformation result in breach of all waste packages that are engulfed by magma. When the waste packages are breached, they are considered to be essentially removed from the environment—there are so many holes and breaks in the wall that they provide no barrier to groundwater flow or radionuclide mobilization.

10.4.3.4 Mobilization of Waste-Package Contents

Most of the same processes applicable to the direct-release incorporation of waste into the magma flow apply to this scenario also. High temperatures can volatilize radionuclides (such as iodine, cesium, etc.). The sulfur and chlorine in the magma can form low-temperature eutectics with components of the waste. The UO_2 can come to solution equilibrium with the magma. Westrich (1982, Table 2) reports that at the lower tested temperatures ($\sim 1,200^\circ C$), the UO_2 is primarily found as a liquidus-phase $Mg_yU_{1-y}O_{2+x}$, while the remainder of the mixture was solid silicate glass. The uranium (and any congruently dissolved radionuclides) therefore can be much more mobile than would be thought from the temperature of the magma. The TSPA waste-form degradation model allows for taking credit for the presence of the Zircaloy cladding by means of a fractional multiplier for the waste-surface area. For the spent fuel exposed to magma, the cladding credit is set to zero.

In a 21-PWR waste package, the spent fuel assemblies occupy about 1.7 m^3 volume. The UO_2 itself is some smaller volume. The void space inside a waste package is about 4.5 m^3 . If the void volume fills with liquid magma (with density 2.65), between 0.2 and 0.4 m^3 of the UO_2 (with density 11) will dissolve. We model this with a uniform distribution, lacking any other insights.

Parameter	Minimum	Maximum	Distribution Type
Amount of UO_2 dissolved	0.0 m^3	0.4 m^3	uniform

10.4.3.4.1 Dissolution Rates

When the intrusion cools, the final state is a mixture of basalt contaminated with the dissolved UO_2 and inclusions of spent-fuel fragments that did not dissolve. As the basalt cools, it cracks, permitting groundwater to penetrate the mass and possibly reach contaminated regions of the basalt and the spent-fuel inclusions. At later times when groundwater flows through this mixture, the uranium oxides will alter to form secondary minerals, such as schoepite (uranyl oxide hydrate), soddyite (uranyl silicate oxide hydrate), and uranophane (calcium uranyl silicate oxide hydrate). In general, the progression of mineralization is schoepite to soddyite to uranophane. The rate of alteration of spent-fuel fragments exposed to dripping J-13 water has been measured at approximately 3% by weight over 3.1 years (Finn et al. 1997, p. 531). (Note

that Finn et al. consider the release rate of Tc-99 as a marker for matrix dissolution). Further tests indicate that the alteration is continuing at the same rate (Finn et al. 1998, p. 123). The alteration rate depends on the temperature and surface area of the UO₂, as well as the availability of water. As is discussed in the next section, the spent fuel is expected to be finely divided by the mechanical and thermal stresses. Approximately ten years after the emplacement of the dike the waste has cooled to its pre-intrusion temperature. At this time, if ambient conditions allow, water can return to the waste and begin the alteration process. At the rate of alteration observed above, UO₂ can be almost completely altered in approximately 100 years.

The dissolution rate for spent fuel has been developed for the TSPA-VA base case. The analysis assumes that adsorbed water films on spent fuel in a waste package cause degradation represented by an intrinsic dissolution rate that is a function of temperature, pH, carbonate concentration, oxygen fugacity, and fuel burnup. Dissolution data under a number of test conditions have been fit with a regression analysis (memo, W. O'Connell, LLNL, to R. Stout, LLNL, December 23, 1997, LLNL reference Number LL YMP98 05049 (MOL.19980605.0424). For conditions typical of waste in air in a repository drift, dissolution rates range between 0.9 and 8 mg/m²-day. For spent fuel encapsulated in basalt, the oxygen availability is much lower than in open air. For example, if the oxygen concentration were 10⁻⁵%, (compared with 20% in air), the dissolution rate would be reduced to the order of 0.2 mg/m²-day (all other conditions remaining the same).

The dissolution rates of secondary uranium minerals are given in Table 10-19. They have been calculated by using molar dissolution rates provided in the cited references multiplied by the molecular weights of the minerals.

A dissolution rate for basalt can be estimated from dissolution rates for some of its constituent minerals. These rates have been calculated from molar dissolution rates provided in Bruno et al. (1995, Table 1). An average molecular weight of basalt, including 30% dissolved UO₂, has been used. The basalt dissolution parameters range from 0.0002 to 0.035 mg/m²-day.

The range of dissolution rates goes from 0.0002 for contaminated basalt to 40.7 for soddyite. Because the proportions of basalt, UO₂ from spent fuel, and UO₂ secondary phases are not known, and because the range of dissolution rates is five orders of magnitude, we assume a log-uniform distribution of dissolution rates (units of mg/m²-day). The dissolution rate for basalt specifically is also taken to be log-uniform over the range given above. The following parameters are given as natural logs.

Parameter	Minimum	Maximum	Type
Overall dissolution rate	-8.35	3.71	log-uniform
Basalt dissolution rate	-8.52	-3.35	log-uniform

10.4.3.4.2 Particle Size Distributions

The size distribution of spent-fuel particles is discussed in Sections 10.4.2.4.1 and 10.4.2.4.2 of this document. The range of particle sizes is 0.01 cm to 1 cm, as shown in Figure 10-33. Under disruptive conditions produced by a magmatic intrusion, it is expected that the uranium dioxide pellets will be extensively fragmented, so that the size distribution is revised to weight it toward the smaller sizes. Figure 10-45 illustrates the revised PDF for uranium dioxide spent-fuel particle sizes. It is a log-normal distribution with a mean of 0.1 cm and a standard deviation of 4.48.

The surface area of the spent fuel and basalt is a function of the mechanical and thermal disturbances it has experienced, as well as chemical alteration processes. Gray and Wilson (1995, Table 2.2) measured specific surface areas for spent fuel. Two methods of measuring surface areas were used: BET and PSD (Gray and Wilson 1995, Section 2.1.3). The PSD method (as adjusted by Gray and Wilson) appears to be more appropriate for dissolution processes (Gray and Wilson 1995, p. 2.6). For extensively oxidized uranium (e.g., U_4O_{9+x}) they reported values ranging from approximately 900 cm^2/g for grains to 20 cm^2/g for particles to 7.2 cm^2/g for spent-fuel "chunks." The specific areas are assumed to be correlated with the particle sizes shown in Figure 10-45. For the TSPA-VA analyses, particle sizes of 0.01 cm are assumed to have specific surface areas of 900 cm^2/g , decreasing to 20 cm^2/g for 1-cm particles. The relationship between specific surface area and particle size is

$$\text{Specific surface area} = [-191.09 \cdot \ln(\text{diameter}) + 20.] \cdot 10^{-7}, \quad (10-9)$$

where diameter is in cm, and specific surface area is now in m^2/mg .

The basalt intrusion that flows down drifts is expected to fracture after emplacement. Observations of fractures for dikes in the Nevada Test Site region show fractures parallel with the country rock with a spacing of approximately 1 cm on the margins (approximately 10 to 20 cm from the dike-country-rock contact, and the same distance from the dike-waste-package contact). The central parts of the dikes are fractured perpendicular to the dike walls, with a fracture spacing of 10 to 20 cm (Greg Valentine, Los Alamos National Laboratory, personal communication 1998).

For basalt that fills the drift to one-half its diameter, the cross section of rock and waste package form an almost semi-circular area (see Figure 10-46). At the centerline of the waste package on its pedestal, the horizontal distance to the drift wall is 2.4 m. Assuming that the margins of the emplaced basalt are fractured on 1-cm spacing, and that the interior of the waste package (0.83 m radius) is similarly fractured, approximately 50% of the cross-sectional area of the basalt intrusion has the closely spaced fractures. An estimate of the average hydraulic conductivity of both the fractured and unfractured basalt, assuming 100-mm fracture apertures and using the parallel-plate model for fracture flow (Barnard et al. 1992, p. 4-41 ff.) gives 1.29×10^5 m/yr. A 100-mm fracture running the entire 5.5-m length of a waste package has a volume capacity of 0.001 m^3 (for a depth of basalt of approximately 2 m). Based on the fracture spacing of 1 cm at the margins of the basalt, there could be approximately 100 fractures, giving a volume capacity of 0.1 m^3 of water. The seepage rate into drifts onto each waste package under long-term-

average climate conditions has been modeled in the base case as ranging from 0 to 3.4 m³/year, with a mean of 0.2 m³/year.

Using the hydraulic conductivity estimate and the maximum seepage rate given above, water entering the drift can be completely accommodated by the fractured basalt. We therefore assume that all the water entering the drift is available to dissolve the contaminated basalt, the UO₂ spent fuel, and the contaminated secondary phases of UO₂.

Combining the information on dissolution of the various forms of contaminated rock with surface areas gotten from particle sizes, the amount of water available, and the amount of waste in a single waste package, we can estimate the rate of mobilization of radionuclides into groundwater. Figure 10-46 illustrates the physical layout of a cross-section through a drift half filled with basalt.

The area of the cross-section containing the basalt is the semi-circular area minus the area of the invert at the bottom of the drift. For a 5.3-m drift diameter, the basalt and the remains of the waste package cover approximately 9 m². Of this area, the spent fuel in the waste package occupies approximately 0.3 m², and the basalt most contaminated by the spent fuel (i.e., that in the void space of the waste package) occupies approximately 0.8 m². We assume that the spent fuel and nearby basalt are extensively pulverized, so it has the largest specific surface area. The remaining basalt, with fracture spacing of 1 cm, is assumed to have lower specific surface area. For the purposes of simulating dissolution, between 20% and 40% of the spent fuel is assumed to be dissolved in basalt; the balance is UO₂ or one of the secondary phases. Spent-fuel particle sizes are described by the distribution given in Figure 10-45, and fractured-basalt sizes are uniformly distributed around the 1-cm fracture spacing.

10.4.3.4.3 Low-Melting Elements

Table 10-20 lists those radionuclides (taken from the list of 39 being used for TSPA-VA base-case analyses) that have melting points in the range of magmatic temperatures. Additionally, there are a few radionuclides that have boiling points in this range, or form low-melting eutectic mixtures with sulfur or silicon (Hansen and Anderko 1958). Approximate amounts of the elements (based on the number of curies in typical commercial spent fuel and defense high-level waste inventories) are also presented in the table.

Thus, a waste package containing between 5.6 and 9 MTU (depending on waste type) could have between 177 and 290 moles of plutonium (42 to 69 kg) available to be mobilized by melting into the basalt; as much as 10 kg of cesium and 1.5 kg of iodine can be released by vaporization.

As an abstraction for TSPA-VA, assume that the low-temperature radionuclides boil off and are deposited on the basalt and tuff rocks in the drift. The higher-temperature radionuclides are mobilized congruently with the UO₂. This contaminated rock becomes the contaminant source term for groundwater flow when water can return to the drift.

10.4.3.5 Development of Enhanced-Source-Term Modeling Analysis Parameters

The realizations for the direct-release scenario that produced simulations of a liquid-magma interaction with the repository are used as the basis for the enhanced source-term modeling. As was done for the direct-release modeling, dike orientations and lengths are randomly selected, and the length of the dike inside the repository is expressed as a fraction of the total dike length. Table 10-21a illustrates some of these realizations.

The dike-length fraction is the product of the length of dike inside the repository and the fraction of inter-drift spacing that is open drifts (i.e., 5.3 m of the 28.6-m inter-drift spacing). When the dike-length fraction shown in Table 10-21a above is 0.185, then the entire dike lies inside the repository. Realization 33 produced a dike that has zero length inside the repository. The number of drifts crossed is calculated the same way as is done for the direct-release scenario — by dividing the north-south component of the dike length by the 28.6-m drift spacing.

The number of packages contacted by the magma is now calculated. Only liquid-magma interactions with waste packages are considered, because the higher heat capacity of the liquid makes waste-package breach more likely. In Table 10-21b, those realizations where the fragmentation depth is below the repository (indicated by an eruption type of "ash") are not considered further. As is discussed in Section 10.4.3.2, we assume that two packages per drift are breached by the intrusion.

The groundwater flow and transport calculation requires the fractional dissolution rate of the waste. As is described in Section 10.4.3.4.1 above, radionuclide dissolution occurs from UO_2 , altered UO_2 , and UO_2 dissolved in basalt. Table 10-21c shows the simulations for dissolution of UO_2 and altered UO_2 .

The amount of UO_2 in the form of spent fuel or secondary phases of UO_2 is determined by the temperature; the higher the temperature, the more UO_2 is dissolved into the basalt (in the range 20% to 40%). Dissolution of contaminated basalt is shown in Table 10-21d.

10.4.3.6 Analysis Procedures

The effect of the enhanced source term on PA consequences has been modeled by applying the intrusion-enhanced source term to the base-case groundwater flow and transport analyses. These calculations are made using the RIP computer code system (see Section 11.1 of this document).

10.4.3.6.1 Summary of Changes to the RIP Base Case for the Volcano Scenarios

The RIP base-case model was modified to allow simulations of disruption of the repository by a volcanic event. To disrupt a specific number of containers throughout the repository during a volcanic event, three new source terms were added to the base-case model. One of these new source terms represents the commercial-spent-fuel containers disrupted by the volcanic event, one represents the DOE-spent-fuel containers disrupted, and the third represents the high-level-waste containers disrupted. These three source terms were used to remove a particular portion of

the waste containers from the repository container population and set them aside to be disrupted only when the volcanic event occurred.

The new commercial-spent-fuel source term for the volcanic event was created by copying (within RIP using the F5—copy source term—command) an existing commercial-spent-fuel source term so that the inventories would be automatically copied to the new source term. Similarly, this same method was used for creating the new high-level-waste and DOE-spent-fuel source terms by copying existing high-level-waste and DOE-spent-fuel source terms.

The number of containers in the new commercial-spent-fuel source term is calculated by a new parameter that is computed by dividing the total number of commercial-spent-fuel containers by the total number of containers in the repository, and then multiplying that fraction by the number of waste containers to be disrupted by the volcanic event. The number of containers for the new high-level-waste and DOE-spent-fuel source terms was calculated in a similar fashion. New parameters for the number of containers in each of the original, base-case source terms were created to adjust for the containers allocated to the three new source terms.

A new parameter was defined for the matrix degradation rate for the three new source terms. The matrix-degradation rate, the number of containers disrupted, and the time of the volcanic event were predetermined and input into RIP before each simulation.

Both the primary and secondary container-failure definitions for the three new source terms were given a distribution type of *degenerate*, with the start time set to the value of the parameter that defines the time of the start of the volcanic event. Also, no "Local Environments" were defined for these new source terms, so essentially, the predetermined numbers of containers to be disrupted by the volcanic event remain intact until the time at which the volcanic event is to occur, then they are all disrupted.

A new waste-form cell pathway was created for each of the three new volcano source terms. Each of these three new waste-form cell pathways connects (via an "advective mass transfer connection") to each of the six EBS region outflow cells (R1OUT, R2OUT, etc.). This makes the volcano source terms available for direct release to the unsaturated zone.

The water flow from each of the new waste-form cells to each of the six "RnOUTs" was scaled based on the area in each region of the repository. This was approximated by using the fraction of containers in each region of the repository. For example, the flow out of the commercial-spent-fuel waste-form cell to EBS region 1 (R1OUT) is the total outflow from the commercial-spent-fuel cell multiplied by the fraction of commercial-spent-fuel containers in EBS region 1.

The results from the initial simulations of volcanic events showed dose time-histories that were higher than the base case even before the volcanic event occurred. A problem with RIP Version 5.19.01 was discovered when a cell network fed an external pathway along multiple connections. To work around this problem, the option to "break" the cell network connections between each of the three new waste-form cells and each of the RnOUT connections was used. The effect of "breaking" these connections is that there is a one-time-step delay in discharges from the three new waste-form cells to the six RnOUT cells. This is unlikely to have a noticeable effect on the simulation results.

10.4.3.6.2 Results of Enhanced-Source-Term Modeling

Approximately 65 percent of the realizations resulted in an enhanced-source term. Because the waste packages are expected to fail regardless of their prior state of degradation, failures occur over the whole time period modeled. Figure 10-47 shows a scatter plot of the times of failure and the fractional release rates. The modeling approach has resulted in there being no discernible trend to the data, although release rates could vary as a function of the degree of degradation of the waste that occurred before the onset of the igneous activity.

The CCDFs comparing base-case and enhanced-source-term dose rates are shown in Figures 10-48 and 10-49. Figure 10-48 compares the ranges of peak individual dose rates at 100,000 years. Applying the maximum probability of occurrence for direct magmatic interactions with the repository (i.e., 10^{-7} events/year) gives the dotted curve in Figure 10-48. Using the mean probability of occurrence of 1.5×10^{-8} /year gives the solid CCDF in the figure. Only 9 percent of the realizations simulating igneous activity occur within the first 100,000 years. Of those nine events in the simulation, five produce no enhanced source term. When events result in radionuclide releases, the dose rates generally range from about 200 to 500 mrem/yr, as shown by the shape of the CCDF curves. The CCDF is essentially flat for dose rates less than about 200 mrem/yr (meaning that most of the dose rates fall in this range) and then it drops steeply (indicating that there are few instances above 200 mrem/yr).

Over 1,000,000 years, approximately 65 percent of the igneous events result in enhanced source terms. Those realizations where there is no source-term enhancement occur when the dike length inside the repository is zero, or if the fragmentation depth is below the repository so the waste packages are impacted by ash rather than liquid magma. Ash has lower heat capacity than liquid magma, and it is assumed that the waste package may survive this environment. Figure 10-49 shows the CCDFs for the million-year igneous analysis and the corresponding base-case, peak dose rates. Comparing the base-case CCDF with the mean-probability CCDF, the maximum dose rate from an enhanced source term is approximately two orders of magnitude less likely than the maximum dose rate for the base case. The maximum igneous-activity dose rate is about one-third of the base-case maximum dose rate.

Over 1,000,000 years the maximum probability of releases is 0.1 (assuming a 10^{-7} annual frequency of occurrence), as is shown in Figure 10-49. As for the 100,000-year case, when there are releases, the dose rates are in the range 200 mrem/yr and above. This is primarily because of the assumption that when the waste package is breached by the magma, the waste becomes readily available for transport when groundwater reaches it.

Figure 10-50 shows dose-rate time histories for some of the releases. They are compared against the base-case dose-rate time history. Examples of an early event (before 100,000 years) and a later event (around 500,000 years) are shown. Because of the travel time for groundwater transport of contaminants, the igneous event occurs several tens of thousands of years before the peak dose rate occurs.

Comparing the base-case peak dose rate with those for igneous events can be seen from Figure 10-50 to be somewhat misleading. The base-case peak dose rate in this example occurs at about 330,000 years, while for the early igneous event, the peak is at about 100,000 years; the

late-event dose peak is at about 550,000 years. Figure 10-51 shows the ratios of igneous-event peak dose rates to the base-case dose rates at the corresponding times. For example, at 100,000 years the enhanced-source-term dose rate is about 600 mrem/yr at the point where the base-case dose rate is about 6 mrem/yr, giving a ratio of approximately 100. The ratios are higher at early times because the base-case dose rates are building up toward their maxima while the magmatically induced dose rates are relatively constant in the range 200 – 500 mrem/yr.

10.4.4 Dike Intrusion Outside Repository Block

If an intrusive event occurs outside the repository block, it can affect the flow and transport of contaminants to the accessible environment. Because most of the flow in the unsaturated zone occurs within the repository footprint, a dike occurring outside the repository block will primarily affect saturated-zone (SZ) flow. This disturbance can be modeled as a alteration in the SZ flow, compared with the base case. These alterations will depend on how permeability of a dike differs from the surrounding rock. A dike that develops large numbers of well-connected cooling fractures would be expected to be more permeable than the country rock, while a dike with few well-connected fractures would be less permeable than the country rock.

Considerable modeling of SZ flow has been done previously (Wilson et al. 1994, Chapter 11; Arnold 1996). Both 2-D (in a horizontal plane) and 3-D models have been used. In order to calculate possible consequences of dike intrusions, assumptions must be made about the location of a dike and its hydrologic properties. The most likely places to consider as locations for new dikes are: 1) along or related to existing structures (identified faults), since their presence of these features suggests structural weakness, or 2) roughly normal to the current least principal stress at Yucca Mountain (Barr et al. 1996; Stock et al. 1985, p. 8701; Stock and Healy 1988, pp. 90-91; Warren and Smith 1985). Both options for location of new dikes—along existing structures and roughly normal to the current least principal stress—have been explored in a series of calculations for comparison to a reference, calibrated model of the SZ.

Three possibilities for dikes modifying the existing SZ flow domain are considered — insertion of dikes singly along existing structures, splays from existing structures aligned approximately normal to the regional least principal stress, or dikes not at all associated with existing features. Intrusion of a dike north or west of the existing structures is not thought capable of adversely affecting saturated-zone flow and has not been considered further. This assertion is predicated on the assumption that calculations can be limited to the tuff aquifers and that the Paleozoic systems (carbonates) can be ignored*. Some examples of the new features are shown in Figure 10-52.

We assume that hydrologic properties of the dikes could vary from being more conductive than the country rock to substantially less conductive than the country rock and that the properties are

* Based on observations in the region (head measurements at well USW-P1 and temperature measurements at other wells) the approximation can be made that the tuff and carbonate aquifers behave independently near the repository. Insertion of a dike to the north of the repository would be primarily in the carbonate aquifer, while dikes to the south/southeast are in the tuff aquifer. Thus, alteration of carbonate-aquifer conditions are assumed to have no influence on tuff-aquifer flow, which can affect contaminant transport from the repository.

isotropic and apply uniformly along the entire length of the dike. For an actual dike, one would expect that hydrologic properties might be anisotropic and vary along the dike. Since these analyses are intended to develop qualitative understanding of changes produced by hypothetical dikes, this simplification is not restrictive for the analyses.

10.4.4.1 Reference Saturated-Zone Model

The reference case model is a calibrated model that is abstracted from a larger regional model (D'Agnese et al. 1997, pp. 59 ff.) which supplies boundary conditions. The reference case depends on the presence of faults or equivalent structures along certain structural features (Solitario Canyon Fault, Drill Hole Wash, H-5 Splay, Yucca Wash and Bow Ridge Fault). These features are included in the model to calibrate calculated heads to observed data. In all cases, it is necessary to model the structures as low-permeability features to obtain calibration. A water-table aquifer model is used, rather than a representation as a confined aquifer so that a rise in the water table, which could put the saturated zone into new rock not part of a confined system, could be accounted for. The water-table aquifer model consists of 14 layers of 2,300 nodes each, of which the lowest 6 represent rock consistently below the water table. It is those six layers for which saturated-zone transport is possible.

The flow field calculated from the reference saturated zone model is then used to simulate contaminant transport. A unit contaminant source is located within the repository footprint at the water-table elevation. This provides contaminants for calculation of concentration contours and breakthrough curves (calculated along a line located 5 km down-gradient of the repository boundary). Figure 10-53 shows the potentiometric surface (heads), representative concentration contours (after 4,375 years' transport), and breakthrough curves for the reference case.

10.4.4.2 Modeling of dikes

The inserted dikes are located along existing structures, or in the region of low hydraulic gradient, either along, or to the south and east of the Solitario Canyon and Drill Hole Wash faults.

10.4.4.2.1 Dikes along existing structures

Dikes inserted along Solitario Canyon fault, Drill Hole Wash fault, Yucca Wash fault, or the H-5 splay fault all resulted in essentially no change from the reference-case potentiometric surface when the hydraulic conductivities of the inserted dikes were reduced by four orders of magnitude. Consequently, there was no change in the concentration contours or breakthrough curves for these cases. When the hydraulic conductivity was increased by four orders of magnitude, the potentiometric surface changed from the reference case. Generally, the changes produced an extremely flat gradient to the south-southeast of the repository. Figure 10-54 illustrates examples of this effect for a dike located along the Solitario Canyon fault.

Compare Figures 10-53a and 10-54a; the 730-m head contour has been shifted southeastward by about 5,000 m, reducing the gradient in this region. Comparing concentration contours

(Figures 10-53b and 10-54b) shows that the contaminant flow is focused in a more easterly direction. The primary effect of the flat potentiometric gradient is to reduce the driving potential for contaminant transport. Compare Figure 10-53c with 10-54c to see the reduced contaminant concentration along an arc 5 km from the repository boundary after 4,375 years.

10.4.4.2.2 Dikes not located along existing structures

Except for the expectation that a new trace for insertion of a dike would be roughly perpendicular to the direction of the least principal stress, location is arbitrary. Guidance for the location of new dikes has been obtained from the Probabilistic Seismic Hazard Analysis (PSHA) work (CRWMS M&O 1998a). Because dikes injected north of Yucca Wash or Drill Hole Wash, west of Solitario Canyon or east of the current model domain are probably irrelevant to transport away from a repository, two locations (one beneath the repository footprint and one south/southeast of the repository) were selected. In each case, these traces were first considered as separate dike segments and then extended to connect with Solitario Canyon Fault. Because the new dikes are not associated with the structures used for calibration, there is no restriction on their hydraulic conductivity. Both increases and decreases of about four orders of magnitude have been modeled.

For the dikes beneath the repository (both connected to and separate from the Solitario Canyon fault), a high hydraulic conductivity changes the potentiometric surface, but produces a flat gradient to the southeast. Changes in the head structure, a representative concentration contour, and breakthrough curve for a dike connected to the existing fault are shown in Figure 10-55.

The change in potentiometric surface can be observed by comparing Figure 10-53a with 10-55a. The lower gradient is evident by comparing the lesser extent of the concentration curves for the two cases (Figures 10-53b and 10-55b). Lastly, there is little difference evident for the breakthrough curves for the insertion of this high-conductivity dike (Figures 10-53c and 10-55c). Calculations of the effects of insertion of low-conductivity dikes also indicate little change from the reference case.

A dike about 2 km long has been inserted to the southeast of the repository and oriented approximately normal to the current direction of the least principal stress (Stock et al. 1985, p. 8701; Stock and Healy 1988, pp. 90-91). The case of low hydraulic conductivity ($k=1 \times 10^{-11}$ m/s) yields a potentiometric surface which differs from the reference case in location of the 730-m and 729-m contours. The heads, concentrations, and breakthroughs are shown in Figure 10-56. The net result, however, is that the gradient between 730 m and 728 m is about the same as the reference case. The concentration contours and the breakthrough curves show only slight differences from the reference case (compare Figure 10-53b with 10-56b and Figure 10-53c with 10-56c). The corresponding case for high hydraulic conductivity ($k=1 \times 10^5$ m/s) also differs only slightly from the reference case. Calculations for the dike connected to the Solitario Canyon fault produced similar results.

10.4.4.3 Interpretation of Modeling Results

Insertion of dikes often produces different potentiometric surfaces from the reference case, and alteration of the direction of transport. All these changes to the potentiometric surfaces result in very low gradients in regions immediately down-gradient from the repository. Transport, while sometimes redirected, is not significantly enhanced. As the breakthrough curves show (Figures 10-53c through 10-56c), in no cases are the contaminant concentrations for the altered flow paths even as large as that for the base case. Consequently, little impact on performance of the repository is expected.

10.5 SEISMIC ACTIVITY

There are several effects that seismic disturbances can have on repository performance, including direct effects such as rockfall damage to waste packages or container disruption by vibratory ground motion or fault displacement. Indirect effects, such as alteration of flow paths near the repository or in the saturated-zone, or changes in the water table elevation are also possible. Additionally, transient groundwater flow resulting from seismic pumping has also been suggested as a possible disruptive mechanism.

Rockfall is expected to be the primary source of waste-package disturbances. Waste-package damage could result in significantly increased radionuclide source terms for groundwater-based releases. These are analyzed here. Alteration of unsaturated-zone flow around the waste packages is of secondary concern for the TSPA-VA analyses. Such alterations could change the environment for waste-package corrosion, which in turn may increase the radionuclide source term for groundwater-flow transport. Saturated-zone flow and transport alterations from seismic disturbances have the same potential to affect doses as was discussed in the volcanic section, and are modeled in the same way, as are the saturated-zone indirect volcanic effects.

Prior analyses have investigated water table rise and seismic pumping (Carrigan et al. 1991). These phenomena have been shown to be transitory and of limited extent, as documented in the PSHA.

10.5.1 Rockfall

Rockfall is induced by both ground shaking and thermo-mechanical stress changes. The superposition of ground shaking on rock already experiencing thermo-mechanical stresses may cause more, or larger, sections of the repository tunnels to fall. It is not expected that there will be any significant difference in the response of the packages to rockfall from the two sources.

An important assumption about the rockfall analysis is that the repository drifts are assumed to remain open for the life of the facility. This represents a "worst case" condition because the waste packages are not slowly covered by small rockfalls that could eventually protect the packages from direct impact of larger rocks.

10.5.1.1 Events and Processes that can Cause Rockfall

Excavating a tunnel alters the local stress state in the surrounding rock by creating a free surface. The rock comprising the wall of a repository tunnel can relax into the opening to relieve the stress. Depending on the quality and type of rock, this stress relaxation may result in rockfall. The sizes of rocks that fall depend on the competency of the rock and the number of fractures present (see Table 10-22). A survey of fractures exposed by the Exploratory Studies Facility tunnel has been conducted (CRWMS M&O 1997d, Section 7.4). The observed joint spacings have been interpreted as rock block sizes potentially available to fall, if conditions permit. The joint spacings (and by interpretation block sizes) have been grouped into ranges for this analysis. Table 10-23 gives the probabilities of occurrence for block-size ranges for the ESF observations.

10.5.1.1.1 Thermo-Mechanical Rockfall

Thermal loading of the rock surrounding the drifts alters the stress field from ambient conditions (CRWMS M&O 1998f, Figures 7-17 and 7-18). Immediately before excavation, the vertical stress from overburden is approximately three times the horizontal stress. Immediately after excavation, the in-situ stresses are redistributed around the openings. At the boundary of the openings, the radial stresses become zero and a tangential or hoop stress is created. In the wall the tangential stress is vertical and is about 2.5 times the vertical stress before excavation. In the roof the tangential stress is horizontal and has a magnitude close to zero or tensile. Thus, the conditions after excavation could promote some rockfall of loose rock in the roof. See Figure 10-57a. As the repository heats, thermal loading causes an increase in the tangential stresses in the roof and wall of the openings. The roof can experience very high compressive stresses as a result of the combined thermal loading from adjacent drifts, as is shown in Figure 10-57b. These high stresses can damage the rock in the roof and cause blocks to shift from a combination of joint slip and local rock failure. The likelihood of rockfall is increased after this damage, even after the repository has cooled. If an earthquake occurs anytime after the maximum heating of the repository, the most likely blocks to fall are in those areas that were damaged from the thermal loading. Depending on the fracture-network orientation, the falling blocks may be located directly over the centerline of the drift, or they may be at the side of the drift. The former can cause impact damage, while the latter can put the waste package under compressive stress.

The stress change can cause block shifts of varying amounts, depending on rock quality. An analysis of the extent of thermally driven spalling for various rock quality designators is given in Table 10-24 (EPRI 1996, Chapter 12). The EPRI analysis assumed a thermal loading of 83 MTU/acre, with a peak rock temperature of 165°C at 100 years. The stability indices, based on interpretations in EPRI (1996), in the table are as follows:

1. No Spalling
2. Very minor spalling (10% chance of rockfall, spall depth < 0.5 m)
3. Minor spalling (20% chance of rockfall, spall depth < 0.5 m)
4. Moderate spalling (40% chance of rockfall, spall depth < 1 m)
5. Drift filled with rubble (80% chance of rockfall).

These stability indices have not been confirmed in Yucca Mountain tuffs, but for TSPA-VA analyses, they are considered an acceptable starting point.

Table 10-24 shows that the highest probabilities for block movement occur at the time of peak wall temperature (100 years). At later times, as the repository is cooling, the areas with strong and medium rock quality become quite stable. During this time, the conditions for seismically initiated fall of rocks big enough to damage a waste package obtain.

Because the highest indices for thermally driven rockfall occur at early times, when waste-package walls are relatively undegraded, this mechanism does not contribute significantly to overall repository rockfall damage.

10.5.1.1.2 Rockfall Induced by Ground Shaking

An empirical relationship for rockfall caused by shaking (Kaiser et al. 1992, Figure 2) is used to estimate the likelihood that rocks of the four quality designations falling in the drifts. The amount and nature of rockfall are expressed in terms of a damage level *DL*, where

< <i>DL</i> 1:	No damage
<i>DL</i> 1 – 2:	First signs of damage
<i>DL</i> 2 – 3:	Minor damage
<i>DL</i> 3 – 4:	Moderate damage
<i>DL</i> 4 – 5:	Significant damage
> <i>DL</i> 5:	Severe damage.

The term “damage level” as used above refers to the amount and type of rock that falls—not damage to waste packages. Table 1 of Kaiser et al. (1992) provides additional descriptions of degrees of rockfall. For example, up through *DL* 2, only loose rock is displaced by rockburst. Small shards and a few chunks of rock are displaced, and there is only minor new fracturing. Rockfall associated with level 2 would occur with only the Very Weak rock quality, because Very Weak rock is composed of these small pieces. At level 3, small-to-large pieces are dislodged, and there is new rock fracturing. This is interpreted as describing the fall of rock designated as Weak. At level 4, there is violent displacement of loose rock and freshly broken rock. Rock is heavily fractured and violently displaced. Medium-quality rock is assumed to fall at level 4. Lastly, at level 5 substantial amounts of rock are displaced, and there is extensive fracturing. Strong-quality rock can fall at these levels.

An equation for peak particle velocity (*ppv*) as a function of rockfall damage is given in Kaiser et al. (1992, eq. 4). It can be rewritten to express *DL* in terms of *ppv* as follows:

$$DL = \frac{\ln\left(\frac{ppv}{50}\right)}{\ln(2)} + 1 \quad (10-10)$$

where, *ppv* is in mms, and *IC* is a measure of initial conditions related to rock wall quality, failure potential, local mining stiffness, and support effectiveness (all factors considered in

mining engineering analyses of tunnel stability). *IC* varies with rock quality and temperature. For example, rock wall quality ranges from 1 to 4 for strong to very weak rock-quality designators. Kaiser et al, (1992) show that this equation is appropriate for an average level of *IC*; i.e., *IC*=2.5. For values of *IC* less than 2.5, on average damage is less, and for *IC* values greater than 2.5, damage is greater. Kaiser et al, (1992) note that the effect of *IC* can result in damage levels up to 2 points higher or lower than the average. Based on these attributes of the data in Kaiser et al, (1992), the equation has been modified to take into account the effect of *IC*. The assumption made here is that very good rock quality (*IC*=1) results in a *DL* value 2 points lower than the average, and the highest possible *IC* value (*IC*=4, for very poor rock quality) will cause the damage level to be 2 points higher than average. Using this *IC* range, the equation is modified as follows:

$$DL = \frac{\ln\left(\frac{PGV}{5}\right)}{\ln(2)} - 2.33 + 1.33 * IC \quad (10-11)$$

where, the relationship also assumes that *ppv* is the same as *PGV* (*PGV* is now expressed in cm/s.) Table 10-25 shows the *IC* values that have been assigned to the rock-quality designators, based on an assessment of *ESF* data. *IC* calculations use equation 1 of Kaiser et al. (1992). The lower the value of *IC*, the lower the *DL* value for a given *PGV* value.

Values of *IC* values less than 2.5 are indicators of “good” rock quality. Table 10-26 gives the ranges of *PGV* values for various damage levels and initial conditions. The table shows that for the Strong-quality rock a *PGV* in excess of 135 cm/s is required to cause maximum damage levels. In contrast, the Very Weak rock experiences maximum damage levels at *PGV* values, less than half those for Strong rock.

The *PSHA* report (CRWMS M&O 1998a, Figures 7-7 and 7-8) provides integrated seismic hazard results for the horizontal *PGV* and vertical *PGV*, respectively. The figures show the 15th, median, 85th, and mean for annual exceedence frequencies to 10⁻⁷. The *PSHA* evaluated accelerations in two oscillation frequency ranges: 1 to 2 Hz and 5 to 10 Hz. The latter oscillation frequencies are of concern for rockfall. The acceleration spectra have been converted to *PGV* values in the 5–10 Hz oscillation range for probabilities from approximately 10⁻¹ to 10⁻⁶. Figure 10-58 shows the probability curves for horizontal *PGV*. The figure shows the median and fractile (15th and 85th) values for horizontal peak ground velocity. The fractile values represent the ±1σ range provided by the *PSHA* experts.

The *PGV* values are provided at a rock outcropping located at the elevation of the repository (Point “A” in *PSHA* notation — CRWMS M&O 1998a, Figure 1-1). For the rockfall calculations, vertical *PGV* values at the repository (i.e., under approximately 300 m of overburden at Point “B,” in *PSHA* notation) are required. Point B values are derived from Point A calculations, and vertical *PGV* can be scaled from horizontal values using the ratio 2/3.

The data in Figure 10-59 are reported as probabilities for mean and fractiles for a given *PGV* value. Hazard values for *PGV* are constructed by inverting the data to give the range of *PGV* values for a given probability. The inversion is done by interpolating between the supplied *PGV*

and probability values after doing a log-transform of the data. The distribution of PGV values around the mean is assumed to be log-normal.

For any time period, the earthquake hazard is the integral over all hazard estimates (i.e., annual probabilities of exceedence). For example, at 10,000 years, the integrated frequency of occurrence is 10^4 times the annual probability of exceedence at the 10^{-3} level plus 10^4 times the annual probability of exceedence at the 10^{-4} level, etc. (Reiter 1990, p. 184, eq. 10.2). The integrated hazard over a time period therefore reflects the fact that there is a relatively high probability of having small-magnitude events, but a non-zero probability of having large events also. Table 10-27 gives the integrated frequencies of occurrence for various time periods for several PGV values.

The table shows that over a 1,000-year period the frequency of occurrence for an earthquake that results in a PGV of 500 cm/s is greater than 10^{-6} . Over a 100,000-year period, the frequency increases to almost 10^{-3} . Over this 100,000-year period 2,850 1-cm/s PGV events are expected.

To reflect the uncertainty in PGV values indicated by the PSHA experts, a log-normal distribution based on the median and fractiles is sampled to obtain values used in the analyses. The $\pm 1\sigma$ points of the distribution are given approximately by the 15th and 85th fractile values.

The DL indicator is related to the quality of rock (as indicated by IC) and PGV. All rocks, up to those of highest-quality descriptor indicated by the IC value are assumed to fall everywhere in the repository. Table 10-28 lists several DL values for various rock qualities for several PGV values.

For PGV values less than 79 and 61 cm/s, the DL values are 3 or below for strong or medium rock, respectively. Such damage levels are not expected to cause rock of these qualities to fall. Whether the falling rock damages waste packages depends on several factors that are listed here and discussed in the following sections.

- Whether the rock hits a package or falls between packages
- Whether the waste-package wall is so thin that the rock can damage it
- The availability of sufficiently big rock.

10.5.1.2 Minimum Size Rock that can Breach a Waste Package

Rockfall on a waste package can rupture the package, permitting premature water entry. If the package is not ruptured, the impact points may become the sites for localized enhanced corrosion of the waste package. Additionally, even if the waste package is not breached, the shock and container-wall deformation can cause mechanical failure of spent-fuel rods or shattering of a glass/ceramic waste form. When the package finally is breached, water may have more direct access to the waste form.

The rockfall problem for waste-package damage (consequences analysis) can be divided into three parts:

- Determining the minimum rock size that can rupture a waste package as a function of waste-package wall thickness
- Determining the rate of thinning of the waste-package walls at various locations in the repository (i.e., the corrosion rates of the CAM and CRM)
- Determining the range of sizes of rocks available to fall onto the containers.

For cases where the package is not breached, damage to fuel rods or DHLW ceramic can be assessed as follows:

- Assume the rock that dropped on the waste package was not big enough to fracture the container for the specified wall thickness
- Determine the shock and deformation transmitted to the waste-package interior from that rock
- Determine the number of fuel rods broken, and fraction of fuel exposed by the impact.

The M&O Waste Package Development group has made two analyses of rockfall effects on waste packages at various levels of degradation. One analyzes the rock size required to cause a *through crack* in a waste package (CRWMS M&O 1997c); the other provides maximum rock size that will cause *crack initiation* on the container without causing failure (CRWMS M&O 1996e). In both cases, the results are reported as functions of waste-package wall thickness remaining. The analysis assumed the CAM is A-516 carbon steel, approximately 10 cm thick, and the CRM is 2-cm thick alloy 625. The new CRM (nickel-based alloy 22) is expected to have similar mechanical behavior. Rock density is given as 2,297 kg/m³, and rocks are assumed to be spherical. Table 10-29 lists the critical rock sizes for causing crack initiation and for causing a through crack.

A plot of the maximum rock masses that can cause crack initiation or through cracks is shown in Figure 10-60. The slope of the "Through Crack" line appears to be different because the scales of the ordinate are different above and below the axis break.

As a TSPA-VA abstraction, one models rockfall damage by assuming that any rock larger than the crack-initiation value for a given wall thickness causes an enhancement in the corrosion rate as a result of localized corrosion. The extent of enhancement is given by the amount the rock mass exceeds the crack-initiation threshold. If a rock larger than the through-crack mass falls on the packages, one assumes that the package is breached (i.e., there is a sufficiently large crack that water can readily enter).

10.5.1.3 Rate of Thinning of Waste-Package Walls

The rates of degradation of the waste-package walls (both the CAM and CRM) have been determined as part of the TSPA-VA base-case abstractions. Figure 10-61 shows the times to corrode the CAM and CRM expressed as a fraction of wall thickness. The CRM values are for

the "drip" conditions in the repository (assumed continuous drips on the waste package – one of two modeled states – drip and no-drip). Combining the data in Figures 10-60 and 10-61, one can display the sizes of rocks that cause the two levels of damage as a function of time (Figure 10-62).

10.5.1.4 Distribution of Rock Sizes

An analysis of potential block sizes for rock falling from the drift ceiling has been completed (CRWMS M&O 1997d, Attachments III and IV). The analysis is based on observations of joint frequencies in the ESF, and on the assumption that joint frequencies are related to rock block sizes. Block-volume data from this analysis have been expressed as rock mass by multiplying the volumes by the density – 2297 kg/m³. The data for all observations are presented in Figure 10-63 as a histogram, with the bin values selected to match the rock masses determined in the analysis listed in Section 10.5.1.2.

Approximately 27 percent of the rock masses are less than 50 kg, meaning that even a substantially degraded waste package would not be further damaged. Another 24 percent are less than 350 kg, meaning that waste packages that have all of the CAM corroded away would be at varying degrees of risk of having cracks form in the CRM. Only 1 percent of the rocks is larger than 2,500 kg. These rocks could cause failure in waste packages that have most of the CAM corroded away. The study identified only one joint spacing that could produce a block greater than 20,000 kg.

The distribution for block sizes in the TSw2 unit only is quite similar, as is shown in Figure 10-64. There are no rocks greater than 3,500 kg found in this sample.

10.5.1.5 Damage to Fuel Rods

CSNF rods are assumed to be damaged by rockfall only if the rock or the waste-package wall directly contacts the assemblies. Shock transmitted by waste-package internal supports could also damage fuel rods. An analysis (CRWMS M&O 1997e, Section 7.8) provides the fractions of rods broken and fractions of fuel exposed for rocks of various configurations. One configuration used a circular point of contact (a "punch") between the rock and the fuel rods and is intended to represent the vertex of an angular rock impacting the rods. The focusing parameter is the ratio of the diameter of the punch to the diameter of the entire rock; thus a focusing parameter of 0.1 means that the entire weight of the rock is focused onto an area given by a diameter one-tenth the diameter of the rock. The other rock configuration assumed the point of contact was a linear blade defined by two parallel chords and the arcs connecting them. This configuration represents the edge of a block striking the rods. The focusing parameter is the width of the blade; for the linear configuration, the angle of blade impact also influences the results.

For the circular punch, the results are shown in Figure 10-65. The results have been calculated assuming a range of rock masses similar to the distribution provided in Section 10.5.1.4. The maximum fraction of rods damaged is about 0.23, occurring from a small circular punch

(focusing parameter of 0.10). At larger values of the focusing parameter, the impact is distributed sufficiently that the rods are not broken. The fraction of fuel exposed is calculated by assuming that the punch removes all the cladding upon impact. This fraction can be seen to be relatively independent of the size of the punch until it gets very small.

For the linear point of contact, Figure 10-66 illustrates the results. As before, a distribution of rock sizes was used, and the results were averaged over many blade orientations. The linear blade punch damages a maximum of approximately 10 percent of the rods, but about the same amount of fuel is exposed as occurs for the circular punch. The differences between the maximum number of rods broken is possibly due to the circular punch representing a more severe load on the rods (CRWMS M&O 1997e, Section 7.8.2).

10.5.1.6 Development of Rockfall Model Source Term

Thermo-mechanical processes are not considered as a likely initiator for rockfall in these analyses. Thermo-mechanical rockfall is expected to occur early in the lifetime of the repository, when the waste-package walls have corroded only slightly. As is discussed in Section 10.5.1.2, block sizes are too small to rupture a waste package with a full thickness of inner and outer barriers. Because the magnitude of PGV is correlated with waste-package thickness (both are treated as functions of time), waste-package damage is calculated for four time periods: 0 to 1,000 years, 0 to 10,000 years, 0 to 100,000 years, and 0 to 1,000,000 years.

To model rockfall initiation, a time of occurrence is randomly picked within each time period. The corresponding frequency-of-occurrence range (shown in Table 10-27) is randomly sampled to give a median PGV value. The median PGV and the corresponding standard deviation are then used to define a log-normal distribution from which the PGV value used in the analysis is sampled. The vertical PGV value is obtained by multiplying by the 2/3 vertical-to-horizontal factor. In each time period, 500 event times are randomly drawn. Next, the damage levels for strong and medium rock qualities are calculated using the formula given above. Table 10-30a illustrates this.

As can be seen from the table above, for times less than 100,000 years the DL values are very small. As the analysis will subsequently show, no waste-package breach occurs for times in the 1,000-year range because of the small magnitude of PGV and the relatively full thickness of waste package walls. Similarly, in the range 0 to 10,000 years, occasionally rockfall resulting in accelerated waste-package corrosion occurs (i.e., there are no breaches of packages). The table above also shows several results from the 0 to 100,000 and 0 to 1,000,000 year simulations. Damage level can be seen to vary widely, resulting from the wide range of median PGV values. Damage levels above 3.0 have the potential to cause fall of rocks large enough to damage waste packages.

The time of occurrence is also used to calculate extent of waste-package degradation that has occurred up to the time of the earthquake. The waste-package degradation values reported here have combined the drip and no-drip simulations done for the base case for the CAM, and use the drip simulations for the CRM. The base-case modeling assumes that the CRM is not degraded until the CAM is substantially removed. To model this, an "adjusted time" is used, which is the

difference between the time it takes for the CAM to corrode to 5 percent (or less) of its original thickness and the time of occurrence of the earthquake. The adjusted time is thus the time available for the CRM to corrode. Table 10-30b shows the amounts of waste-package degradation for the selected realizations.

Based on waste-package wall thickness, the critical rock sizes for initiation of localized corrosion and breach can be determined from Figure 10-62. The analyses done by the Waste-Package Design group provided critical rock masses at selected values of wall thickness. For values other than those calculated by the WPD group, interpolations or extrapolations have been made. Particularly, it is assumed that there is some difference in the rock mass necessary to initiate localized corrosion and to rupture the CRM in the degradation conditions where the CAM is completely gone. From the discussion of rock quality, we have the fractions of the various rock qualities in the repository (Table 10-23). From the observations of joint spacing in the ESF we have the distribution of rock sizes (Figure 10-64). The DL values shown in Table 10-30a allow us to simulate the size rocks that could fall for a given DL value. This is done by associating DL values with the CDF for rock sizes in the ESF. Table 10-30c illustrates this.

Thus, damage levels from 3 to 4 cause medium-quality rocks to fall, with masses ranging from 350 to 1000 kg. DL values greater than 4 cause strong-quality rocks to fall, with masses greater than 1000 kg. Table 10-30d shows the rock sizes for the selected realizations.

The column "Size of Rock Expected from DL" gives the rock mass that could fall based on the DL calculated for the magnitude of ground shaking. The column "Size of Rock from PDF" gives the rock mass drawn from the PDF; this is the rock that is modeled for this realization as actually falling. In some instances in Table 10-30d, the rock that is available to fall is smaller than the size expected. If the rock is smaller than expected, but larger than that needed to damage the waste package, then waste-package damage occurs (note the realization at 730,808 years). In other cases, the rock that falls is larger than the expected size, but smaller than the size that can do damage, so no damage occurs (the realization at 98,921 years). Lastly, there are several instances in Table 10-30d where waste-package breach occurs because the rock that falls is of sufficient size. In two instances, the rock is big enough to do damage, but not large enough to rupture the package. The fractional increase in corrosion rate (modeled as an increase in localized rate) is given in these two cases as approximately 6 percent and 24 percent.

The last factor to consider is the probability that a falling rock will hit a waste package, rather than falling between packages to the drift floor. The average waste package occupies 5.5 m of the 14.2-m average spacing between packages, or approximately 39 percent of the space in a drift. The probability that falling rock that would otherwise damage a waste package actually strikes a package is thus 0.39 of the frequencies calculated above. Table 10-31 summarizes the results for waste-package damage and breach for the hazard levels modeled. Each simulation at a given hazard level consists of 500 realizations. The fractions given in the table reflect the probability of the falling rock hitting a package. Note that the column "Mean PGV" in Table 10-31 is derived from Figure 10-59. Maximum PGV is found by treating the mean PGV as the mean of a log-normal distribution with a standard deviation determined from the 15th and 85th fractiles. Maximum PGV is then the largest value samples in the 500 realizations. Mean Time of Occurrence is for each of the time periods listed. In each case it can be seen to be approximately half the time period, as would be expected for uniform random sampling.

Over all time periods, the mean PGV values remain quite similar, primarily because they are dominated by the high-annual-frequency-low PGV events. When 500 random samples are drawn for the 1,000,000-year time period, for example, there may be no instances of high PGVs included. At late times the waste package walls are sufficiently degraded that they can be breached by rocks that comprise the bulk of the observed distribution, and are thus more likely to fall.

There is only a narrow time window for rockfall damage. For most of the time the waste-package wall is too robust to be damaged by the size rocks available to fall. When the waste package finally corrodes sufficiently, the difference in rock size between damage and breach is quite small.

The WAPDEG (CRWMS M&O 1998e) program calculates the time and extent of failure of waste packages and generates a distribution for use by the PA code RIP. Normally, waste-package penetration is caused only by corrosion. The times of breach caused by rockfall are used instead for this analysis. The distribution of times for waste-package failure resulting from breach is given in Figure 10-67. To that distribution is added the failures that occur as a result of accelerated corrosion from rockfall.

WAPDEG also requires the number of waste-package "patches" that are penetrated at time of failure. A patch is a small area (approximately 310 cm²) of the waste-package skin that is assumed to fail as an entity. It is thus larger than a pit in the waste package and more suitable for describing rockfall damage. As a model for this parameter, we use the mass of the rock that breached the package. The rock mass is expressed as a spherical volume whose radius is used to calculate the number of square patches that are hit.

Figure 10-68 shows the CDF for waste-package breaches for the rockfall analysis. Out to 200,000 years, there are very few rockfall failures. The probability then rises sharply as more waste packages corrode sufficiently that they are susceptible to rockfall failure.

Because rockfall is expected to be a perturbation on the distribution of failures from normal corrosion, the distributions for the two processes have been combined. Figure 10-69 compares the distributions of base-case corrosion (for the northeast region, alpha-mean, always dripping) with the distribution for rockfall and corrosion combined. Most of the waste-package failures from corrosion occur in the first 300,000 years. During this time, rockfall contributes little to any increase in failures. After about 400,000 years, if any packages fail they do so from rockfall.

Future versions of WAPDEG will incorporate seismic rockfall directly into the calculations. This will permit a more coherent treatment of the methods of waste package failure, by using the several repository conditions to calculate prior waste-package corrosion. Stochastically modeled rockfall can then be applied to the corroded packages.

10.5.1.7 Results of Rockfall Modeling

Waste-package degradation is normally calculated using the code WAPDEG. For the rockfall analysis, WAPDEG input has been modified to incorporate failures from rockfall. Two

modifications have been made: the CDF for waste-package failures including rockfall was used, and a modification was made to the distribution of waste-package patches that fail. Figure 10-70 compares the waste-package failure CDF for the base case (corrosion only) with the modified CDF that includes rockfall.

Figure 10-70 shows that relatively more packages fail at later times when rockfall is included. Whereas the base-case CDF rises less steeply (meaning that there are fewer failures) after approximately 300,000 years, the combined CDF increases sharply in this time period. This is probably an artifact of the independent calculation of failures resulting from rockfall and corrosion. The radionuclide inventory available to be transported to the dose-receptor point is smaller for failures at late times because of decay.

Comparing the numbers of failed patches on waste packages resulting from the two failure mechanisms (Figure 10-71), we see that there is only a slight increase for rockfall over the corrosion base case. The difference is greatest at late times, when most packages fail by rockfall.

It is expected, however, that additional patch openings by rockfall may not cause significant differences in radionuclide release rate from the breached waste packages. The patch openings from general corrosion can occur anywhere on the waste package: top, side, or bottom. Rockfall patch openings are assumed to occur only on the top. In the base-case model, once a waste package is breached, radionuclides are released through all openings, regardless of their location. Release rate is dependent on several factors, including seepage flow rate into the package. In the current waste-package degradation model, the limiting factor for waste mobilization is the amount of water that flows through the packages. Thus, additional patch openings in the top do not necessarily increase the mobilization rate of the waste form. Two of the radionuclides that contribute significantly to doses are technetium and neptunium. Technetium is highly soluble, and its advective release is generally limited by its mobilization rate from the waste form. Neptunium is solubility limited, and its release is affected by the advective flow rate.

The total-system analysis code RIP was used to calculate doses. An example time history of dose rates for a rockfall case and the base case is shown in Figure 10-72. The lower dose rates when rockfall is included is undoubtedly a consequence of the modeling assumptions and limitations discussed above.

10.5.2 Water-Table Rise

As part of their evaluation of the likelihood that groundwater level could rise to the height of the repository by any plausible geological process, a panel convened by the National Research Council (the Panel on Coupled Hydrologic/Tectonic/ Hydrothermal Systems at Yucca Mountain) considered the effects of earthquake-induced changes in crustal stresses on the water table. They concluded, based on a review of recent historical earthquakes and the results of modeling, that a water-table response to seismically induced changes in crustal stresses is at least an order of magnitude less than the amount needed to affect the unsaturated status of the proposed repository (NAS/NRC 1992, p. 138). The modeling results suggested that water-table rises of more than a few tens of meters are unlikely to result from earthquake strain release mechanisms (or "seismic pumping"). The EPRI model (McGuire 1990, Sections 3.3.3 and 5.3) estimated rises in the water table following a normal faulting earthquake of 1 to 15 m resulting from a large

(magnitude 7) normal faulting earthquake near Yucca Mountain. Subsequent modeling results by Kemeny and Cook (1992, Table 6.3) explicitly considered uncertainties in stress drop, saturation above the water table, and material properties. These results also suggested that water-table rise as a result of an earthquake likely will be 15 meters or less.

Water-table rise resulting from seismic effects has also been analyzed as supporting investigations for prior YMP TSPAs (Carrigan et al. 1991; Arnold 1996, Gauthier et al. 1995). These calculations also show that the direct effects are transitory, and have little impact on performance. However, a potential PA impact could occur if the water-table-rise event occurred when the unsaturated zone beneath the repository contained a large quantity of radionuclides in transit. Under this scenario, the contaminants would be more rapidly flushed from the unsaturated zone into the saturated zone for transport to the dose receptor point. A higher concentration of radionuclides in the unsaturated zone could occur during a wet climate cycle.

10.5.3 Fault Altering Saturated Zone Flow

The modeling of faulting that occurs outside the repository block is substantially similar to that done for dikes intruding outside the block (see Section 10.4.4). If faults have significantly different hydrologic properties then the country rock, groundwater flow and contaminant transport in the saturated zone could be affected.

Prior analyses (Barr et al. 1996, p. 31) suggest that the most likely locations for faulting are displacement along existing features and splays from, or extensions of, existing faults. Any faulting is expected to be controlled by the regional stresses, with fault reinitiation occurring roughly perpendicular to the least principal stress. Characteristic faulting in the Yucca Mountain region is dip/slip or strike/slip.

As with the dike analysis, the modeling does not address how or why faults can have different hydrologic properties. Hydraulic-conductivity changes of ± 5 orders of magnitude have been assumed in the modeling. Because the analysis makes no distinction between faults or dikes with different hydrologic properties, the same results apply to this case as to the dike analysis. The modeling results can be summarized by noting that contaminant transport can be redirected by faulting, but there is essentially no effect on repository performance.

10.6 NUCLEAR CRITICALITY

The potential for nuclear criticality associated with a geological repository must be considered because the emplaced waste contains fissile materials. The repository systems, particularly the waste package, have been engineered to ensure that criticality is impossible as designed as long as the waste packages are intact. However, over the period of performance of the repository, there are sufficient variabilities and uncertainties in the processes affecting repository systems that the possibility of criticality cannot be positively excluded. Scenarios have been developed to identify events and processes that could lead to criticality. These scenarios are discussed in CRWMS M&O (1997f, Section 5.0). To facilitate the analysis, the types of criticality can be characterized by dividing the possible locations into three categories: inside the waste package, in the rock comprising the repository drifts and the first few meters into the rock beneath the drift

(the near field), and in the far-field rock away from the repository (CRWMS M&O 1997f, Section 4.0).

10.6.1 Nuclear Criticality Analysis Methodology

The general methodology for analysis of scenarios for TSPA-VA that may result in criticality involves five steps (listed below). This methodology is consistent with the evaluations performed by the M&O Waste Package Operations (CRWMS M&O 1998d, Section 3). These steps include the following considerations:

- A. Environmental drivers, including geohydrological, geochemical, and materials-properties events and processes that could lead to a potentially critical configuration. Specify the models and parameters that describe the potentially critical configuration.
- B. Degradation of the waste package internal components, including the removal of the neutron absorber material according to models and parameters that describe the processes leading to the potentially critical configuration.
- C. Neutronics of potentially critical configurations to see if they can sustain a nuclear-critical reaction. For those configurations that can go critical, probability that the environmental, degradation, and waste form properties identified in the previous steps will combine to produce the critical configurations.
- D. Fission output of those configurations that can go critical to determine the steady state effects (e.g., increase in radionuclide inventory and total thermal energy released) and transient effects (e.g., power or radiation pulse).
- E. Impact of criticality effects (e.g., heat, radiation, and chemical changes) on the near-field environment model, particularly the groundwater flow. The increased inventory, together with the groundwater flow, is used to revise the source term for radionuclide transport. Finally, the impacts, if any, on performance-assessment measures (such as dose rate for a critical population) are evaluated.

The considerations listed in Items A and B above determine whether a potentially critical configuration can occur. If a potentially critical configuration does occur, Item C determines whether it actually is critical. If it is critical, Items D and E determine the impacts (if any) on the repository and/or the environment. In general, the following conditions must occur to sustain a criticality: sufficient fissile material, sufficient neutron moderator, a limitation on neutron absorbers, and the geometry of the fissile material and moderator must be favorable. It should be noted that few of the waste forms have sufficient fissile material, or are able to go critical without the presence of neutron moderators.

10.6.1.1 Environmental and Degradation Conditions Required for Potential Critical Configurations

As is discussed in detail in CRWMS M&O (1997f, Section 2), the probability of a nuclear criticality occurring in a dry waste package with intact contents is designed to be zero. The first requirement for development of a potential critical configuration is therefore that the waste package be breached, allowing water to enter and corrode the waste form and waste-package internal criticality-control structures. Potentially critical in-package configurations can then form if the neutron-absorbing material released by this corrosion process becomes soluble so that it can be removed from the waste package by the flowing groundwater. It is also possible for the fissile material released by corrosion of the waste-form to become soluble and to be transported from the corroded waste package to the near-field or far-field rock and form potentially critical configurations there.

The nature of the configurations internal to the waste package is strongly determined by the relative degradation rates of the waste form and the other internal structures. If the waste form degrades faster than the waste-package internal structures, fissile materials can accumulate in the bottom of the waste package away from the neutron absorbers. Conversely, if the waste form is more resistant to corrosion, the waste package can degrade first. Neutron absorbers can then be removed from the vicinity of the fissile material. The former condition is characteristic of the aluminum-matrix DOE spent nuclear fuel, while the latter describes most commercial spent nuclear fuel. Details of these scenarios are given in CRWMS M&O (1997f, Section 4.1.1.3). Plutonium immobilized in glass or ceramic (which will be co-disposed with defense high-level waste) may have the fissile material and waste-package materials degrading at approximately the same rate (also discussed in CRWMS M&O 1997f, Section 4.1.1.1).

Potentially critical configurations that form external to the waste package require that the fissile material be transported from the waste package to another location and be concentrated at that place to provide sufficient fissile fuel for a criticality. The transport process could permit the separation of the mobilized fissile material from mobilized absorbers by sorption or speciation (CRWMS M&O 1997f, Section 4.1.1.2).

As is discussed in detail elsewhere, most of the waste forms have insufficient fissile material to form potentially critical configurations (those for which k_{∞} is less than 1.13) (CRWMS M&O 1997i, Figure 6.1-1). Furthermore, the waste-package design and loading strategy will positively prevent criticality for most conditions in the waste package (CRWMS M&O 1997i, Section 4.1). It is only specific configurations or extreme environmental conditions that may result in potential critical configurations. Identifying and modeling these conditions and parameter values is the ongoing work of the PA and Waste-Package Design organizations.

10.6.1.2 Neutronics Conditions Required for Critical Configurations

Criticality calculations are quite complex, and do not lend themselves directly to abstraction into TSPA analyses. A self-sustaining reaction requires several components. (1) There must be sufficient fissile material present, either U-235 or Pu-239. Other fissile or fissionable nuclides are present, and must be accounted for in the precise criticality calculations required for

regulatory purposes, but their nuclear reactivities and/or amounts are too small to be of significance in determining potentially critical configurations. (2) For spent nuclear fuel with an effective enrichment (ratio of total fissile material, U-235 plus Pu-239, to total U) of approximately 5 percent or less, a neutron moderator is required (Knief 1993, p. 13). Water is the most effective moderator, but silica and carbonates also have moderating properties. For high enrichment, an unmoderated (fast) criticality is possible; however, preliminary analysis indicates that there are no physical mechanisms for achieving the necessary concentration of the fissile material. (3) As part of criticality-control engineering and design, neutron-absorbing materials are incorporated in the waste package. Their presence will prevent criticality even if all the other conditions obtain. Neutron-absorbing material must be limited (proportional to the amount of fissile material) to achieve criticality. (4) Lastly, the fissile material and moderator must be in a geometry favorable for maintaining a sufficiently large neutron population (Knief 1993, p. 9). The occurrence of criticality is measured by the effective neutron multiplication factor, k_{eff} . Criticality requires that $k_{eff} \geq 1.0$; however, NRC regulations may require values below 1.0 to account for inferred model bias, uncertainty in the method of calculation, and safety.

The following is a summary of the k_{eff} calculation methodology; this methodology is described in detail in CRWMS M&O (1998d). The calculation consists of first determining the specifics of the models and parameters describing the potentially critical configuration. Examples are the time of waste-package failure, the type of failure (i.e., bathtub or flow-through), the rate of water seepage into the waste package (all required for in-package criticalities). Examples specifically for external criticalities include processes or geologic features for concentration of fissile material. The next step is determining the fissile isotopic composition of the waste form and the reactivity of the geometric configuration. Isotopic concentrations for commercial SNF are obtained from computer codes contained in the SAS2H sequence of SCALE 4.3 (ORNL 1995), based on the burnup and initial enrichment of individual assemblies, as given in the EIA database. Values of K_{eff} are calculated using the MCNP 4B code (ORNL 1997); this code uses the isotopic compositions of the fissile materials and a detailed model of the geometry to determine a stochastic time history of the neutron population. From this k_{eff} is calculated.

Determination of isotopic concentrations is itself a stochastic process because the relative amounts of fission products generated during reactor operations can vary. The range of isotopic concentrations covered by commercial SNF requires a number of MCNP runs to be made with varying input compositions to get a range of k_{eff} values. The bias and uncertainty in the k_{eff} calculations for a family of waste forms (e.g., commercial SNF) are determined by comparing a suite of measured values for k_{eff} (from commercial reactor critical experiments and other criticality experiments) against the value calculated when using nominal isotopic concentrations. Regulations require that calculated k_{eff} values be adjusted for bias and uncertainty (NRC 1996, 10 CFR 60.131(h)). If k_{eff} is calculated to be 1.0 or above (after taking into account bias and uncertainty), then a critical configuration is presumed to exist and fission output occurs.

10.6.1.3 Calculation of Fission Output from Criticality Events

Fission reactions in a repository environment are controlled by geologic processes. In general, these are much different from the controls available in engineered systems such as reactors. For

a fission reaction to persist, the conditions that resulted in its formation must persist. Changes in any of the required conditions for criticality could either increase or decrease the reaction rate. For example, the water that is required for neutron moderation is provided by flow through geologic media. If heat output from the nuclear reaction evaporates moderating water faster than it is being replenished by dripping the k_{eff} will drop below 1.0, stopping the criticality reaction. Other feedback mechanisms caused by the heat generated include chemical or mechanical changes to the initial configuration. Because the greatest fission output is expected to come from steady-state criticalities (CRWMS M&O 1997i, Section 9.5), violent mechanical changes, such as explosions, are extremely unlikely (see Section 10.6.5).

After determining the conditions under which a steady-state criticality can operate, the duration can be estimated. Limits to the duration include climate changes that reduce the availability of water, exhaustion of the fissile fuel, or reduction in the neutron population as a result of mechanical or physical changes to the geometry of the critical configuration. The increased radionuclide inventory resulting from the criticality can be calculated using a code such as ORIGEN-S (ORNL 1995).

10.6.1.4 Performance-Assessment Analyses

The heat output of the criticality event can be evaluated to see if it represents a significant perturbation on the thermal history of the repository. If not, then groundwater flow and transport from the repository are not affected, so the increased radionuclide inventory can be treated solely as a perturbation on the base-case inventory. Assessment of the impact of the increased radionuclide inventory can be done by a three-stage method.

- *Assume that a critical configuration exists, and calculate the consequences.* As a measure of the PA impact, estimate the number of fissions that occur from the criticality. Compare this number with the number of fissions that have occurred in commercial spent nuclear fuel. For example, assume that the contents of one waste package containing commercial spent nuclear fuel of a given burnup and age have formed a configuration with k_{eff} of 1.0. For these conditions (e.g., the geometry, the amounts of fissile material, moderator, and neutron absorbers present), estimate the duration of the criticality and the number of fissions that would occur. One of the factors that determines whether the additional inventory is a significant perturbation depends on the time at which the criticality event occurs. If the perturbation to the inventory warrants further investigation, then do the next step.
- *Investigate the geologic processes and conditions necessary to create the critical configuration.* By modeling the processes, rates, and timings of the FEPs that must occur to create the critical configuration, additional information can be developed that may change the parameters of the criticality (such as fissile-material availability, moderator, etc.). By recalculating k_{eff} , the power and duration of the criticality and the resulting radionuclide inventory, the significance of the criticality to repository performance (in the form of an alteration to the radionuclide inventory) can be reevaluated. Again, if the

criticality appears to cause a significant perturbation to the inventory, the final step can be undertaken.

- *Perform a TSPA analysis using the modified inventory.* The radionuclide inventory becomes the source term for groundwater flow and transport analyses and dose calculations. Again, the timing of the creation of the additional source term may be a factor. Impact of the criticality on repository performance can be directly reported as an increase in dose or releases as a function of time, or other measure.

10.6.2 Scenarios and Criticality Calculations for Potentially Critical Configurations

CRWMS M&O (1997f, Sections 5.1, 5.2, and 5.3, respectively) identified numerous scenarios that could lead to in-package, near-field, and far-field criticalities. They are summarized in Tables 10-32 through 10-34, from CRWMS M&O (1997f). The terms in the tables are explained in CRWMS M&O (1997f) and this section. The scenarios for TSPA-VA are chosen to be representative of most of the waste types that are emplaced.

10.6.2.1 In-Package Potentially Critical Configurations

Thirteen in-package potentially critical configurations were identified in CRWMS M&O (1997f). Three general classes of fissile waste forms have been evaluated thus far: commercial spent nuclear fuel (CSNF), aluminum-matrix research reactor SNF (owned by DOE), and immobilized Pu-239 (from surplus weapons plutonium) co-disposed with defense high-level waste (DHLW). The CSNF consists of either Zircaloy- or stainless-steel-clad reactor fuel rods; DOE SNF is modeled as being aluminum-clad, with many assemblies having higher enrichment than the CSNF. The immobilized Pu waste form is planned as a very corrosion-resistant ceramic in which the plutonium is dispersed.

Two general moderator configurations were considered: "bathtub," in which only the top of the waste package is breached, so the container fills with water; and "flow-through," where water can flow out the bottom of a waste package. In the bathtub case, the moderator can be liquid water or hydrated clays; in the flow-through case water trapped in the clay serves as the moderator.

Mechanisms to remove the neutron-absorbing materials from the waste-package, criticality-control structures include dissolution of the material containing the absorber and flushing of any dissolved species. The solubility of most of the materials is enhanced by both high and low pH, with solubility typically being lowest for pH close to 7.0.

Table 10-32 lists the potentially critical configurations. In the "Relative Probability" column, 1 means unlikely and 5 means certain. Referring to Table 10-32, the potentially critical configurations considered relatively more likely are IP-1b, IP-2b, IP-3a, IP-3b, IP-4b, and IP-5a. Note that the single most likely configuration identified in Table 10-32, IP-3c, is not considered because the waste package for which it is applicable is not currently planned to be emplaced.

Configurations IP-1b and IP-4b both apply to DOE Al-clad SNF (IP-1b is bathtub, the other is flow-through). Configurations IP-2b and IP-5a apply to Pu-ceramic with the two waste-package failure modes. IP-3a and IP-3b apply to the bathtub configuration for stainless-steel or Zircaloy-clad CSNF, respectively.

The following sections summarize environmental and geologic processes that can lead to potential critical configurations, and analyses done by the M&O Waste-Package Design organization to evaluate some potential critical configurations.

10.6.2.1.1 DOE SNF In-Package Criticalities

The only DOE spent nuclear fuel evaluated thus far is the aluminum-clad/aluminum-matrix research-reactor fuel, most of which has high initial enrichment (typically 93.5 percent) and low burnup (relative to commercial spent nuclear fuel). In the presence of water, the aluminum cladding corrodes to produce a gelatinous degradation product that retains water (CRWMS M&O 1997g, Section 6.3.2). Although the degradation products are relatively insoluble, the uranium oxide (typically hydrated and occupying a larger volume than the original fuel) can be displaced mechanically, ending up in locations ranging from the bottom of the waste package to uniformly distributed throughout the water (approximating a very thick coating on the still intact basket). These are scenarios IP-1b and IP-1a, respectively. CRWMS M&O (1997g, Section 6.5) analyzes several configurations for degraded aluminum-clad spent fuel. The analyses calculate k_{eff} parameterized by the amount of the principal neutron-absorber (gadolinium) present. Additionally, iron oxides can reduce k_{eff} by displacing moderator. CRWMS M&O (1997g, Table 6.5.1.2-2) indicates that k_{eff} ranges from 0.83 to 1.01 depending on the amount of iron oxides and/or gadolinium present. The values of k_{eff} for which criticality is possible or of regulatory concern ($k_{eff} > 0.98$) have 0.10 kg or less of gadolinium present. Waste-package design specifies at least 1 kg of gadolinium; this is 10 times the minimum necessary to prevent criticality; geochemistry analysis indicates that even under the worst case assumptions concerning gadolinium solubility, there will still be 0.4 kg of gadolinium left, which is four times as much absorber present to meet the criticality criterion CRWMS M&O (1997g, Section 7.1).

10.6.2.1.2 In-Package Criticalities of Pu-Ceramic

Consideration is being given to disposal of excess weapons plutonium with defense high-level waste (DHLW). The plutonium would be immobilized in ceramic and included with other (non-fissile) DHLW waste in a waste package (CRWMS M&O 1997h, Section 2.2). In the can-in-canister design, plutonium is loaded into a ceramic, which is embedded in DHLW filler glass inside a pour canister. Five pour canisters fit inside one waste package. If all five canisters are used for co-disposal of plutonium, there is 143 kg plutonium per waste package. However, the analysis summarized in the report (CRWMS M&O 1997h, Sections 2.2, 7.4.1) was based on an earlier formulation of the ceramic. The plutonium can become mobilized as the ceramic degrades; however, the plutonium is very insoluble so any mobilization is very slow. Plutonium-239 has an approximately 24,000-year half-life, decaying to uranium-235, which is generally somewhat less reactive (up to 20 percent) with respect to criticality. Gadolinium is incorporated into the ceramic as the principal neutron absorber. The solubility of gadolinium depends on the pH; at pH 5.5, it can be over 500 times more soluble than at pH 6.5 (CRWMS M&O 1997h,

Table 5.3.4-1). The pH of groundwater is controlled by its passage through country rock, through any concrete drift liner, and through the waste-package and waste-form materials.

The model for formation of a potentially critical configuration assumes the pour canisters are made of stainless steel, which contains chromium. As the stainless steel dissolves, the chromium may form chromic acid, which lowers the pH sufficiently to dissolve gadolinium. The dissolved gadolinium can subsequently be flushed from the waste package. Since this model for the removal of gadolinium is only valid while the stainless steel is corroding, the amount of gadolinium removed will be proportional to the rate of dissolution of the waste form. For a waste-form dissolution rate of $0.003 \text{ g/m}^2/\text{day}$ (a value between the minimum and maximum assigned to this parameter [CRWMS M&O 1997h, Table 7.3-1]), k_{eff} increases from approximately 0.84 at 50,000 years to 0.98 at 80,000 years (CRWMS M&O 1997h, Figure 7.3.2-1). After the stainless steel has completely corroded, (which might occur before 100,000 years), the pH rises to approximately neutral, reducing the solubility of gadolinium so that little more can be flushed from the waste package. At the waste-form corrosion rate used here, the plutonium loading of each waste package would have to be reduced to approximately 50 kg per waste package to preclude criticality (CRWMS M&O 1997h, Section 8.1). The ceramic waste form has subsequently been redesigned to avoid this limitation by the following: (1) use of insoluble hafnium as a supplemental neutron absorber; (2) development of a more robust ceramic formulation to have lower degradation rate.

10.6.2.1.3 Commercial Spent Nuclear Fuel In-Package Criticalities

The characteristic of this class of scenario is that the waste form is much more corrosion resistant than the waste-package internal structures. For some spent fuels, criticality control is provided by borated stainless-steel plates separating spent-fuel assemblies (the basket). (Other spent fuel is sufficiently unreactive that no criticality-control measures are required; some requires absorbers in control rods within the assemblies.) This analysis focuses on the absorber-plate waste packages.

Commercial spent nuclear fuel assemblies include spacers to maintain optimal distance for nuclear reactivity between the individual fuel rods. Fuel-pin spacers are made of highly corrosion-resistant materials. The borated stainless steel is more susceptible to corrosion than either the fuel-pin cladding or the assembly spacers. Three scenarios for waste-form and waste-package degradation are considered: partially degraded basket with intact fuel, fully degraded basket with intact fuel, and fully degraded basket with degraded fuel.

As the waste-package basket degrades, iron oxide accumulates in the waste package while the boron dissolves from the corroded portion of the borated stainless steel, and is flushed from the waste package. The iron oxide may be distributed in various ways throughout the package void space. The two extremes for the spatial distribution of this material are settled to the point of lowest gravitational energy (leaving some fuel rods exposed to clear water), or uniformly distributed throughout the package void space. In general in a flooded package with completely degraded carbon steel structural components, degradation of the borated stainless steel results in a 12% increase in K_{eff} with the settled oxide cases having k_{eff} values 3 to 5% higher than the uniform cases. For a given configuration, K_{eff} values peak in the 10,000 to 35,000 year time frame, and drop by as much as 5% by 100,000 years. (CRWMS M&O 1997i, Section 6.2.1).

When the basket is fully degraded, over half the original void space at the bottom of the waste package is filled with oxide. The balance of the fuel assemblies can be covered by water, depending on the amount filling the waste package. The reactivity of the spent fuel depends on its initial enrichment and the amount of burnup in the reactor. Although high burnup reduces the amount of U-235 remaining, plutonium isotopes are present at higher concentrations. At the time of peak reactivity, k_{eff} is approximately 0.95 for 3 percent-enrichment, 23.5 GWd/MTU spent fuel, and 0.94 for 4.9 percent enrichment, 44 GWd/MTU fuel. Both calculations assume a flooded package with settled oxide at the bottom, covering all but the top 20 cm of the stacked assemblies (CRWMS M&O 1997i, Section 6.2.2).

When both the fuel assemblies and the basket degrade, the fuel rods collapse in the iron oxide at the bottom of the waste package. Collapse of the rods reduces the space available for moderator surrounding the fissile material so that as the rods get closer together, the k_{eff} value decreases. This effect is most strongly demonstrated for the case with iron oxide uniformly distributed throughout the waste package, because the settled oxide already has the water largely excluded from the lower portion of the SNF assembly stack. In this case, using one of the most reactive commercial SNF, assemblies k_{eff} goes from 0.99 for rods with original spacing to 0.65 for all rods touching in a cylindrical segment at the bottom of the waste package (CRWMS M&O 1997i, Section 6.2.3).

A preliminary evaluation of the cumulative probability that a commercial PWR waste package would exceed a K_{eff} of 0.98 as result of flooding and internal degradation was performed using a monte carlo simulation (CRWMS M&O 1998d, Appendix C). For each trial, distributions were sampled to determine time of package breach, presence of a dripping fracture above the package, duration of flooding (if any), corrosion rate of borated stainless steel, and burnup/enrichment of contained fuel. If k_{eff} was calculated to exceed 0.98 at any time during the degradation of the package, that time was recorded and the next realization begun. The summation of the number of times the limit was exceeded, divided by the total number of trials, represents the cumulative probability of criticality to that time. The results indicate that not more than one PWR package would be expected to exceed this limit within 1 million years.

10.6.2.2 External Potentially Critical Configurations

External critical configurations include those that develop immediately outside the waste package and those in the country rock, potentially a great distance from the repository. After the waste package is breached, the waste form can be mobilized, to its limit of solubility, and be transported into the drift and into the fractures of the rock beneath the drift. Both fissile materials and absorbers can be transported. Because of different solubilities, chemical reactions with the fracture walls, and retardation characteristics, the fissile material and absorbers may preferentially separate into spatially distinct concentrations after being transported away from the waste package. This is a mechanism analogous to the chromatographic separation used extensively in chemical testing. The solubilities of fissile nuclides used in the TSPA-VA analyses range from approximately 1.2×10^{-4} g/L to 8.8×10^{-3} g/L (data from the RIP total-system analyzer code). To achieve a potentially critical configuration requires concentrations of fissile materials on the order of several g/L (ANSI 1983, Tables 6 and 7).

Tables 10-33 and 10-34 list scenarios developed describing potential critical configurations for near-field and far-field locations, respectively. Only scenarios NF-4a, for the near field, and FF-3d for the far field were considered even remotely likely scenarios (CRWMS M&O 1997f, Sections 5.2 and 5.3, and p. 43).

10.6.2.2.1 Near-Field Criticalities for Immobilized Plutonium

Scenario NF-4a considers ponding of a fissile solute in a topographic low spot in a repository drift. The low rate of water seepage into the drifts and the large permeability of the invert material and drift walls make this scenario quite unlikely. However, processes to plug the pore and fractures in the drift materials have been suggested, so this scenario has been investigated (CRWMS M&O 1996f, Section 4.2.2).

Fissile solutes from several waste packages could potentially accumulate at a single low spot in the drift. The Waste-Package Design organization has analyzed the geochemical reactions that could lead to concentration of fissile material in a pond (CRWMS M&O 1998b, Section 6.1). Potential reactions are sorption of solutes onto the concrete or tuff forming the drift invert. The reaction-path geochemistry code EQ6 (Wolery and Daveler 1992) was used to calculate the deposition of solutes in the drift materials. The amount of deposition will generally be proportional to the amount of solute in solution. The solubilities of uranium and plutonium are near their maxima at pH 10 (approximately 6000 parts per million uranium and 78 ppm plutonium, compared with 10^{-3} ppm uranium and 1.6×10^{-7} ppm plutonium at pH 7 [CRWMS M&O 1998b, Section 5.3]). Hence the amount of fissile material carried out of the waste package, to become the source term for external criticality, will be highest during the period of high pH. In the immobilized plutonium co-disposal waste package, the degradation of DHLW glass is the principal agent for an increase in pH to values over 10, so the period of greatest fissile deposition potential will correspond to the period of highest potential for increased fissile deposition.

Preliminary EQ6 analyses predict that considerable total solids can be deposited in the invert material from the degradation of defense high-level waste glass, but that most are non-fissile materials. Consequently, less than 0.08 percent of the invert void space is filled by fissile materials (CRWMS M&O 1998b, Section 6.1.3). Criticality calculations show that volume fractions of 1 percent to 4 percent, in fractures having aperture volume equal to 10 percent of the total rock volume (very conservative assumptions), are required to have k_{eff} values near 1.0 (CRWMS M&O 1998b, Section 7.2).

10.6.2.2.2 Far-Field Criticalities for Immobilized Plutonium

Several scenarios for potentially critical-configuration formation in the far field are identified in CRWMS M&O (1997c, Section 4.3.2.1). The probabilities of most scenarios are considered very low because of the very dilute groundwater solution and the extremely low density of deposits that could be efficient accumulators (if such deposits could even exist at Yucca Mountain). Processes based on uranium ore-body analogs have been investigated as possible ways to form critical configurations (CRWMS M&O 1998b, Section 6.2). The primary requirements for epigenetic ore-body formation are a source of dissolved uranium (e.g., the repository), and a localized region where the uranium can accumulate by some geochemical or

physical means. Most uranium deposits have occurred in reducing environments (CRWMS M&O 1998b, Section 6.2.4). Deposition in unconformities could occur by precipitation in void spaces caused by fracturing or faulting; the reducing environment could be hydrocarbon-containing fluids moving upward from basement rock through the unconformity. Calcrete uranium deposits rely on the oxidation of vanadium ions and the simultaneous reduction and precipitation of uranium as groundwaters move through constricted channels. Vanadium is not found in sufficient abundance in the Yucca Mountain area to make this scenario credible.

Sandstone uranium deposits are relatively common in the Southwest; reducing agents include organic deposits such as paleo-logs, coal or lignite, or petroleum-bearing sands and shales. Such reducing agents are thought to have created the Colorado Plateau uranium deposits. The uranium content of most deposits are in the range 0.1 percent to 0.35 percent UO_2 . This concentration is too low to form a critical configuration, although some petrified logs have been found in the Colorado Plateau with uranium contents of more than 15 percent (CRWMS M&O 1998b, Section 6.2.4.2). Buried logs are frequently associated with ash deposits, so their existence in the Yucca Mountain region cannot be ruled out. Although it is conceivable that critical configurations could form in the tuffs at Yucca Mountain, the current understanding of the Yucca Mountain site makes it extremely unlikely that reducing features or processes will be discovered (CRWMS M&O 1998b, Section 6.2.5).

Lastly, if uranium is transported unmixed to the Franklin Lake Playa (an expected outfall for the regional flow system), organic and inorganic materials associated with the lake-bed deposits there can reduce and potentially concentrate it. Potential critical configurations could develop where there is sufficient water. The water that transports the uranium to the point of concentration is likely sufficient to provide the moderator for the critical configuration. However, the Nevada and California desert area is known for its deposits of borates (Lyday 1985, pp.91-92); it is therefore not unlikely that such deposits will be found at Franklin Lake Playa. The existence of these naturally occurring absorbers must be considered when evaluating these potential critical configurations.

10.6.3 Fission-Output Calculations for Critical Configurations

The Waste-Package Design organization has performed fission-output calculations on several critical configurations; two are discussed here. These analyses determine the radionuclide-inventory increase resulting from the criticality event and other transient effects, such as heat output. Both an in-package and an external criticality have been analyzed (CRWMS M&O 1996c).

10.6.3.1 Fission-Output Calculations for In-Package Criticality

For a critical configuration to operate as a nuclear reactor in a geological environment, the processes increasing nuclear reactivity and those reducing it must be in balance. Reactivity increases as water dissolves and removes iron and boron from the waste-package interior. Reactivity decreases as water is removed by boiling or evaporation from the heat generated by the fission reaction. The maximum steady-state reactivity is estimated by calculating the power output that balances the bulk waste-package water removal by evaporation against the water

input from drips into the package. As modeled in CRWMS M&O (1996c, Section 7.1.2), the steady-state power output of the reactor is 2.18 kW, using a dripping rate of 191 L/yr, based on the drip rates provided in CRWMS M&O (1995, Section 7.4), (equivalent to a percolation rate of 42 mm/year – see Chapter 2 of this document). The equilibrium temperature is 57.4°C.

The heat output from the criticality is compared with the thermal profile of an average 21-PWR waste package during the time of the 10,000-year criticality. Figure 10-73 shows the incremental heat output from the criticality. At the time of the criticality, the average 21-PWR waste package emits about 100 watts of heat (see Section 3.5.3.6, this document). The additional 2 kW from the criticality raises the heat output equivalent to that of waste emplaced for 100 years.

The criticality is assumed to start at 15,000 years after emplacement. Because of radioactive decay, this is the time at which the reactivity of the PWR design-basis fuel is at its peak (CRWMS M&O 1997i, Section 6.2.2). The critical configuration is assumed to be a bathtub waste-package failure, removal of boron and iron oxides by flushing (i.e., overflowing of the bathtub), and complete basket collapse. Reaction durations of 1,000, 5,000 and 10,000 years have been modeled; 10,000 years is considered the upper limit for maintaining the conditions permitting criticality, including high water-drip rate, sufficient fissile material, and no failure in the bottom of the waste package that would drain the water (CRWMS M&O 1996c, Section 7.2.1). After a 10,000-year criticality, the total increase in radioactivity, compared with the radioactive inventory for the same waste that had not undergone a criticality, is 24 percent. The events leading to criticality are sufficiently improbable that only individual waste packages are expected to form critical configurations. Comparisons of radionuclide inventory increments for the nine radionuclides used in TSPA-VA analyses are presented in Figure 10-74. The total inventory difference for the nine radionuclides is only about 9%. The nine radionuclides included in the TSPA-VA analyses are the dominant ones for dose-rate calculations. Thus, the overall 24% increase is not relevant from a risk perspective. The fissile nuclides change very little; both U-234 and Pu-239 increase by less than 10 percent, while Pu-242 decreases by about 5 percent. The essentially constant Pu-239 inventory is a consequence of competing burnup and breeding processes. Pu-242 is burnt up by the criticality.

10.6.4 PA Consequences of Critical Configurations

Applying the three-levels of discrimination listed in Section 10.6.1.4 above to estimate PA consequences of a criticality, it is expected that a 9 percent inventory increase has no measurable effect on dose rates. Despite the indications of this screening, the increased radionuclide inventory has been used as the source term for a groundwater-flow and transport analysis using the RIP TSPA analyzer. The RIP analysis assumes base-case hydrologic conditions (i.e., there is no alteration of the EBS or near-field models to account for the increased heat output of the criticality). The radionuclide source term is identical with the base-case source until 15,000 years, at which point the source is increased by the amounts caused by the 10,000-year criticality. Waste-form release rates are the same as the base-case rates. The PA consequences of the increased radionuclide inventory are shown in Figure 10-75. As expected, there is no significant contribution to the dose rates from the criticality.

These results are for a criticality in a single waste package. A qualitative estimate of the probability of criticality occurring in the entire repository can be made. Fissile material

undergoing an in-package criticality is the most reactive (from a postclosure criticality standpoint) about 15,000 years after emplacement. In this period, most waste packages have not corroded sufficiently to permit water to fill the package. The bathtub mode for waste-package failure is not the most common way that waste packages corrode. Failure modes are discussed in Chapter 5.4. About half the time, holes form in the top of the waste package. Sometime thereafter, holes also develop in the bottom, allowing the water to drain. In the summary, the probabilities of in-package criticalities require several unlikely events to occur and are therefore quite unlikely. The following is a summary of the physical and chemical processes that act to make repository criticality an unlikely event:

- Most of the waste packages cannot go critical because they do not have sufficient fissile material (or have sufficient enrichment) to form a critical mass.
- Of the waste packages that can go critical, commercial spent fuel waste packages form the majority. For these waste packages the criticality potential drops by 30% for times beyond 40,000 years, which significantly decreases the criticality probability because only 10% of the waste packages are expected to even be breached by 40,000 years.
- Of the waste packages that can go critical, most require some form of water retention to provide moderation. Models of the waste package corrosion process indicate that only 25% of the waste packages will hold a significant amount of water for the time required to flush the neutron absorbers that have been added for criticality prevention.

Figure 10-76 shows the difference between the total radionuclide inventories between the base case and the base case plus criticality. The greatest difference (a dose rate difference of 0.035 mrem/yr) occurs at approximately 30,000 years. There is another peak in the dose rate difference at 70,000 years. The first occurs from Tc-99 and I-129 reaching the dose-receptor point, and the peak at 70,000 years is from the presence of Np-237. Both Tc-99 and I-129 are not significantly retarded during groundwater transport, so their doses occur shortly after they are created by the criticality.

Figure 10-77 shows the time histories for four of the radionuclides. (At this early time in repository history, most of the other radionuclide doses are essentially zero.) The peak in dose-rate difference in Figure 10-76 occurring at 30,000 years can be seen to be caused by the Tc-99 and, to a lesser extent, the I-129. The difference at 70,000 years is from the Np-237.

The contributions of individual radionuclides to the increase in the dose rate from criticality is shown in Figure 10-78. The maximum increase in dose rate is approximately 0.035 mrem/year. One peak occurs at 30,000 years from Tc-99, and another at 75,000 years from Np-237.

The fact that radionuclide inventory increases and thermal output from transient events is small, even compared with steady-state criticalities, means that mechanical disruption of the waste package or the EBS from criticality is considered incredible.

The extremely low probability of having a criticality outside the waste package means that external criticalities have essentially no PA impact. For example, in CRWMS M&O (1998b), the consequences of a 4,000-year criticality of Pu-239 in fractured tuff has been evaluated. The

findings are that immediately after the criticality shuts down, the total radioactivity is 560 Ci. Of this amount, 479 Ci result from radioactive decay of the plutonium remaining, and 81 Ci are from fission products. Thus, in this example, the criticality increases the radioactivity by 14%. At 20000 years after the end of the criticality, the excess radiation from the fission products is only 3% of the total.

10.6.5 Potential for Autocatalytic Criticality in a Geologic Repository

It has been suggested (Bowman and Venneri 1996) that a transient external criticality with a large mass of highly enriched fissile material could have sufficient positive reactivity feedback (due to overmoderation, a condition that can increase k_{eff} as water is removed from the system), and could be sufficiently confined by the rock, to produce a power pulse large enough to be classified as an explosion (Bowman and Venneri 1996, p. 280). The following are reasons why such a positive-feedback transient event is far less likely than the already incredible external criticality:

- It will be nearly impossible to accumulate a large enough mass because the few waste packages containing highly enriched uranium (or plutonium) will be widely interspersed among the much greater number of packages containing low enriched material. As multiple waste packages fail in the vicinity of the highly enriched material, the effective enrichment would be reduced (Van Konynenburg 1996, p. 306).
- The slow accumulation of such a large mass of fissile material (over approximately a million years) is entirely inconsistent with the rapid reactivity insertion necessary for a transient criticality. With slow accumulation, it would be nearly impossible to accumulate an overmoderated mass without going through a small criticality that would disrupt the mass and consequently preclude the possibility of reaching the overmoderated condition (Van Konynenburg 1996, pp. 316 ff.).

10.7 HUMAN INTRUSION

Human intrusion analyses are handled differently from the other three disturbances in TSPA-VA. Based on the recommendation of the National Academy of Sciences panel on technical bases for Yucca Mountain standards (NAS/NRC 1995, Chapter 4), human-intrusion risks are not incorporated into the overall total-system risk evaluation. Instead, the consequences of a stylized human-intrusion scenario are calculated to judge whether the repository system is inherently resilient to this class of disturbance. Additionally, only a few cases are analyzed, rather than a sufficient number to provide a stochastic measure of performance.

Prior TSPA analyses have modeled direct surface releases that result from inadvertent drilling activities at the repository (Barnard et al. 1992, Chapter 6; Wilson et al. 1994, Chapter 16). The analyses showed that significant releases of radionuclides did not occur from this disturbance. Furthermore, releases of this type (i.e., to drillers or others at the surface where the radionuclides are deposited) are not a discriminatory measure of the quality of repository design or siting choices.

As suggested by the NAS panel, a drilling scenario in which waste is transported directly to the saturated zone is an example of a stylized analysis. Additionally, the Environmental Protection Agency has informally provided guidelines for a similar human-intrusion scenario that specifies more information on what should be modeled. Details of the suggested scenario are:

- Drilling techniques and drill size are characteristic of groundwater exploration in the Yucca Mountain region; one borehole is drilled.
- At some time in the future after repository closure, a waste package is damaged by a drilling operation; the time should be the earliest time that current drilling technology and practices can lead to waste-package penetration.
- Drilling continues in such a way that a continuous path is created from the repository horizon to an aquifer underlying Yucca Mountain.
- Waste from the damaged package falls down the drill hole to the bottom, where it remains under water.
- As the waste degrades (by dissolution or colloid formation), it is transported to the accessible environment.

Modeling of this scenario does not dwell on the mechanics of penetration of the waste package. We assume that the drill passes vertically through the waste package along the diameter and continues to the water table. The calculation is based on one drilling event into the repository. Determining the potential number of drill holes into the repository over any length of time requires making predictions about future human behavior and technology, neither of which can be substantiated. If more than one drill hole is assumed, the results can be scaled for the number selected.

We also assume that the drilling process thoroughly breaks up the waste form, so CSNF is unprotected by the Zircaloy cladding, and DHLW glass is shattered. Furthermore, because unsaturated zone transport is bypassed, radionuclides that would otherwise not be transported are also available (in this analysis no additional radionuclides are considered, however).

One assumption of the stylized drilling scenario is that the borehole is improperly sealed after it is abandoned by the driller. An open borehole could permit surface water to flow down the borehole and dissolve waste from the waste package. Eventually the hole will seal itself and this process stops. Additional surface water is not expected to contribute significantly to the dissolution of waste and is not considered in the analysis.

10.7.1 Time of Occurrence of Drilling Incident

The informal EPA guidance states that "... the time should be the earliest time that current drilling technology and practices can lead to waste-package penetration...". Because standard diamond-tipped tri-cone drilling bits are designed to chip away rock, rather than drill through metal as an auger can, it is an open question whether the rock bit would penetrate a metal waste package at all. If we assume it can, it is more likely that penetration could occur when the CAM

was substantially degraded or absent. As other work on waste-package degradation has shown (see Figure 10-61), the CAM requires approximately 10,000 years to degrade by 50 percent, and about 30,000 years to degrade by 70 to 80 percent. As a TSPA-VA abstraction, we assume CAM degradation by over 50 percent is necessary in order to allow waste package penetration.

10.7.2 Amount of Waste Removed by drilling

When a drill goes through a waste package, more than the drilled-out volume of waste can be removed from the package by action of the drilling fluid. Based on TSPA-93 analyses, neither the size of the drill bit nor the amount of waste removed from the package has a significant effect on the consequences (Wilson et al. 1994, Section 16.4). The TSPA-93 analysis assumed that a volume of waste defined by a cylinder twice the diameter of the drill bit was removed from the container. (TSPA-93 also modeled the case where the entire 10 metric tons of waste were removed from a package; radionuclide releases increased by about two orders of magnitude.) Drill-bit sizes range from 16 cm for exploration boreholes to 61 cm for oil-production. A large-size groundwater-exploration bit is 21 cm (8.5 in); this size is assumed for the analysis. A 21-cm drill bit removes 0.05 m³ of waste in the hole that is drilled through the waste package (whose diameter is approximately 1.5 m). Circulation of drilling fluids inside the waste package is assumed to double the diameter of the hole cut through the waste. Furthermore, the circulating fluid could remove any loose material or fines elsewhere inside the waste package. Although the circulation flow is designed to bring these materials to the surface, we assume they are available to fall down the borehole to the saturated zone. To include this uncertainty, we assume that between 0.05 and 0.25 m³ of waste is removed from the waste package, and is a uniform distribution. (Causing all 10 metric tons of waste to fall down the borehole does not seem remotely realistic. Even if it could all be mobilized by the drilling fluid, most would be carried to the surface by the circulating fluid.)

Parameter	Minimum	Maximum	Distribution Type
Volume of waste dropped down borehole	0.05m ³	0.25m ³	Uniform

10.7.3 Source Term Calculation

To calculate the source term for the human-intrusion analyses we must develop two factors:

- The amount of waste carried to the saturated zone
- The rate of mobilization of waste in saturated-zone waters.

The volume of waste removed by drilling is assumed to be between 0.05 and 0.25 m³, as discussed in the section above. Using the density of UO₂ (11000 kg/m³), masses range between 550 and 2750 kg of waste. The rate of mobilization of waste is a function of several factors.

- The dissolution rate of spent fuel in saturated-zone waters
- The specific surface area of the waste
- Solubilities of the radionuclides being tracked by the PA code RIP.

10.7.3.1 Waste-Form Dissolution Rate in Saturated-Zone Waters

The waste-form degradation task for TSPA-VA has developed a model for the intrinsic dissolution rate for CSNF. See Chapter 6 of this document. The model is a function of temperature, pH, total carbonate, oxygen, and fissile-material burnup. The model was developed for dissolution in waste packages under atmospheric conditions where the fuel is exposed to dripping water. A regression fit against "flow-through" test data has been determined. The investigations were high-flow-rate experiments (Gray et al. 1992) performed on single grains of fuel for several tens of days. All distributions are assumed to be uniform. The variables addressed in the tests are given in the following table:

Parameter	Minimum	Maximum	Units	Distribution Type
Temperature	21	78	°C	uniform
Carbonate	0.2	20	mmole/L	uniform
Oxygen	0.2	20	% atm	uniform
pH	8	10	—	uniform
Burnup	20	25	MWd/kg U	uniform

The details of the regression fit to dissolution data are given in Chapter 6 of this document. Dissolution rates calculated for spent fuel in waste packages range from 1.3 mg/m²-day to 7 mg/m²-day.

Waste immersed in saturated-zone water is exposed to a different environment. Saturated-zone waters are modeled as having the following parameter values.

Parameter	Minimum	Maximum	Units	Distribution Type
temperature	22.7	57	°C	Uniform
carbonate	0.00059	0.196	mmole/L	Uniform
oxygen	3.5	6.1	mg/L	Log-uniform
pH	6.6	9	—	Uniform

For the human-intrusion scenario, we apply the waste-form dissolution-rate model using conditions characteristic of the saturated-zone waters. Primarily, there is less oxygen because the waste is assumed to be submerged, rather than in air. Saturated-zone waters are also considered to have less carbonate than those in the unsaturated zone have. The waste-form dissolution model assumes the pH is in the range 8 to 10. The model may not be applicable at lower pH values.

Using the saturated-zone parameters, a range of dissolution rates has been calculated. Parameter values for the model have been randomly selected from the ranges given above. (To convert the

oxygen parameter in the above table into units used in the model, we apply the ideal gas law for air at 1 atm, and 30°C. Under these conditions there are 0.04 moles of air per liter, and an equal number of moles of oxygen. With a molecular weight of 32, 3.5 mg/L O₂ is 0.27 percent, and 6.1 mg/L O₂ is 0.47 percent.) Because of the potential inapplicability of the model at lower pH values, a minimum pH of 7 was used. A range of dissolution rates in saturated-zone water of 0.0037 to 1.55 mg/m²-day is calculated. Figure 10-79 shows the distribution of rates for the regular-burnup case (burnup in the range 20 to 25 GWd/MTU).

10.7.3.2 Surface-Area Determinations of Spent-Fuel

The surface area of the spent fuel is used to determine the fractional dissolution for use in the PA analysis code. As is discussed in the volcanic enhanced source-term analysis (Section 10.4.3.4.2), specific area of spent fuel ranges from 980 cm²/g for spent-fuel grains to 20 cm²/g for particles (Gray and Wilson 1995, Table 2.2). As a TSPA-VA abstraction, we assume the waste is extensively pulverized, and that the range of specific surface areas is from 800 to 980 cm²/g. Larger specific surface areas provide more area for dissolution, and are thus conservative. When UO₂ oxidizes it expands and becomes pulverized. The surface-area values used are therefore also appropriate for mechanically pulverized spent fuel.

Parameter	Minimum	Maximum	Distribution Type
Specific surface area of waste	800 cm ² /g	980 cm ² /g	uniform

These two factors are used to calculate a fractional dissolution rate per year. Using the range of dissolution rates developed in Section 10.7.3.1 and the range of specific surface areas given above, 100 random samples of these parameters produces a range of fractional dissolution rates. Figure 10-80 shows the distribution:

For the human-intrusion calculation, the minimum and maximum rates have been used in the source-term determination. The minimum is 0.0005/year, and the maximum is 0.05/year. The inverse of the fractional dissolution rate is the number of years it would take to dissolve all the waste, assuming a sufficiently large volume of water is available.

10.7.3.3 Amount of water flowing over waste

The saturated-zone flow and transport analysis (Chapter 8 of this document) uses six source zones to model the interface between the water arriving from the unsaturated zone and the flow tubes used to represent saturated-zone flow (see Figure 8-25 in Chapter 8). The volumetric fluxes through these source zones are considered to be the water available to dissolve the waste that has fallen to the water table. The values for long-term-average climate range from 11,303 m³/year in zone 6 to 55,000 m³/year in zone 5 (see Table 8-13 in Chapter 8). The long-term-average is used because the time of the occurrence of the drilling incident is 10000 years. For

the human-intrusion analysis, a volumetric flux value of 24,000 m³/year has been used, representing the average over all six zones.

The rock in the saturated zone surrounding the 21-cm borehole is a source for water for dissolution of the waste. As a conservative assumption, a rock volume given by 10 times the borehole diameter as the source of water for dissolution is used. Depending on the fracture connectivity, the water available for dissolution could vary greatly, but the volume used in this analysis should be bounding. For a repository area of 3×10^6 m² (741 acres), the average source zone area is 5×10^5 m². A 2.1-m-diameter source area represents approximately 7×10^{-6} of the average source zone. Thus, of the 24,380 m³/year volumetric flux in the source zone, 0.169 m³/year flows over the waste through this source area.

10.7.3.4 Mass of contaminants dissolved

The nine radionuclides tracked for the base-case analyses are also used for this analysis (see Section 7.5 of this document). To determine the amounts available to be transported, one first determines the inventories of the radionuclides at the 10,000-year time of the drilling incident. This is done using the Characteristics Database (discussed in Section 10.4.2.10.1). The fractional dissolution rate of spent fuel is then used to calculate the maximum mass per year that can dissolve. Next, the solubilities of each radionuclide (given in grams of each radionuclide per m³ of water) are used to determine the volumes of water necessary per year to dissolve the masses of each radionuclide available. From Section 10.7.3.3 we have the volume of water flowing over the waste per year, so this number can be compared with the volume required for dissolution to see if the availability of the radionuclide is solubility limited. If the radionuclide is solubility limited, then the mass per year available for transport is reduced to the amount available from dissolution. Table 10-35 gives the parameters used to determine dissolved contaminant mass.

The table shows that there are 0.0845 g/MTU of C-14 contained in the waste after 10,000 years. Therefore, 550 kg (0.55 MTU) of waste contains 0.047 g of C-14. At a fractional dissolution rate of 0.0501/year, 0.0023 g of C-14 can dissolve in one year. With a solubility limit of 12,000 g/m³, it requires only 1.95×10^{-7} m³/year to dissolve the 0.0023 g of C-14. Since 0.169 m³/year flows into the borehole, the C-14 source is not solubility limited, and its solubility factor is 1.0. The amount of C-14 available as a radionuclide source is therefore 0.0023 g/year. Lastly, because the C-14 is not solubility limited, it can be mobilized at the rate of the waste dissolution. A fractional rate of 0.0501/year implies that it takes 19.9 years to dissolve all the waste.

In contrast, the 1760 g/MTU of Np-237 in the 10,000-year inventory (shown in Table 10-35) has limited solubility. It requires 144 m³/year of water to dissolve the Np-237, but there is only 0.169 m³/year flowing through the borehole. Thus, there is only 0.057 g/year of Np-237 that is available to be transported. Because of the low dissolution rate, the Np-237 dissolves for 16,946 years before being exhausted from the waste.

10.7.3.5 RIP Analysis

The base-case model was modified to allow for simulations of the disruption of the repository as a result of a human-intrusion event by creating a new source term. The new source term contains the mass of the inventory that is affected by the human-intrusion event. The initial mass of individual radionuclides is obtained from the Characteristics Database (CDB) System LWR Radiological PC Database (DOE 1992). This program contains information generated by ORIGEN2 on the radiological characteristics of spent nuclear fuel from commercial light water reactors. The inputs to this program are that the spent fuel was PWR fuel with a burnup of 33,000 MWd with the standard initial enrichment of 3.30 percent. The mass of radionuclides given by the CDB is then input into the new source term and RIP accounts for decay. There are two exceptions though; since the base-case model does not directly account for ingrowth of the radionuclides, those that incur ingrowth (Np-237 and U-234) must have their masses adjusted. The Np-237 and U-234 masses were adjusted by using the CDB to estimate the masses of Np-237 and U-234 at 10,000 years and then using the decay equation to calculate the necessary starting masses. This is consistent with the treatment of radionuclides with ingrowth in the base-case analyses. For the cases in which 2.7 metric tons of spent fuel is disrupted by the human-intrusion event, the initial inventory of the nine radionuclides in the human-intrusion source term are given in Table 10-36.

For the cases in which 0.55 MTU metric tons of spent fuel is disrupted by the human-intrusion event, the initial inventory of the nine radionuclides in the human-intrusion source term are given in Table 10-37.

The RIP simulations used two matrix-degradation rates for the human-intrusion, source-term inventory, 0.0501 and 1.0×10^4 (fraction/year).

The human-intrusion source-term-container, failure definitions (primary and secondary) are defined in such a way that none of the inventory is available until the time of the intrusion event (10,000 years); then all of it is available in accordance with the defined matrix degradation rate.

Finally, a new waste-form cell pathway is created for the human-intrusion source term. This cell pathway (WFHIS) is advectively connected to the existing UZ6OUT cell with a flow rate of $0.169 \text{ m}^3/\text{year}$.

10.7.3.6 Cases Modeled

Four cases have been modeled. All modeling assumes that the drilling incident occurs at 10,000 years, when at least 50 percent of the waste-package outer barrier has corroded away. The four cases are combinations of the mass of waste dropped down the borehole and dissolution rate of the spent-fuel in the saturated-zone water. The two masses used are the minimum and maximum of 100 randomly chosen samples falling between the limits specified in Section 10.7.2 above. The dissolution rates used are the maximum and minimum of 100 random simulations of the waste-form dissolution model given in Section 10.7.3.1. The cases are labeled as follows:

- Large mass of waste/High spent-fuel dissolution rate: Hi-Hi

- Large mass of waste/Low spent-fuel dissolution rate: Hi-Lo
- Small mass of waste/High spent-fuel dissolution rate: Lo-Hi
- Small mass of waste/Low spent-fuel dissolution rate: Lo-Lo

10.7.3.7 Results of Human-Intrusion Modeling

Figure 10-81 shows the individual time histories of the nine radionuclides modeled. The first contaminants from the human-intrusion incident arrive at the dose-receptor point about 2,000 years after the incident. Because of their high solubilities, Tc-99, I-129, and C-14 are all quickly flushed through the system. Np-237 and U-234 both increase to higher, approximately constant values by about 20,000 years. The other contaminants either have low dissolution rates or their transport is retarded so they arrive later and increase more slowly.

Figure 10-82 shows the dose-rate time histories for the extreme human-intrusion cases analyzed (i.e., cases Hi-Hi and Lo-Lo). The inset graph in Figure 10-82 shows the dose rates from 10,000 to 20,000 years. The Hi-Hi peak in this time period is approximately 145 times the base-case dose rate at 12,000 years. The Lo-Lo dose rate is approximately 3.7 times that of the base case at the same time. By about 15,000 years, the dose rates again closely track the base case. At about 50,000 years, the dose rates diverge again, as can be seen in Figure 10-82. After about 150,000 years, the dose rates for all human-intrusion cases again track the base-case time history.

Dissolution rate has the greatest effect on the dose rate. Figure 10-83 shows the sensitivity of results to the dissolution rate. There is a noticeable difference between the high-dissolution-rate and low-dissolution-rate cases, but the large-mass and small-mass dose-rate profiles are indistinguishable.

Figure 10-83 also shows that, at approximately 50,000 years, there is a plateau in the dose rates for the human-intrusion cases. The low-mass/low-dissolution rate case decreases to the base-case level by about 130,000 years, but the high-mass/high-dissolution rate case remains higher than the base case until about 200,000 years.

In terms of the dose to a critical group over 100,000 years, the effects of human intrusion are small (an approximate four-times increase over the base-case dose rate for about 50,000 years). Over 1,000,000 years, this increase over the base case is unlikely to be significant. At times closer to the human-intrusion incident, the increased dose rates can be much larger than the corresponding base-case rates.

10.8 SUMMARY AND RECOMMENDATIONS

Four disturbed scenario classes have been incorporated for TSPA-VA.

- Igneous activity
- Seismic activity
- Nuclear criticality
- Human intrusion.

Altogether, eight different scenarios have been investigated.

- Direct volcanic releases
- Magmatic-enhanced groundwater-transport radionuclide source term
- Indirect igneous effects
- Rockfall
- Indirect seismic effects
- In-package criticality
- External criticality
- Human-intrusion drilling.

Repository performance measures (i.e., radiation dose rates at 20 km from the repository) have been calculated for five of these scenarios.

- Direct volcanic releases
- Magmatic-enhanced source term
- Rockfall
- In-package criticality
- Human intrusion.

Performance measures for indirect igneous effects, indirect seismic effects, and external criticality have not been calculated. In all cases, the performance effects on the base case would have been undetectable. Refer to Section 10.4.4.3 for a discussion of the performance consequences of indirect igneous effects. Section 10.6.4 gives the increase in source term for an external criticality.

The emphasis for the igneous and seismic analyses has been to develop a credible, physically based radionuclide source term to be used by the TSPA radionuclide-transport and dispersal models.

10.8.1 Summary of Source-Term Model Development

The source term for igneous interactions considers several processes that are required for waste-package mechanical breach. These include probabilities and mechanisms for contact between an intrusion and a waste package, and mechanisms for mechanical breach of the affected waste packages. For direct volcanic releases, the source term incorporates mechanisms for ejection of waste from the breached waste packages and entrainment of waste in the ascending magma/pyroclast flow. For enhanced source term, mechanisms for dissolution and alteration of waste by magma are included. The rockfall-scenario source term considers the degradation rate of waste packages by corrosion, and probabilities and mechanisms for breach by falling rock.

The probabilities and mechanisms of the interactions between intrusions and waste packages are developed from the PVHA (CRWMS M&O 1996a). The model of igneous activity at the Yucca Mountain site indicates that the primary factor controlling the intersection of an eruptive conduit with waste packages is the number of volcanic vents likely to occur inside the repository. Although eruptive vents are likely to occur somewhere along a dike intrusion in the Yucca

Mountain region, the probability that the vent is inside the repository is less than 50 percent (discussed in Section 10.4.2.1).

Interpretations of studies of waste-package material properties under conditions similar to magmatic environments indicate that the waste-package inner barrier is fairly robust. The most likely failure mechanism is blowout of the waste-package end caps from the high temperatures. Corrosion and mechanical collapse of the waste packages are likely to be failure mechanisms only if the waste package inner barrier has been previously corroded to at least half its original thickness by aqueous corrosion (Section 10.4.2.3).

Ejection and entrainment of waste are modeled by recognizing the density difference between the magma/pyroclasts and the waste form. Because the waste is significantly heavier than the magma or pyroclasts, a relatively large intrusion velocity is required in order to eject the waste and entrain it to the surface (Sections 10.4.2.4 and 10.4.2.5).

Waste encapsulated in magma can be altered by heat, chemicals in the magma, and groundwater to become available to be transported. Alteration processes and the absence of a waste package are modeled as resulting in higher mobilization rates for radionuclides for the enhanced-source-term scenario (Section 10.4.3.4).

The probabilities of various magnitudes of ground motion in repository drifts have been obtained from the PSHA (CRWMS M&O 1998a). The sizes of rocks available to fall from the drift walls onto waste packages have been used to determine the extent of prior waste-package degradation necessary before the rock can breach the waste-package wall (Section 10.5.1). The sizes of rocks available to fall imply that most of the waste-package outer barrier must be corroded away before the wall becomes weak enough to be breached by the falling rock.

The human-intrusion source term assumes a quantity of waste falls down a borehole into saturated-zone water. It therefore bypasses unsaturated-zone transport and is mobilized in the saturated zone (Section 10.7.3).

10.8.2 Summary of Modeling Results

Dose rates from base-case processes change relatively slowly because the processes creating the radionuclide source terms are driven by geologic processes such as groundwater flow. In contrast, disruptive events can occur at any time in the life of the repository and can cause essentially instantaneous changes in sources for radioactive dose rates. This difference can make comparison of the impact of disturbances not completely straightforward.

Of the four classes of disruptive events modeled for TSPA-VA, the greatest impact (as measured by dose rate CCDF) comes from the igneous, enhanced-source-term scenario. The probability of an igneous event at the Yucca Mountain repository is small, and when the processes required to release radionuclides under this scenario are considered, the probability of releases becomes even lower. Consequences, as measured by the maximum dose rate calculated, are approximately 40 percent of the maximum base-case dose rate for both the 100,000-year and 1,000,000-year comparisons (Section 10.4.3.7).

Modeling shows direct volcanic release to be a low-consequence/low-probability disturbance. There are no direct surface releases in 100,000 years, and such releases occur less than 6 percent of the time over 1,000,000 years. When the risk (probability of occurrence times consequence) of a volcanic eruption at the Yucca Mountain repository is included, the probability becomes insignificant. Consequences, as measured by maximum dose rates, are about 5 orders of magnitude below the maximum base-case dose rates (Section 10.4.2.10).

Models for rockfall show that there is no impact on the repository performance. The models for waste-package degradation by corrosion and rockfall are not well integrated, and this may influence this conclusion. However, the basic finding that the sizes of rocks available in the repository to fall are too small to damage any but already degraded waste packages still holds (Section 10.5.1.7).

Nuclear criticality has no impact on repository performance. The increase in radionuclides from an in-package criticality is too small to change the dose rates (Section 10.6.4). The potential consequences of a far-field criticality could be more significant, because of closer distance to dose-receptor locations, but the probability of such criticalities occurring is vanishingly small. This finding is independent of the question of whether criticality events of any magnitude should be regulated.

Human intrusion can cause a significant perturbation in repository behavior at times shortly after the event. Because future human activities and technologies cannot be predicted, only the consequences are considered. A human-intrusion event that occurs early in the repository lifetime (for example, at 10000 years) produces a detectable impact on dose rates for approximately the next 90,000 years (Section 10.7.3.7).

10.8.3 Caveats, Conservatism, and Modeling Artifacts

Investigations of the behavior of engineered materials in volcanic environments have shown that little is known that can be directly applied to the processes modeled for TSPA-VA. Although waste-package behavior is not the largest factor in defining the source term for igneous releases, any reduction in this area of uncertainty would significantly improve the credibility of the models.

The models for interactions of dikes with country rock contain several conservatisms. For example, the models assume that an eruptive conduit will actually pass through repository drifts. A crack-propagation study is necessary to determine if the preferential path is to avoid stress-relieved zones (such as drift openings) and to remain in undisturbed rock in the inter-drift volumes. Secondly, volcanic gases are assumed to attack waste packages at distances away from the intersection of the dike and drift. A reactive flow analysis could determine the extent of reactions along drifts from these gases. At early times when the repository is hot, the least principal stress of the rock could rotate such that lateral flow (sills) may be more likely. This stress rotation could have implications for igneous interactions with the repository.

The rockfall analyses assumed that the drifts remain open until a rock that potentially could damage a waste package falls. It is much more likely that the drifts will slowly fill with large

and small rocks that will eventually surround, and perhaps cover, the waste packages. The presence of this rock fill could mitigate the shock of large rocks falling.

There are numerous conservative assumptions made by the Waste-Package Development modelers in their criticality calculations. Additional conservatisms, such as the occurrence of the bathtub waste-package failure mode, must also be recognized.

Of all the disturbed analyses, the rockfall modeling depends most completely on a close integration with waste-package degradation models from the base-case analyses. Rockfall damage occurs only when the waste package has corroded sufficiently that the wall can be breached by the falling rock. Rockfall damage was applied to waste-package failure distributions determined independently, resulting in failure distributions that did not reflect the combined events.

Modeling did not consider thermo-mechanical and thermo-chemical alteration of rock near and below the repository. Such alterations could change groundwater flow and transport.

10.8.4 Recommendations for License-Application Analyses

The low probability of igneous activity at Yucca Mountain should permit DOE to dismiss this class of disturbed scenarios. Additionally, the further reduction in probability when the processes for radionuclide releases are included should be taken into account. If investigations of igneous disturbances are included in the TSPA for License Application, additional investigations of waste-package materials behavior in magmatic environments can reduce the uncertainties in the calculations.

The results of the rockfall modeling are ambiguous, probably as a result of modeling artifacts. An integrated model of waste-package corrosion and rockfall damage should be developed for License-Application analyses. Waste-package failure distributions for input to PA models should include both corrosion and breach from rockfall. In addition, the modeling of waste-form degradation as parameterized by the number of holes in the waste-package ("patches") should better reflect the effects of rockfall. Additionally, the likely environment of rubble-filled drifts should be included in the models.

The likely impacts of nuclear criticality on repository performance can generally be estimated from calculations that provide the radionuclide inventory increment. However, any additional criticality consequence calculations should integrate the latest geohydrological and material-degradation information developed by the PA organization with the criticality modeling done by the Waste-Package Development organization.

Because human intrusion appears to cause the greatest consequences (dose rates) at times early in repository lifetime of any disturbance modeled, a more comprehensive modeling should be included in the TSPA for License Application. When the EPA releases its regulations for treatment of human intrusion, additional modeling should be done to address the regulations.

10.9 REFERENCES

- Aki, K. and Koyanagi, R. 1981. "Deep Volcanic Tremor and Magma Ascent Mechanism Under Kilauea, Hawaii." *Journal of Geophysical Research*, 86, 8, 7095-7109. Washington, D.C.: American Geophysical Union. TIC Catalog Number: 224964.
- (ANSI) American National Standards Institute. 1983. *Nuclear Criticality Safety in Operations with Fissionable Materials Outside Reactors*. ANSI/ANS 8.1-1983. La Grange Park, Illinois: American Nuclear Society. TIC Catalog Number: 231616.
- Andersson, J., Editor. 1989. *The Joint SKI/SKB Scenario Development Project*. SKB Technical Report 89-35, 163 pp. Stockholm: Swedish Nuclear Fuel and Waste Management Co. TIC Catalog Number: 208568.
- Andersson, J. and Eng, T. 1990. "The Joint SKI/SKB Scenario Development Project." *Proceedings of the Symposium on Safety Assessment of Radioactive Waste Repositories, Paris, France, October 9-13, 1989*, 397-404. Paris, France: Organization for Economic Co-Operation and Development.
- Arnold, B.W. 1996. "Changes in Water Table Elevation at Yucca Mountain in Response to Seismic Events." High Level Radioactive Waste Management, Proceedings of the 7th Annual International Conference, Las Vegas, Nevada, April 29-May 3, 1996, 102-104. La Grange Park, Illinois: American Nuclear Society, Inc.; New York, New York: American Society of Civil Engineers. Also available as SAND95-2550A. MOL.19960508.0258.
- ASME (American Society of Mechanical Engineers). 1995. *The 1995 ASME Boiler and Pressure Vessel Code*, Volume II, Part 2, p. 370, Table 2B. New York, New York: American Society of Mechanical Engineers.
- Ayer, J.E.; Clark, A.T.; Loysen, P.; Ballinger, M.Y.; Mishima, J.; Owczarski, P.C.; Gregory, W.S.; and Nichols, B.D. 1988. *Nuclear Fuel Cycle Facility Accident Analysis Handbook*. NUREG-1320. Washington, D.C.: Division of Industrial and Medical Nuclear Safety, Office of Nuclear Material Safety and Safeguards, U.S. Nuclear Regulatory Commission. TIC Catalog Number: 206914.
- Barnard, R.W.; Wilson, M.L.; Dockery, H.A.; Gauthier, J.H.; Kaplan, P.G.; Eaton, R.R.; Bingham, F.W.; and Robey, T.H. 1992. *TSPA 1991: An Initial Total-System Performance Assessment for Yucca Mountain*. SAND91-2795, 376 pp. Albuquerque, New Mexico: Sandia National Laboratories. NNA.19920630.0033.
- Barr, G.E.; Dunn, E.; Dockery, H.A.; Barnard, R.W.; Valentine, G.; and Crowe, B. 1993. *Scenarios Constructed for Basaltic Igneous Activity at Yucca Mountain and Vicinity*. SAND91-1653, 149 pp. Albuquerque, New Mexico: Sandia National Laboratories. NNA.19930811.0013.
- Barr, G.E.; Borns, D.J.; and Fridrich, C. 1996. *Scenarios Constructed for the Effects of the Tectonic Processes on the Potential Nuclear Waste Repository at Yucca Mountain*. SAND96-1132, 106 pp. Albuquerque, New Mexico: Sandia National Laboratories. MOL.19970610.0644.

Bowman, C.D. and Venneri, F. 1996. "Underground Supercriticality from Plutonium and Other Fissile Material." *Science & Global Security*, 5, 279-302. Amsterdam, Netherlands: Gordon and Breach Science Publishers SA.

Bruhn, R.L. and Schultz, R.A. 1996. "Geometry and Slip Distribution in Normal Fault Systems: Implications for Mechanics and Fault-Related Hazards." *Journal of Geophysical Research, B, Solid Earth and Planets*, 101, B2, 3401-3412. Washington, D.C.: American Geophysical Union.

Bruno, J.; Casas, I.; Cera, E.; Ewing, R.C.; Finch, R.J.; and Werme, L.O. 1995. "Assessment of the Long-Term Evolution of the Spent Nuclear Fuel Matrikinetic, Thermodynamic and Spectroscopic Studies of Uranium Minerals." *Scientific Basis for Nuclear Waste Management XVIII, Materials Research Society Symposium Proceedings, Kyoto, Japan, October 23-27, 1994*, 353, 1, 633-639. Pittsburgh, Pennsylvania: Materials Research Society. TIC Catalog Number: 216341.

Burke, P.A. 1984. "Synopsis: Recent Progress in the Understanding of CO₂ Corrosion." *Advances in CO₂ Corrosion. Volume 1: Proceedings of the CORROSION/83 Symposium on CO₂ Corrosion in the Oil and Gas Industry, Anaheim, California, April 18-19, 1983*, 1, 3-9. Editors: Hausler, R.H. and Godard, H.P. Houston, Texas: National Association of Corrosion Engineers.

Carmichael, I.S.E.; Nicholls, J.; Spera, F.J.; Wood, B.J.; and Nelson, S.A. 1977. "High-Temperature Properties of Silicate Liquids: Applications to the Equilibration and Ascent of Basic Magma." *Philosophical Transactions of the Royal Society of London A*, 286, 1336, 373-431. London: Royal Society of London. NNA.19900306.0047.

Carr, W.J. and Parrish, L.D. 1985. *Geology of Drill Hole USW VH-2, and Structure of Crater Flat, Southwestern Nevada*. Open-File Report 85-475, 41 pp. Denver, Colorado: U.S. Geological Survey. TIC Catalog Number: 201300.

Carr, W.J. 1990. "Styles of Extension in the Nevada Test Site Region, Southern Walker Lane Belt; An Integration of Volcano-Tectonic and Detachment Fault Models." *Basin and Range Extensional Tectonics Near the Latitude of Las Vegas, Nevada*, 283-303. Editor: Wernicke, B.P. Memoir 176. Boulder, Colorado: Geological Society of America. NNA.19920811.0124.

Carrigan, C.R.; King, G.C.P.; Barr, G.E.; and Bixler, N.E. 1991. "Potential for Water-Table Excursions Induced by Seismic Events at Yucca Mountain, Nevada." *Geology*, 19, 12, 1157-1160. Boulder, Colorado: Geological Society of America. TIC Catalog Number: 203414.

Carlsaw, H.S. and Jaeger, J.C. 1986. *Conduction of Heat in Solids*. Second Edition, p. 258, eq. 1. Oxford: Clarendon Press; New York, New York: Oxford University Press. NNA.19900522.0259.

Champion, D.E. 1991. "Volcanic Episodes Near Yucca Mountain as Determined by Paleomagnetic Studies at Lathrop Wells, Crater Flat, and Sleeping Butte, Nevada." *High Level Radioactive Waste Management, Proceedings of the Second International Conference, Las Vegas, Nevada, April 28-May 3, 1991*, 1, 61-67. La Grange Park, Illinois: American Nuclear

Society, Inc.; New York, New York: American Society of Civil Engineers. NNA.19920131.0231.

Chapman, N.A.; Andersson, J.; Robinson, P.; Skagius, K.; Wene, C-O.; Wiborgh, M.; and Wingefors, S. 1995. *Systems Analysis, Scenario Construction and Consequence Analysis Definition for SITE-94*. SKI Report 95:26, 172 pp. Stockholm, Sweden: Swedish Nuclear Fuel and Waste Management Co.

Cranwell, R.M.; Guzowski, R.W.; Campbell, J.E.; and Ortiz, N.R. 1990. *Risk Methodology for Geologic Disposal of Radioactive Waste: Scenario Selection Procedure*. SAND80-1429, 109 pp. Albuquerque, New Mexico: Sandia National Laboratories. NNA.19900611.0073.

Crowe, B.M.; Amos, R.; Perry, F.; Self, S.; and Vaniman, D. 1982. *Aspects of Possible Magmatic Disruption of a High-Level Radioactive Waste Repository in Southern Nevada*. LA-9326-MS, 42 pp. Los Alamos, New Mexico: Los Alamos National Laboratory. TIC Catalog Number: 202326.

Crowe, B.; Self, S.; Vaniman, D.; Amos, R.; and Perry, F. 1983b. "Aspects of Potential Magmatic Disruption of a High-Level Radioactive Waste Repository in Southern Nevada." *Journal of Geology*, 91, 3, 259-276. Chicago, Illinois: University of Chicago Press. NNA.19870407.0404.

Crowe, B.M. and Perry, F.V. 1990. "Volcanic Probability Calculations for the Yucca Mountain Site: Estimation of Volcanic Rates." *Proceedings of the Topical Meeting on Nuclear Waste Isolation in the Unsaturated Zone, FOCUS '89, Las Vegas, Nevada, September 17-21, 1989*, 326-334. La Grange Park, Illinois: American Nuclear Society. NNA.19910617.0005.

Crowe, B.; Perry, F.; Geissman, J.; McFadden, L.; Wells, S.; Murrell, M.; Poths, J.; Valentine, G.A.; Bowker, L.; and Finnegan, K. 1995. *Status of Volcanism Studies for the Yucca Mountain Site Characterization Project*. LA-12908-MS, 396 pp. Los Alamos, New Mexico: Los Alamos National Laboratory. MOL.19951127.0106.

CRWMS M&O. 1995. *Total System Performance Assessment – 1995: An Evaluation of the Potential Yucca Mountain Repository*. B00000000-01717-2200-00136, Rev. 1. Las Vegas, Nevada: TRW Environmental Safety Systems. MOL.19960724.0188.

CRWMS M&O. 1996a. *Probabilistic Volcanic Hazard Analysis for Yucca Mountain, Nevada*. BA0000000-01717-2200-00082, Rev. 0. Las Vegas, Nevada: TRW Environmental Safety Systems. MOL.19971201.0221.

CRWMS M&O. 1996b. *Static Structural Analyses of Waste Packages in Degraded States*. BBAA00000-01717-0200-00014 REV.00. Las Vegas, Nevada: TRW Environmental Safety Systems. MOL.19970402.0069.

CRWMS M&O. 1996c. *Probabilistic Criticality Consequence Evaluation*. BBA000000-01717-0200-00021 REV. 00. Las Vegas, Nevada: TRW Environmental Safety Systems. MOL.19970113.0002.

CRWMS M&O. 1996d. *Rock Size Required to Breach Barriers at Different Corrosion Levels*. BBAA00000-01717-0200-00012 Rev. 00. Las Vegas, Nevada: TRW Environmental Safety Systems. MOL.19961217.0318.

CRWMS M&O. 1997a. *Subsurface Repository VA Design Layout Plan*. BCAA00000-01717-2700-81024 REV 00. Las Vegas, Nevada: TRW Environmental Safety Systems. MOL.19971210.0063.

CRWMS M&O. 1997b. *Controlled Design Assumptions Document*. B00000000-01717-4600-00032, REV 04, ICN 3. Las Vegas, Nevada: TRW Environmental Safety Systems. MOL.19980408.0604.

CRWMS M&O. 1997c. *Rock Size Required to Cause a Through Crack in Containment Barriers*. BBAA00000-01717-0200-00015 REV 00. Las Vegas, Nevada: TRW Environmental Safety Systems. MOL.19970813.0531.

CRWMS M&O. 1997d. *Confirmation of Empirical Design Methodologies*. BABEE0000-01717-5705-00002 REV 00. Las Vegas, Nevada: TRW Environmental Safety Systems. MOL.19980219.0104.

CRWMS M&O. 1997e. *Design Basis Cladding Analysis* BBA000000-01717-0200-00054 REV 01A. Las Vegas, Nevada: TRW Environmental Safety Systems.

CRWMS M&O. 1997f. *Construction of Scenarios for Nuclear Criticality at the Potential Repository at Yucca Mountain, Nevada*. B00000000-01717-2200-00194. Las Vegas, Nevada: TRW Environmental Safety Systems. MOL.19980204.0281.

CRWMS M&O. 1997g. *Evaluation of Codisposal Viability for Aluminum-Clad DOE-Owned Spent Fuel: Phase II Degraded Codisposal Waste Package Internal Criticality*. BBA000000-01717-5705-00017 REV. 00. Las Vegas, Nevada: TRW Environmental Safety Systems. MOL.19980218.0192.

CRWMS M&O. 1997h. *Degraded Mode Criticality Analysis of Immobilized Plutonium Waste Forms in a Geologic Repository*. A00000000-01717-5705-00014 REV. 01. Las Vegas, Nevada: TRW Environmental Safety Systems. MOL.19971001.0246.

CRWMS M&O. 1997i. *Waste Package Probabilistic Criticality Analysis: Summary Report of Evaluations in 1997*. BBA000000-01717-5705-00015 REV. 00. Las Vegas, Nevada: TRW Environmental Safety Systems. MOL.19980105.0081.

CRWMS M&O. 1997j. *Waste Package Design Basis Events*. BBA000000-01717-0200-00037C REV. 00. Las Vegas, Nevada: TRW Environmental Safety Systems. MOL.19971006.0075.

CRWMS M&O. 1998a. *Probabilistic Seismic Hazard Analyses for Fault Displacement and Vibratory Ground Motion at Yucca Mountain, Nevada Final Report Volume 1 Text* June 15

1998... Las Vegas, Nevada: TRW Environmental Safety Systems. (M&O hasn't decided if this will be a USGS or M&O document)

CRWMS M&O. 1998b. *Report on External Criticality of Plutonium Waste Forms in a Geologic Repository*. BBA000000-01717-5705-00018 REV. 01. Las Vegas, Nevada: TRW Environmental Safety Systems. MOL.19980318.0412.

CRWMS M&O. 1998c. *Yucca Mountain Site Description: Book 1 – Sections 1,2,3*. B00000000-01717-5700-00019 REV 00, Draft A. Las Vegas, Nevada: TRW Environmental Safety Systems.

CRWMS M&O. 1998d. *Disposal Criticality Analysis Methodology Topical Report*. B00000000-01717-5705-00095 REV 00B, June 8, 1998. Las Vegas, Nevada: TRW Environmental Safety Systems.

CRWMS M&O. 1998e. *Software Routine Report for WAPDEG (Version 3.07)*. B00000000-xxxx-xxxx-xxxx. Las Vegas, Nevada: TRW Environmental Safety Systems. MOL.19980715.0166

CRWMS M&O. 1998f. *Repository Ground Support Analysis for Viability Assessment*. BCAA000000-01717-0200-00004 REV 01B, April 22, 1998. Las Vegas, Nevada: TRW Environmental Safety Systems. MOL.19980512.0336

D'Agnese, F.A.; Faunt, C.C.; Turner, A.K.; and Hill, M.C. 1997. *Hydrogeologic Evaluation and Numerical Simulation of the Death Valley Regional Ground-Water Flow System, Nevada and California*. Water-Resources Investigations Report 96-4300. Denver, Colorado: U.S. Geological Survey. MOL.19980306.0253.

DOE (U.S. Department of Energy). 1988. *Consultation Draft Site Characterization Plan Overview Yucca Mountain Site, Nevada Research and Development Area, Nevada*. DOE/RW-0161. Washington, D.C.: U.S. Department of Energy, Office of Civilian Radioactive Waste Management. TIC Catalog Number: 203432.

DOE 1992. *Characteristics of Potential Repository Wastes*. DOE/RW-0184-R1. Prepared for the U.S. Department of Energy, Office of Civilian Radioactive Waste Management, Washington, D.C. Oak Ridge, Tennessee: Oak Ridge National Laboratory. Volumes 1-4. HQO.19920827.0001 through HQO.19920827.0004.

DOE 1996. *Title 40 CFR Part 191 Compliance Certification Application for the Waste Isolation Pilot Plant*. DOE/CAO-1996-2184. Carlsbad, New Mexico: Department of Energy, Waste Isolation Pilot Plant, Carlsbad Area Office. (Full text available at <http://reserve.wipp.carlsbad.nm.us>. Accessed: July 11, 1998.)

Douglass, D.L. and Healey, J.T. 1979. *The Corrosion of Some Pure Metals in Basaltic Lava and Simulated Magmatic Gas at 1150°C*. SAND79-1981, 77 pp. Albuquerque, New Mexico: Sandia National Laboratories. NNA.19890626.0386.

Ehrlich, S.A. and Douglass, D.L. 1982. *The Effect of Molybdenum Plus Chromium on the Corrosion of Iron-, Nickel-, and Cobalt-Base Alloys in Basaltic Lava and Simulated Magmatic Gas at 1150°C.* SAND82-7055, 79 pp. Albuquerque, New Mexico: Sandia National Laboratories.

EPRI (Electric Power Research Institute). 1996. *Yucca Mountain Total System Performance Assessment, Phase 3.* TR-107191, 572 pp. Palo Alto, California: Electric Power Research Institute. MOL.19980211.0367.

Gauthier, J.H.; Wilson, M.L.; Borns, D.J.; and Arnold, B.W. 1995. "Impacts of Seismic Activity on Long-Term Repository Performance at Yucca Mountain." *Proceedings of the Topical Meeting on Methods of Seismic Hazards Evaluation, Focus '95, Las Vegas, Nevada, September 18-20, 1995*, 159-168. La Grange Park, Illinois: American Nuclear Society. Also available as SAND95-1917C. MOL.19960327.0356.

Gerlach, T.M. 1980. "Evaluation of Volcanic Gas Analyses from Kilauea Volcano." *Journal of Volcanology and Geothermal Research*, 7, 3-4, 295-317. Amsterdam; New York, New York: Elsevier Scientific Publishing Company. NNA.19930330.0077

Golder 1998. *RIP Theory and User's [sic] Guide Version 5.18*, March 1998. Redmond, Washington: Golder Associates, Inc.

Goodwin, B.W.; Stephens, M.E.; Davison, C.C.; Johnson, L.H.; and Zach, R. 1994. *Scenario Analysis for the Postclosure Assessment of the Canadian Concept for Nuclear Fuel Waste Disposal.* AECL-10969, COG-94-247, 139 pp. Pinawa, Manitoba: Atomic Energy of Canada Ltd., Whiteshell Laboratories. TIC Catalog Number: 215123.

Gray, W.J.; Leider, H.R.; and Steward, S.A. 1992. "Parametric Study of LWR Spent Fuel Dissolution Kinetics." *Journal of Nuclear Materials*, 190, 46-52. Amsterdam: North-Holland Publishing Co. MOL.19960613.0037.

Gray, W.J. and Wilson, C.N. 1995. *Spent Fuel Dissolution Studies FY 1991 to 1994.* PNL-10540, 150 pp. Richland, Washington: Pacific Northwest National Laboratory. MOL.19960613.0035.

Guzowski, R.V. and Newman, G. 1993. *Preliminary Identification of Potentially Disruptive Scenarios at the Greater Confinement Disposal Facility, Area 5 of the Nevada Test Site.* SAND93-7100, 204 pp. Albuquerque, New Mexico: Sandia National Laboratories. TIC Catalog Number: 209690.

Hansen, M. and Anderko, K. 1958. *Constitution of Binary Alloys.* Second Edition, 823, 909, 911, 918, 920, 922, 926, 932, 1162, 1164, 1168, 1169, 1172, 1196, 1200, 1206. New York, New York: McGraw-Hill Book Company. NNA.19891009.0004.

Jarzemba, M.S. and LaPlante, P.A. 1996. *Preliminary Calculations of Expected Dose from Extrusive Volcanic Events at Yucca Mountain.* San Antonio, Texas: Center for Nuclear Waste Regulatory Analyses (CNWRA).

Jarzemba, M.S.; LaPlante, P.A.; and Poor, K.J. 1997. *ASHPLUME Version 1.0 - A Code for Contaminated Ash Dispersal and Deposition. Technical Description and User's Guide.* CNWRA 97-004 Revision 1. San Antonio, Texas: Center for Nuclear Waste Regulatory Analyses.

Kaiser, P.K.; Tannant, D.D.; McCreath, D.R.; and Jesenak, P. 1992. "Rockburst Damage Assessment Procedure." *Rock Support in Mining and Underground Construction, Proceedings of the International Symposium on Rock Support, Sudbury, Ontario, Canada, June 16-19, 1992*, 639-647. Editors: Kaiser, P.K. and McCreath, D.R. Rotterdam, Netherlands; Brookfield, Vermont: A.A. Balkema.

Kemeny, J.M. and Cook, N.G.W. 1992. "Water Table Change Due to a Normal Faulting Earthquake." *Demonstration of a Risk-Based Approach to High-Level Waste Repository Evaluation: Phase 2*. TR-100384, 6-1 through 6-13. McGuire, R.K. Palo Alto, California: Electric Power Research Institute. NNA.19940225.0126.

Knief, R.A. 1993. *Nuclear Criticality Safety: Theory and Practice*. La Grange Park, Illinois: American Nuclear Society.

Lorenz, R.A.; Collins, J.L.; Malinauskas, A.P.; Kirkland, O.L.; and Towns, R.L. 1980. *Fission Product Release From Highly Irradiated LWR Fuel*. NUREG/CR-0722, ORNL/NUREG/TM-287, 166 pp. Oak Ridge, Tennessee: Oak Ridge National Laboratory. MOL.19891109.0121.

Lyday, P.A. 1985. "Boron." *Mineral Facts and Problems 1985 Edition*. Bureau of Mines Bulletin 675, 91-102. Washington, D.C.: United States Department of the Interior; For Sale by Superintendent of Documents, U.S. Government Printing Office. TIC Catalog Number: 231110.

MacDonald, G.A. 1949. *Petrography of the Island of Hawaii*. U.S. Geological Society Professional Paper 214-D, 51-96. Reston, Virginia: U.S. Geological Society.

MacDonald, G.A. 1972. "Temperature of Magmas." *Volcanoes*, 54-61. Englewood Cliffs, New Jersey: Prentice-Hall. NNA.19940415.0006.

McCormick, N.J. 1981. *Reliability and Risk Analysis: Methods and Nuclear Power Applications*. New York, New York: Academic Press. TIC Catalog Number: 4386.

McGuire, R.K., Editor. 1990. *Demonstration of a Risk-Based Approach to High-Level Waste Repository Evaluation*. EPRI-NP-7057, 248 pp. Palo Alto, California: Electric Power Research Institute. NNA.19910813.0004.

Miller, W.M. and Chapman, N.A., Editors. 1993. *HMIP Assessment of Nirex Proposals: Identification of Relevant Processes (System Concept Group Report)*. UKDOE/HMIP TR-ZI-11, August 1993. London: Environment Agency.

Minor, S.A.; Sawyer, D.A.; Wahl, R.R.; Frizzell, V.A., Jr.; Schilling, S.P.; Warren, R.G.; Orkild, P.P.; Coe, J.A.; Hudson, M.R.; Fleck, R.J.; Lanphere, M.A.; Swadley, W.C.; and Cole, J.C.

1993. *Preliminary Geologic Map of the Pahute Mesa 30'x60' Quadrangle, Nevada*. Open-File Report 93-299, 39 pp. Denver, Colorado: U.S. Geological Survey. MOL.19950307.0143.

Morrall, F.R., Editor. 1984. "Wrought Superalloys." *Superalloys Source Book*, 20-40. Editor: Donachie, M.J., Jr. Metals Park, Ohio: American Society for Metals.

Napier, B.A.; Peloquin, R.A.; Streng, D.L.; and Ramsdell, J.V. 1988. *GENII - The Hanford Environmental Radiation Dosimetry Software System. Volume 1: Conceptual Representation. Volume 2: User's Manual. Volume 3: Code Maintenance Manual*. PNL-6584. Richland, Washington: Pacific Northwest Laboratory. TIC Catalog Number: 206898.

National Academy of Sciences/National Research Council (NAS/NRC). 1995. *Technical Bases for Yucca Mountain Standards*. Committee on Technical Bases for Yucca Mountain Standards, Board on Radioactive Waste Management. 205 p. Washington, D.C.: National Academy Press. TIC Catalog Number: 104273.

National Academy of Sciences/National Research Council. 1992. *Ground Water at Yucca Mountain, How High Can it Rise?* Final Report of the Panel on Coupled Hydrologic/Tectonic/Hydrothermal Systems at Yucca Mountain. 222 pp. Washington, D.C.: National Academy Press. MOL.19960708.0340.

Nuclear Energy Agency (NEA). 1992. *Safety Assessment of Radioactive Waste Repositories: Systematic Approaches to Scenario Development*. Group on the Identification and Selection of Scenarios Paris: Organisation for Economic Co-Operation and Development. TIC Catalog Number: 8083.

Nuclear Regulatory Commission (NRC). 1996. "Disposal of High-Level Radioactive Wastes in Geologic Repositories." *Code of Federal Regulations, Title 10, Part 60*. Washington, D.C.: Superintendent of Documents, U.S. Government Printing Office.

Oak Ridge National Laboratory (ORNL). 1995. *SCALE 4.3: Modular Code System for Performing Standardized Computer Analyses for Licensing Evaluation for Workstations and Personal Computers*. October 1995. CCC-545. Oak Ridge, Tennessee: Oak Ridge National Laboratory, Radiation Safety Information Computational Center (RSICC). (Abstract listed at <http://epicws.cped.ornl.gov/codes/ccc/ccc5/ccc-545.html>. Accessed 7/14/98.

Oak Ridge National Laboratory (ORNL). 1997. *MCNP4B2: Monte Carlo N-Particle Transport Code System*. April 1997. CCC-660. Oak Ridge, Tennessee: Oak Ridge National Laboratory, Radiation Safety Information Computational Center (RSICC). (Abstract listed at <http://epicws.cped.ornl.gov/codes/ccc/ccc6/ccc-660.html>. Accessed 7/14/98.)

Pérez, I.; Casas, I.; Torrero, M.E.; Cera, E.; Duro, L.; and Bruno, J. 1997. "Dissolution Studies of Soddyite as a Long-Term Analogue of the Oxidative Alteration of the Spent Nuclear Fuel Matrix." *Scientific Basis for Nuclear Waste Management XX, Materials Research Society Symposium Proceedings, Boston, Massachusetts, December 2-6, 1996*, 465, 565-572. Pittsburgh, Pennsylvania: Materials Research Society. MOL.19980505.0194.

Perry, F.V.; Crowe, B.M.; and Wells, S.G. and 8 others 1998. "Chapter Two Geology and Geochronology of Basaltic Volcanism in the Yucca Mountain Region." *Synthesis of Volcanism Studies for the Yucca Mountain Site Characterization Project*. Editors: Perry, F.V.; Crowe, B.M.; Valentine, G.A.; and Bowker, L.M. Los Alamos: Los Alamos National Laboratory.

Ramelli, A.R.; Oswald, J.A.; Vadurro, G.; Menges, C.M.; and Paces, J.B. 1996. "Quaternary Faulting on the Solitario Canyon Fault." *Seismotectonic Framework and Characterization of Faulting at Yucca Mountain, Nevada*, Chapter 4.7, 4.7-1 through 4.7-56. Denver, Colorado: U.S. Geological Survey. MOL.19970129.0041.

Reiter, L. 1990. *Earthquake Hazard Analysis: Issues and Insights*. New York, New York: Columbia University Press TIC Catalog Number: 236929.

Rhodes, P.R.; Welch, G.A.; and Abrego, L. 1983. "Stress Corrosion Cracking Susceptibility of Duplex Stainless Steels in Sour Gas Environments." *Duplex Stainless Steels, Conference Proceedings*, 757-803. Editor: Lula, R.A. Metals Parks, Ohio: American Society for Metals.

Roark, R.J. and Young, W.C. 1975. *Formulas for Stress and Strain*. Fifth Edition. New York, New York: McGraw-Hill Publishers.

Robertson, J.A.L. 1969. *Irradiation Effects in Nuclear Fuels*. New York, New York: Gordon and Breach, Science Publishers.

Schweickert, R.A. and Lahren, M.M. 1997. "Strike-Slip Fault System in Amargosa Valley and Yucca Mountain, Nevada." *Tectonophysics*, 272, 25-41. Amsterdam, The Netherlands: Elsevier Science B.V.

Searcy, C.; Dean, K.; and Stringer, W. 1998. "PUFF: A High-Resolution Volcanic Ash Tracking Model." *Journal of Volcanology and Geothermal Research*, 80, 1-16.

Skagius, K. and Wingefors, S. 1992. *Alligator Rivers Analogue Project Final Report. Volume 16 Application of Scenario Development Methods in Evaluation of the Koongarra Analogue*. DOE/HMIP/RR/92/086, SKI TR 92:20-16. Menai, New South Wales, Australia: Australian Nuclear Science and Technology Organisation. TIC Catalog Number: 231268.

Smith, E.I.; Feuerbach, D.L.; Naumann, T.R.; and Faulds, J.E. 1990. "The Area of Most Recent Volcanism Near Yucca Mountain, Nevada: Implications for Volcanic Risk Assessment." *High Level Radioactive Waste Management, Proceedings of the International Topical Meeting, Las Vegas, Nevada, April 8-12, 1990*, 1, 81-90. La Grange Park, Illinois: American Nuclear Society, Inc.; New York, New York: American Society of Civil Engineers. TIC Catalog Number: 216711.

Smith, R.P.; Jackson, S.M.; and Hackett, W.R. 1996. "Paleoseismology and Seismic Hazards Evaluations in Extensional Tectonic Terrains." *Journal of Geophysical Research*, 101, B3, 6277-6292. Washington, D.C.: American Geophysical Union.

- Stephens, M.E. and Goodwin, B.W. 1990. "Scenario Analysis for the Postclosure Assessment of the Canadian Concept for Nuclear Fuel Waste Disposal." *Proceedings of the Symposium on Safety Assessment of Radioactive Waste Repositories, Paris, France, October 9-13, 1989*, 405-415. Paris, France: Organisation for Economic Co-Operation and Development.
- Stock, J.M.; Healy, J.H.; Hickman, S.H.; and Zoback, M.D. 1985. "Hydraulic Fracturing Stress Measurements at Yucca Mountain, Nevada, and Relationship to the Regional Stress Field." *Journal of Geophysical Research*, 90, B10, 8691-8706. Washington, D.C.: American Geophysical Union. TIC Catalog Number: 219009.
- Stock, J.M. and Healy, J.H. 1988. "6. Stress Field at Yucca Mountain, Nevada." *Geologic and Hydrologic Investigations of a Potential Nuclear Waste Disposal Site at Yucca Mountain, Southern Nevada*. U.S. Geological Survey Bulletin 1790, 87-93. Editors: Carr, M.D. and Yount, J.C. Washington: United States Government Printing Office. TIC Catalog Number: 203085.
- Symonds, R.B.; Rose, W.I.; Bluth, G.J.S.; and Gerlach, T.M. 1994. "Chapter 1 Volcanic-Gas Studies: Methods, Results, and Applications." *Volatiles in Magmas*. Reviews in Mineralogy Volume 30, 1-66. Editors: Carroll, M.J. and Holloway, J.R. Washington, D.C.: Mineralogical Society of America. TIC Catalog Number: 238061.
- Turrin, B.D.; Champion, D.; and Fleck, R.J. 1991. "⁴⁰Ar/³⁹Ar Age of the Lathrop Wells Volcanic Center, Yucca Mountain, Nevada." *Science*, 253, 5020, 654-657. Washington, D.C.: American Association for the Advancement of Science. TIC Catalog Number: 225167.
- Valentine, G.A.; Woldegabriel, G.; Rosenberg, N.D. and 8 others 1998. "Chapter 5 Physical Processes of Magmatism and Effects on the Potential Repository: Synthesis of Technical Work Through Fiscal Year 95." *Synthesis of Volcanism Studies for the Yucca Mountain Site Characterization Project*. Editors: Perry, F.V.; Crowe, B.M.; Valentine, G.A.; and Bowker, L.M. Los Alamos: Los Alamos National Laboratory. LA-UR-96-3063, 156 pp. Los Alamos, New Mexico: Los Alamos National Laboratory. TIC Catalog Number: 201799.
- Van Konynenburg, R.A., Compiler. 1996. "Comments on the Draft Paper 'Underground Supercriticality from Plutonium and Other Fissile Material,' Written by C.D. Bowman and F. Venneri (LANL)." *Science & Global Security*, 5, 303-322. Amsterdam, Netherlands: Gordon and Breach Science Publishers SA.
- Vaniman, D.T.; Crowe, B.M.; and Gladney, E.S. 1982. "Petrology and Geochemistry of Hawaiiite Lavas from Crater Flat, Nevada." *Contributions to Mineralogy and Petrology*, 80, 341-357. Berlin, Germany: Springer-Verlag. TIC Catalog Number: 201799.
- Wang, D. and Douglass, D.L. 1983. "The Corrosion of Chromium and Nickel-Chromium Alloys in Oxygen-Sulfur-Carbon Gases at 800°C." *Oxidation of Metals*, 20, 3-4, 111-146. New York, New York: Plenum Press.
- Warren, W.E. and Smith, C.W. 1985. "In Situ Stress Estimates from Hydraulic Fracturing and Direct Observation of Crack Orientation." *Journal of Geophysical Research*, 90, B8, 6829-6839. Washington, D.C.: American Geophysical Union.

U. S. Nuclear Regulatory Commission, NRC Iterative Performance Assessment Phase 2: Development of Capabilities for Review of a Performance Assessment for a High-Level Waste Repository. Wescott, R. G.; Lee, M.P.; Eisenberg, N.A.; McCartin, T.J.; and Baca, R.G., Editors. NUREG-1464. Washington, D.C.: Office of Nuclear Material Safety and Safeguards, Office of Nuclear Regulatory Research; San Antonio, Texas, Center for Nuclear Waste Regulatory Analyses.

Westrich, H.R. 1982. "The Solubility of LWR Core Debris in Sacrificial Floor Material." *Journal of Nuclear Materials*, 110, 324-332. Amsterdam, The Netherlands: North-Holland Publishing Company. NNA.19940301.0032.

Wilson, L. and Head, J.W., III. 1981. "Ascent and Eruption of Basaltic Magma on the Earth and Moon." *Journal of Geophysical Research*, 86, B4, 2971-3001. Washington, D.C.: American Geophysical Union. MOL.19950111.0030.

Wilson, M.L.; Gauthier, J.H.; Barnard, R.W.; Barr, G.E.; Dockery, H.A.; Dunn, E.; Eaton, R.R.; Guerin, D.C.; Lu, N.; Martinez, M.J.; Nilson, R.; Rautman, C.A.; Robey, T.H.; Ross, B.; Ryder, E.E.; Schenker, A.R.; Shannon, S.A.; Skinner, L.H.; Halsey, W.G.; Gansemer, J.D.; Lewis, L.C.; Lamont, A.D.; Triay, I.R.; Meijer, A.; and Morris, D.E. 1994. *Total-System Performance Assessment for Yucca Mountain-SNL Second Iteration (TSPA-1993)*. SAND93-2675. Albuquerque, New Mexico: Sandia National Laboratories. MOL.19940112.0123. Wolery, T.J. and Daveler, S.A. 1992. *EQ6, A Computer Program for Reaction Path Modeling of Aqueous Geochemical Systems; Theoretical Manual, User's Guide, and Related Documentation, Version 7.0*. LA-UCRL-MA-110662, Part IV. Livermore, California: Lawrence Livermore National Laboratory. NNA.19930127.0028.

Zyvoloski, G.A.; Robinson, B.A.; Dash, Z.V.; and Trease, L.L. 1995. *Models and Methods Summary for the FEHMN Application, Revision 1*. LA-UR-94-3787, 70 pp. Los Alamos, New Mexico: Los Alamos National Laboratory. TIC Catalog Number: 222337.

O'Leary, D. W. "Plio-Pleistocene Basaltic Volcanism And Its Relation To Extension In The Crater Flat, Nevada, Tectonic Domain", OFR- in press, US Geological Survey, Denver CO.

R. Youngs, Geomatrix Corporation, personal communication 1998.

G. Valentine and F. Perry, LANL, Minutes of Meeting on volcanic disturbed scenarios, March 1998. Accession number MOL.19980715.0398

Memo, W. O'Connell, LLNL, to R. Stout, LLNL, December 23, 1997, LLNL reference Number LL YMP98 05049 MOL.19980605.0424.

Greg Valentine, Los Alamos National Laboratory, personal communication 1998.

Finn, P.A.; Hoh, J.C.; Wolf, S.F.; Surchik, M.T.; Buck, E.C.; and Bates, J.K. 1997. *Spent Fuel Reaction: The Behavior of the ϵ Phase over 3.1 Years* Materials Research Society Symposium Proceedings, Vol. 465, pp. 527-534.

Finn, P.A.; Finch, R.; Surchik, M.T.; Buck, E.C.; and Bates, J.K. 1998. *Corrosion Mechanisms of Spent Fuel under Oxidizing Conditions* Materials Research Society Symposium Proceedings, Vol. 506, pp. 123-131.

Leigh, C.D.; Thompson, B.M.; Campbell, J.E.; Longsine, D.E.; Kennedy, R.A.; and Napier, B.A. 1993. *User's Guide for GENII-S: A Code for Statistical and Deterministic Simulations of Radiation Doses to Humans from Radionuclides in the Environment*. SAND91-0561. Albuquerque, New Mexico: Sandia National Laboratories. TIC Catalog Number: 231133.

ASM Committee on Stainless Steels and Heat-Resistant Alloys. 1981. "Heat Treating of Heat-Resisting Alloys." *Superalloys Source Book*, 347-368. Editor: Donachie, M.J., Jr. Metals Park, Ohio: American Society for Metals.

INTENTIONALLY LEFT BLANK

Chapter 10
Figures

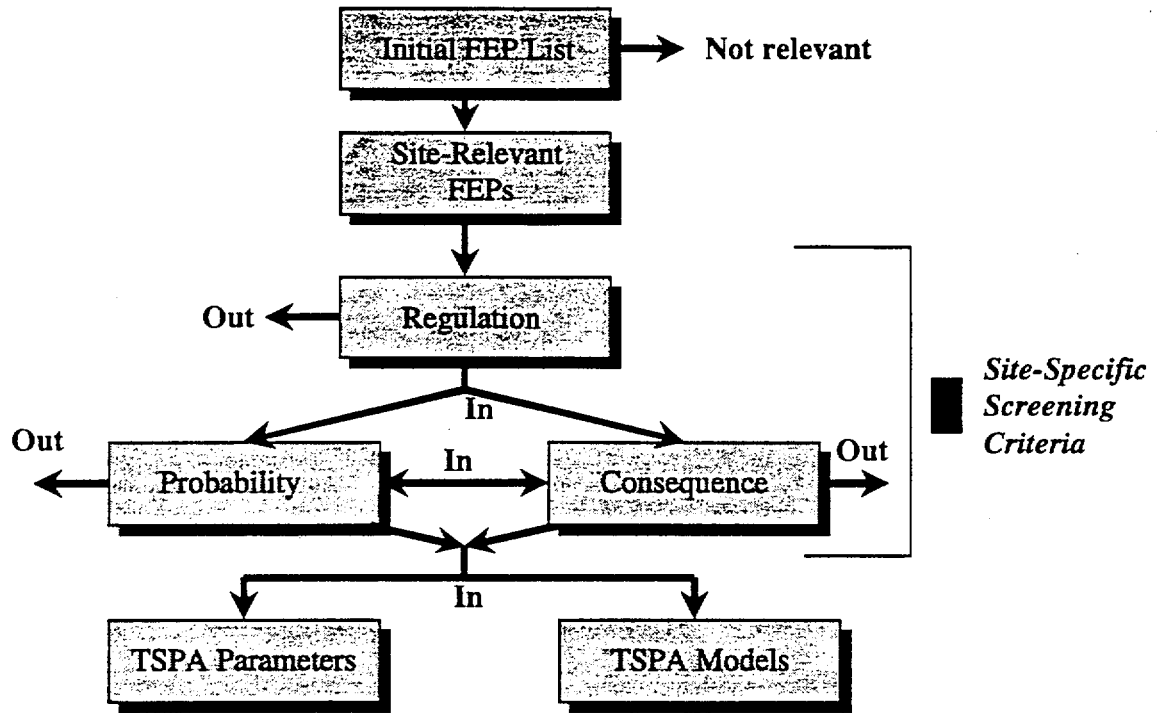


Figure 10-1. Schematic illustration of the FEP screening process.

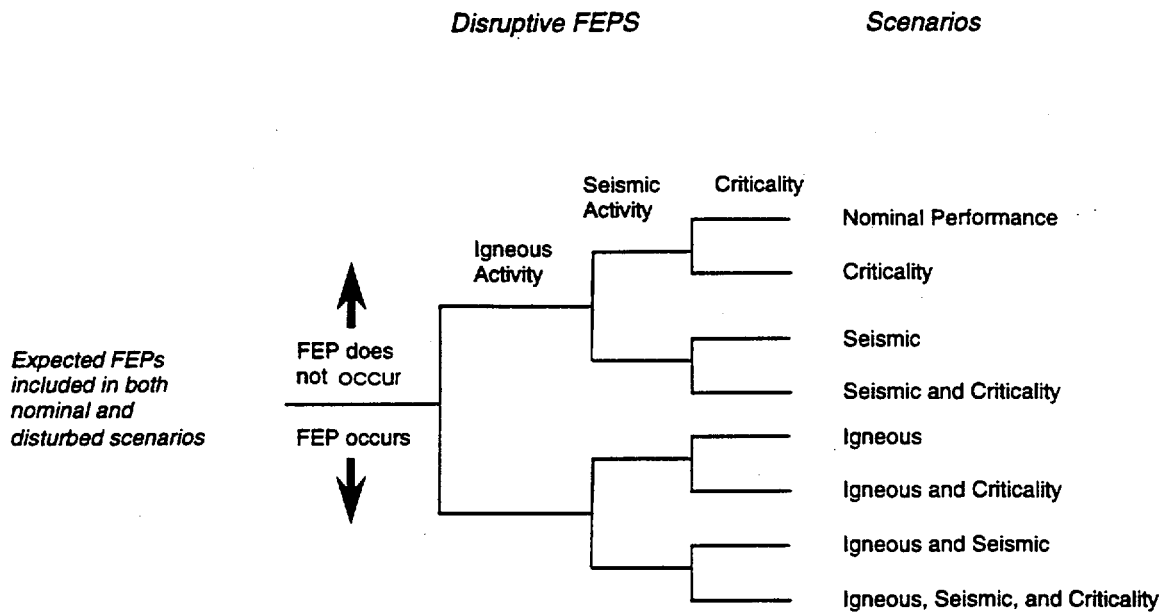
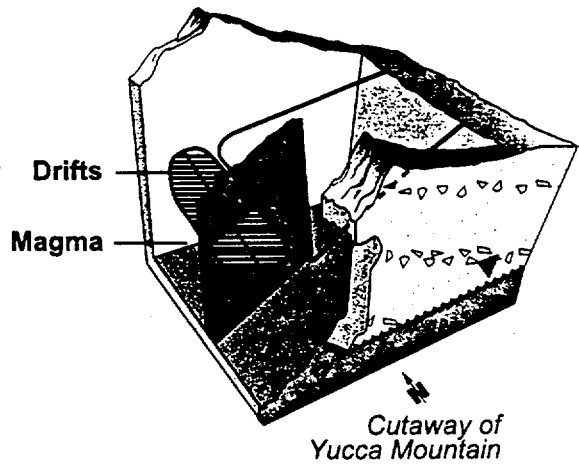
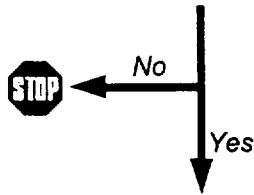


Figure 10-2. Logic Diagram for the YM TSPA-VA, showing the construction of scenarios using combinations of disruptive FEPS.

Igneous intrusion occurs in YM Area?

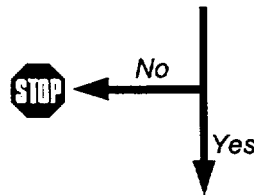
No performance assessment consequence. End Scenario.



Cutaway of Yucca Mountain

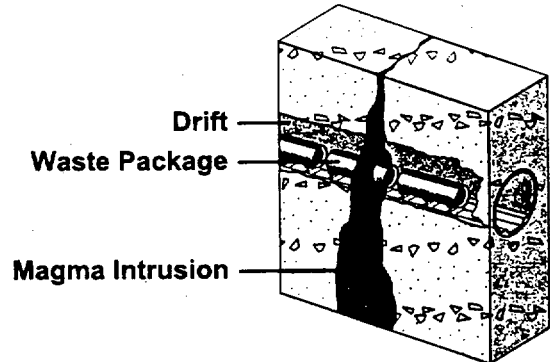
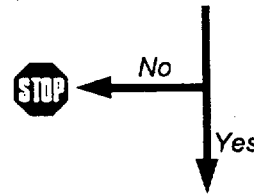
Magmatic dike intrudes into repository?

Alteration of saturated zone flow and transport by a regional dike modeled in indirect scenario



Dike intrusion directly contacts waste packages?

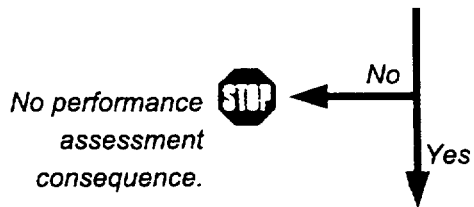
No performance assessment consequence.



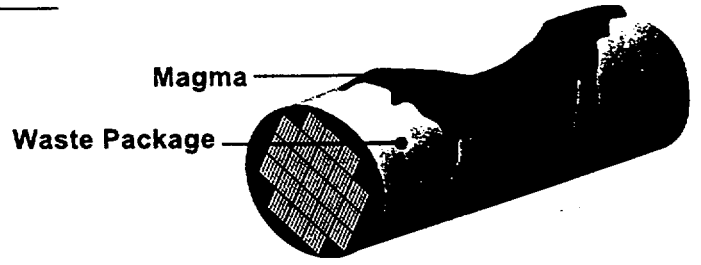
snl/trw abq 02a.eps

Figure 10-3a. Simplified representation of igneous activity scenarios.

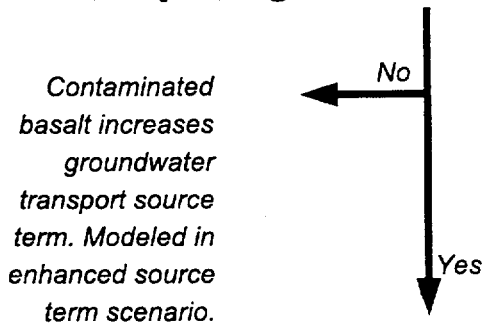
Waste packages are breached?



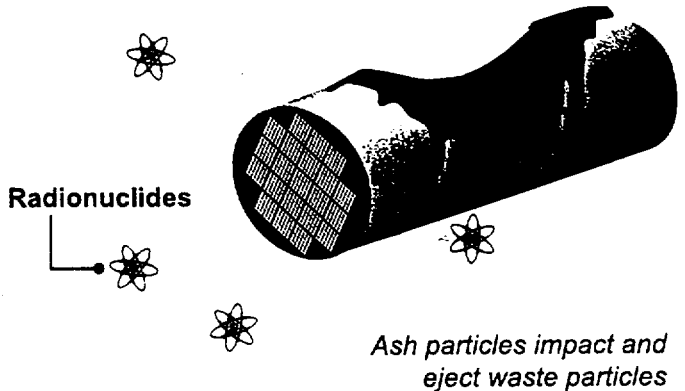
No performance assessment consequence.



Waste is removed from waste package?



Contaminated basalt increases groundwater transport source term. Modeled in enhanced source term scenario.



sni/trw abq 02b.eps

Figure 10-3b. Simplified representation of components of direct-release igneous activity scenarios.

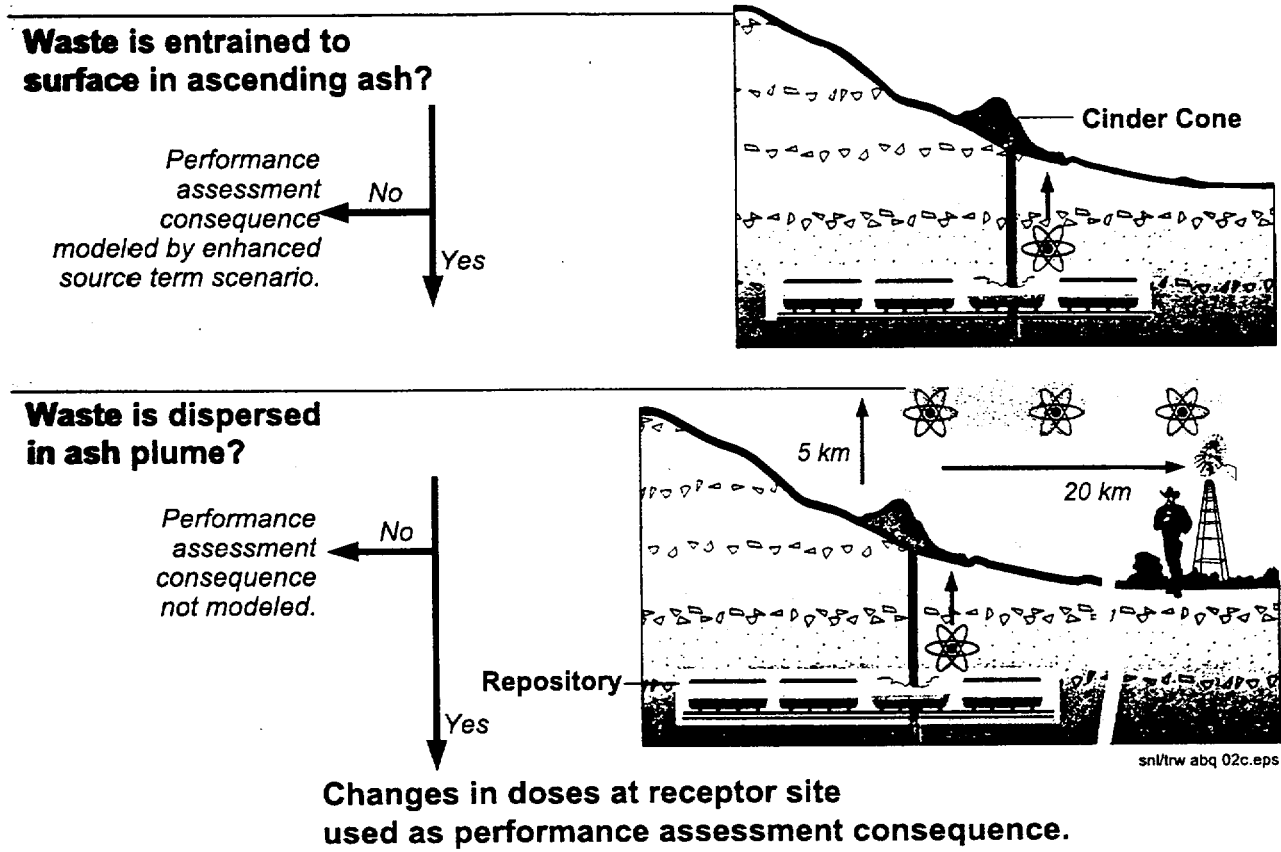
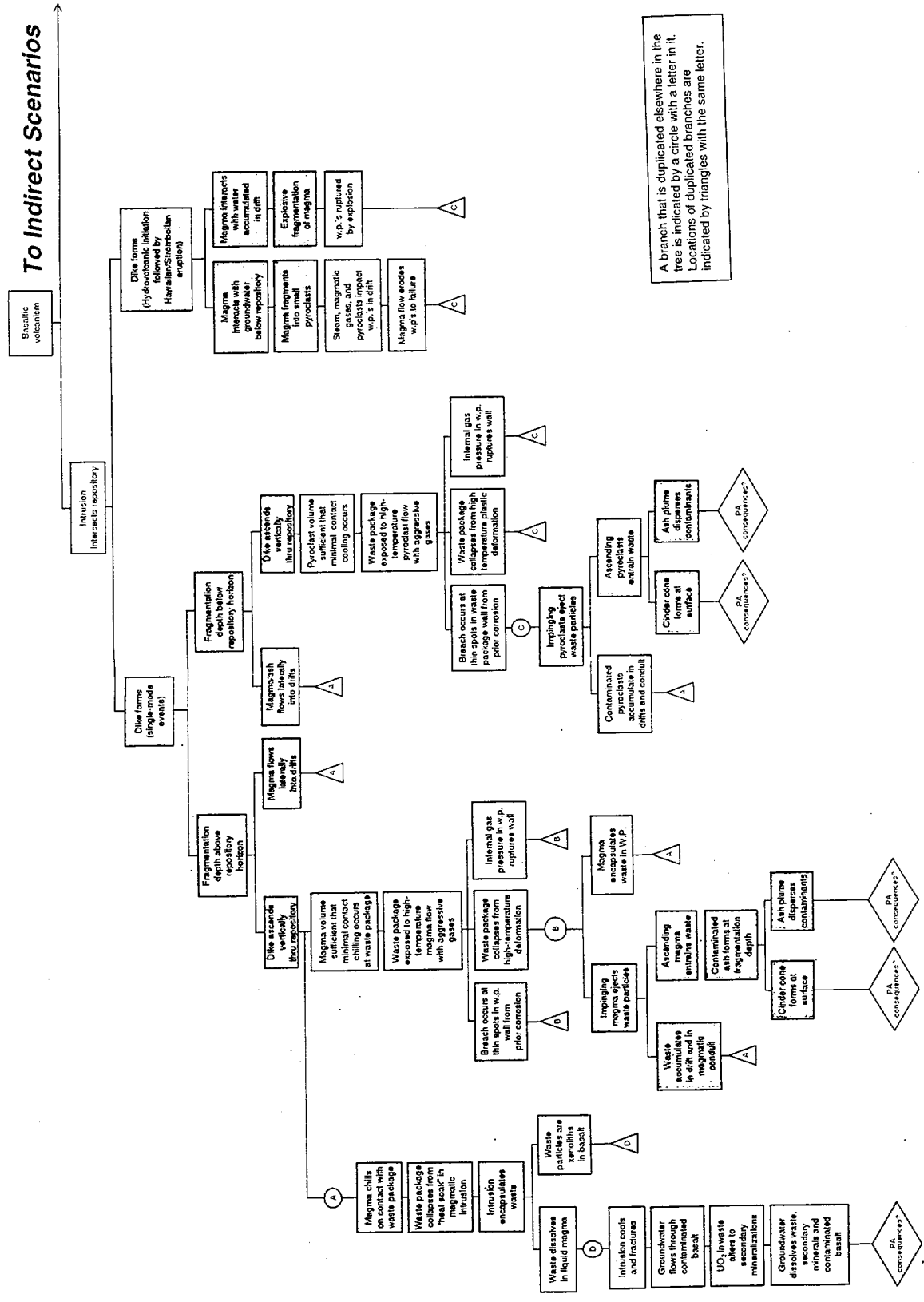


Figure 10-3c. Simplified representation of components of direct-release igneous activity scenarios (continued).

To Indirect Scenarios

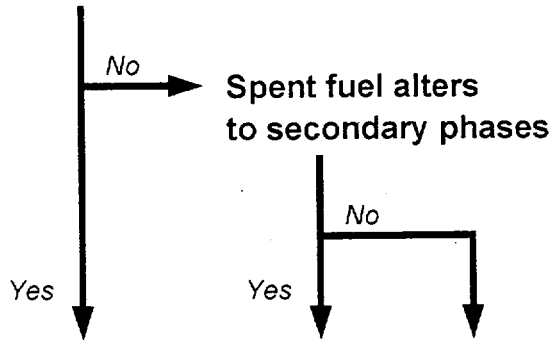


A branch that is duplicated elsewhere in the tree is indicated by a circle with a letter in it. Locations of duplicated branches are indicated by triangles with the same letter.

Figure 10-4a. Direct-release branches of the generalized event tree for igneous activity.

FIG-6

Magma dissolves spent fuel

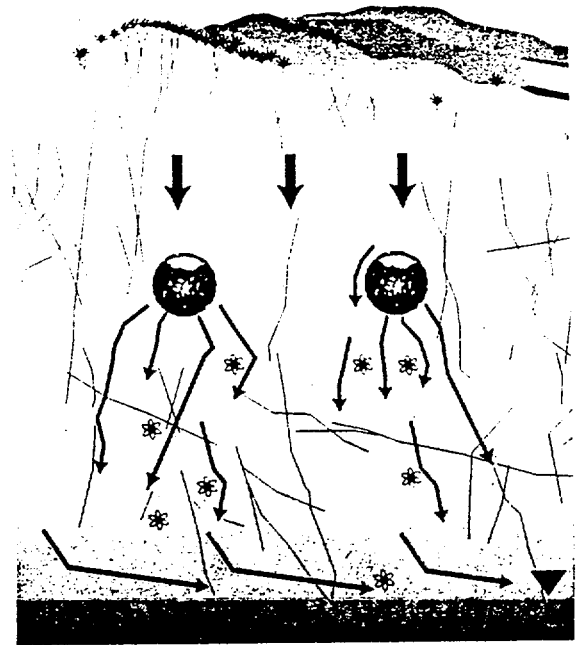
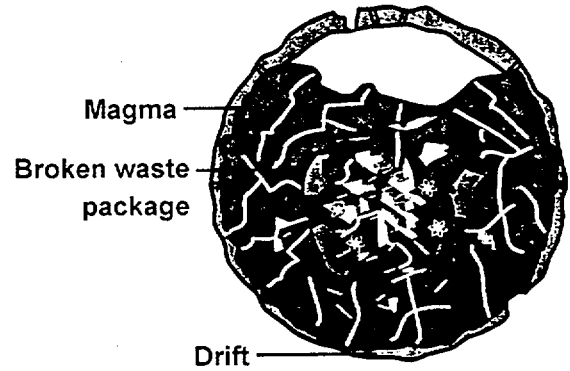


Groundwater dissolves contaminants from basalt and spent fuel

Contaminants transported through unsaturated zone and saturated zone

Changes in doses at receptor site used as performance assessment consequence

Yes

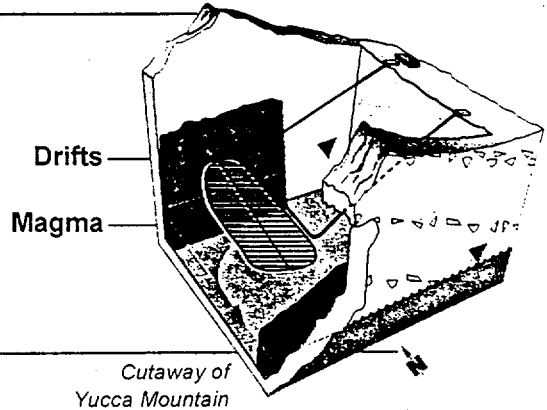
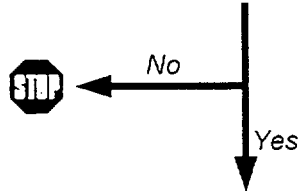


snl/trw abq61.eps

Figure 10-5. Simplified representation of components of enhanced-source-term igneous activity scenario.

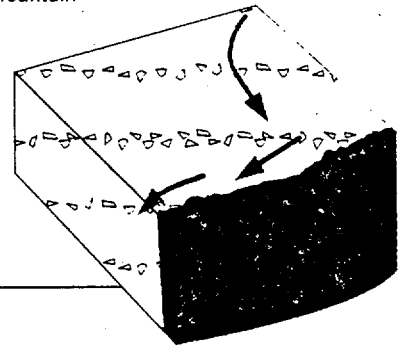
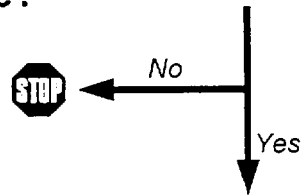
Igneous dike occurs in Yucca Mountain region?

No performance assessment consequence. End Scenario.



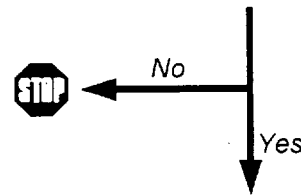
Dike alters groundwater flow and transport in saturated zone?

No performance assessment consequence.

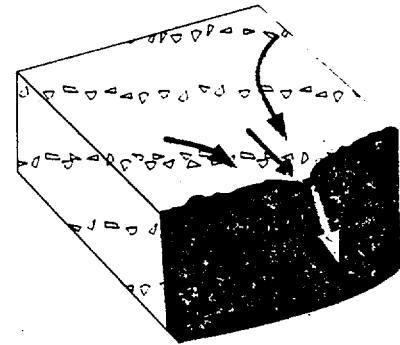


Dike transmits groundwater more readily than surrounding rock?

No performance assessment consequence.



Changes in doses at receptor site are used as performance assessment consequence



snl/trw abq25.eps

Figure 10-6. Simplified representation of components of indirect-effect igneous activity scenario.

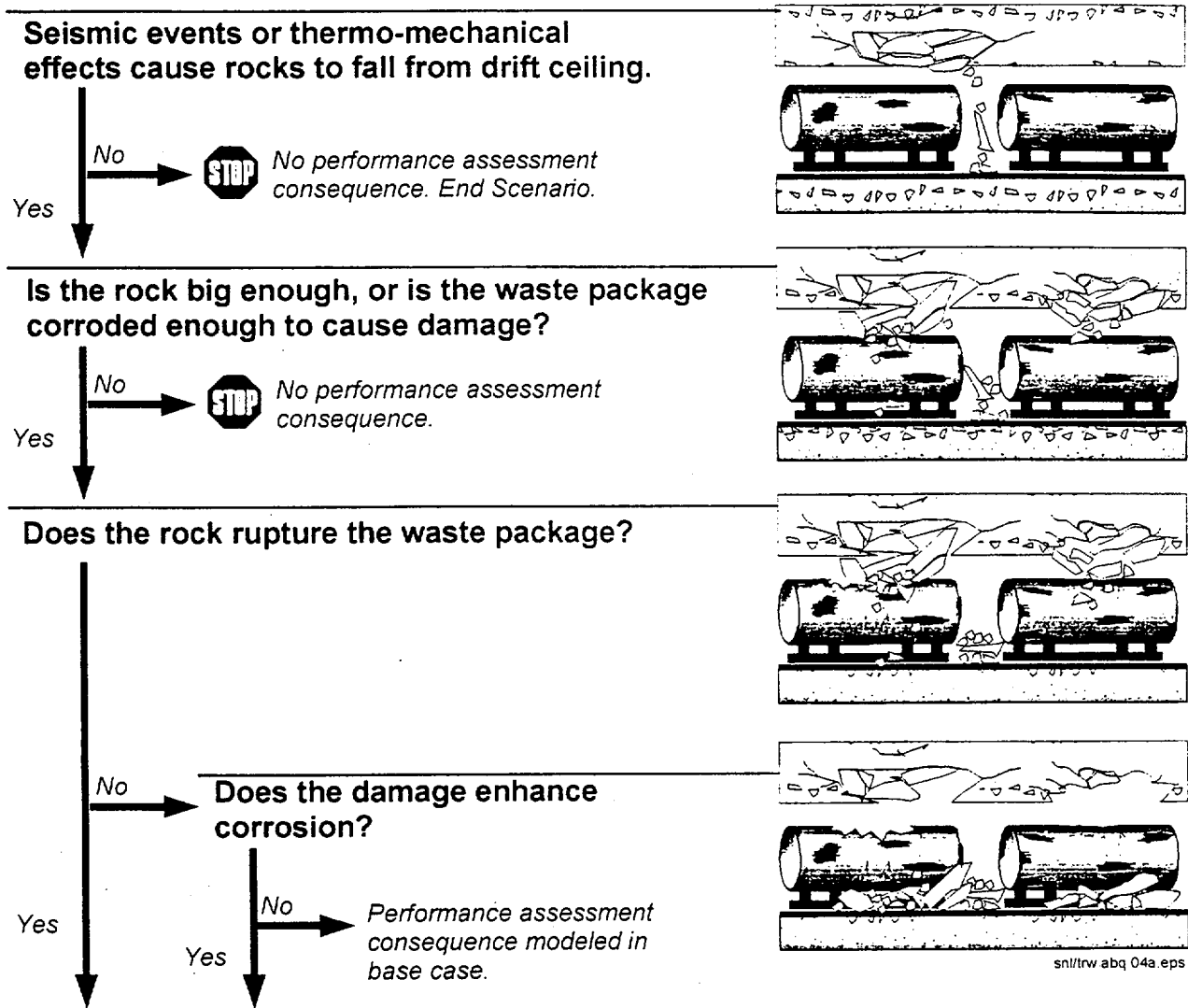


Figure 10-7. Simplified representation of the rockfall scenario.

Displacement occurs on faults in Yucca Mountain region?

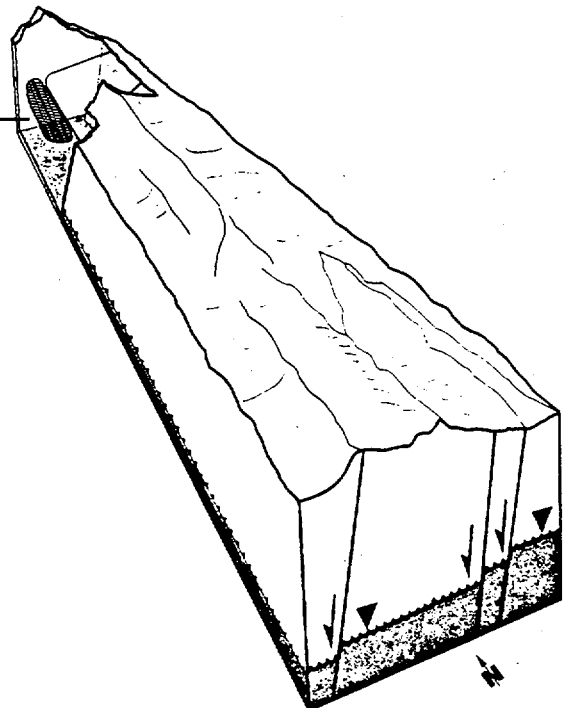
No performance assessment consequence. End Scenario.



No

Yes

Repository



Re-initiation of movement on faults occurs in multiple areas of hydrologic system?

No performance assessment consequence.



No

Yes

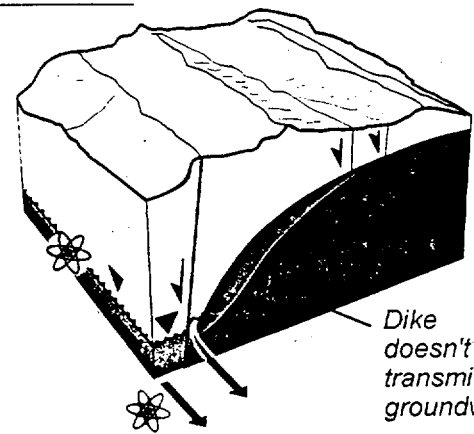
Re-initiated faulting alters groundwater flow and transport in saturated zone?

No performance assessment consequence.



No

Yes



Dike doesn't transmit groundwater.

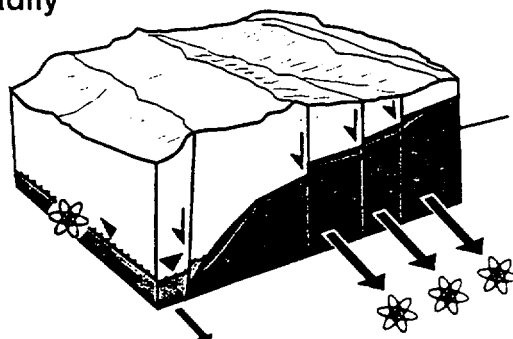
Faults from re-initiated seismic activity transmit water more readily than surrounding rock?

No performance assessment consequence.



No

Yes



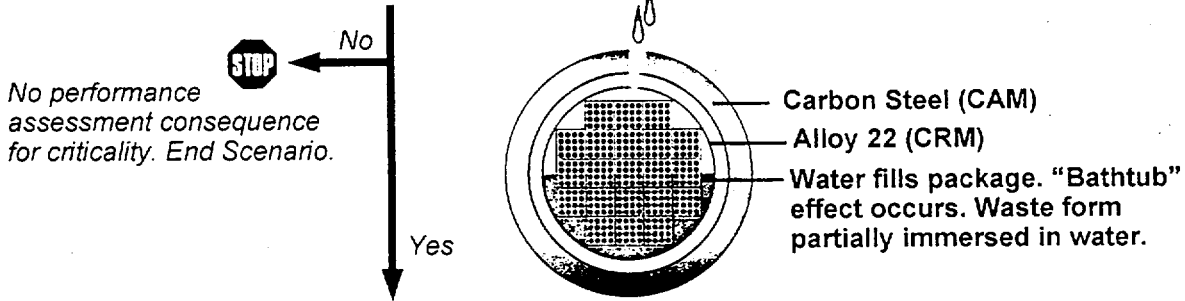
Faulted dike transmits water better than tuffs.

Changes in doses at receptor site are used as performance assessment consequences.

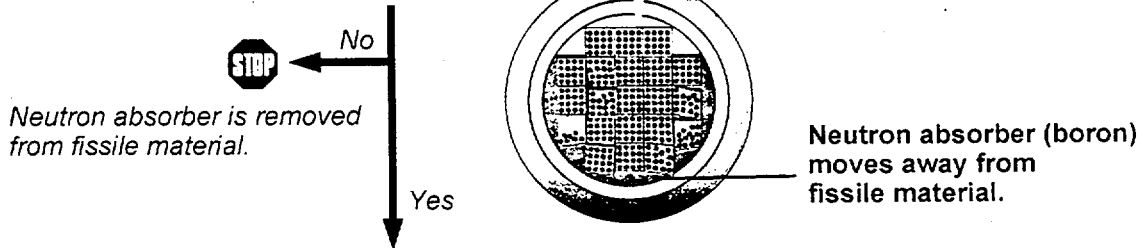
sn/trw abq 68.eps

Figure 10-8. Simplified representation of the seismic indirect-effects scenario.

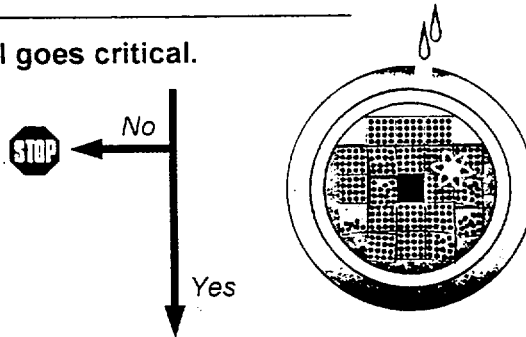
Waste package breached on top half, not breached on bottom half.



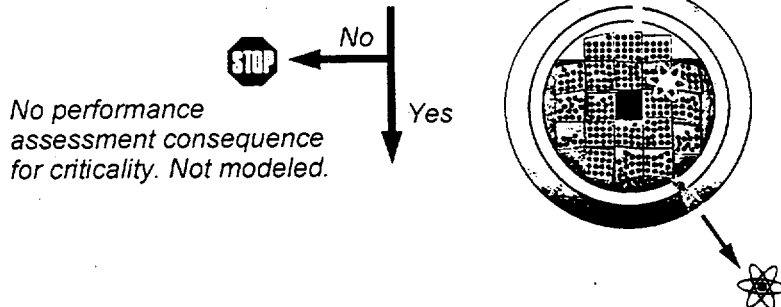
Basket holding assemblies partially degrades, releasing neutron absorber.



Fissile material goes critical.

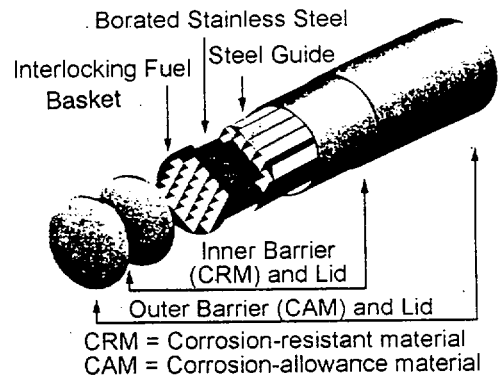


Waste package corrodes, allowing dissolved radionuclides to move out.



Waste Package

Expanded to show parts. Package shown in cross section in pictures to left.

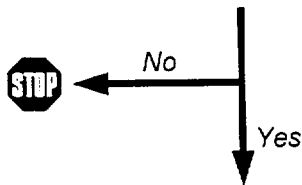


sn/trw abq 01.eps

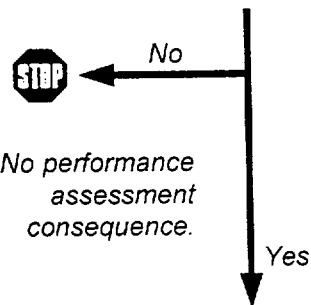
Figure 10-9. Simplified representation of the in-package nuclear criticality scenario.

Radionuclides in groundwater move out of repository and collect in a subsurface trap.

Cutaway of Yucca Mountain

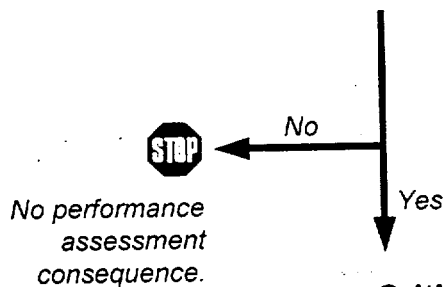


Subsurface feature contains reducing environment that precipitates radionuclides.



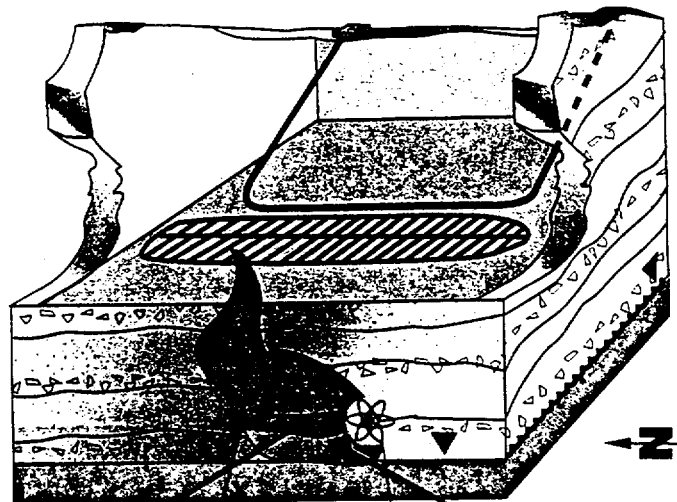
No performance assessment consequence.

Are the following conditions present?
 Sufficient fissile material
 Sufficient water for moderator
 Few neutron absorbers
 Radionuclides collected in a "favorable" geometry.



No performance assessment consequence.

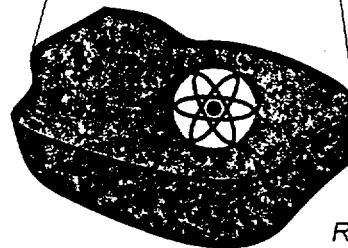
Critical configuration produces additional radionuclides that are transported to dose receptor point.



Organic matter in tuff.

Plume with reduced radionuclide concentration.

Subsurface trap formed within low oxygen (reducing) zone where radionuclides precipitate out and collect (become insoluble).



Radionuclides formed by criticality are more soluble and enter groundwater.

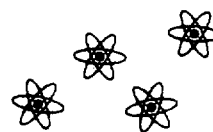
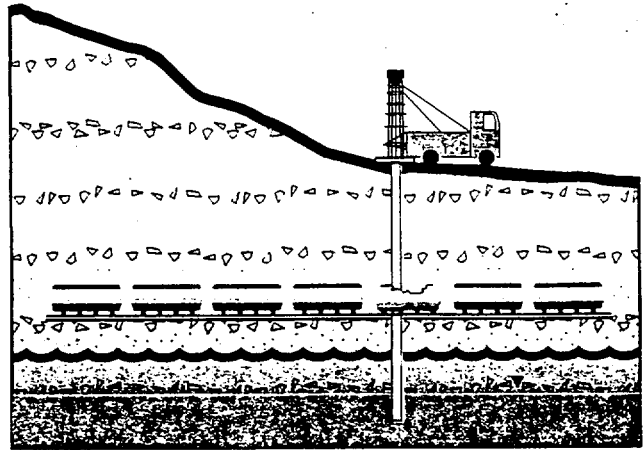


Figure 10-10. Simplified representation of the out-of-package nuclear criticality scenario.

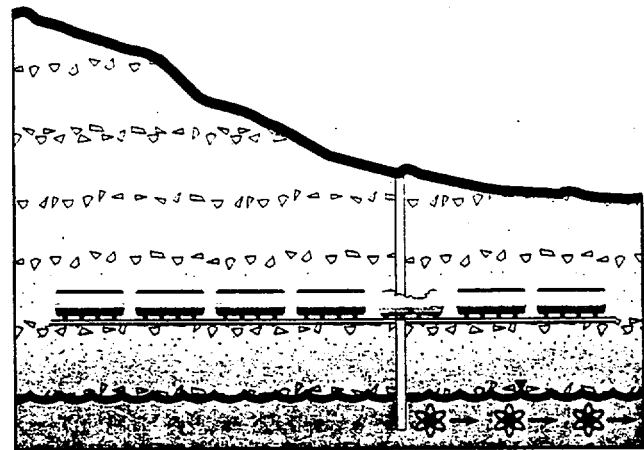
Borehole drilled for water.
Bit hits and breaks waste package.
Drilling continues to water table.

Waste falls down borehole to
water table.



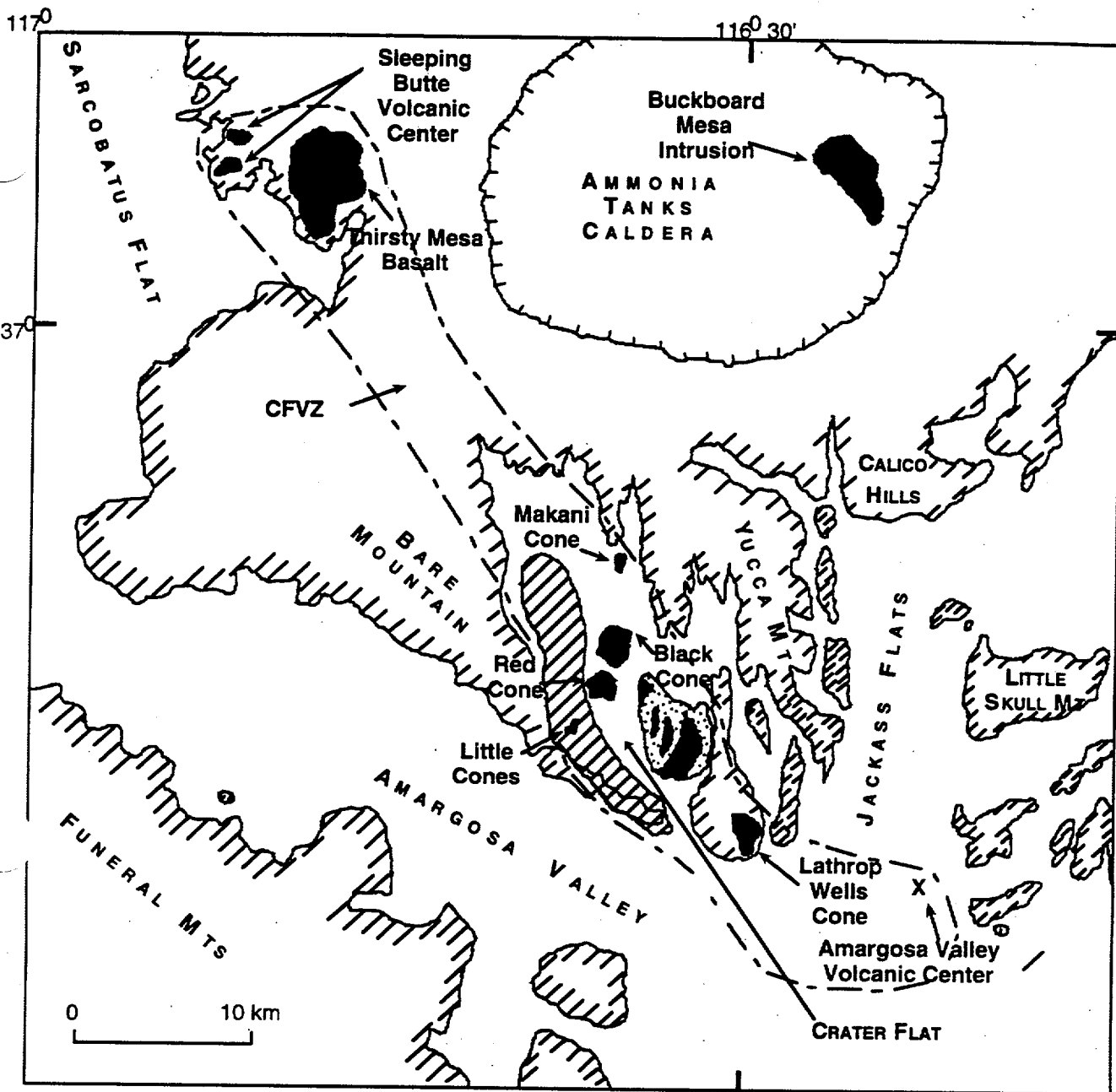
Enhanced concentration of waste
transported to accessible environment.

Performance assessment consequence
is enhanced source term for saturated
zone transport.



snl/trw abq 03.eps

Figure 10-11. Simplified representation of the human-intrusion scenario.



EXPLANATION

-  Generalized outcrop of Precambrian to Pleistocene bedrock
-  Outcrop of and area underlain by 3.7 Ma basalt
-  Area underlain by 10-11 Ma basalt

Figure 10-12. Location of Plio-Pleistocene volcanic centers in the Yucca Mountain area and outline of the Crater Flat Volcanic Zone (CFVZ).

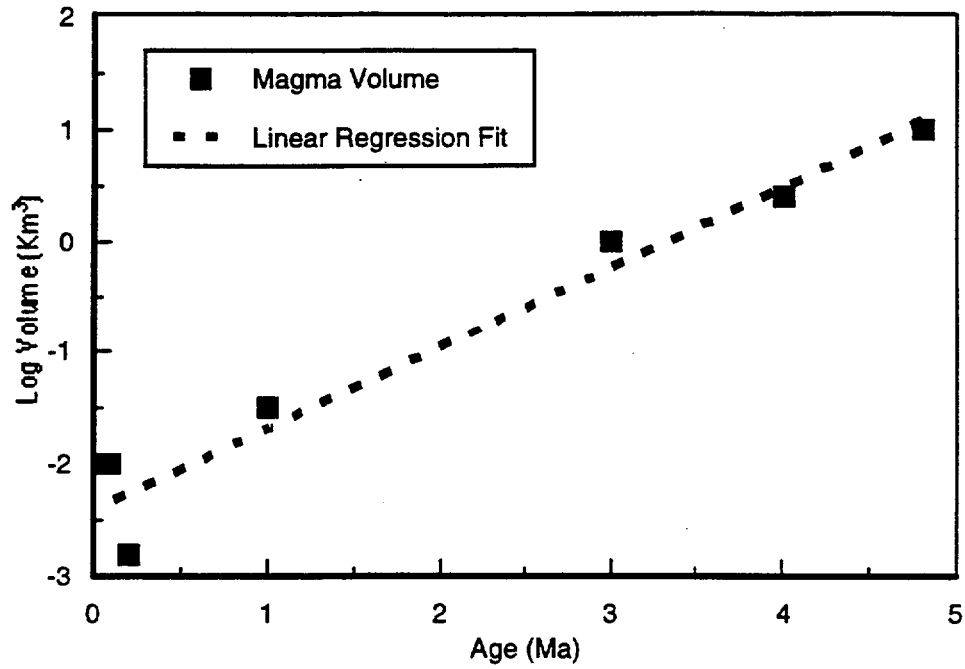


Figure 10-13. Magma volume vs age of eruption for Pliocene and Quaternary volcanic events in the Yucca Mountain region.

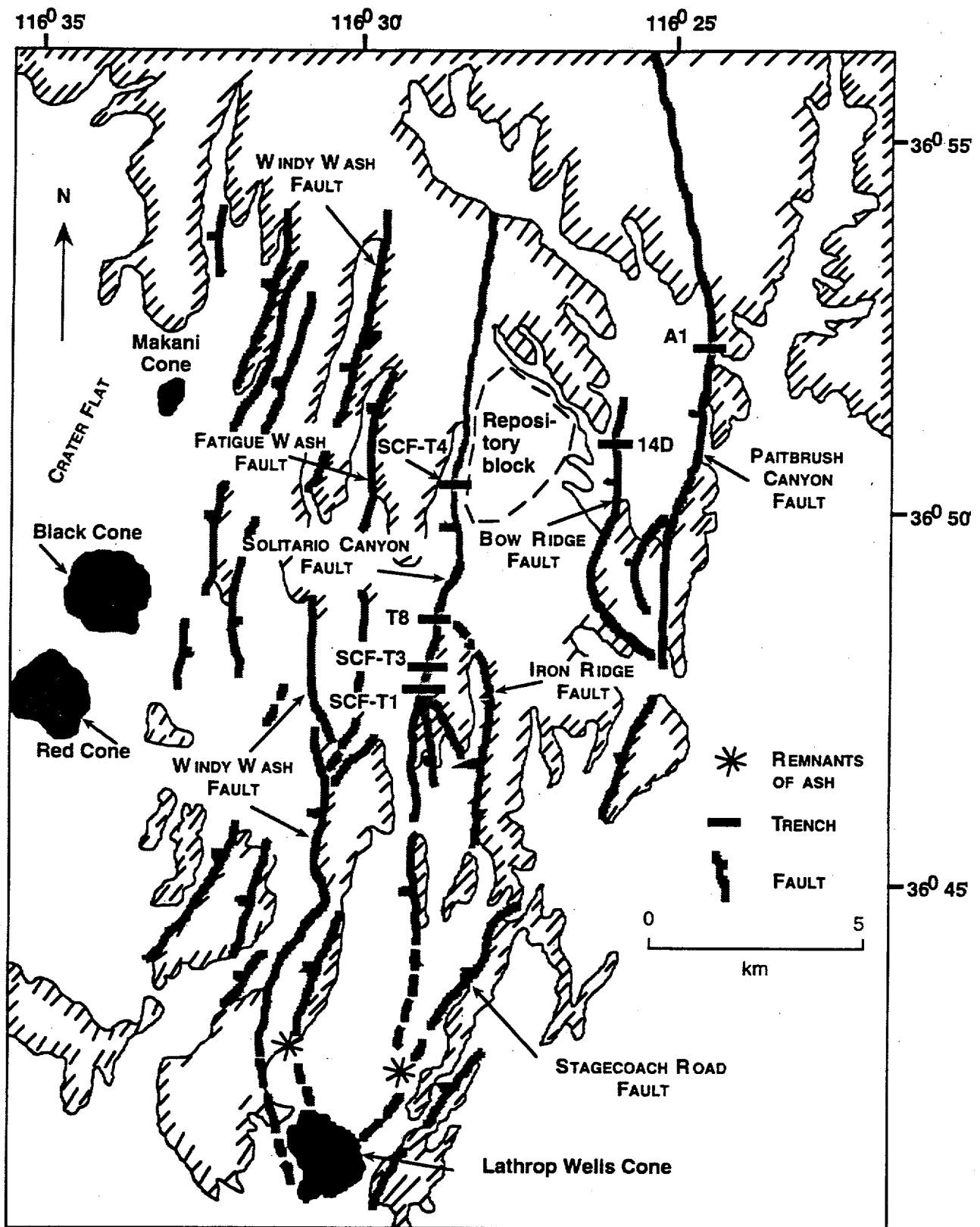


Figure 10-14. Major faults along Yucca Mountain and locations of trenches that contain basaltic ash. Star symbols show locations of ash remnants from Lathrop Wells cone.

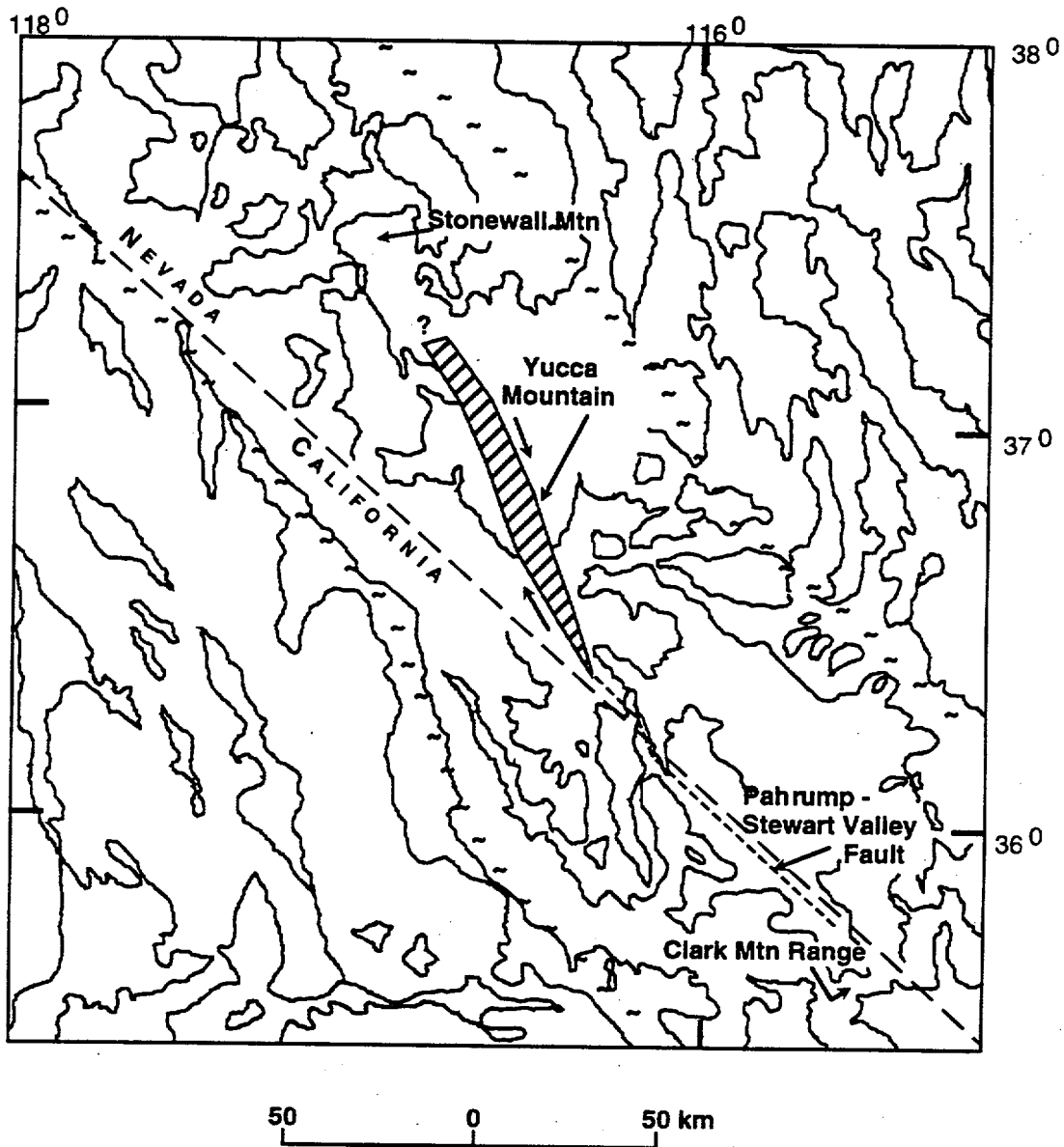


Figure 10-15. Approximate borders of Walker Lane shown by --- pattern. Hatching and strike-slip arrows show location of Amargosa Desert fault system of Schweickert and Lahren (1997).

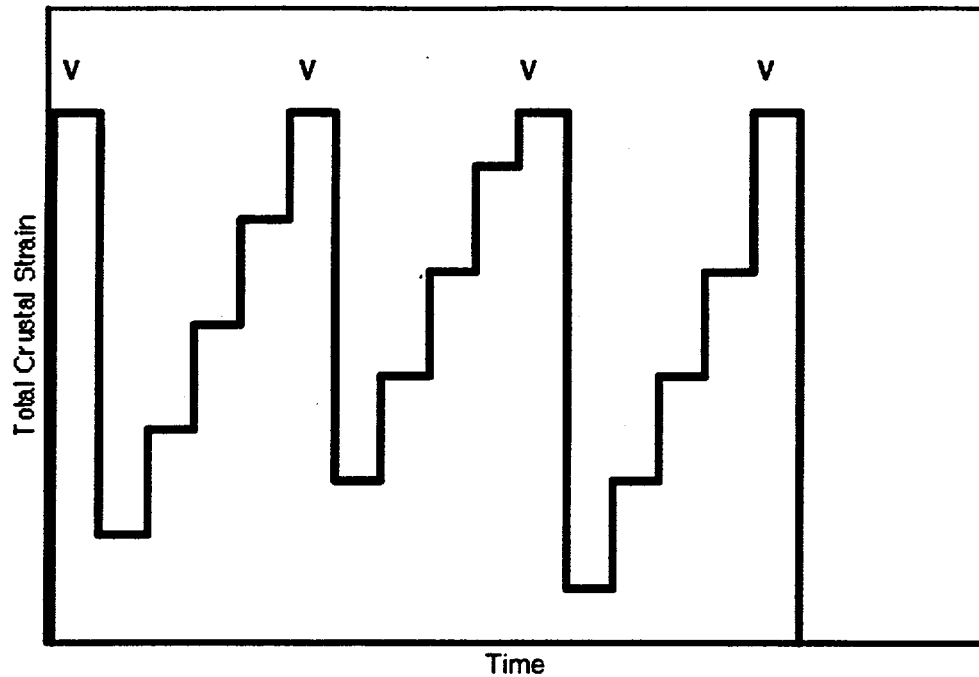


Figure 10-16. Total crustal strain vs time. Initiating event V culminates in volcanism, a high-strain event. Strain then drops to low level; as horizontal stress decreases, extensional strain increases and different parts of crust fail and slip, culminating in another volcanic event.

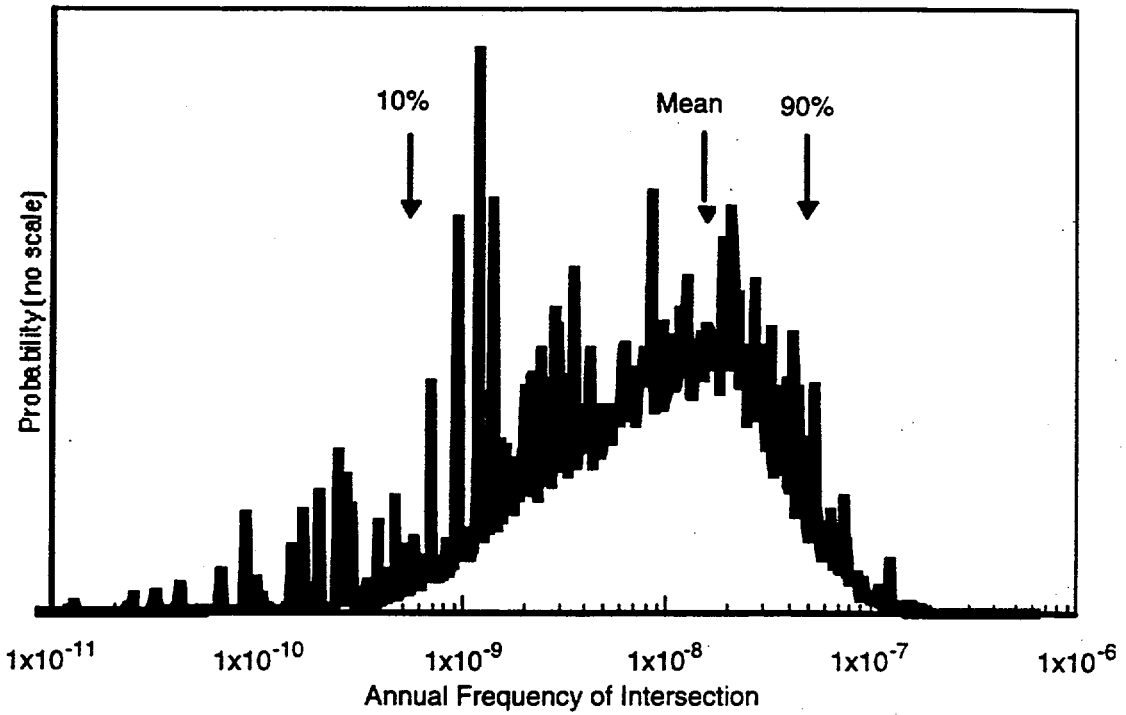


Figure 10-17. Aggregate results for frequency of intersection of an igneous intrusion with the Potential Yucca Mountain repository (after CRWMS M&O 1996a, Figure 4-32a)

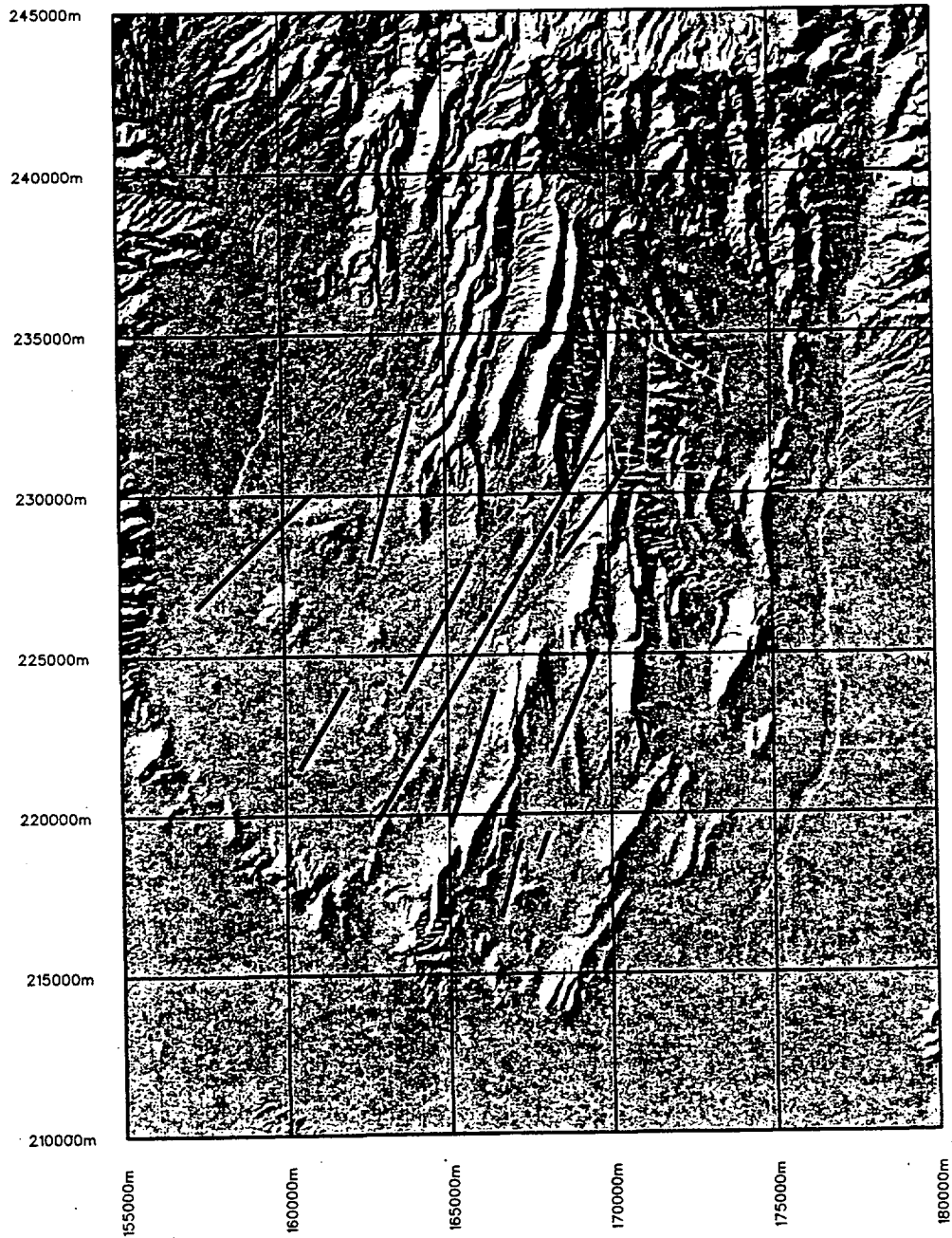


Figure 10-18. Illustration of potential dikes in the Yucca Mountain area (after CRWMS M&O 1996a).

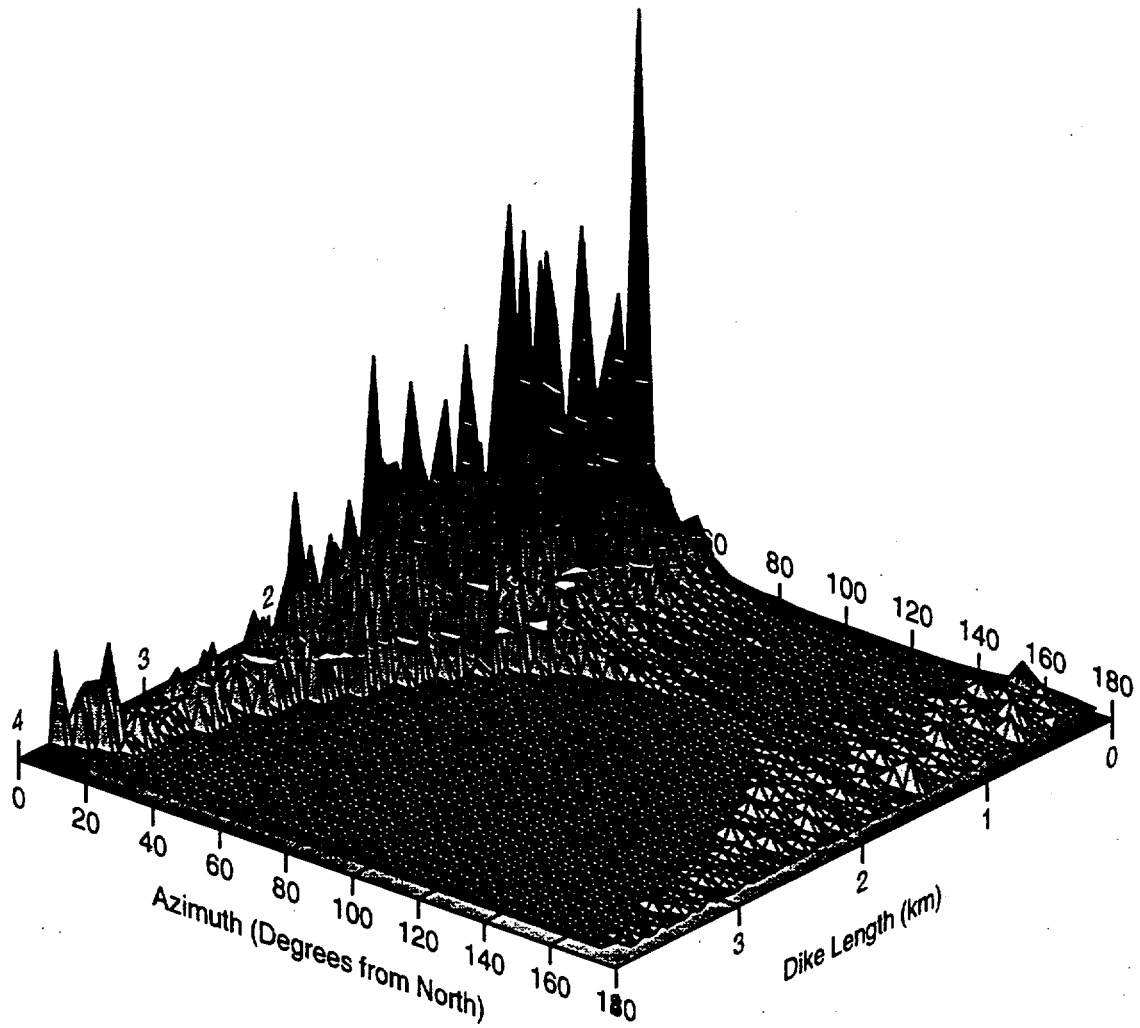


Figure 10-19. Probability density for dike length and orientation inside the repository (after CRWMS M&O 1996a).

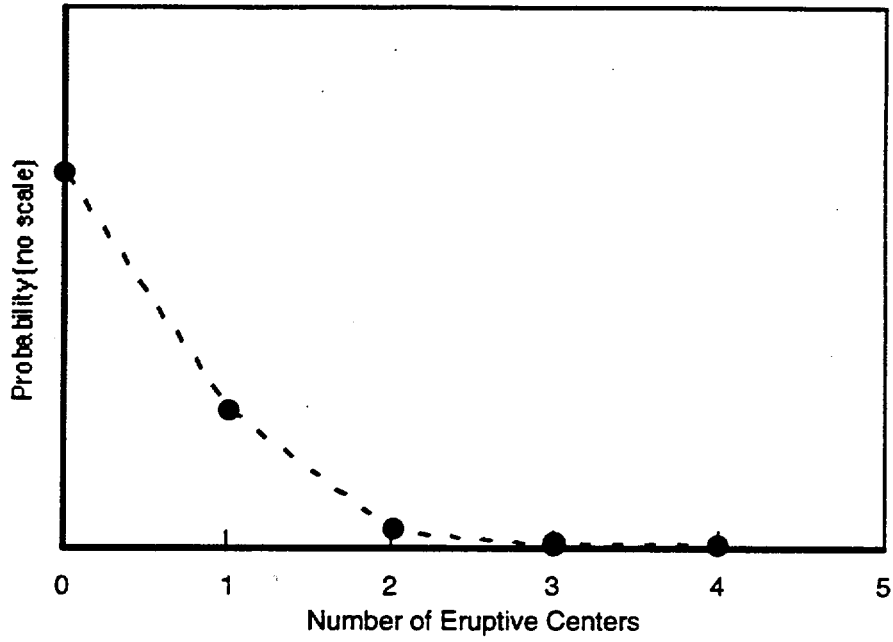


Figure 10-20. PDF for number of vents along a dike inside the repository.

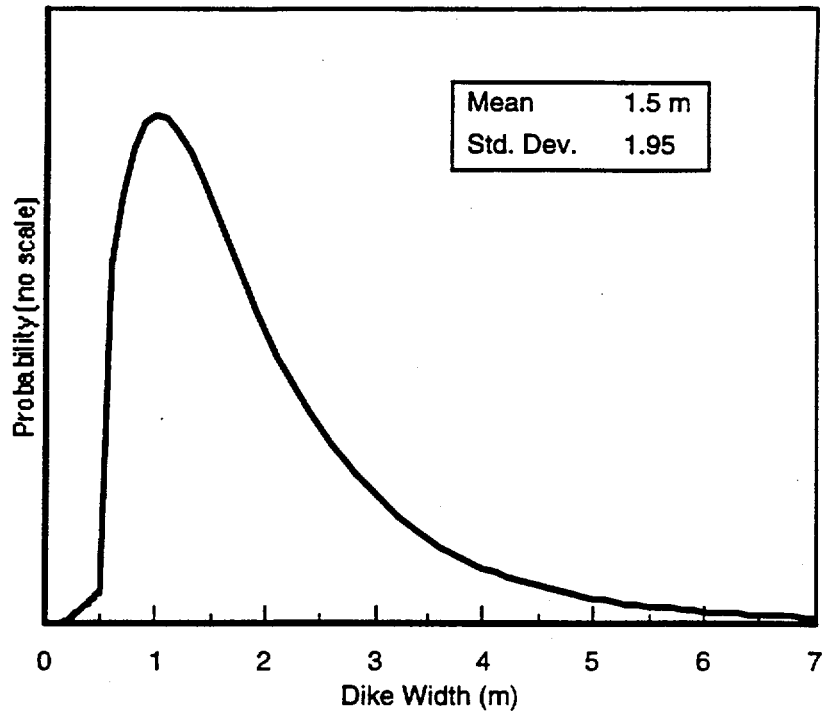


Figure 10-21. PDF for dike width.

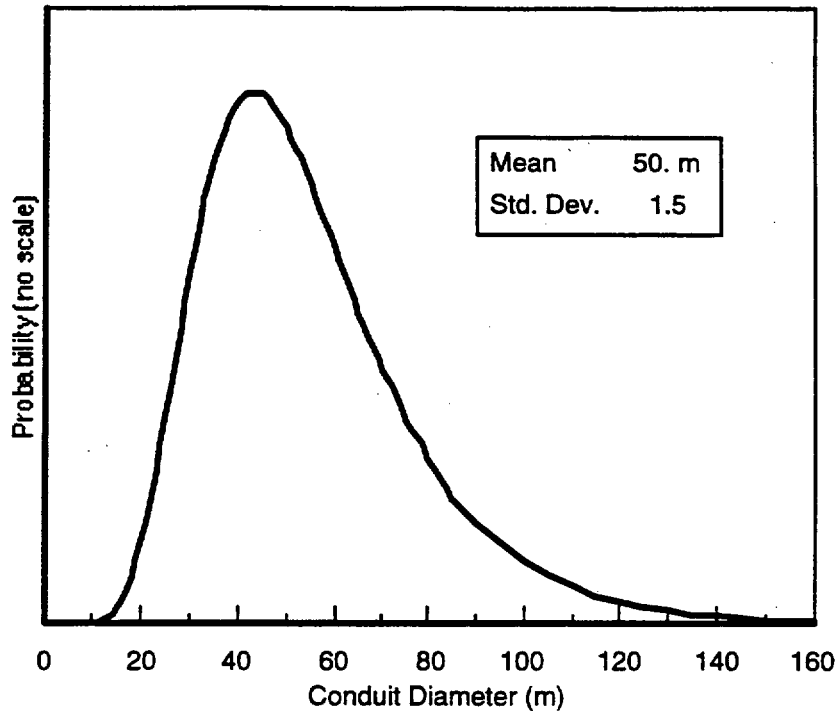


Figure 10-22. PDF for conduit diameter.

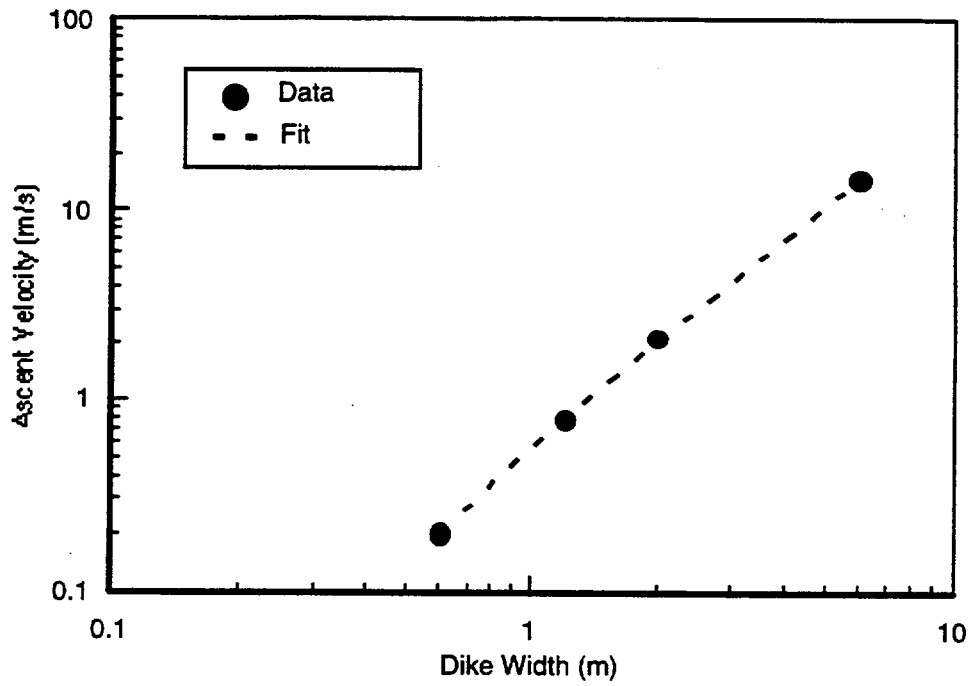


Figure 10-23. Range of liquid magma ascent velocities as a function of dike width.

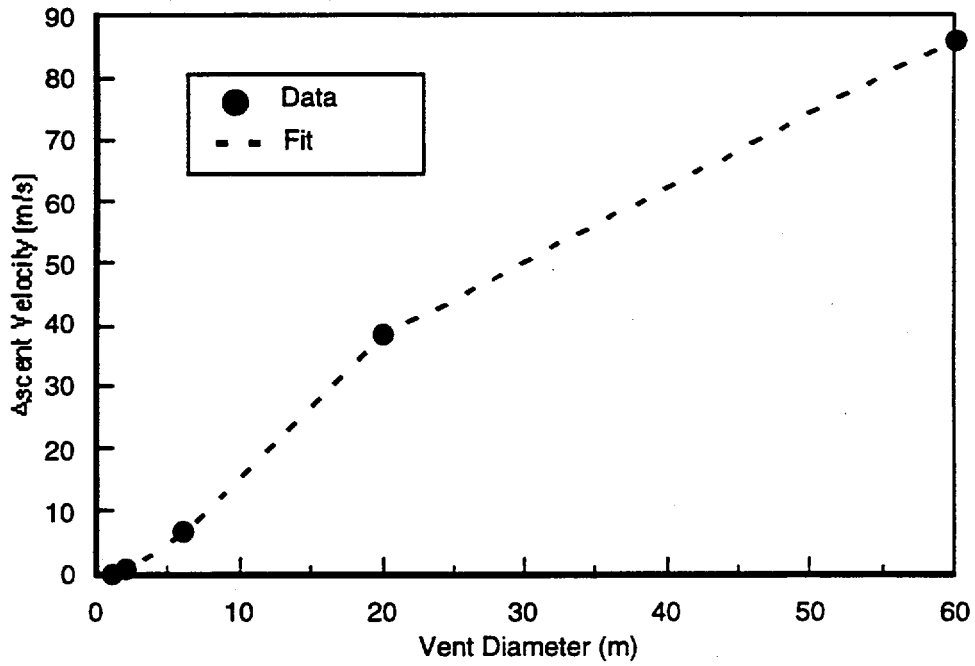


Figure 10-24. Range of ascent velocities as a function of conduit diameter (after Wilson and Head 1981, Table 3).

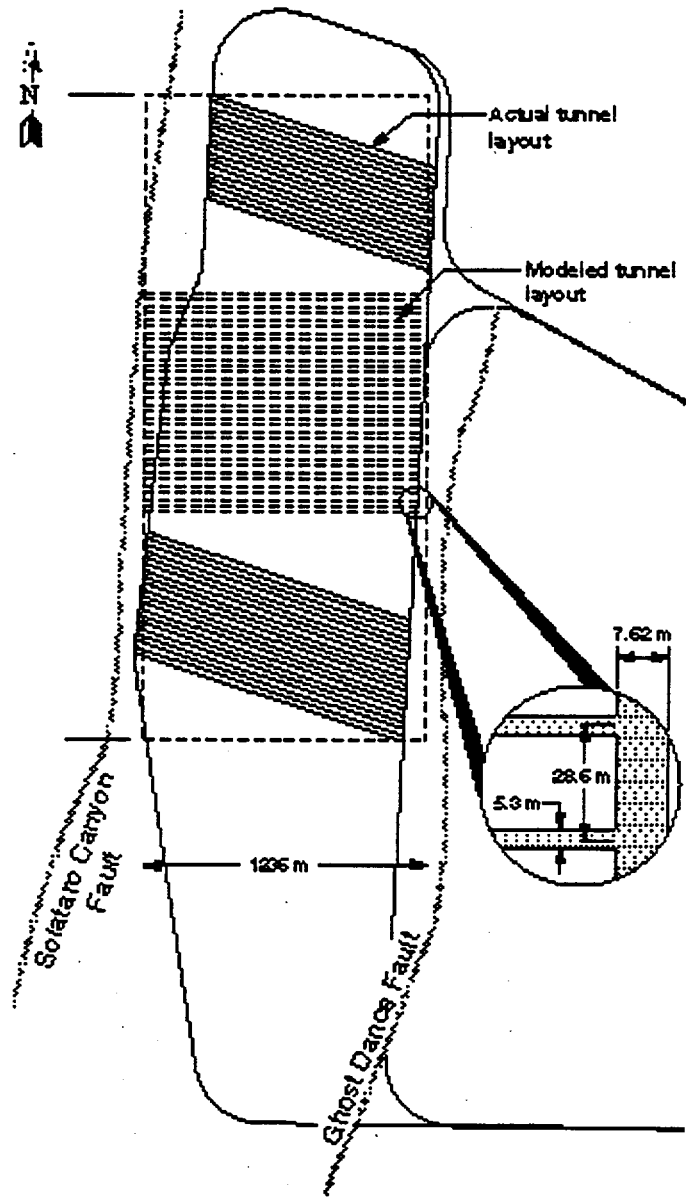


Figure 10-25. Repository outline and modeled configuration (from CRWMS M&O 1997a).

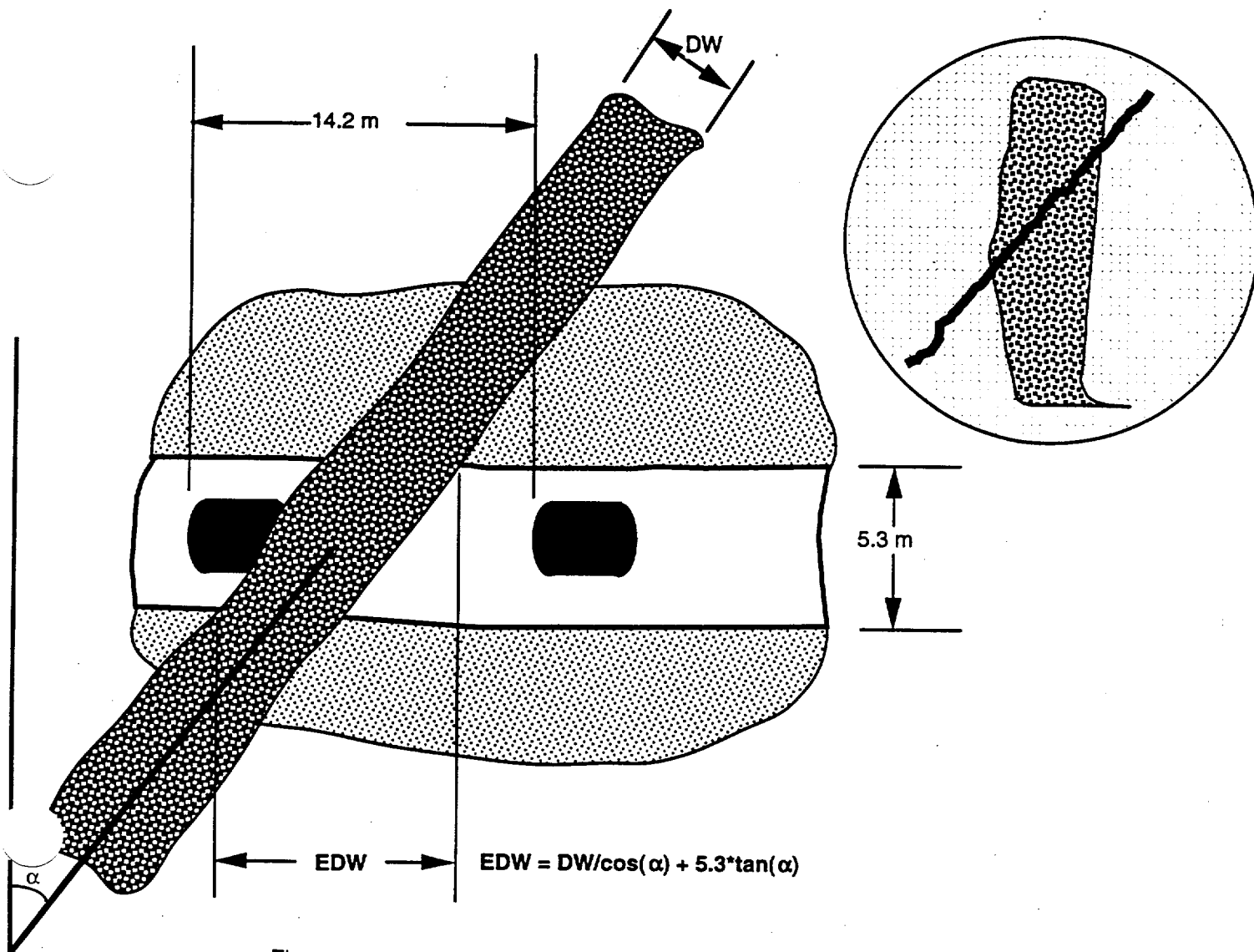


Figure 10-26. Dike intersection with a drift.

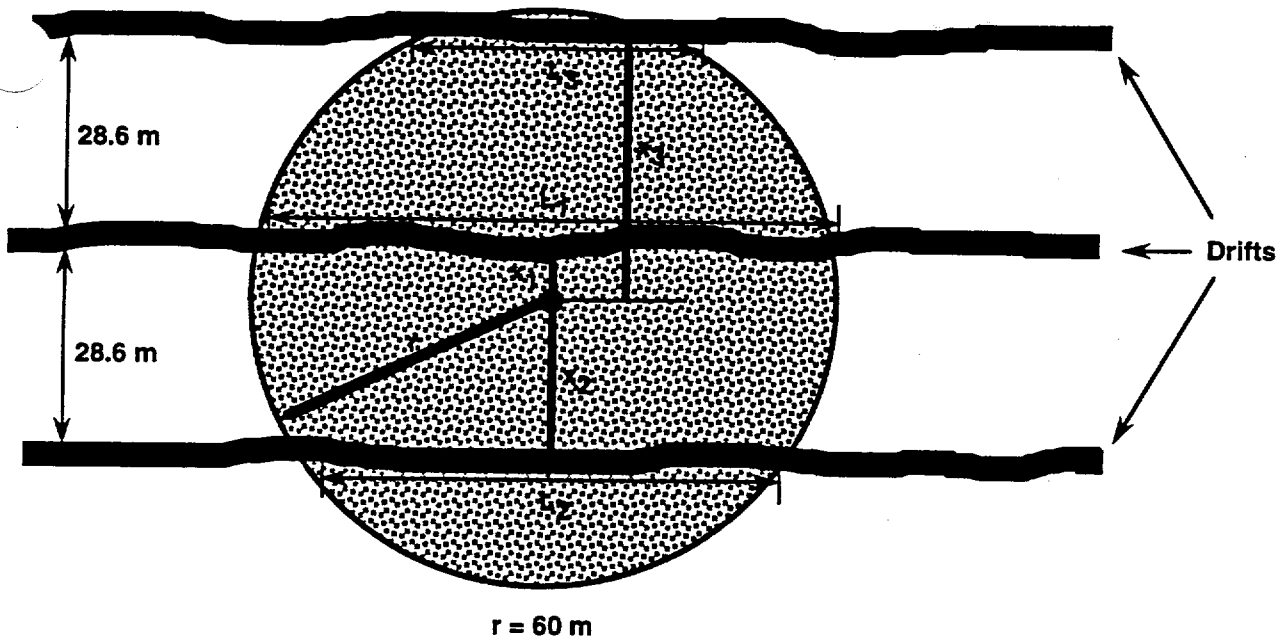


Figure 10-27. Intersection of a circular conduit with drifts.

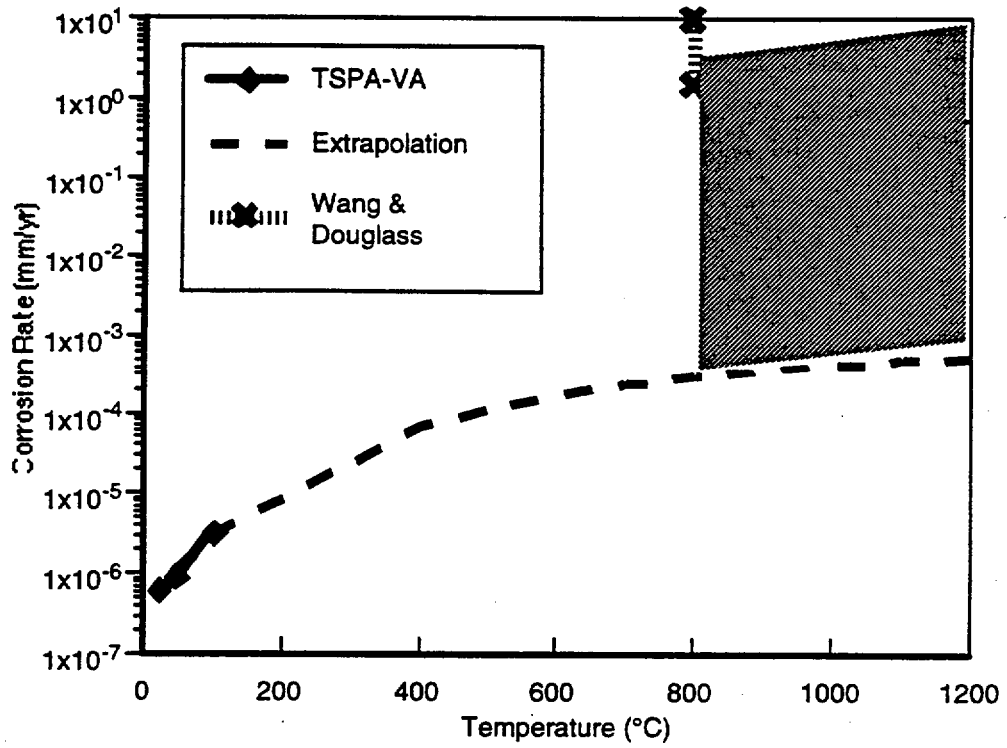


Figure 10-28. Extrapolation of CRM corrosion rates.

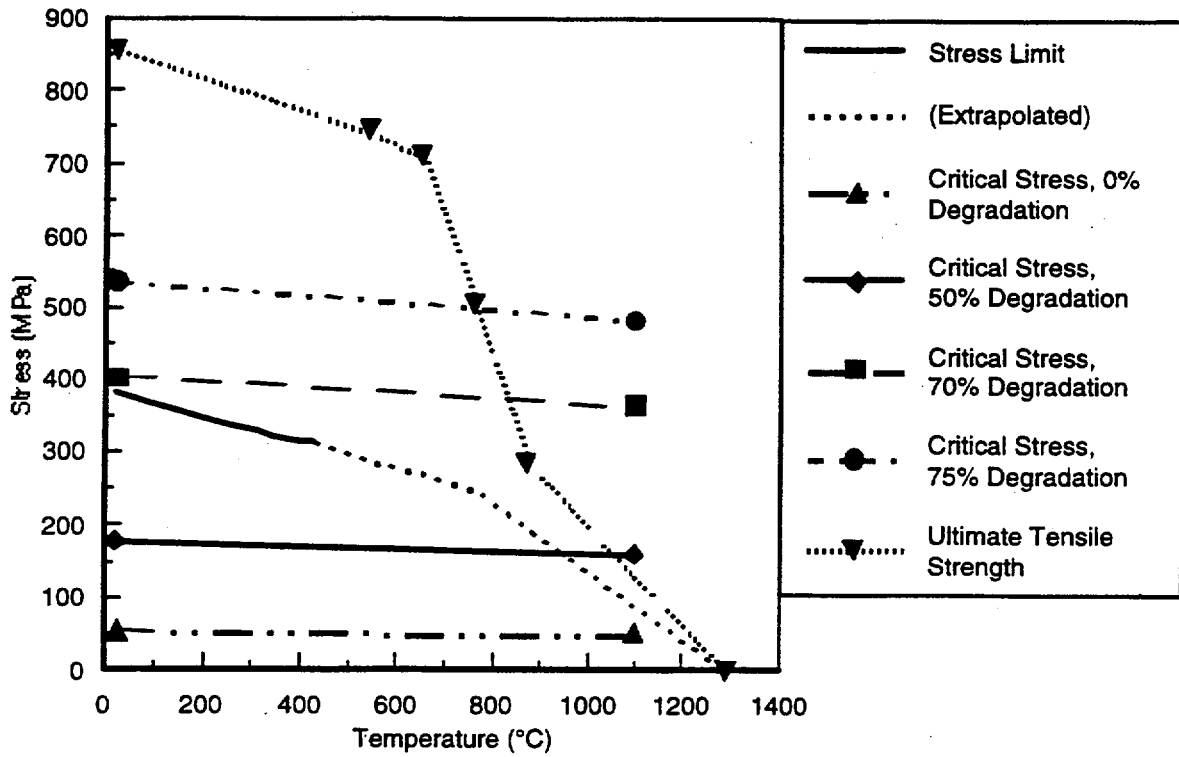


Figure 10-29. Waste-package CRM wall stresses as a function of temperature.

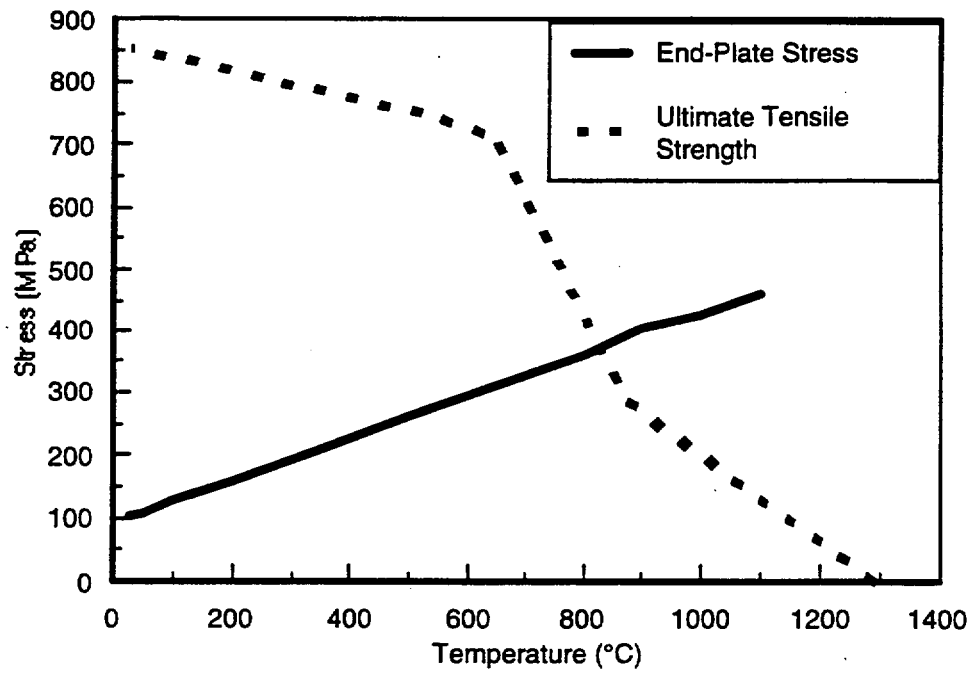


Figure 10-30. Waste-package CRM end-cap stresses as a function of temperature.

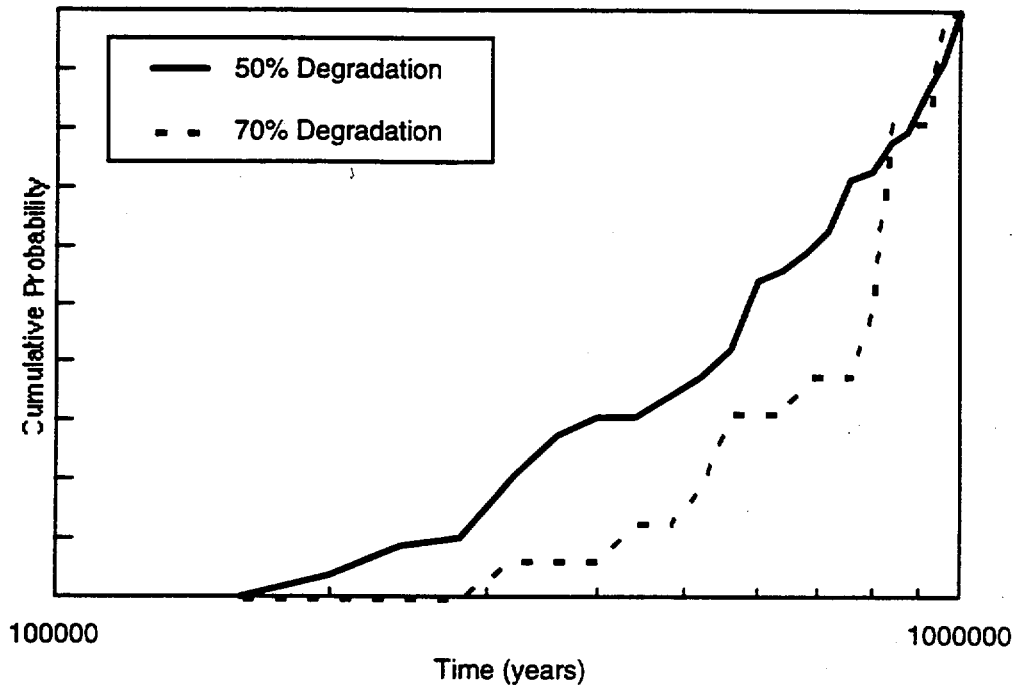


Figure 10-31. Times for 50% and 70% degradation of CRM.

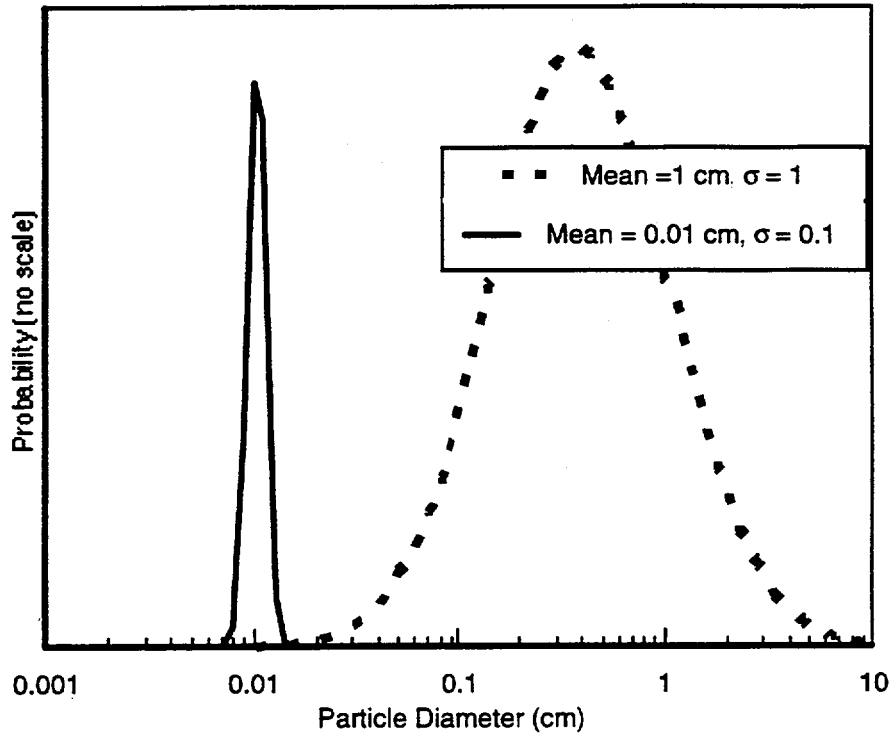


Figure 10-32. PDFs of ash-particle diameters.

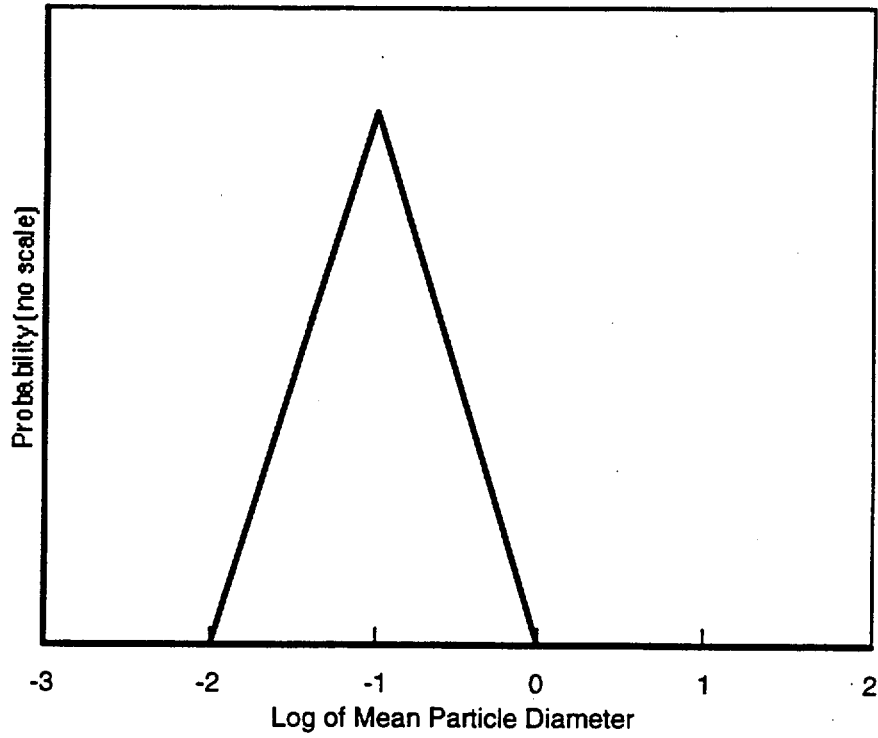


Figure 10-33. PDF for waste-particle sizes (Jarzempa & LaPlante 1996, Figure 4).

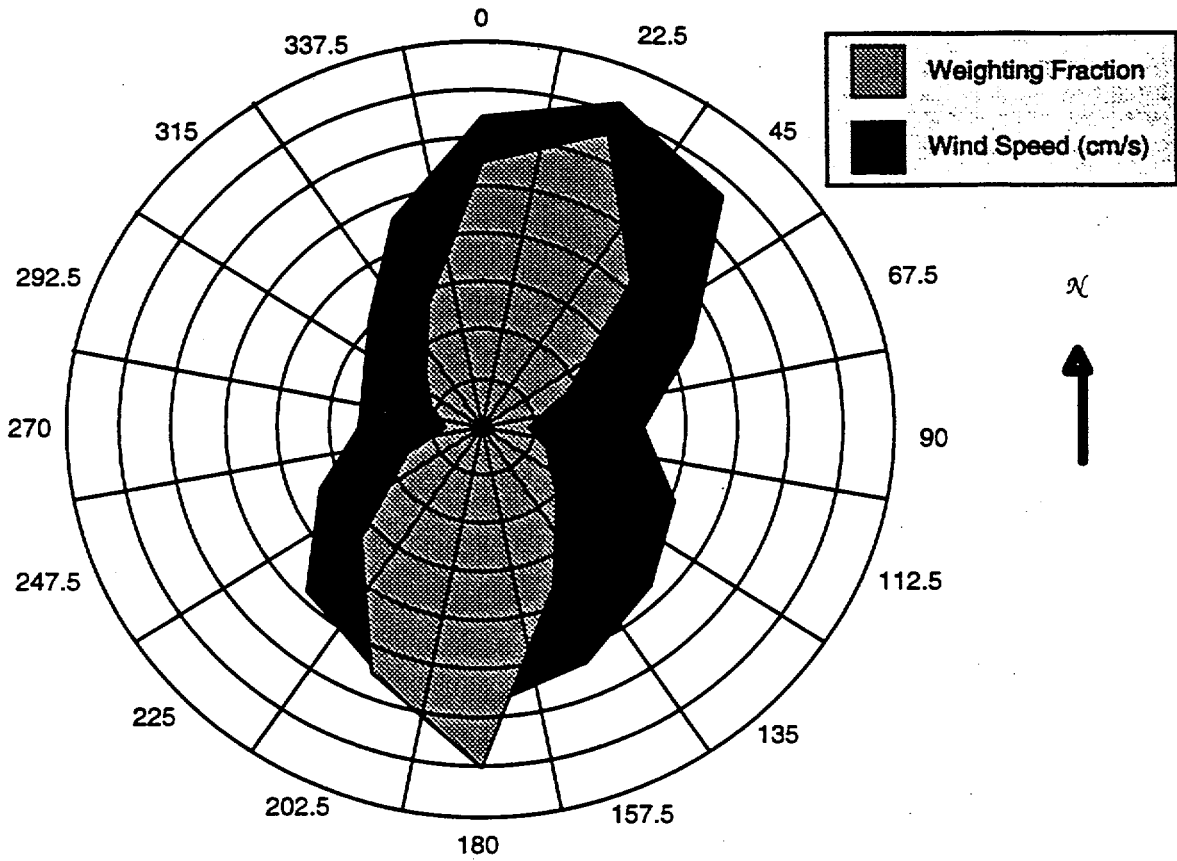


Figure 10-34. Distribution of wind direction and speed at Yucca Mountain.

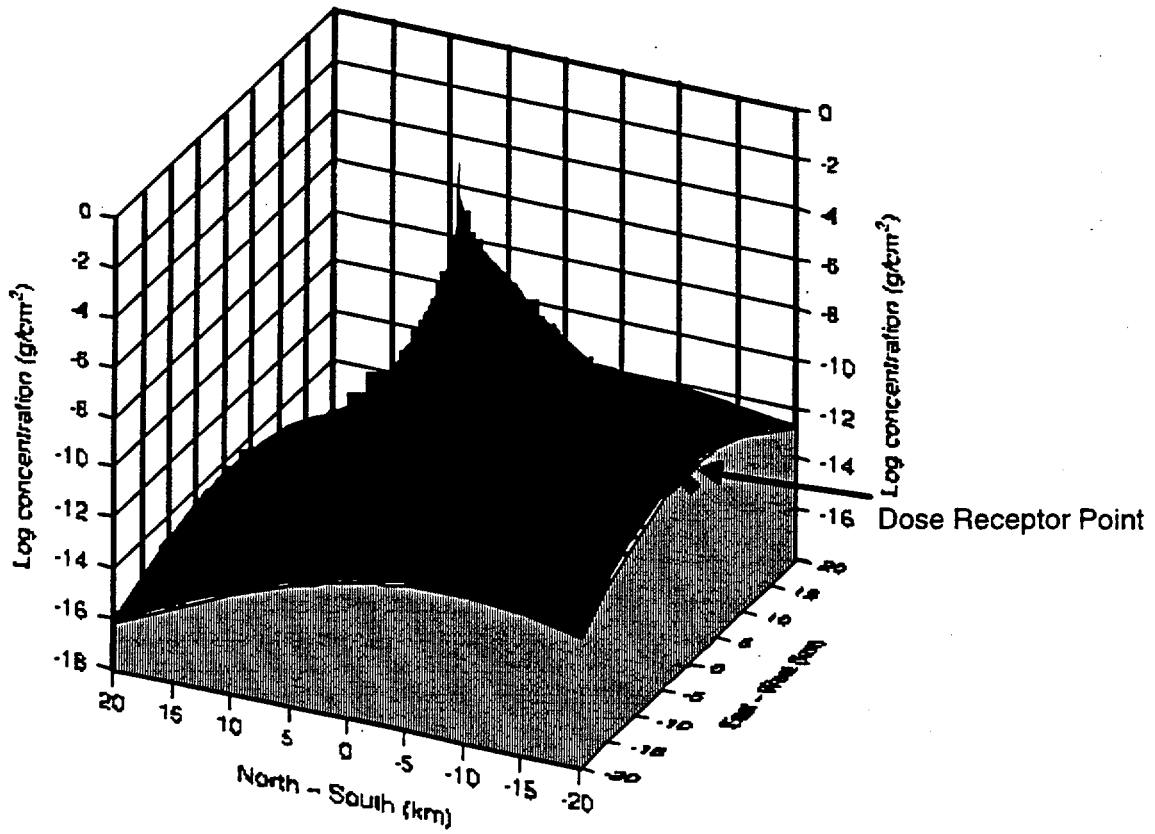


Figure 10-35. Contours for greatest concentration at dose receptor point (Realization 14).

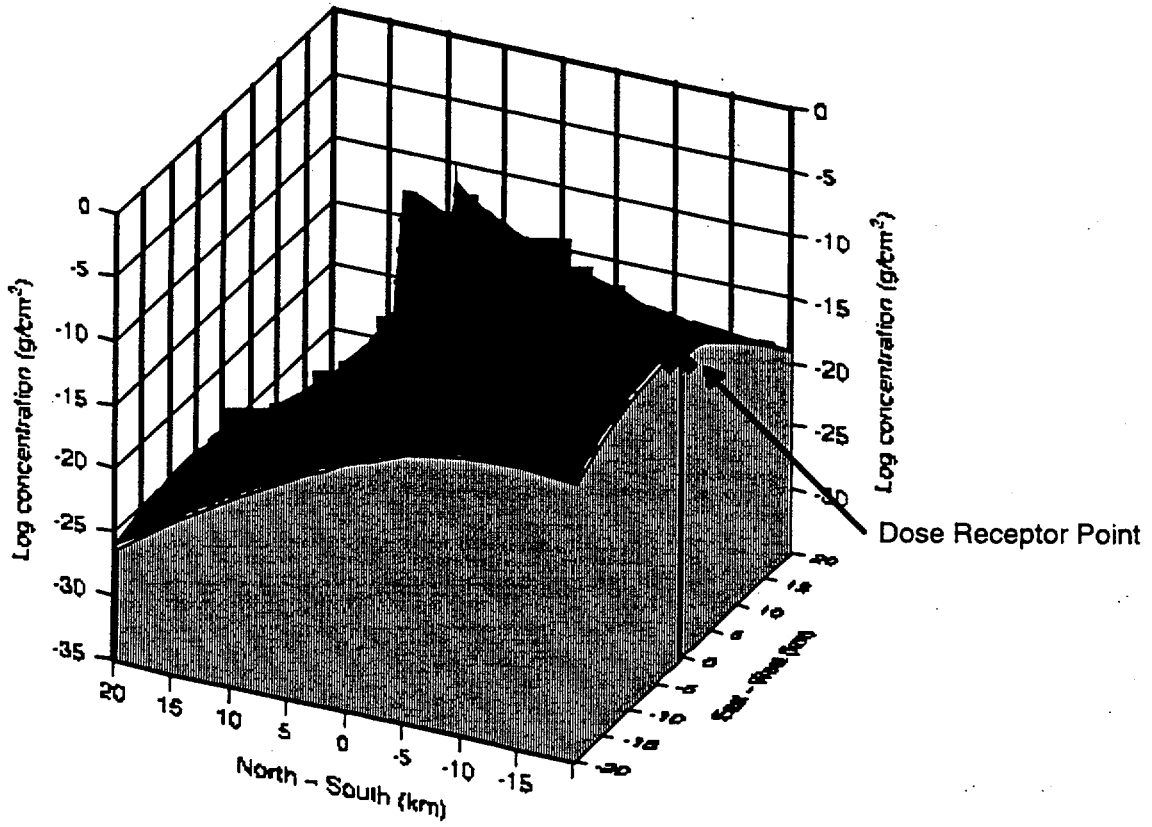


Figure 10-36. Concentration contours for greatest erupted waste amount (Realization 1).

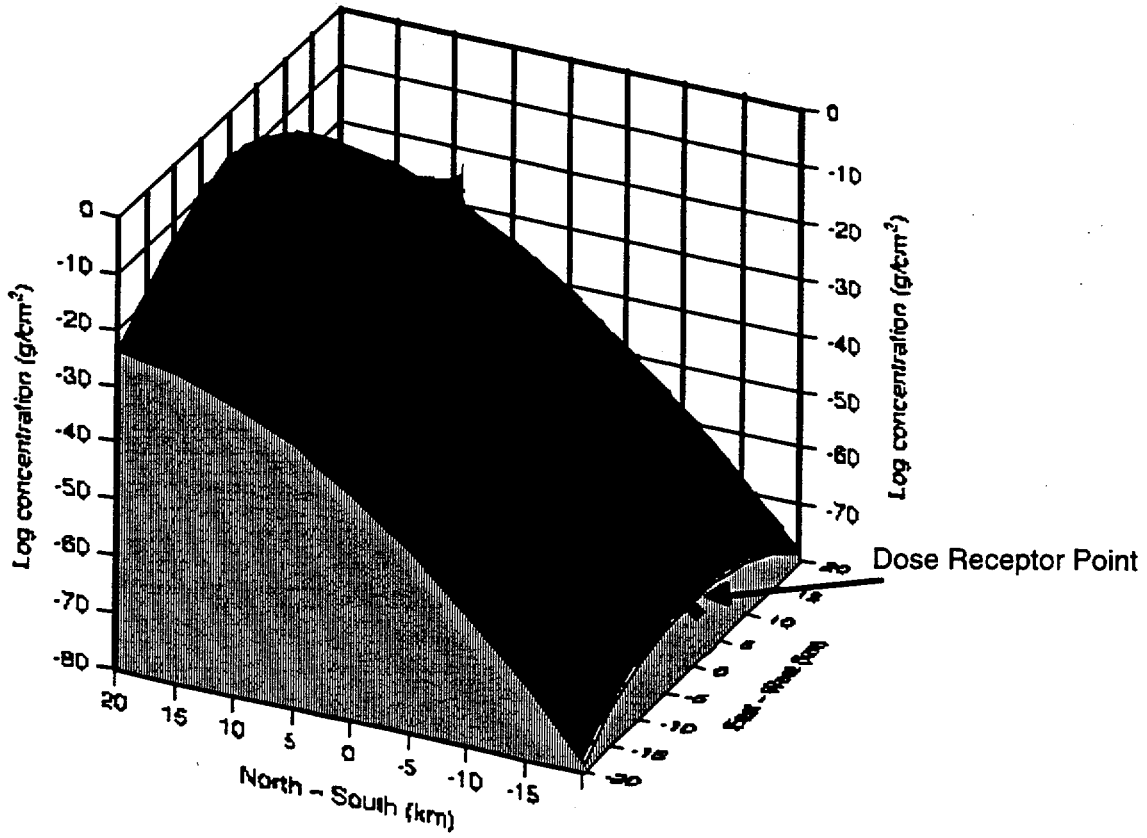


Figure 10-37. Concentration contours for strongest wind blowing away from dose receptor point (Realization 8).

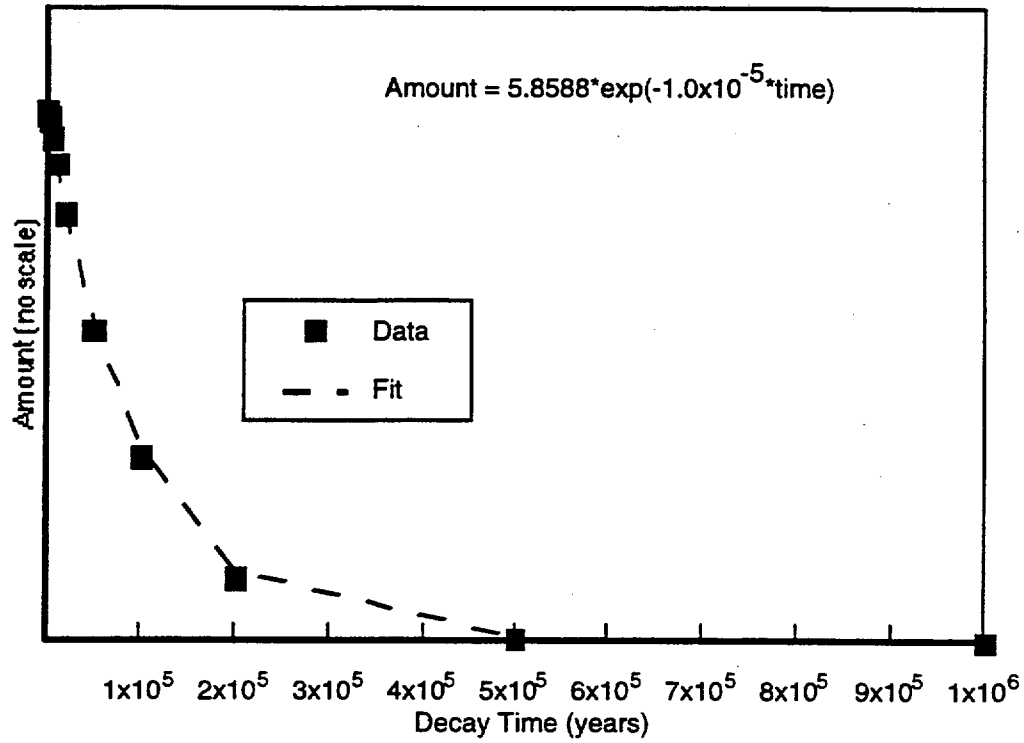


Figure 10-38. Inventory of Se-79 as a function of time.

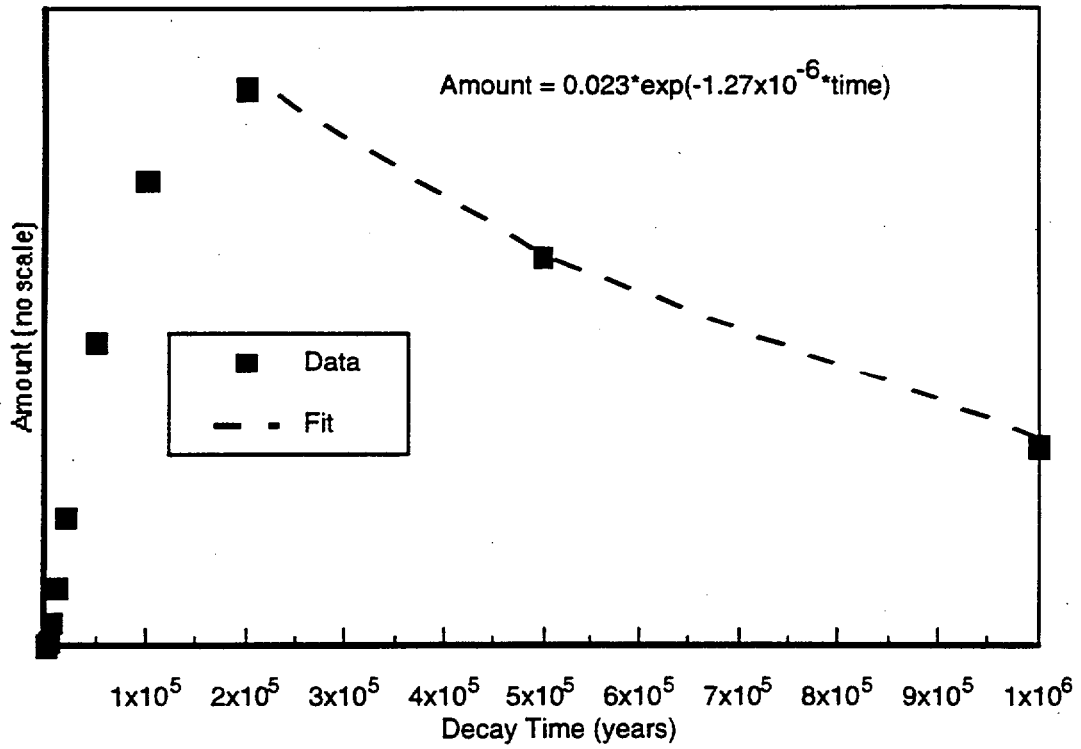


Figure 10-39. Inventory of Pb-210 as a function of time.

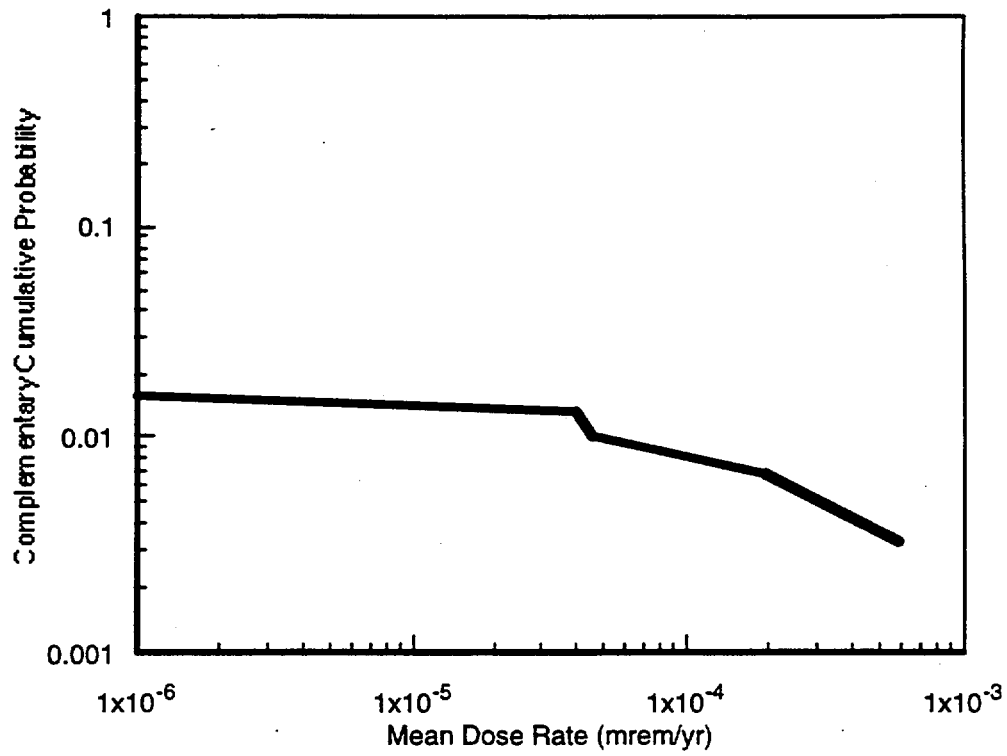


Figure 10-40. Conditional CCDF for mean direct-release volcanic dose rates.

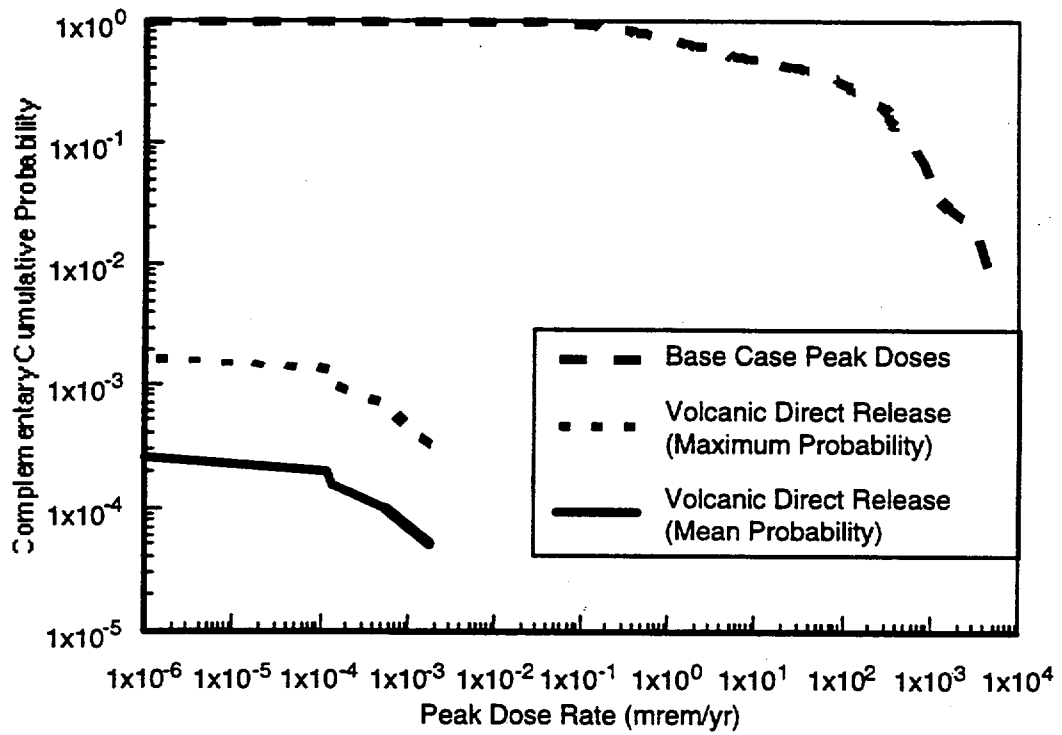
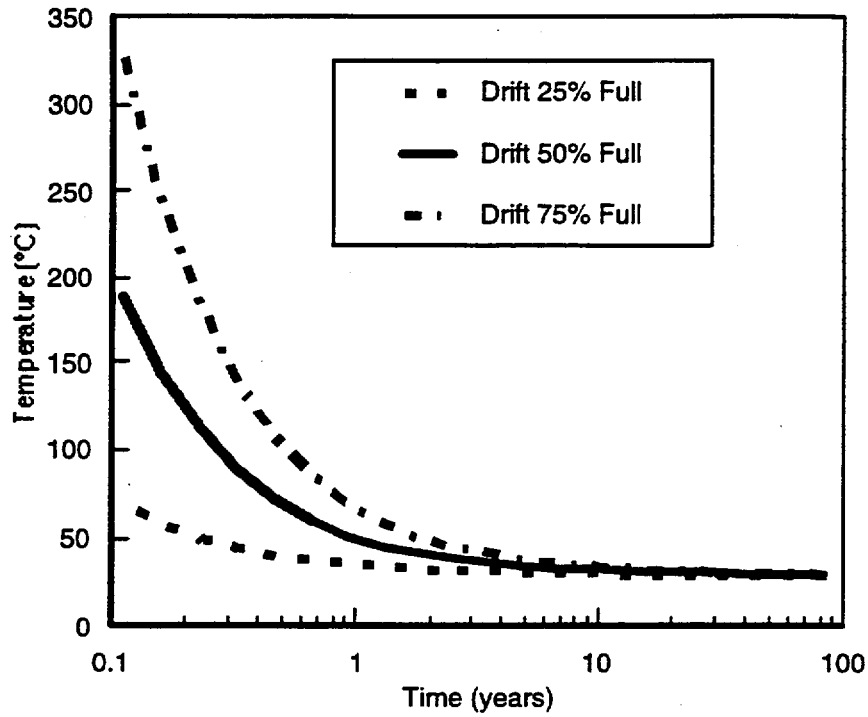
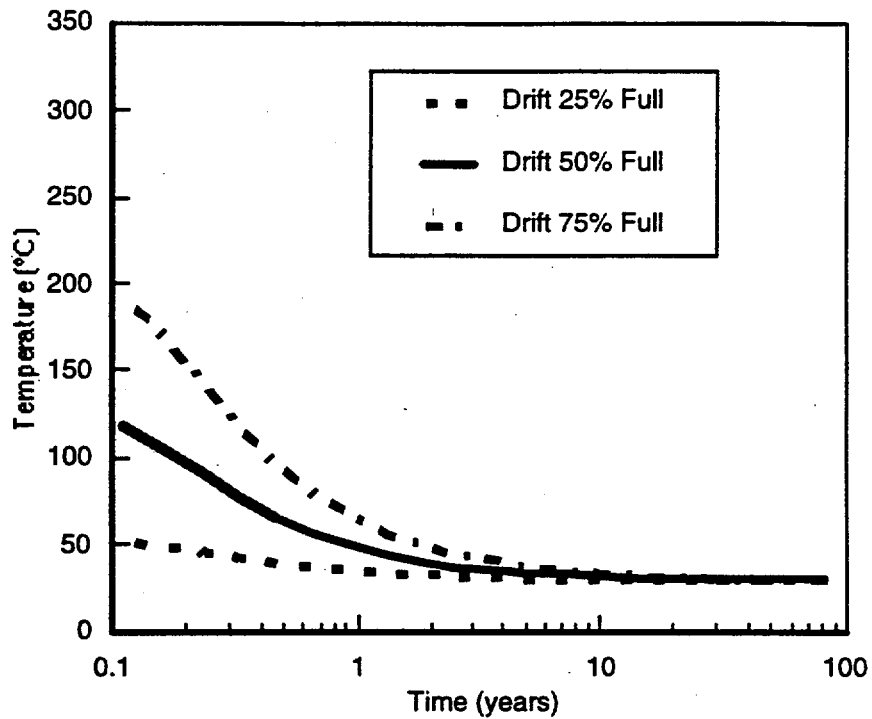


Figure 10-41. CCDFs for peak base-case and direct-volcanic dose rates.



(a) Temperatures at Waste Package



(b) Temperatures at Drift Wall

Figure 10-42. Temperature profiles in repository for various amounts of magma filling drift.

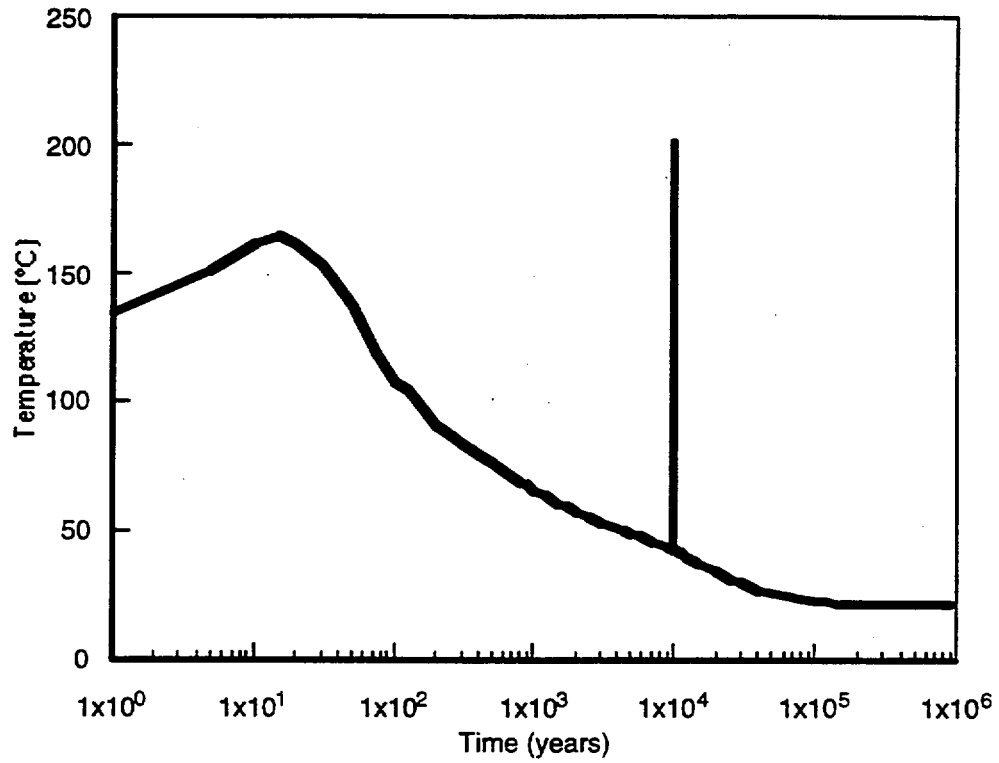


Figure 10-43. Profile for base-case drift-wall temperatures with a magmatic intrusion at 10,000 years.

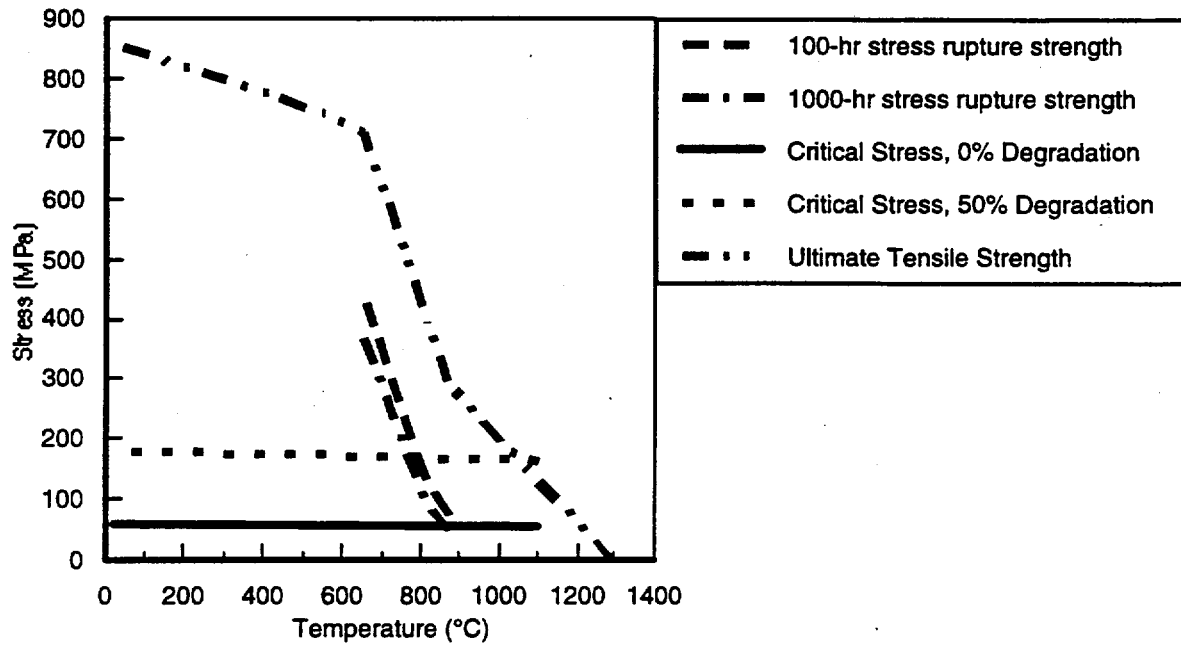


Figure 10-44. Mechanical behavior of alloy 625 as a function of time and temperature.

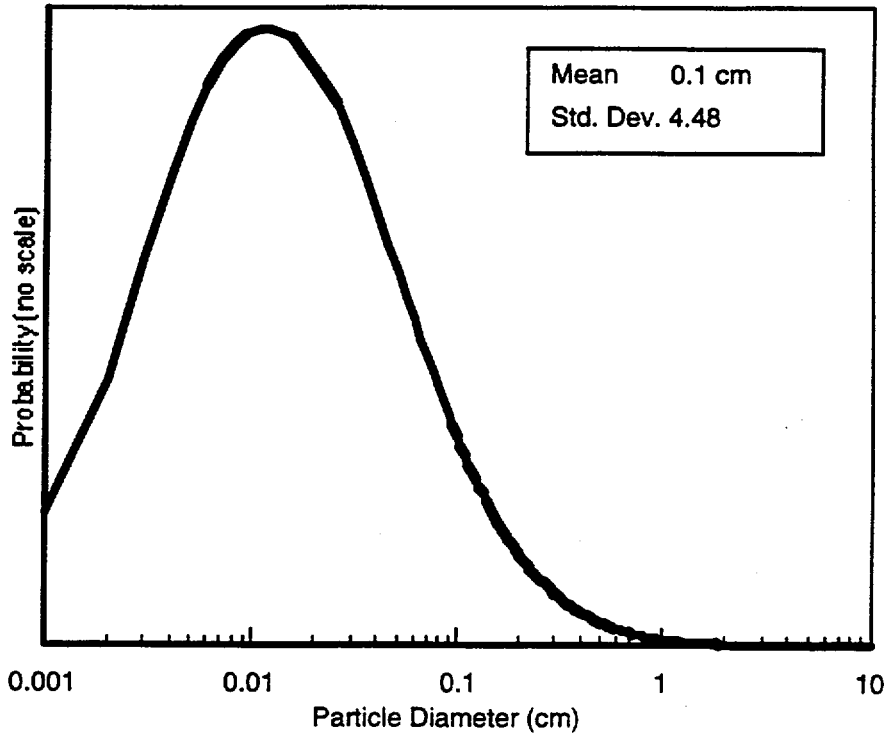


Figure 10-45. PDF for uranium dioxide particle sizes after interaction with magma.

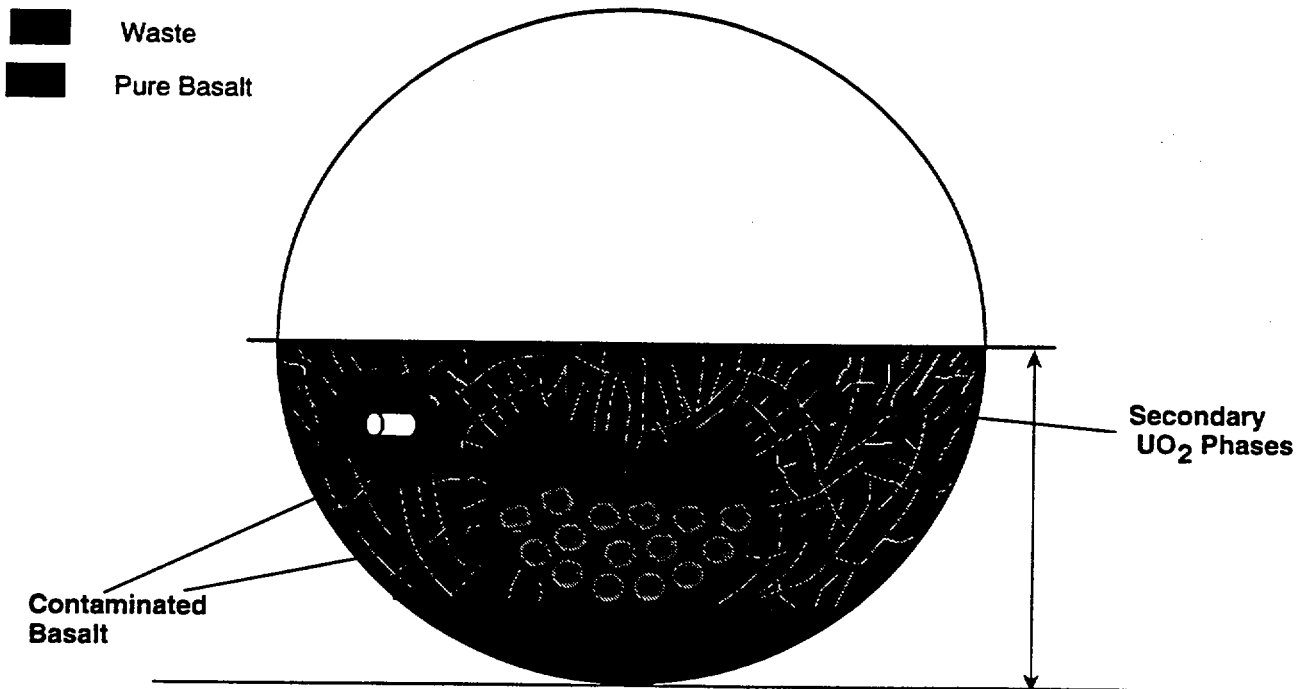


Figure 10-46. Layout of contaminated basalt in a drift.

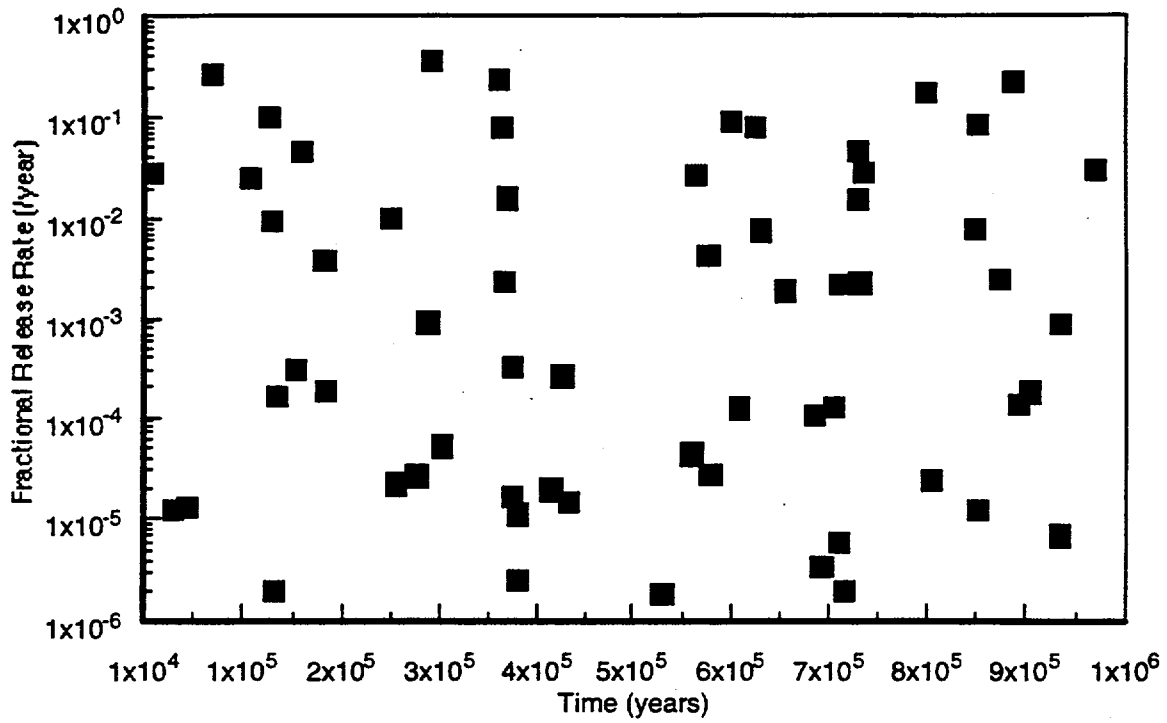


Figure 10-47. Times of failure and fractional release rate.

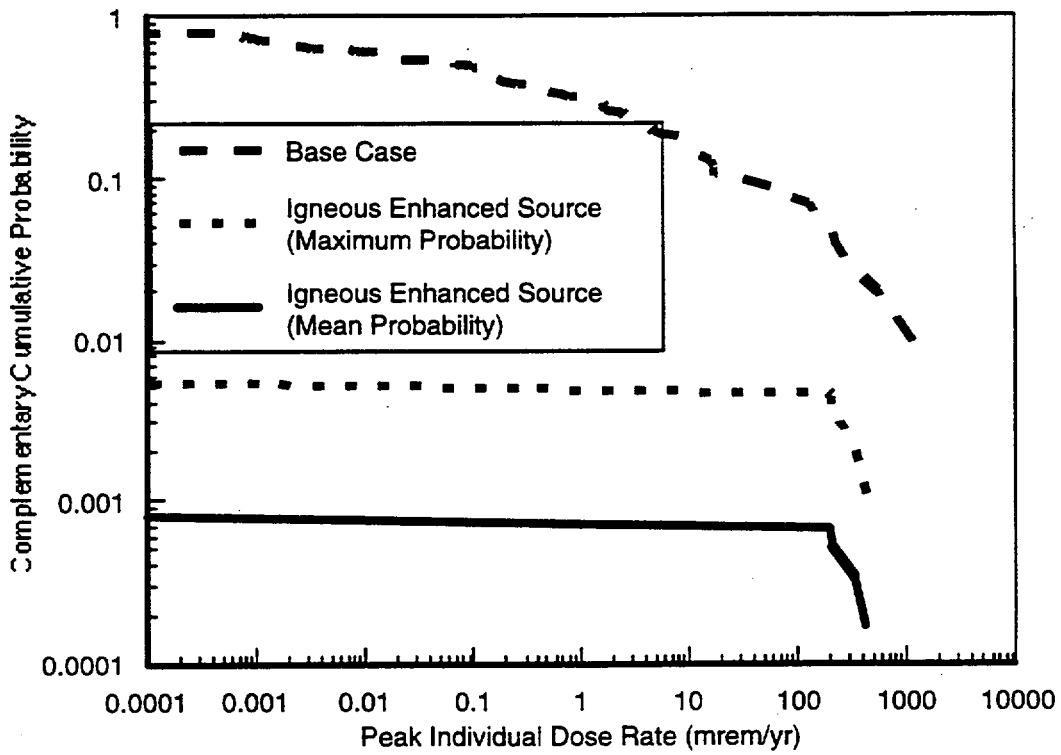


Figure 10-48. Comparison of CCDFs for 100,000-year dose rates.

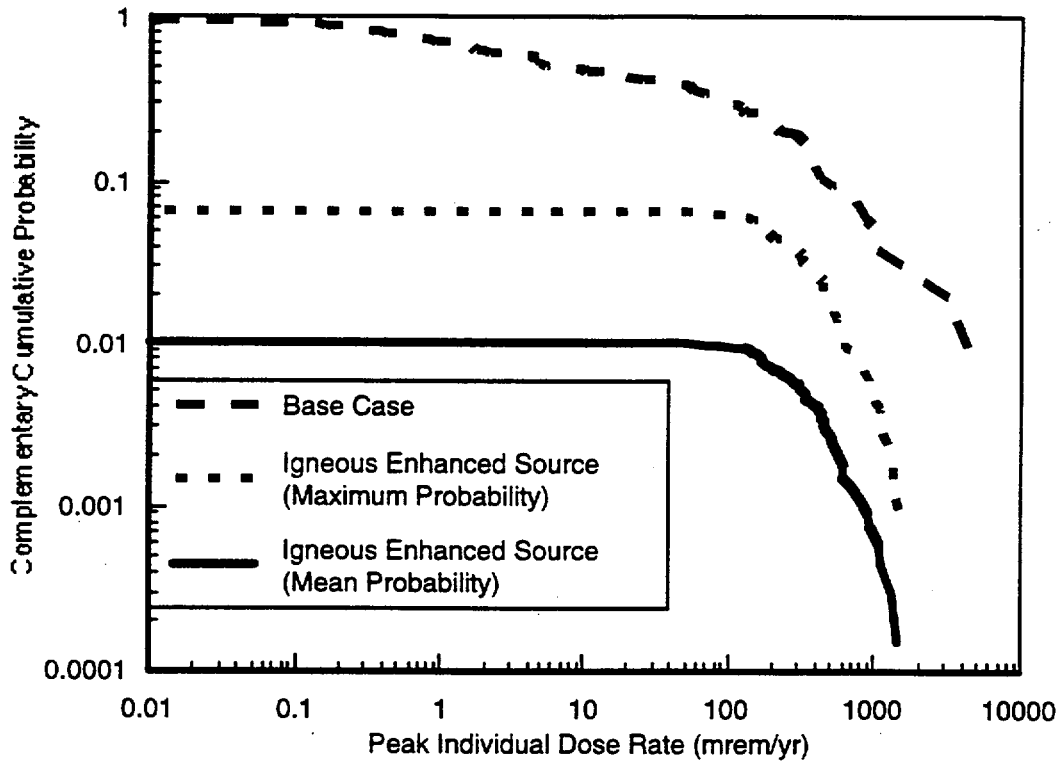


Figure 10-49. Comparison of CCDFs for 1,000,000-year dose rates.

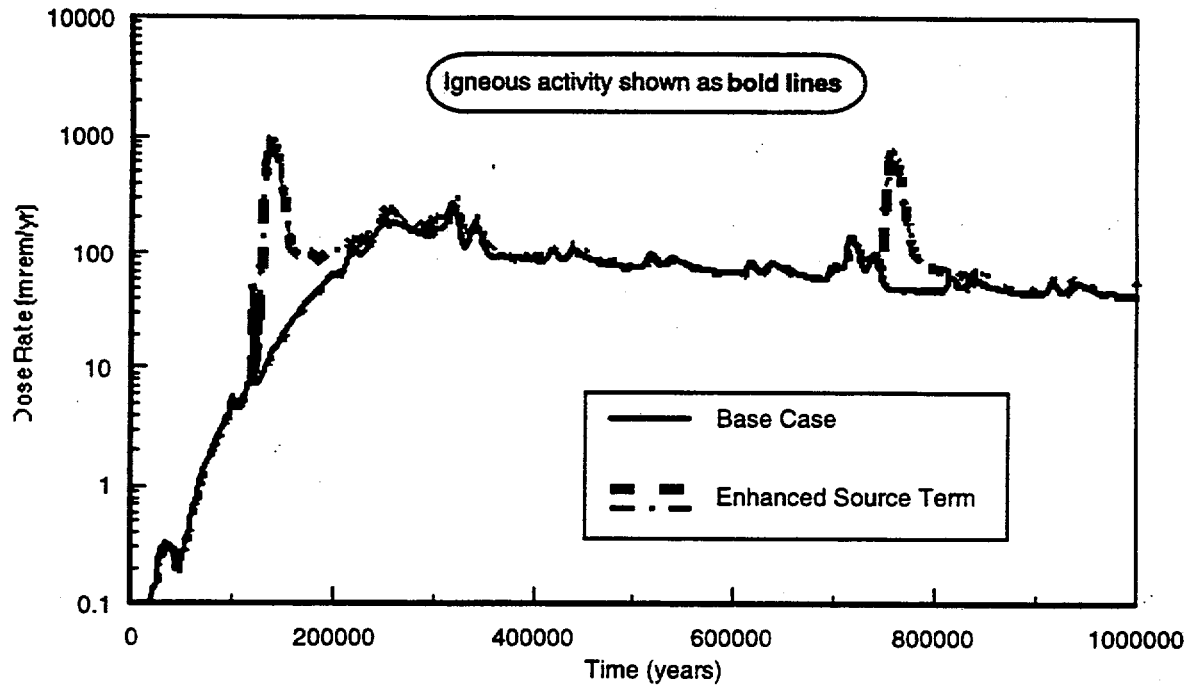


Figure 10-50. Time histories for dose rates over 1,000,000 years.

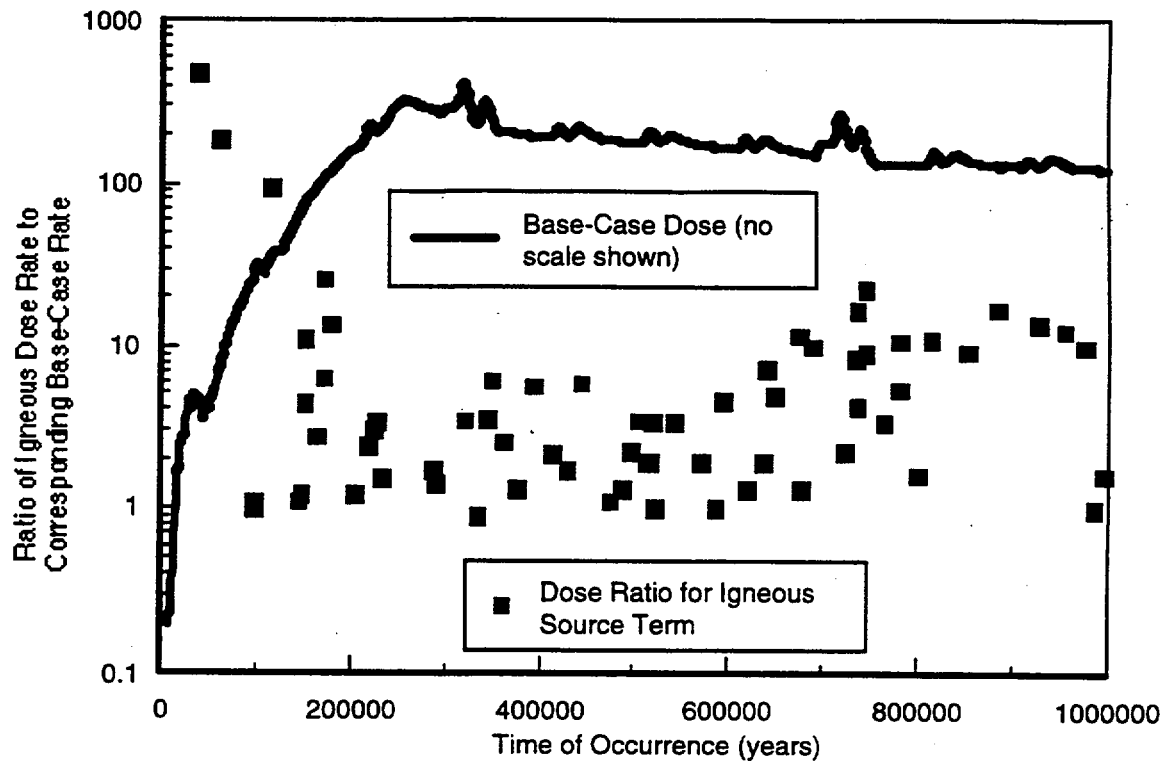
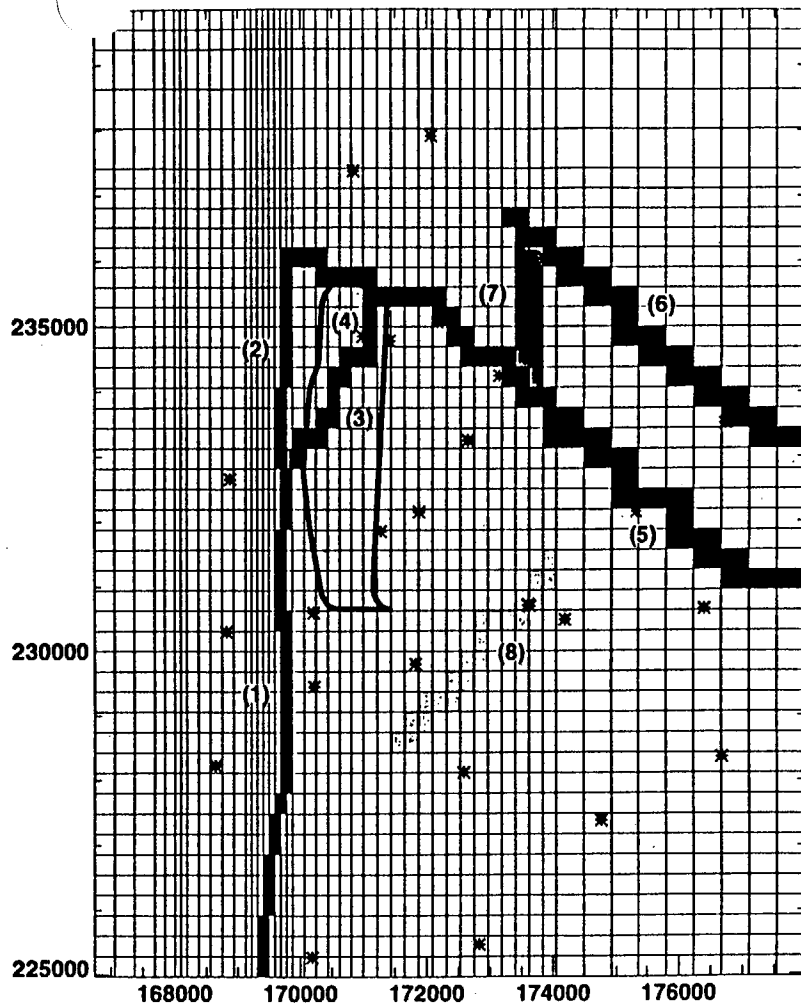
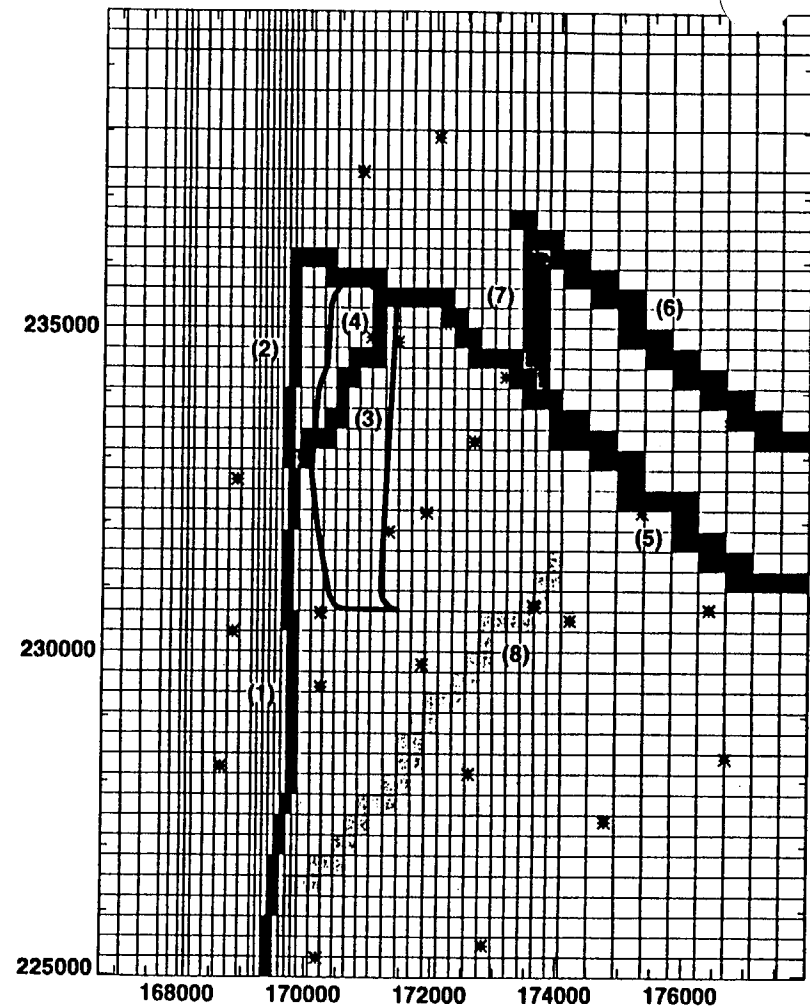


Figure 10-51. Ratios of doses from enhanced source term with corresponding base-case doses.



- | | |
|--|---------------------|
| (1) Solitario Canyon Fault | (5) Drill Hole Wash |
| (2) Solitario Canyon Fault extension (GAP) | (6) Yucca Fault |
| (3) H-5 Splay | (7) Bow Ridge Fault |
| (4) H-5 Splay Extension (Splay X) | (8) New Dike |

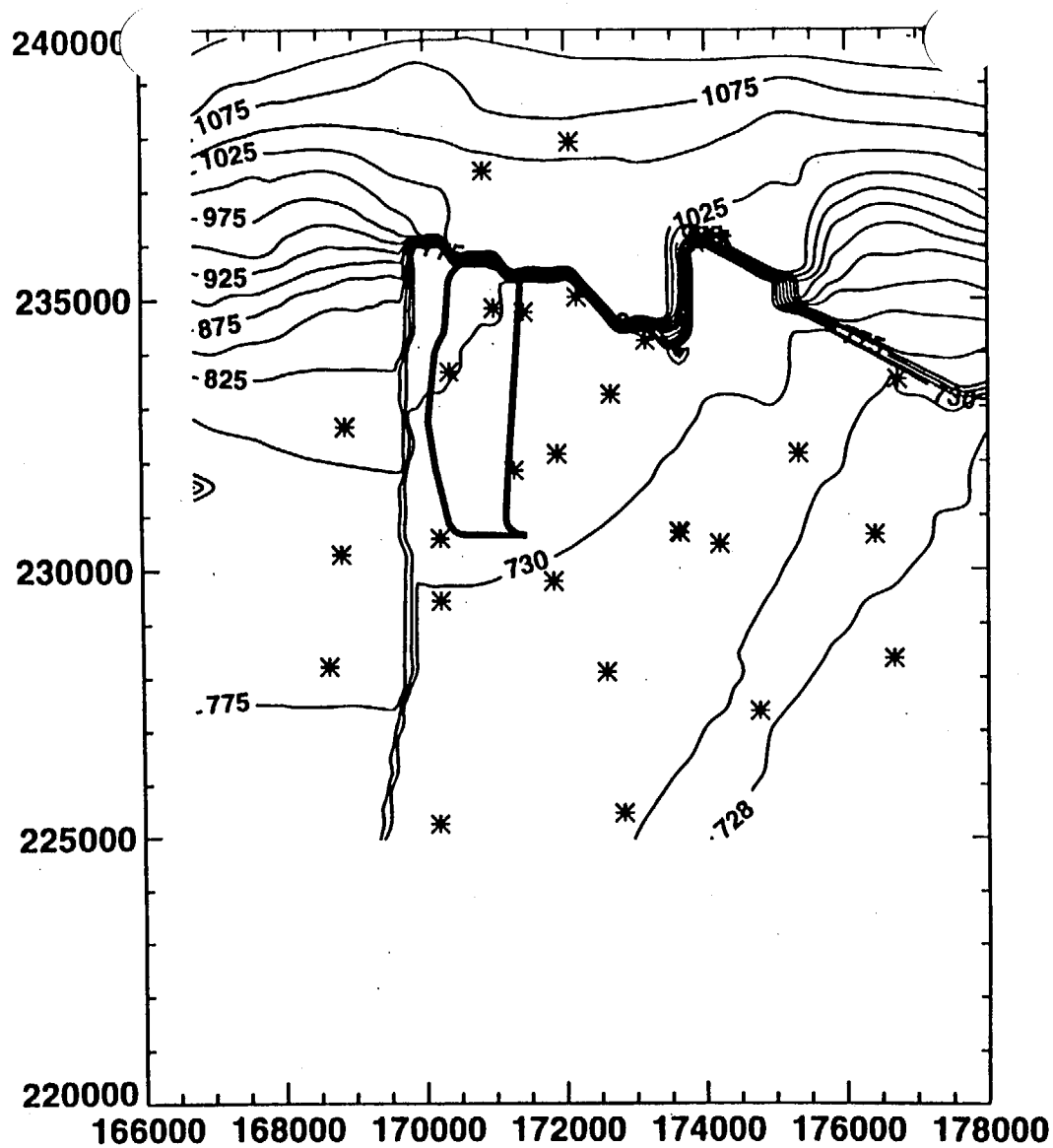
(a)



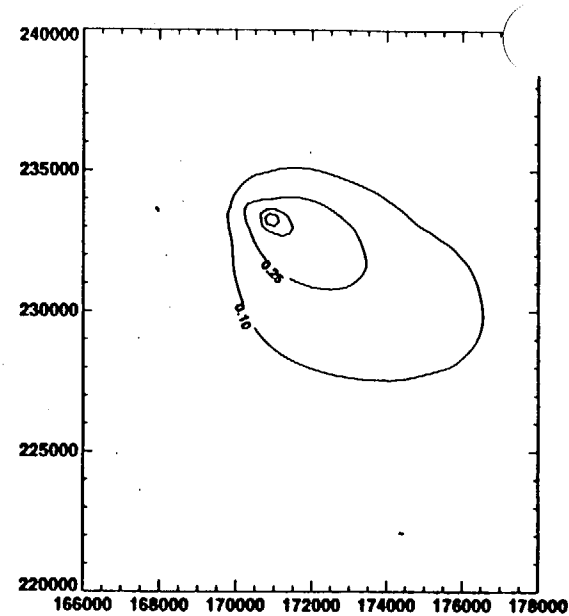
- | | |
|--|---------------------|
| (1) Solitario Canyon Fault | (5) Drill Hole Wash |
| (2) Solitario Canyon Fault extension (GAP) | (6) Yucca Fault |
| (3) H-5 Splay | (7) Bow Ridge Fault |
| (4) H-5 Splay Extension (Splay X) | (8) New Dike |

(b)

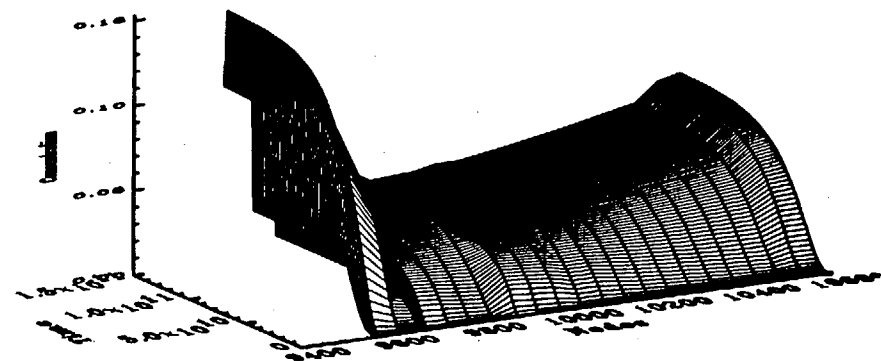
Figure 10-52. Examples of new dikes in the saturated flow domain. (a) Dike not attached to existing structure; (b) dike splayed off Solitario Canyon fault.



(a)

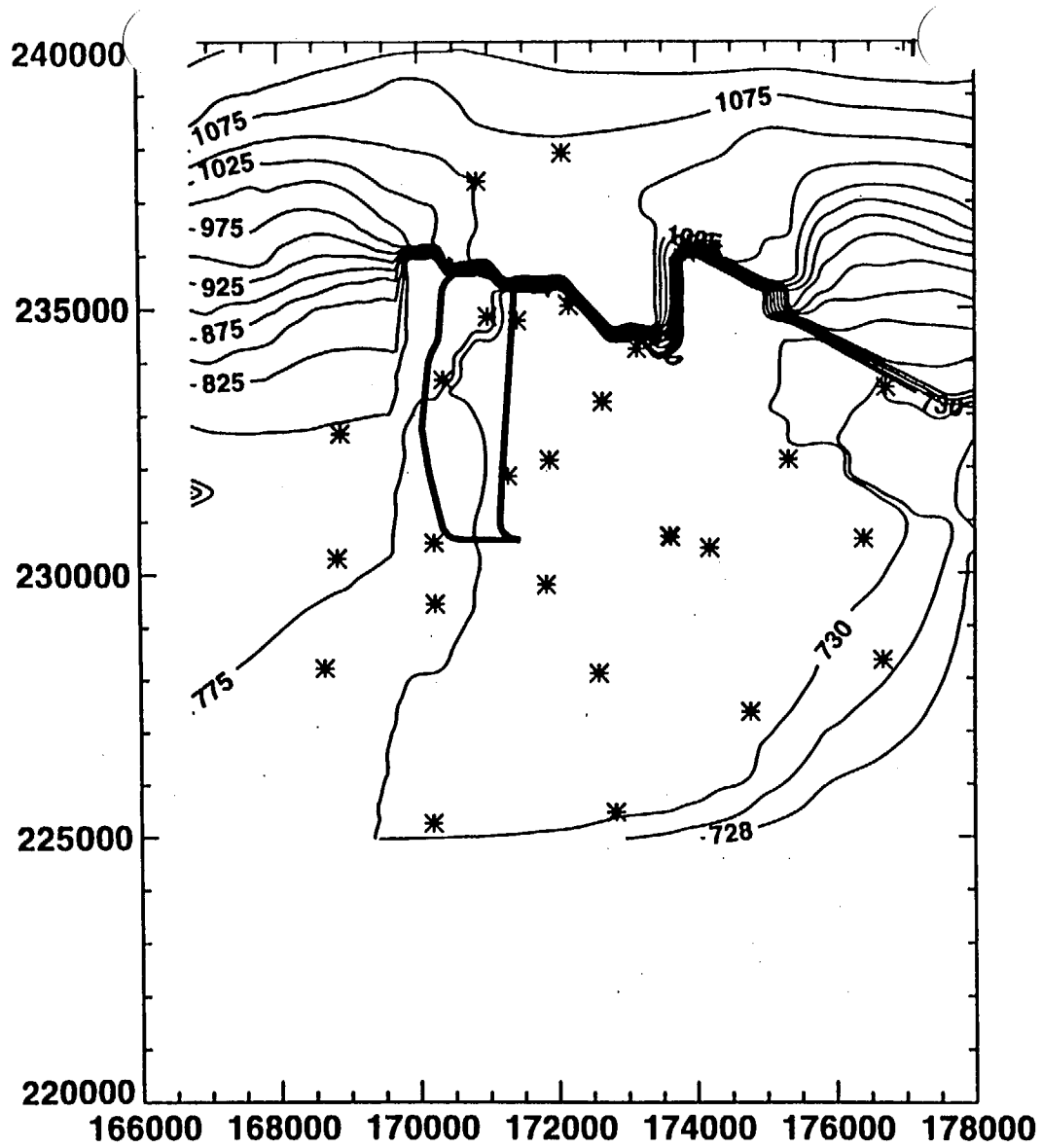


(b)

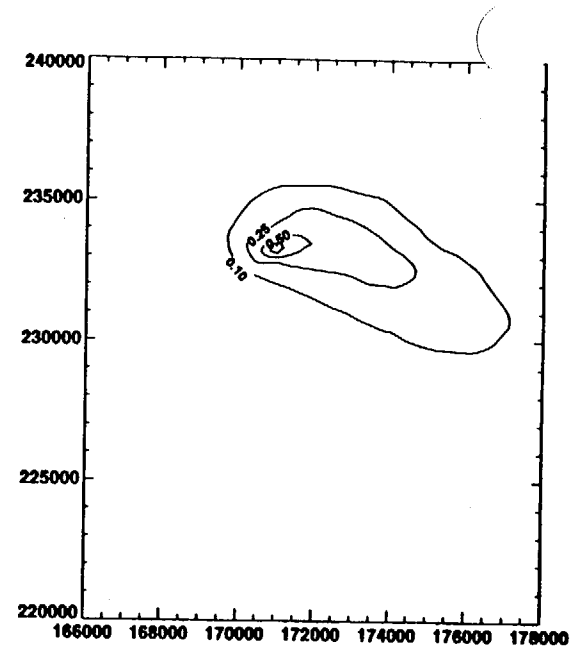


(c)

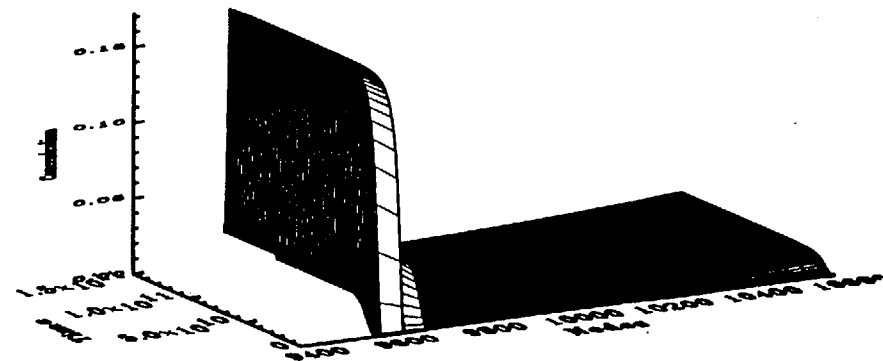
Figure 10-53. SZ reference model: (a) potentiometric surface; (b) representative contaminant concentration contours; (c) representative contaminant breakthrough curve.



(a)

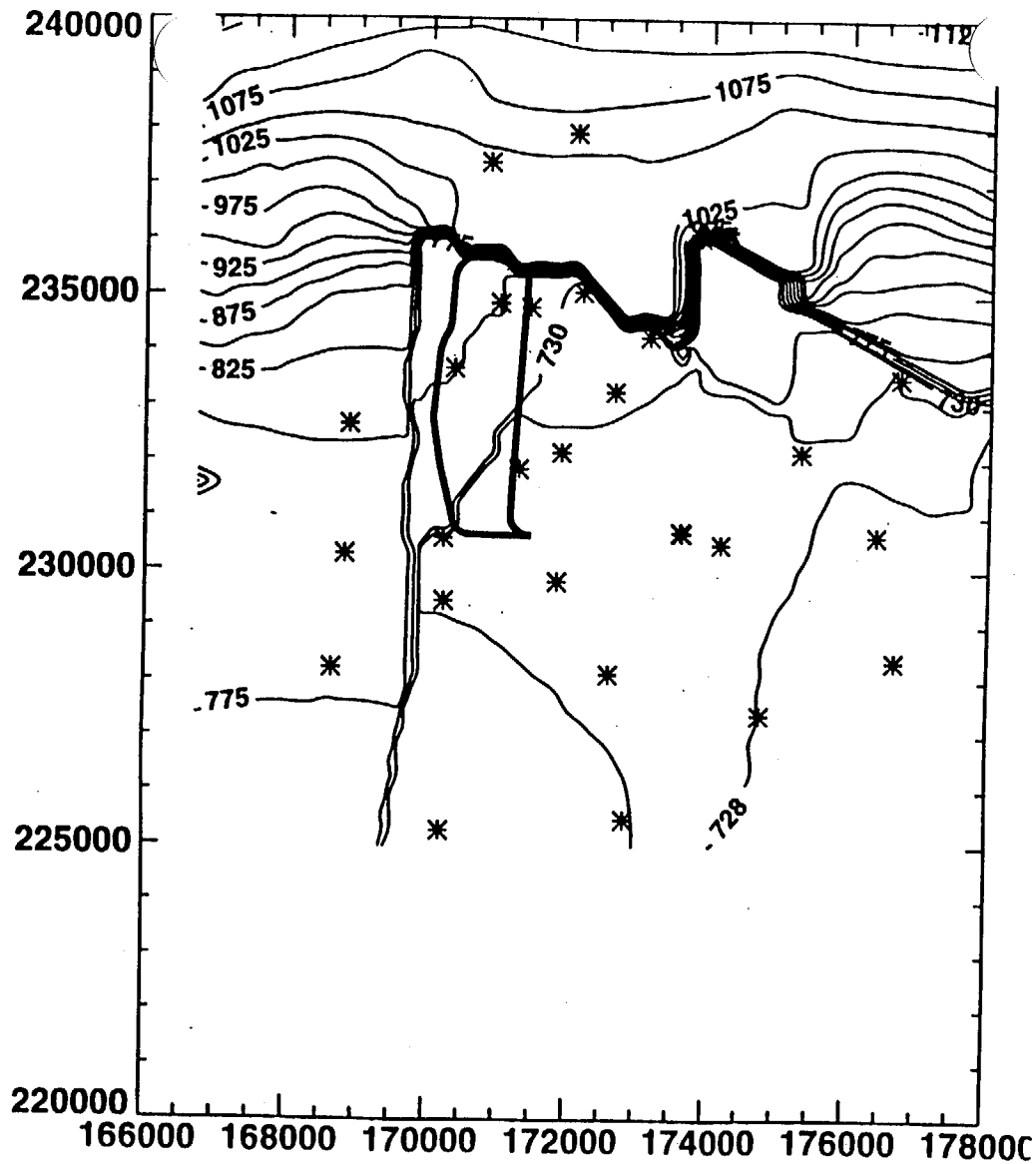


(b)

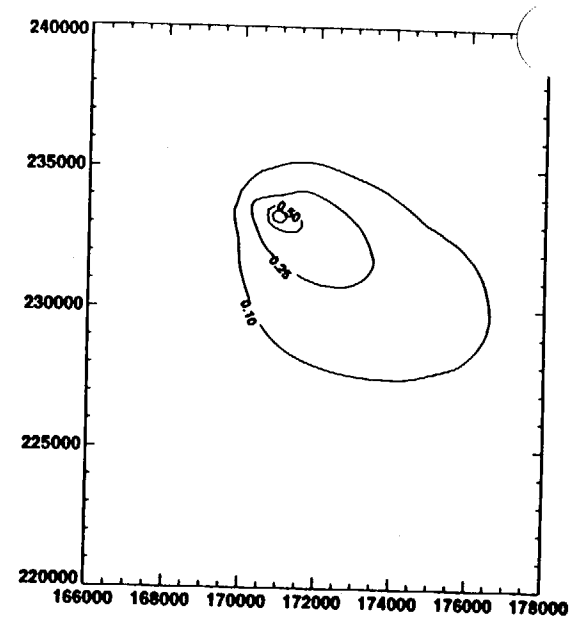


(c)

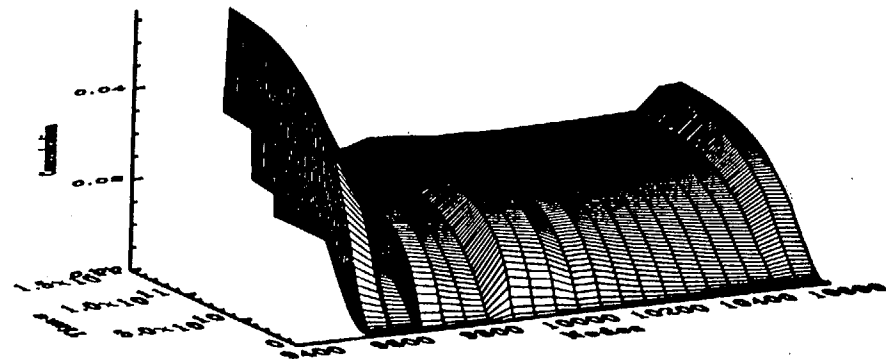
Figure 10-54. Dike inserted along Solitario Canyon fault: (a) potentiometric surface; (b) representative contaminant concentration contours; (c) representative contaminant breakthrough curve.



(a)

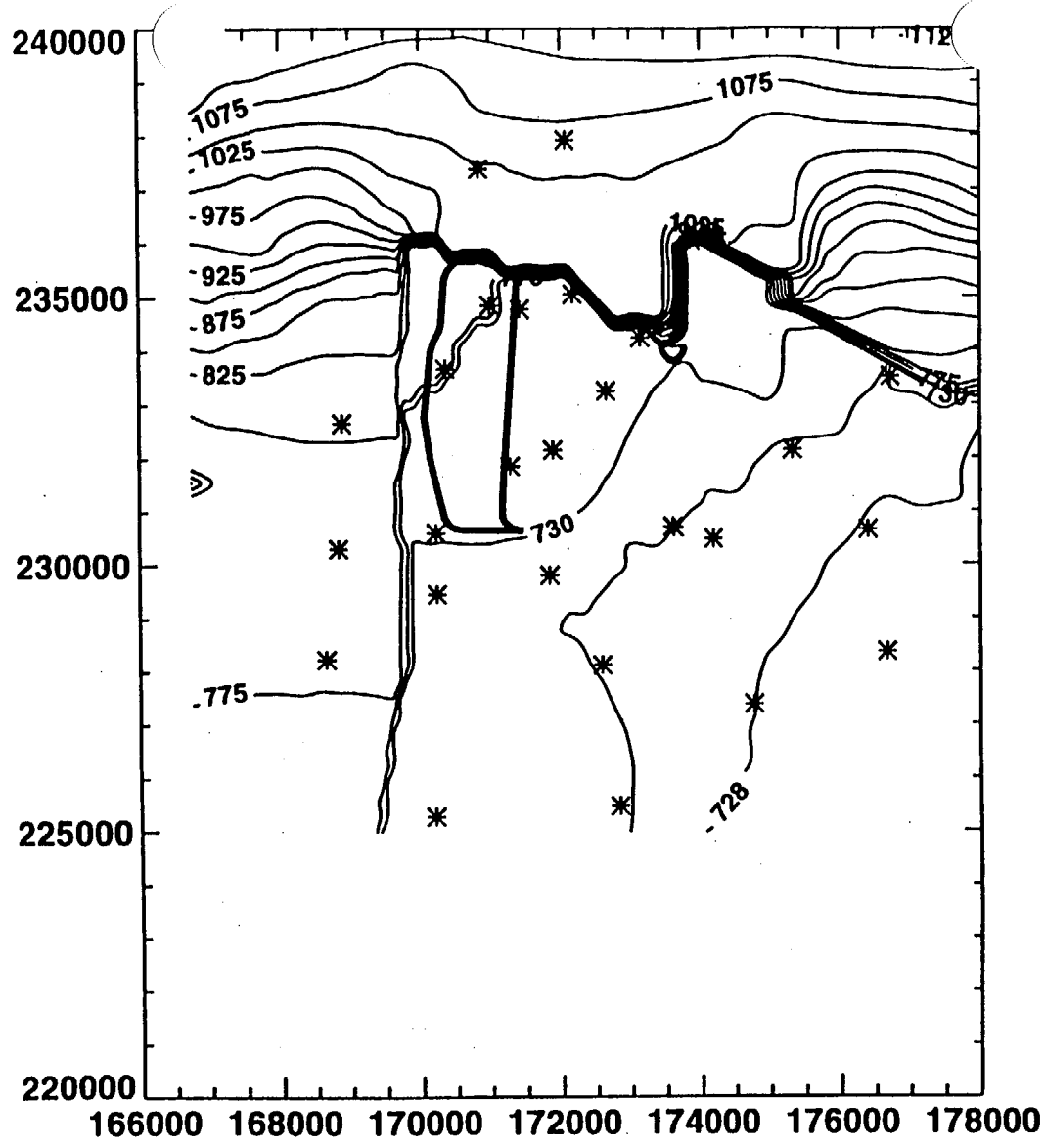


(b)

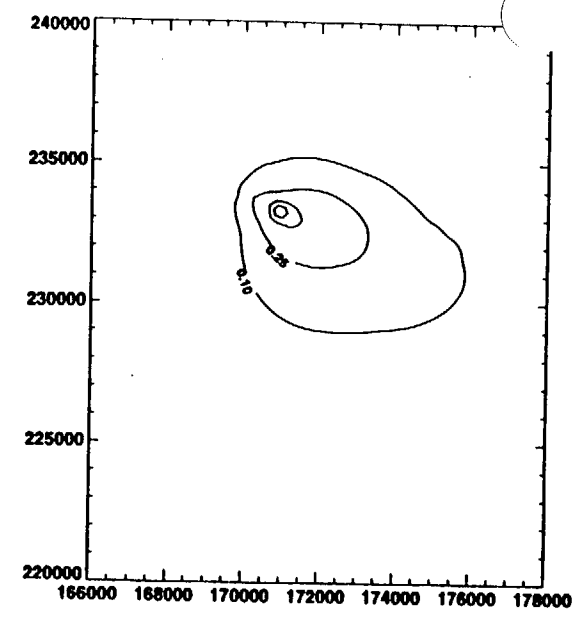


(c)

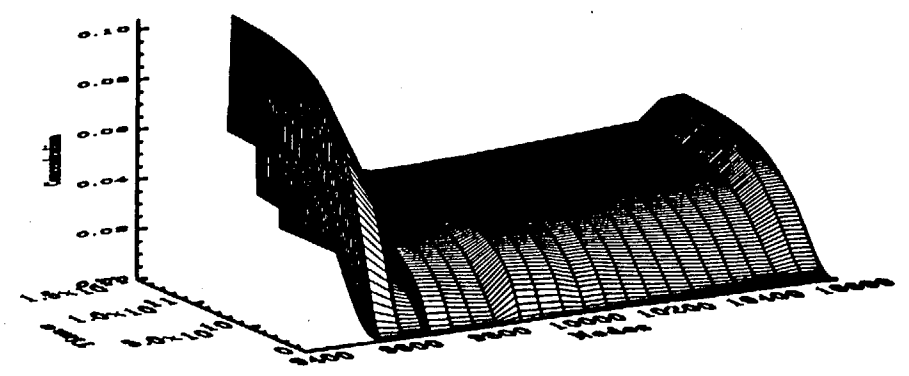
Figure 10-55. Dike inserted beneath repository connected to Solitario Canyon fault: (a) potentiometric surface; (b) representative contaminant concentration contours; (c) representative contaminant breakthrough curve.



(a)

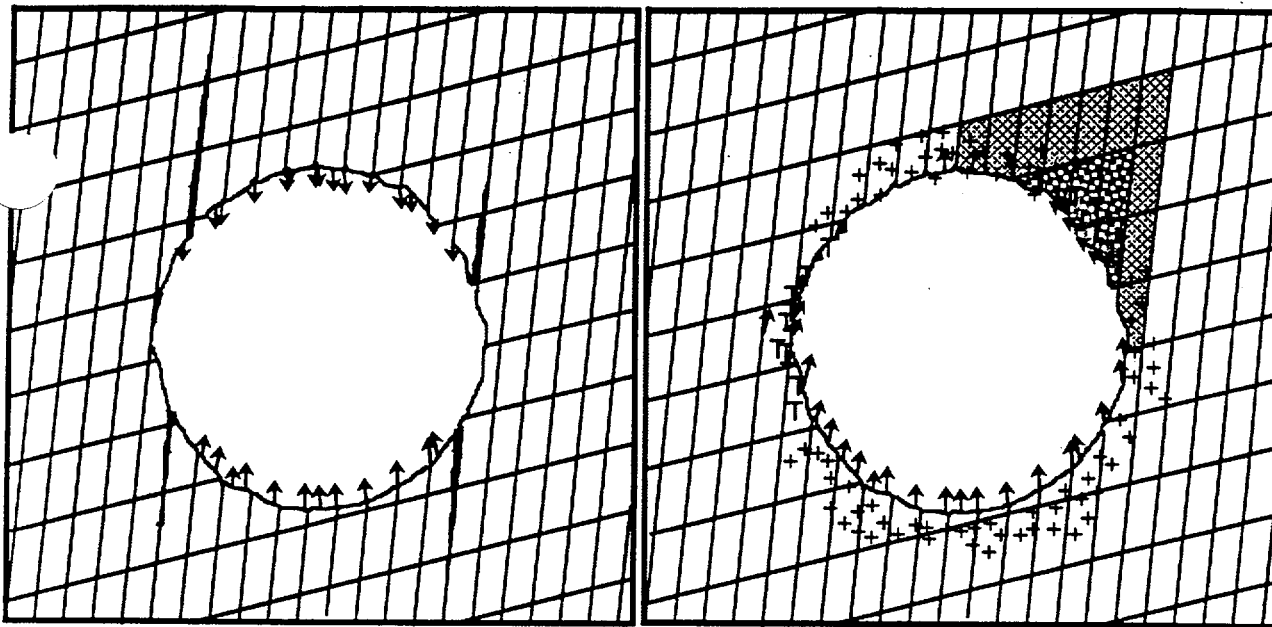


(b)



(c)

Figure 10-56. Dike inserted southeast of repository: (a) potentiometric surface; (b) representative contaminant concentration contours; (c) representative contaminant breakthrough curve.



(a)

(b)

Figure 10-57. (a) Stress state of drift immediately after excavation. (b) Stress state after 50 years of heating.

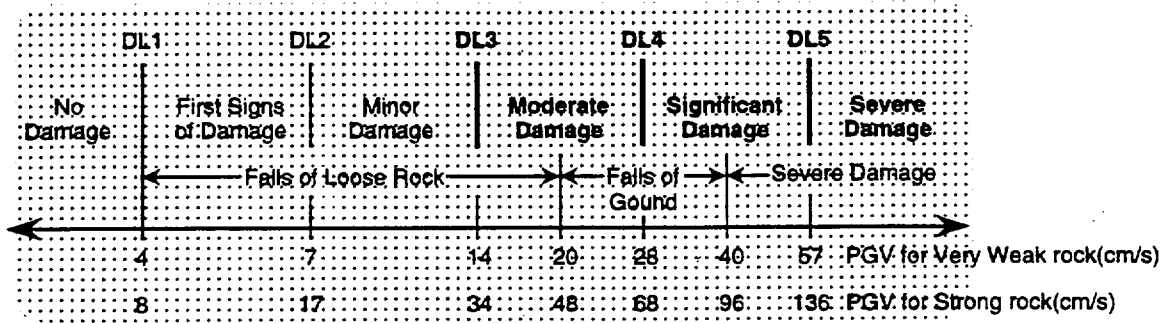


Figure 10-58. PGV that causes a given damage level for various rock qualities.

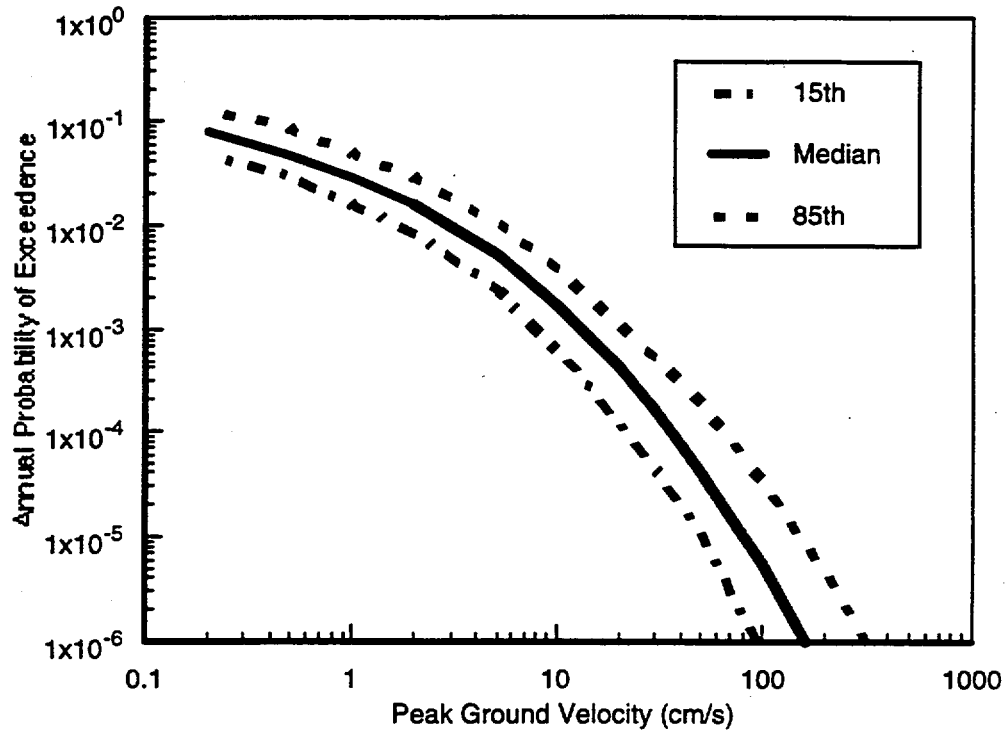


Figure 10-59. Annual probability of exceedence for horizontal PGV (after CRWMS M&O 1998a, Figure 7-8).

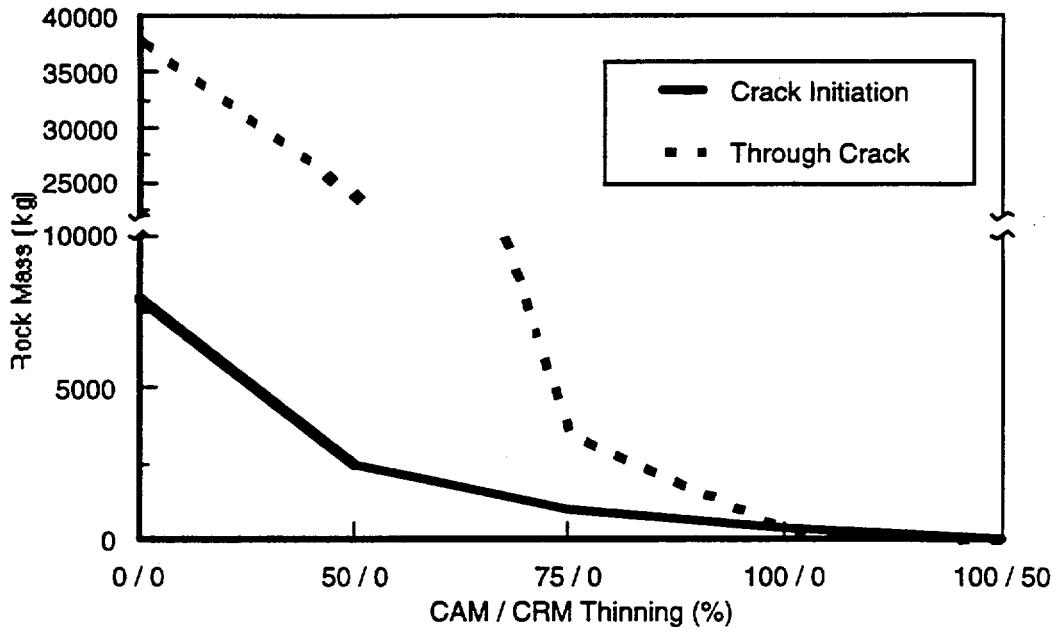


Figure 10-60. Critical rock masses for various waste-package wall thickness.

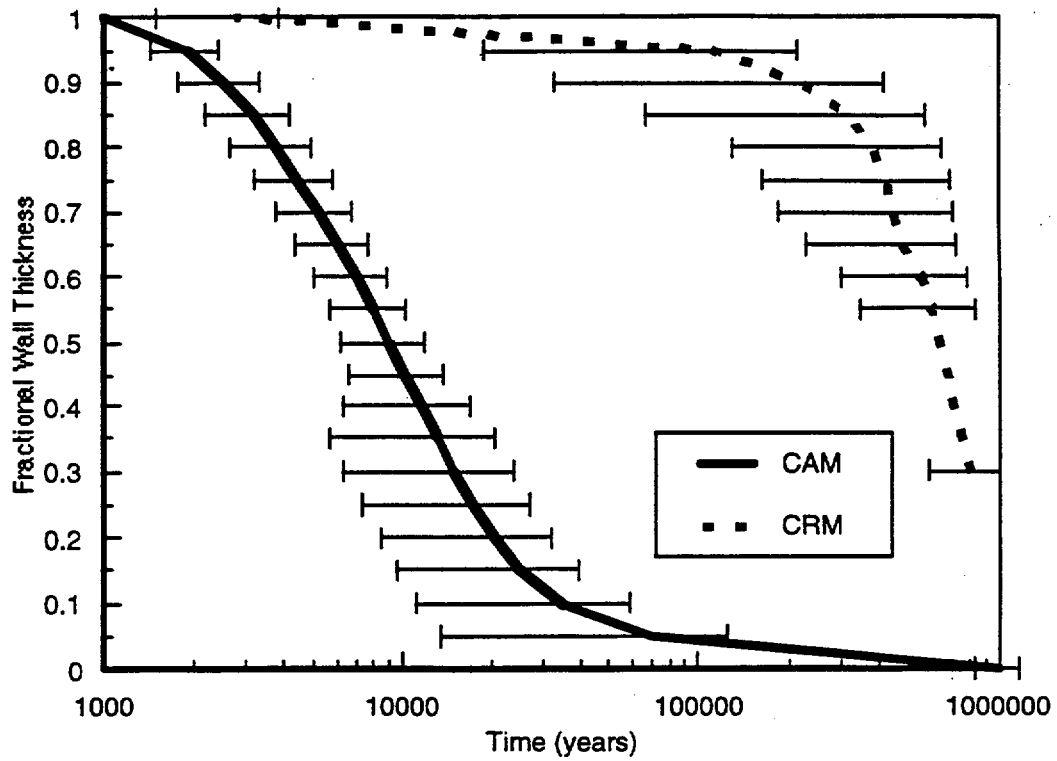


Figure 10-61. Time rate of thinning of waste package wall.

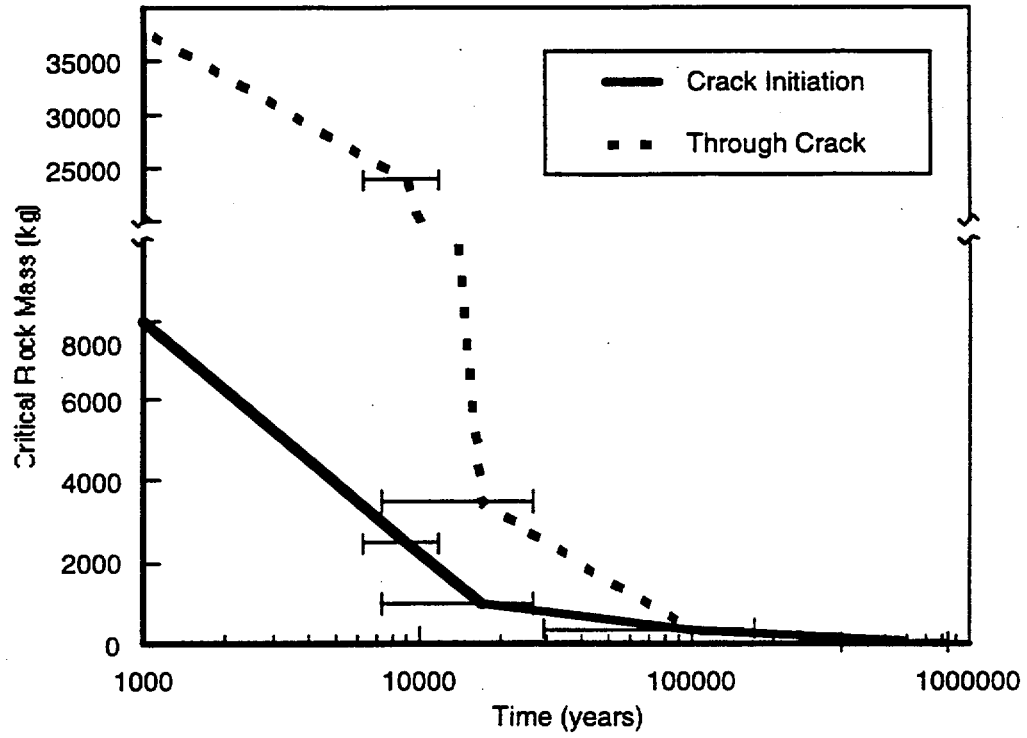


Figure 10-62. Critical rock masses as function of time.

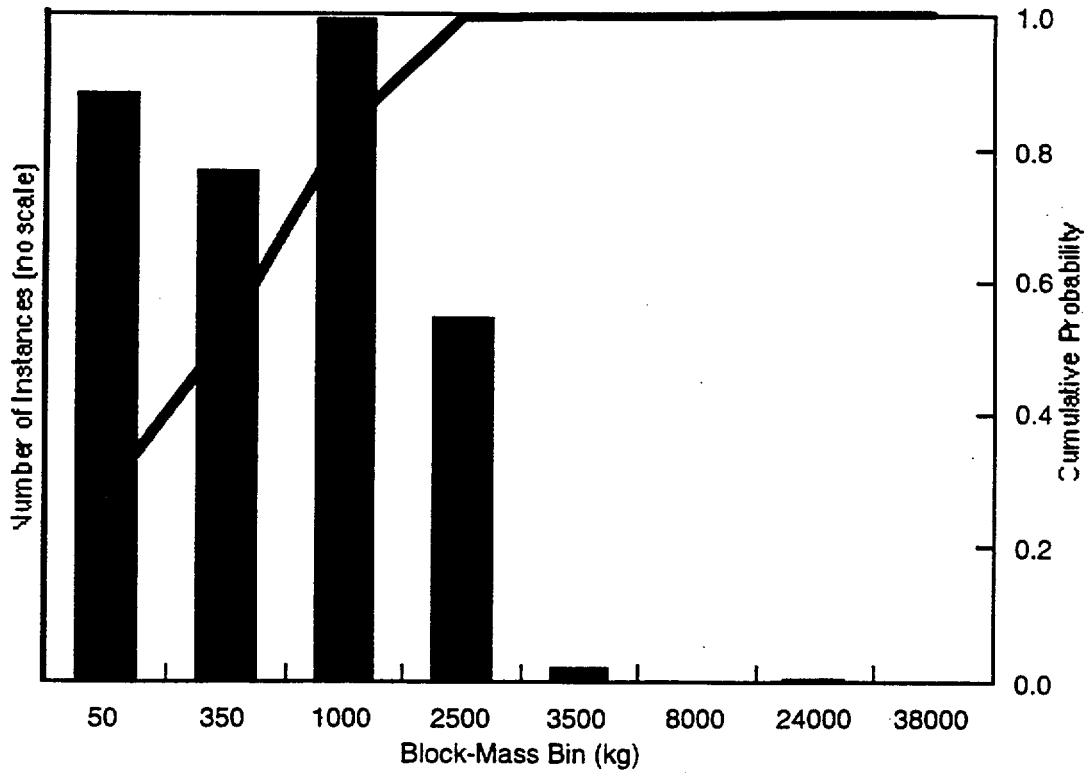


Figure 10-63. Distribution of rock sizes for all units.

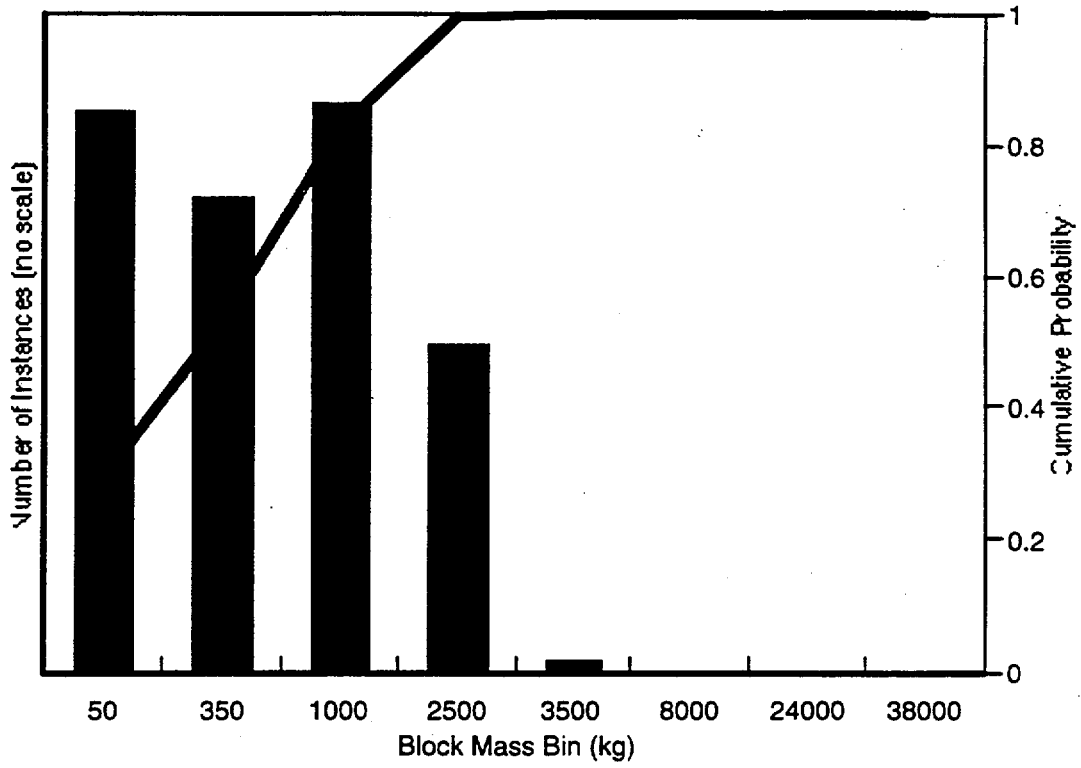


Figure 10-64. Distribution of rock sizes for the TSw unit.

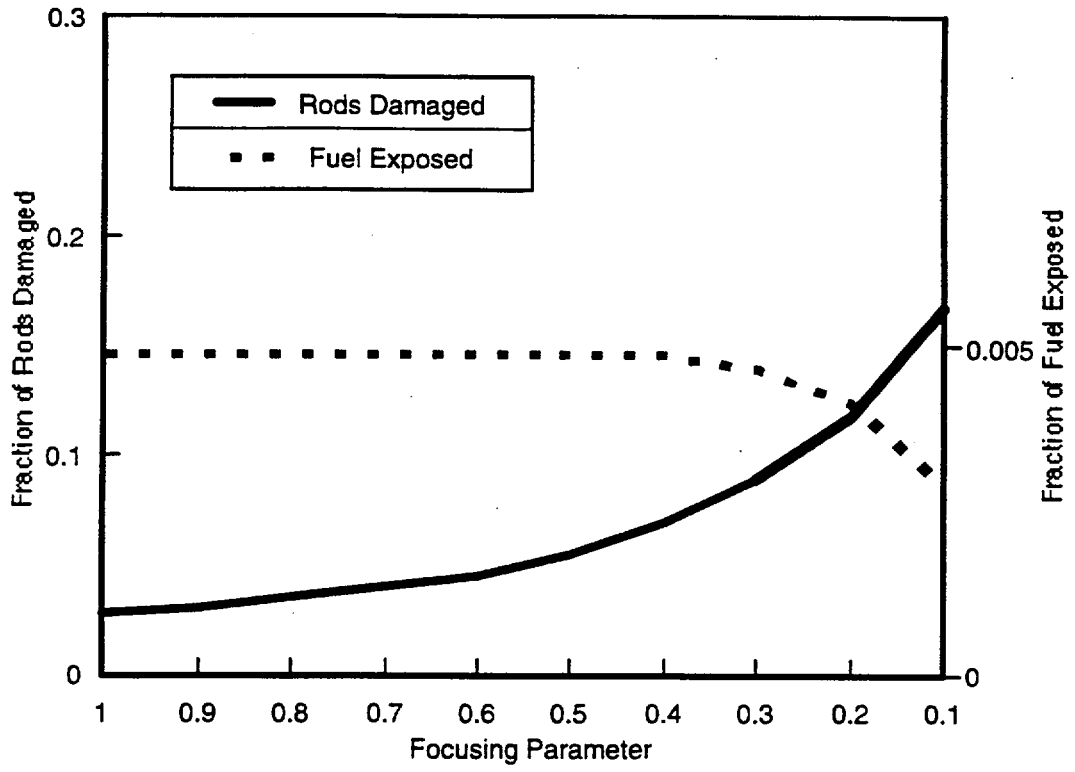


Figure 10-65. Mechanical damage to fuel rods from a circular punch.

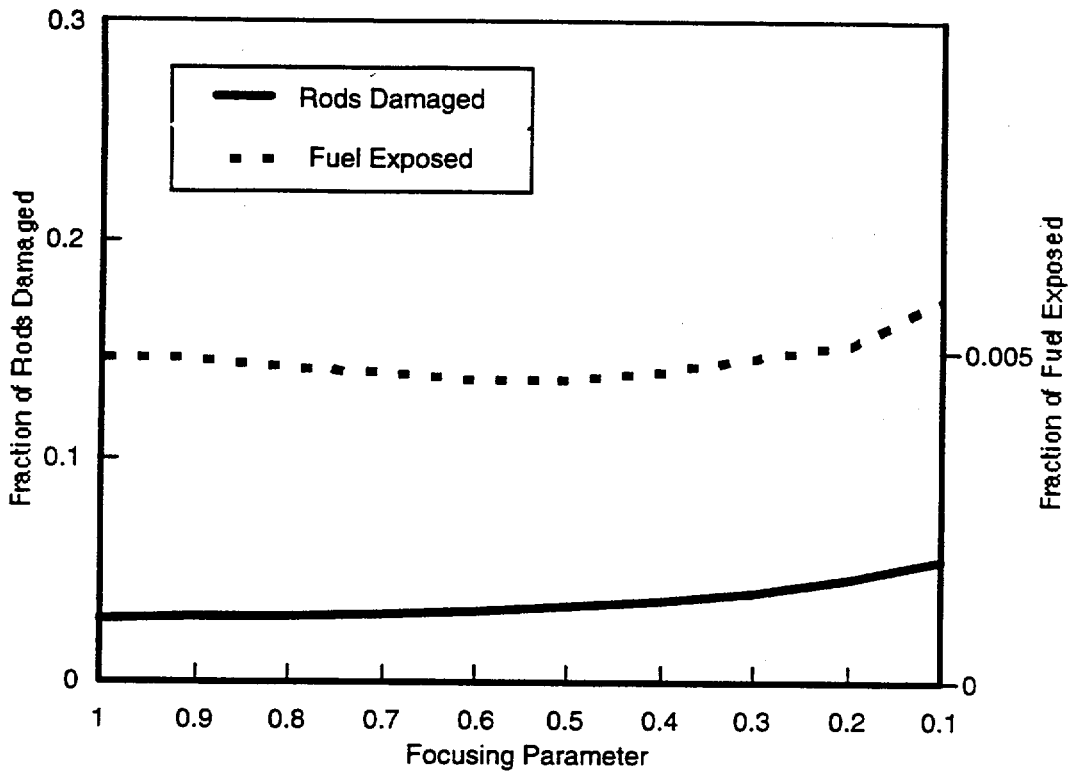


Figure 10-66. Mechanical damage to fuel rods from a linear punch.

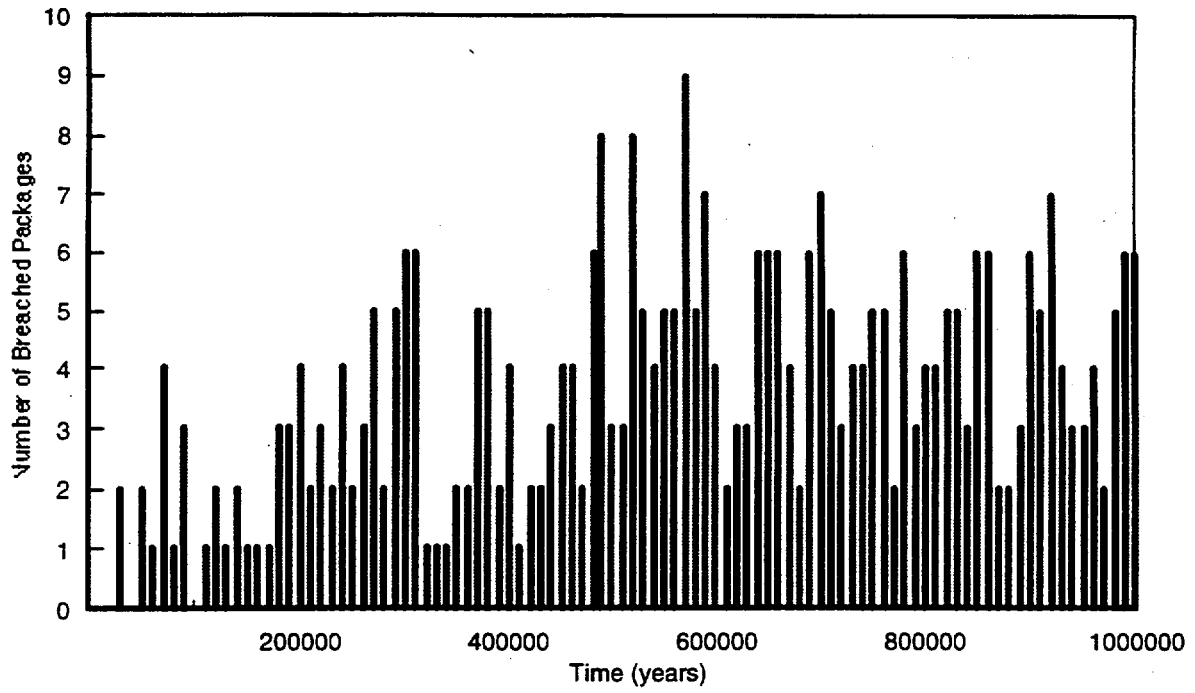


Figure 10-67. Distribution of times for breach of waste packages.

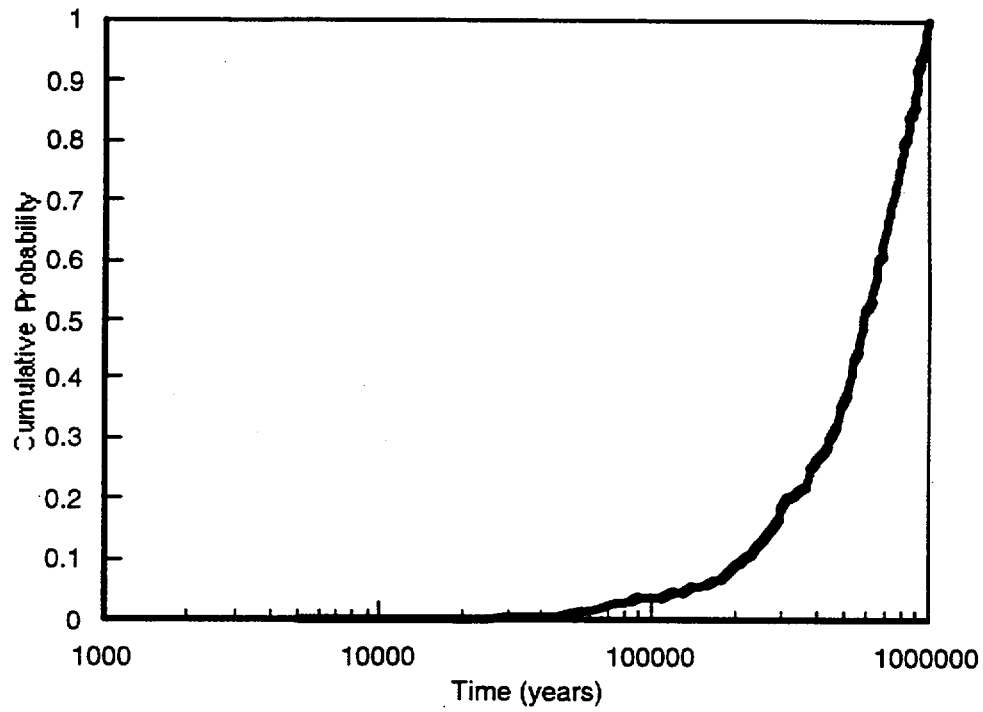


Figure 10-68. CDF for waste-package failures from rockfall.

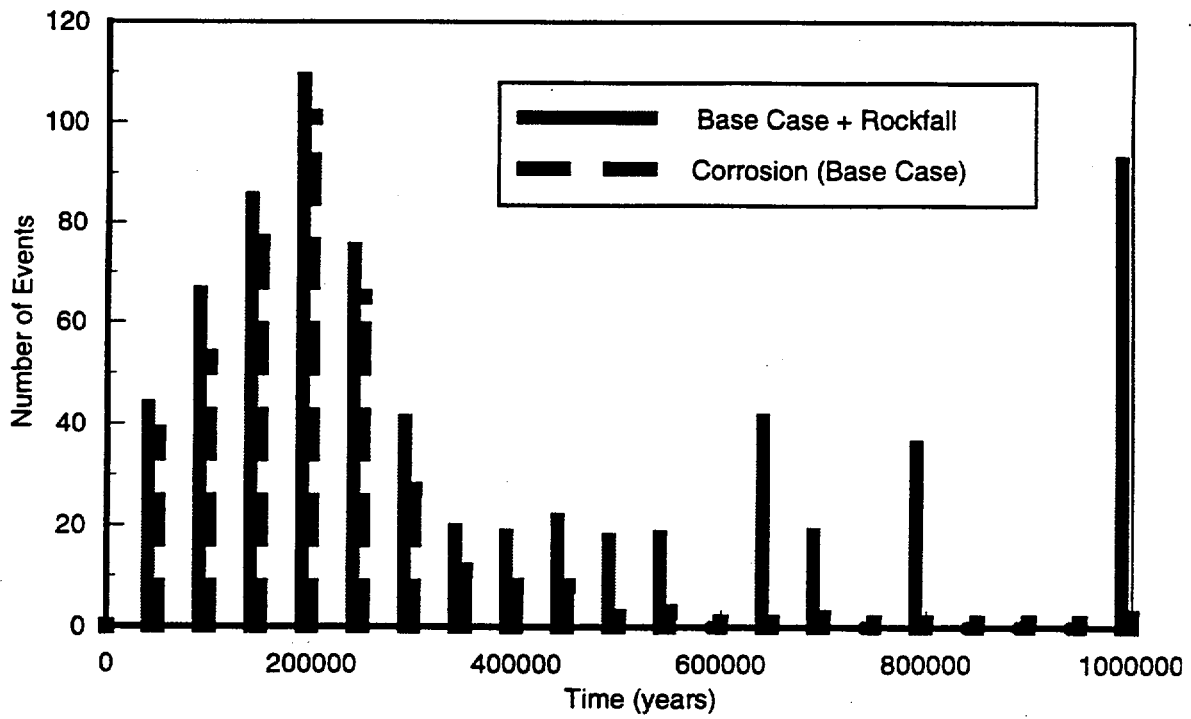


Figure 10-69. Comparison of waste-package failures for corrosion and rockfall

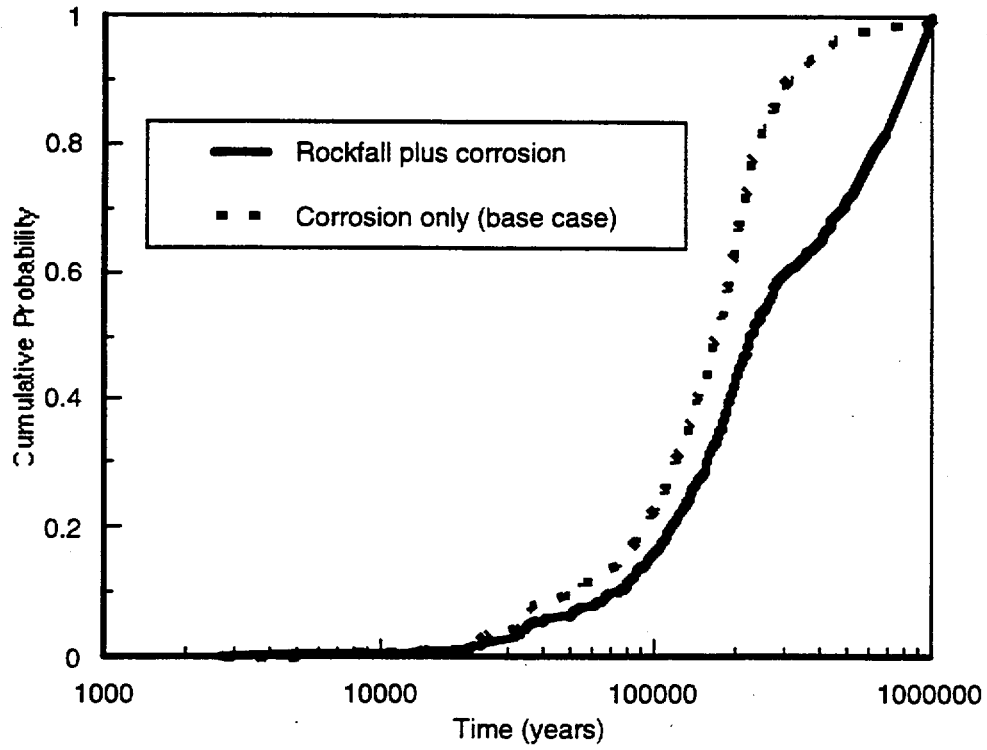


Figure 10-70. CDFs for waste-package failure from corrosion and rockfall.

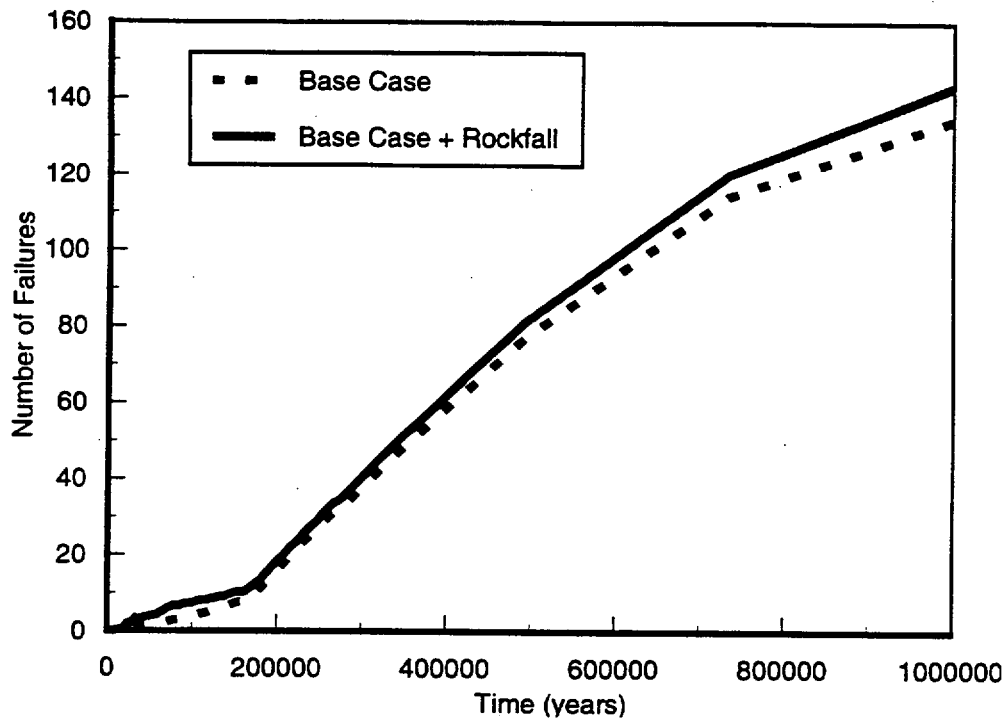


Figure 10-71. Comparison of patch failure from corrosion and rockfall

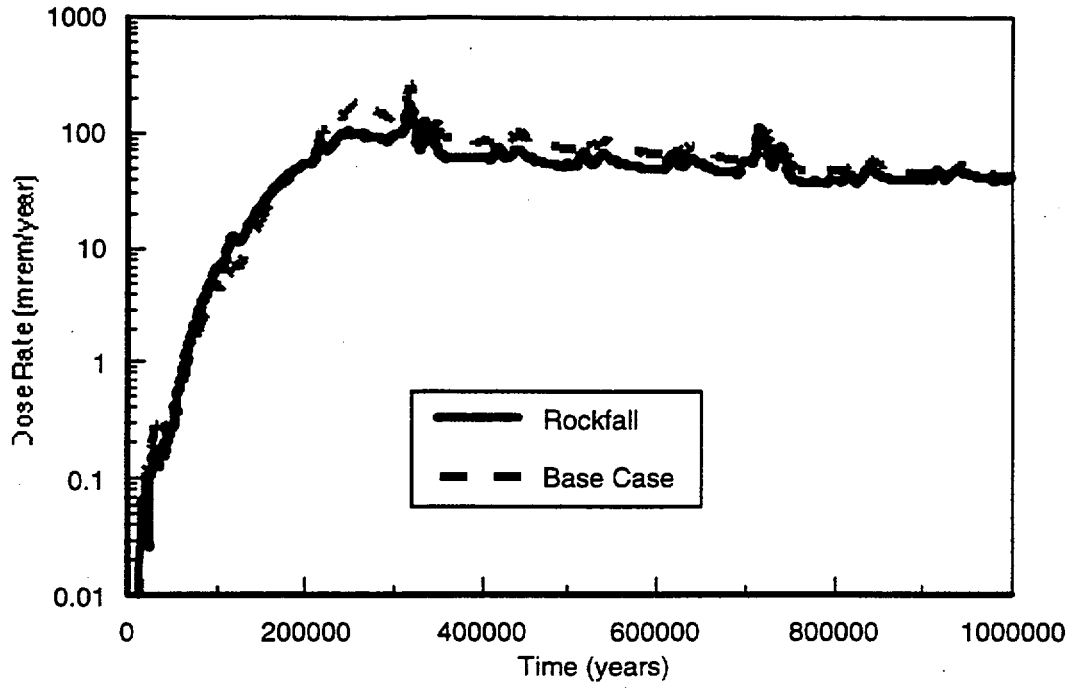


Figure 10-72. Dose-rate time histories for rockfall and base case.

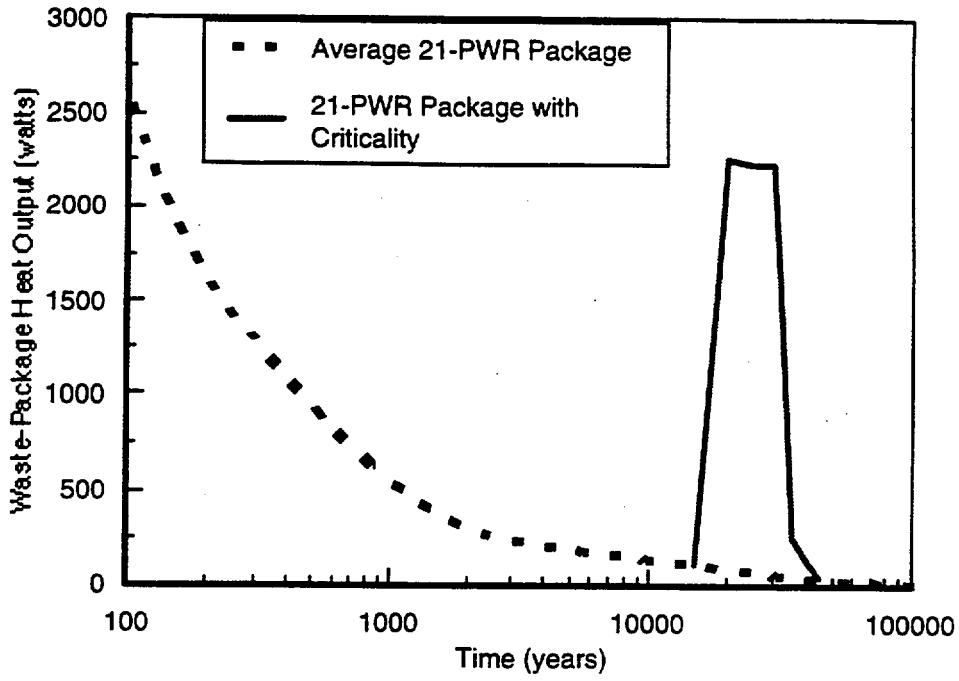


Figure 10-73. Incremental heat output for 10,000-year criticality (data from Section 3 of this document).

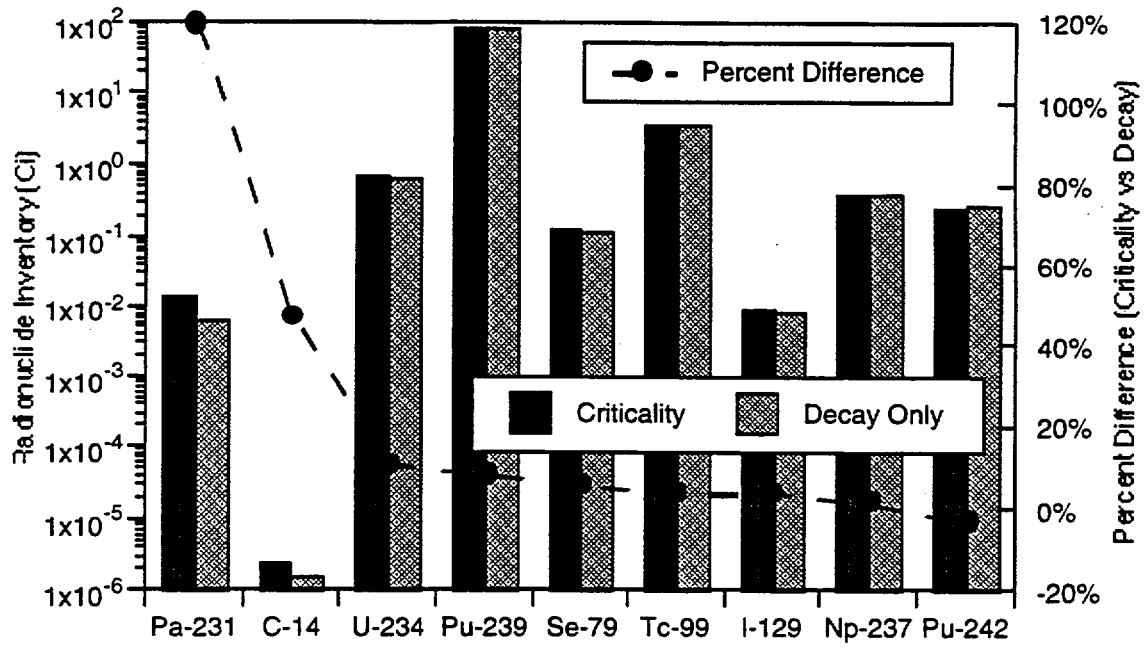


Figure 10-74. Radionuclide inventory differences for 10,000-year criticality (after CRWMS M&O 1996c, Section 7.2.1).

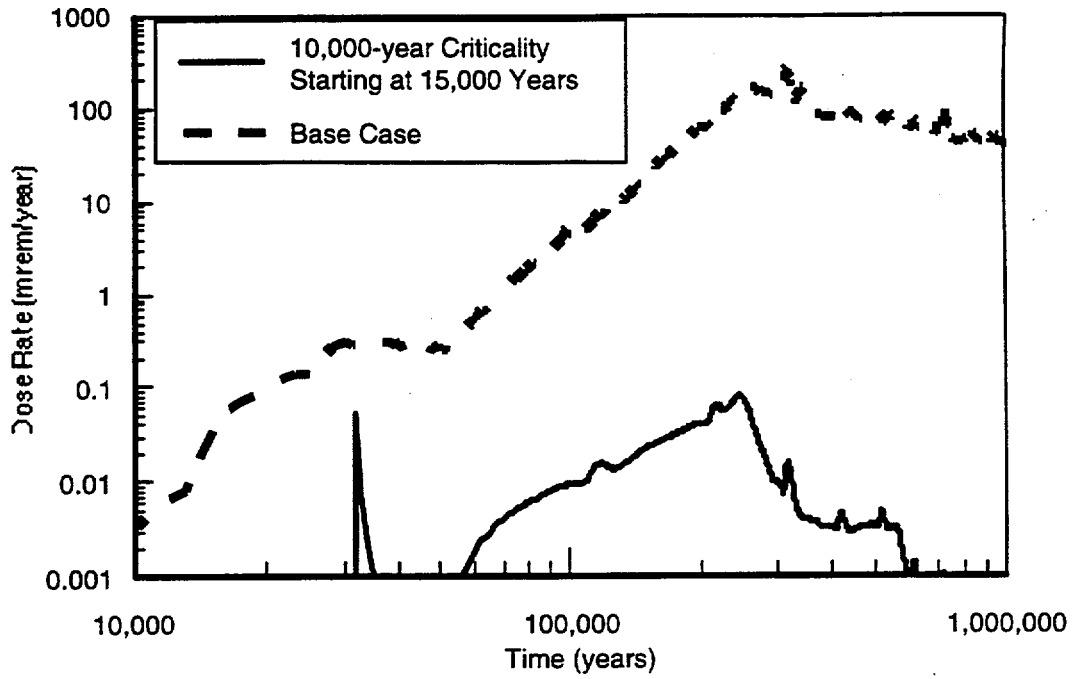


Figure 10-75. Dose rate time history for 10,000-year criticality starting at 15,000 years after emplacement.

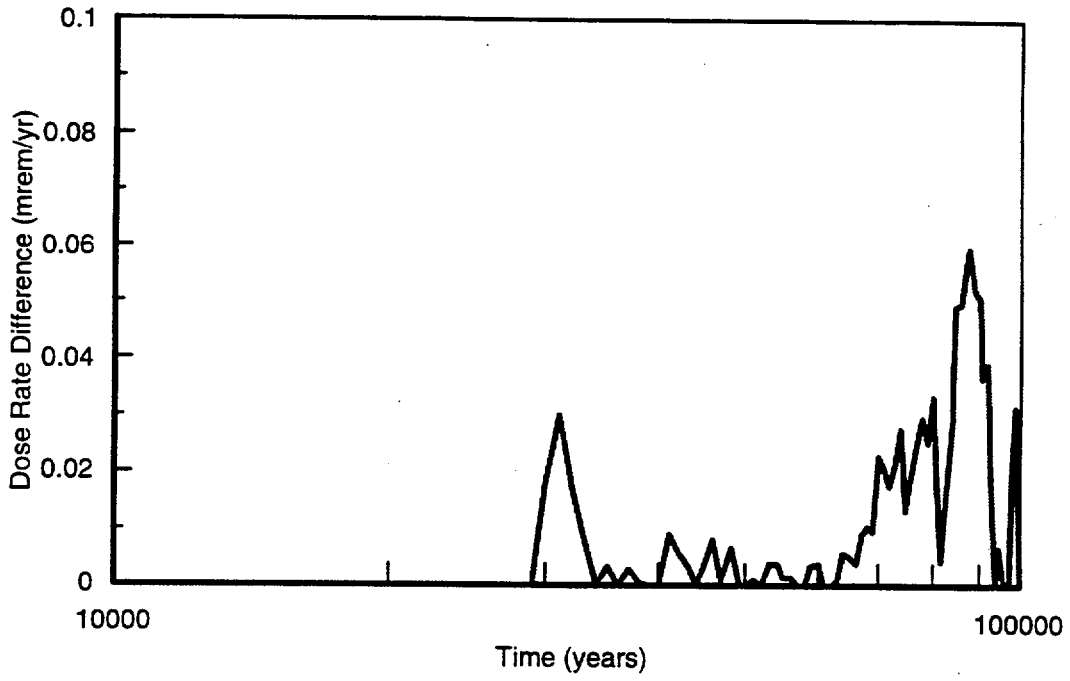


Figure 10-76. Difference in dose rates for criticality vs base case.

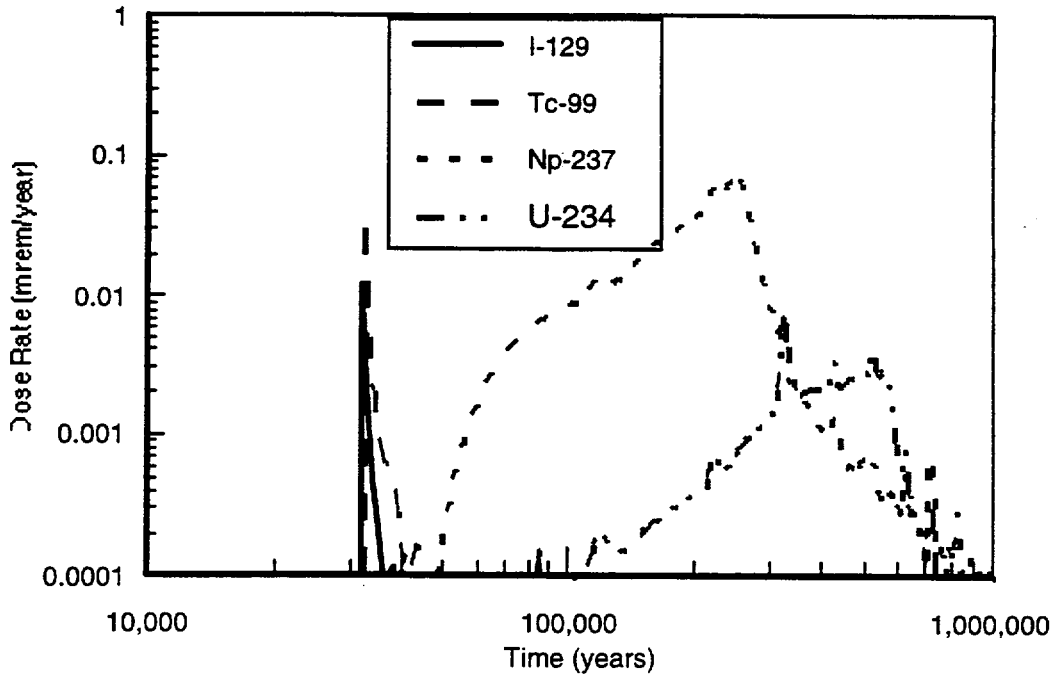


Figure 10-77. Dose rate time histories for the four largest contributors to dose.

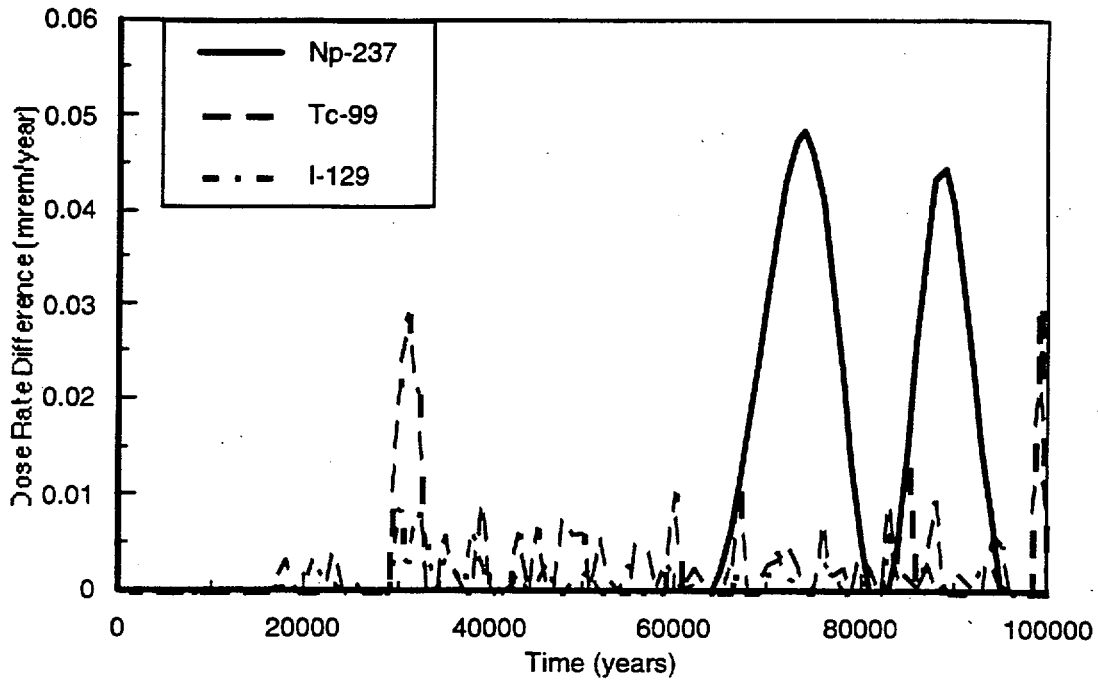


Figure 10-78. Dose-rate increases from criticality from individual radionuclides.

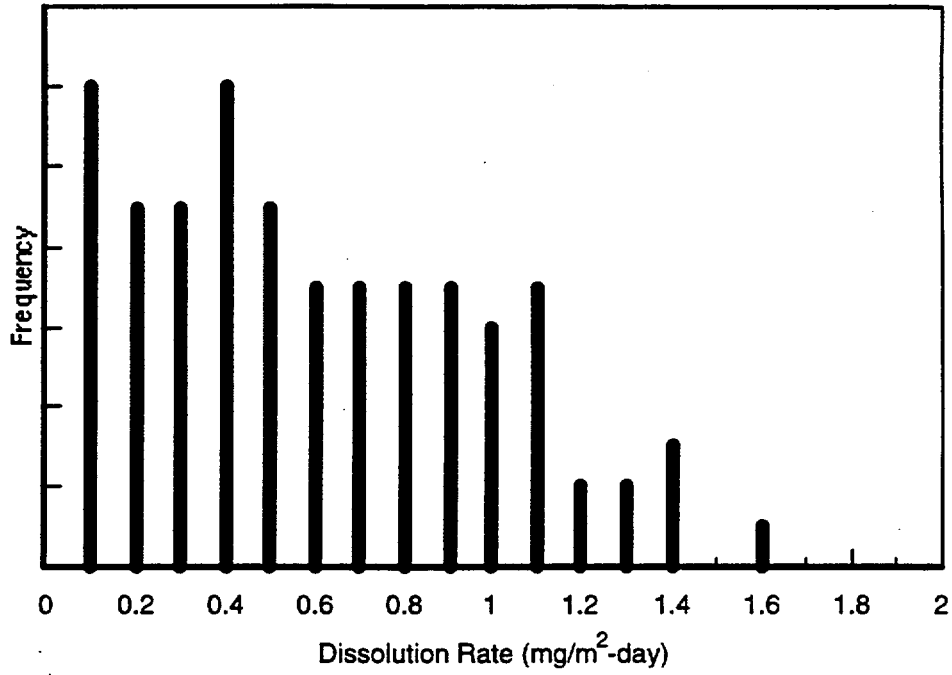


Figure 10-79. Range of waste-form dissolution rates in saturated-zone waters.

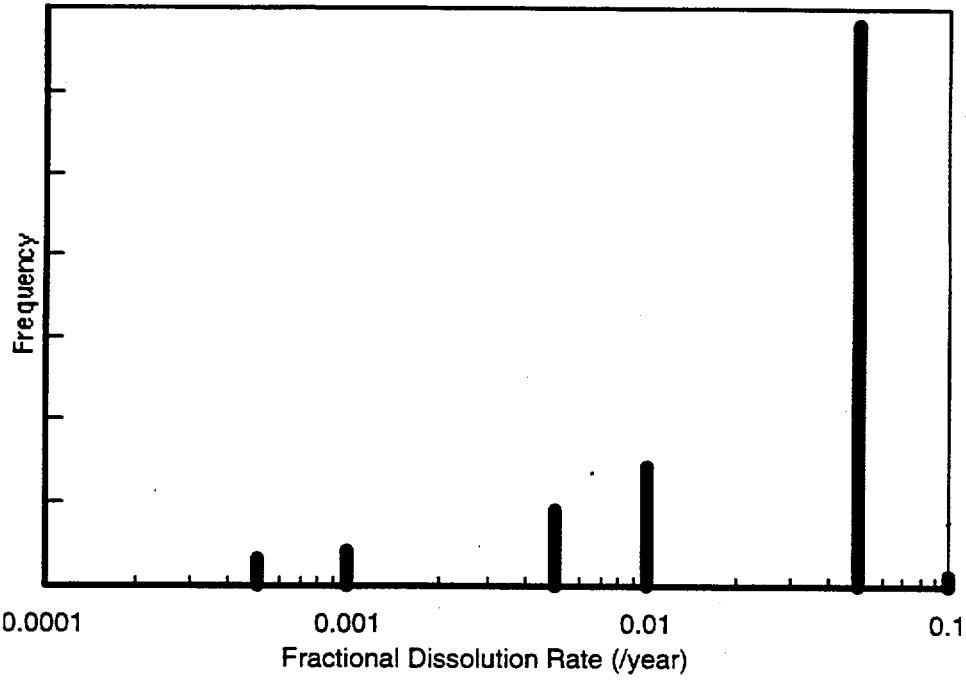


Figure 10-80. Range of waste-form fractional dissolution rates.

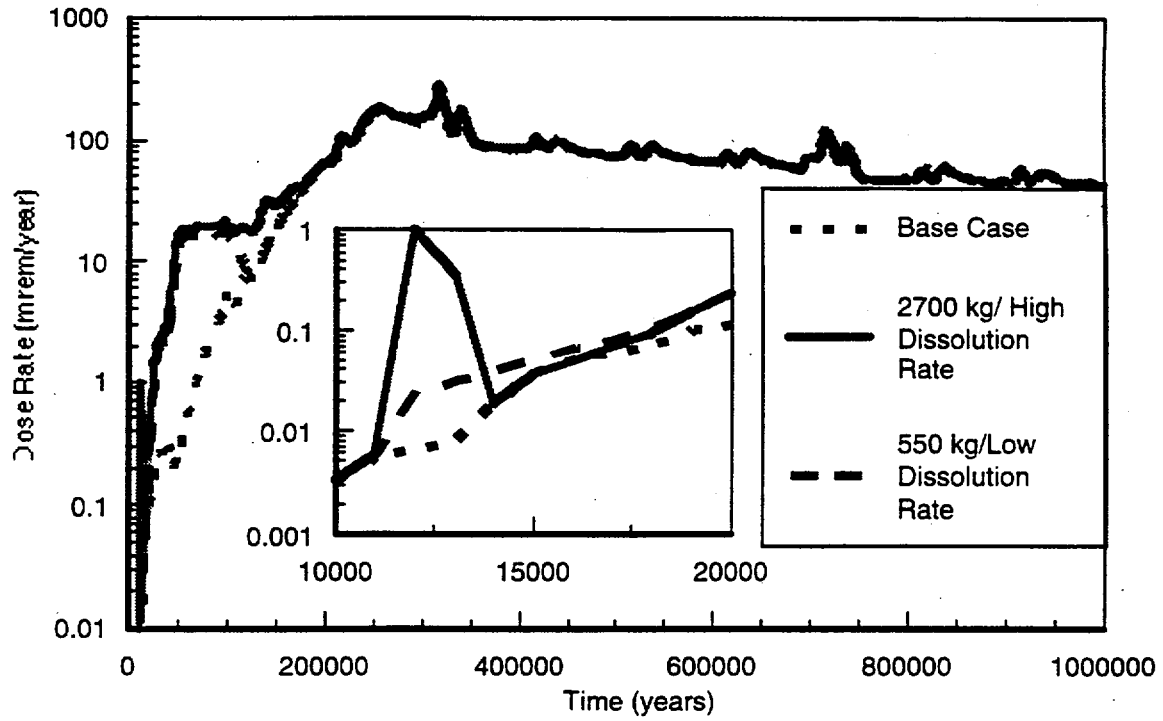


Figure 10-81. Dose-rate time histories for individual radionuclides.

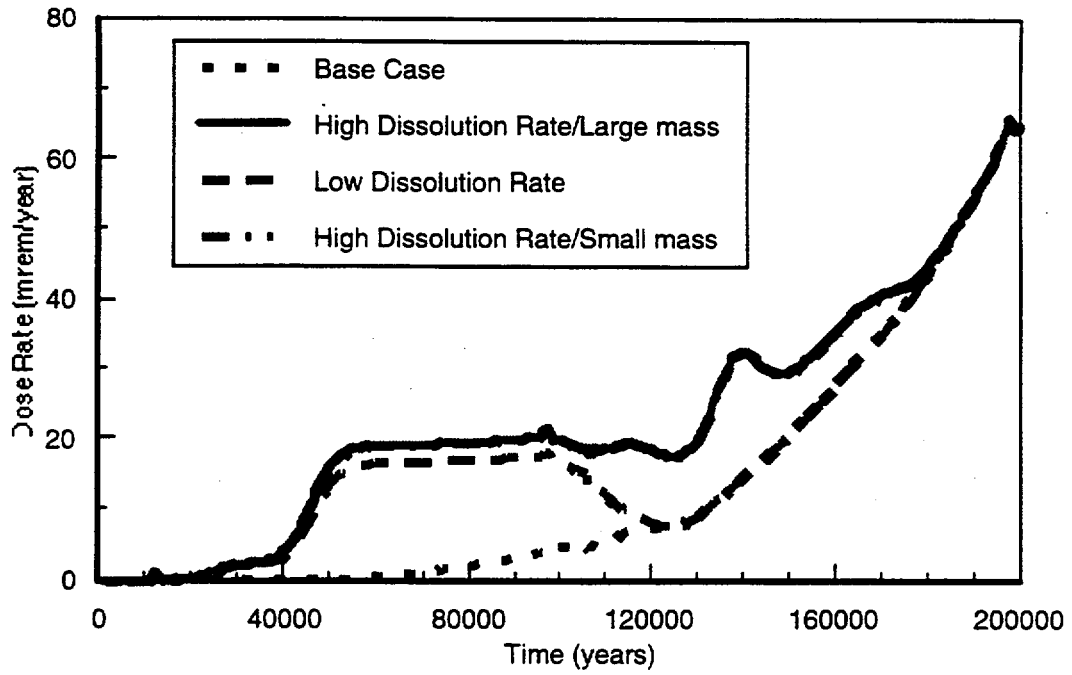


Figure 10-82. Dose-rate time histories for human intrusion.

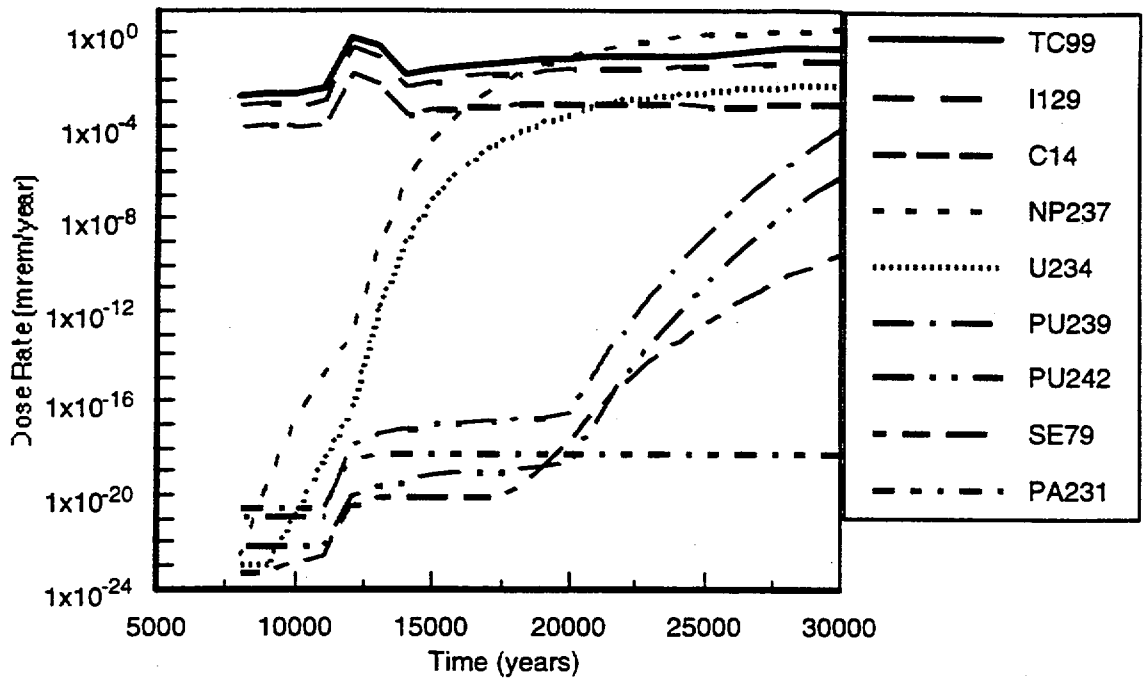


Figure 10-83. Sensitivities of dose rates to model parameters.

Chapter 10
Tables

INTENTIONALLY LEFT BLANK

Table 10-1. Models Used in Disruptive-Events Analyses.

Model	Where Used	Data Tracking Numbers	Q-Status
Volcanic Ash Dispersal	Section 10.4.1	SNT05072098002.001	Non-Q
Volcanic Enhanced Radionuclide Source Term	Section 10.4.2	SNT05072098001.101, TDIF #306979	Non-Q
Rockfall	Section 10.5	DTN: SNT05072098001.103, TDIF #306981	Non-Q
Nuclear Criticality	Section 10.6	SNT05072098001.104 TDIF #306982	Non-Q
Human Intrusion	Section 10.6	SNT05072098001.104 TDIF #306980	Non-Q

Table 10-2. Computer Codes Used in Disruptive-Events Analyses.

Code	Version	Code Usage	Q-Status
ASHPLUME	1.3	Volcanic ash dispersal	Non-Q
RIP	5.19.01	Total-System Integrator	Non-Q
FEHMN	2.0	Site-scale flow and transport	Non-Q

ASHPLUME is described in Jarzempa et al. 1997, RIP is described in Golder (1998), and FEHMN is described in Zivoloski et al. (1995).

Table 10-3. Summary of Codes, Input/Output Files, and DTNs Associated With Technical Figures.

Figure or Table	Subject	Code or Reference	Input filename	Output filename	Data Tracking or Record Accession Number	Q-Status
Figure 10-3	Magma volume vs. age of eruption for Pliocene and Quaternary volcanic events in Yucca Mtn Region	Ref: Crowe et al. 1995)	NA	NA	LA000000000093.001	NQ
Figure 10-12	Aggregate results for frequency of intersection of an igneous intrusion	After CRWMS M&O 1996a, Figure 4-32a	NA	NA	MOL.19971201.02 21	NQ
Figure 10-13	Illustration of potential dikes in the Yucca Mountain Area	After CRWMS M&O 1996a	NA	NA	MOL.19971201.02 21	NQ
Figure 10-14	Probability density for dike length and orientation	After CRWMS M&O 1996a	NA	NA	MOL.19971201.02 21	NQ
Figure 10-15	PDF for number of vents along a dike	Valentine & Perry, 1998	NA	NA	?	NQ
Figure 10-16	PDF for dike width	PVHA experts; Valentine & Perry, 1998	NA	NA	?	NQ
Figure 10-22	PDF for conduit diameter	Valentine & Perry, 1998	NA	NA	?	NQ
Figure 10-23	Range of liquid magma ascent velocities as a function of dike width	Wilson & Head, 1981, Table 5	NA	NA	MOL.19950111.00 30	NQ
Figure 10-24	Range of ascent velocities as a function of conduit diameter	Wilson & Head, 1981, Table 3	NA	NA	MOL.19950111.00 30	NQ
Figure 10-25	Repository outline and modeled configuration	CRWMS M&O, 1997a	NA	NA	MOL.19971210.00 63	NQ
Figure 10-26	Dike intersection with a drift	CRWMS M&O, 1997a	NA	NA	MOL.19971210.00 63	NQ
Figure 10-27	Intersection of a circular conduit with drifts	CRWMS M&O, 1997a	NA	NA	MOL.19971210.00 63	NQ
Figure 10-28	Extrapolation of CRM corrosion rates	Wang & Douglass 1983	NA	NA	NA	NQ

Table 10-3. (continued).

Figure or Table	Subject	Code or Reference	Input filename	Output filename	Data Tracking or Record Accession Number	Q-Status
Figure 10-29	Waste-package CRM wall stresses as a function of temperature	ASME 95, Table 2B; Morral, 1994, Table 9, p. 29 ff.	NA	NA	NA	NQ
Figure 10-30	Waste-package CRM end-cap stresses as a function of temperature	Roark & Young 1975	NA	NA	NA	NQ
Figure 10-31	Times of 50% and 70% degradation of CRM	TSPA-VA Base Case	NA	NA	MO9807MWDRIP 00.000	NQ
Figure 10-32	PDFs of ash-particle diameters	Jarzemba & LaPlante, 1996; Jarzemba et al. 97	NA	NA	SNT05072098002 .001	NQ
Figure 10-33	PDF for waste-particle sizes	Jarzemba & LaPlante, 1996, Figure 4	NA	NA	SNT05072098002 .001	NQ
Figure 10-34	Distribution of wind direction and speed	Jarzemba & LaPlante, 1996	NA	NA	SNT05072098002 .001	NQ
Figure 10-35	Contours for greatest concentration at dose receptor point (Realization 14)	ASHPLUME Version 1.3	RN14z1.in RN14z2.in RN14z3.in	RN14z1.o ut RN14z2.o ut RN14z3.o ut	SNT05072098002 .001	NQ
Figure 10-36	Concentration contours for greatest erupted waste (Realization 1)	ASHPLUME Version 1.3	RN01z3.in RN01z4.in RN01z5.in	RN01z3.o ut RN01z4.o ut RN01z5.o ut	SNT05072098002 .001	NQ
Figure 10-37	Concentration contours for strongest wind blowing away from dose receptor point (Realization 8)	ASHPLUME Version 1.3	RN08z2.in RN08z3.in RN08z4.in	RN08z2.o ut RN08z3.o ut RN08z4.o ut	SNT05072098002 .001	NQ

Table 10-3. (continued).

Figure or Table	Subject	Code or Reference	Input filename	Output filename	Data Tracking or Record Accession Number	Q-Status
Figure 10-38	Inventory of ^{79}Se as a function of time	CDB, DOE 1992 ORIGEN2	?	?	HQO.19920827.0 001 through HQO.19920827.0 004	NQ
Figure 10-39	Inventory of ^{210}Pb as a function of time	CDB, DOE 1992 ORIGEN2	?	?	HQO.19920827.0 001 through HQO.19920827.0 004	NQ
Figure 10-40	Conditional CCDF for mean direct-release volcanic dose rates	Napier et al. 1988 GENII-S	?	?	TIC Catalog No. 206898	NQ
Figure 10-41	CCDFs for peak base-case and direct-volcanic dose rates	Napier et al. 1988 GENII-S	?	?	TIC Catalog No. 206898	NQ
Figure 10-42	Temperature profiles in repository for various amounts of magma filling drift	? Carslaw & Jaeger 1986, p. 258, eqn. 1	NA	NA	NNA.19900522.02 59	NQ
Figure 10-43	Profile for base-case drift-wall temperatures with a magmatic intrusion at 10000 years	? Carslaw & Jaeger 1986, p. 258, eqn. 1	?	?	NNA.19900522.02 59	NQ
Figure 10-44	Mechanical behavior of alloy ASTM N06625 as a function of time and temperature	Morral, 1984, Table 10, p. 33; Morral, 1984, Table 9; CRWMS M&O 1996b	?	?	MOL.19970402.00 69	NQ
Figure 10-45	PDF for uranium dioxide particle size after interaction with magma	?	?	?	?	NQ
Figure 10-46	Layout of contaminated basalt in a drift	?	?	?	?	NQ
Figure 10-47	Times of failure and fractional release rate	?	?	?	?	NQ

Table 10-3. (continued).

Figure or Table	Subject	Code or Reference	Input filename	Output filename	Data Tracking or Record Accession Number	Q-Status
Figure 10-48	Comparison of CCDFs for 100000-year dose rates	RIP Version 5.1901	RIP.IN	RIP.OUT	SNT05072098001 .001MO9807MWD RIP00.000	NQ
Figure 10-49	Comparison of CCDFs for 1000000-year dose rates	RIP Version 5.1901	RIP.IN	RIP.OUT	SNT05072098001 .001MO9807MWD RIP00.000	NQ
Figure 10-50	Time histories for dose rates over 1000000 years	RIP Version 5.1901	RIP.IN	RIP.OUT	SNT05072098001 .001MO9807MWD RIP00.000	NQ
Figure 10-51	Missing?	? RIP Version 5.1901	RIP.IN ?	RIP.OUT ?	?	NQ
Figure 10-52	Examples of new dikes in the saturated flow domain	?	?	?	?	NQ
Figure 10-53	SZ reference model	SZ Code = ? D'Agnese et al 1997, pp. 59 ff.	?	?	?	NQ
Figure 10-54	Dike inserted along Solitario Canyon fault	SZ Code = ?	?	?	?	NQ
Figure 10-55	Dike inserted beneath repository connected to Solitario Canyon fault	SZ Code = ?	?	?	?	NQ
Figure 10-56	Dike inserted southeast of repository	SZ Code = ?	?	?	?	NQ
Figure 10-57	Stress state of drift immediately after excavation	?	NA	NA	?	NQ
Figure 10-58	Assumed relationship btw DL and descriptive damage	Kaiser et al. 1992, Figure 2	NA	NA	NA	NQ
Figure 10-59	Annual probability of exceedence for horizontal PGV	CRWMS M&O 1998e	NA	NA	In press	NQ

Table 10-3. (continued).

Figure or Table	Subject	Code or Reference	Input filename	Output filename	Data Tracking or Record Accession Number	Q-Status
Figure 10-60	Critical rock mass for various waste-package wall thickness	CRWMS M&O 97c; CRWMS M&O 97b	NA	NA	MOL.19970813.05 31 MOL.19961217.03 18	NQ
Figure 10-61	Time rate of thinning of waste package wall	TSPA-VA base-case abstractions	?	?	MO9807MWDRIP 00.000	NQ
Figure 10-62	Critical rock masses as function of time	TSPA-VA base-case abstractions; Figs 23 & 24 ?	?	?	MO9807MWDRIP 00.000	NQ
Figure 10-63	Distribution of rock sizes for all units	CRWMS M&O 1997d	?	?	MOL.19980219.01 04	NQ
Figure 10-64	Distribution of rock sizes for the TSw unit	CRWMS M&O 1997d	?	?	MOL.19980219.01 04	NQ
Figure 10-65	Mechanical damage to fuel rods from a circular point of contact	CRWMS M&O 1997e	?	?	NA	NQ
Figure 10-66	Mechanical damage to fuel rods from a linear point of contact	CRWMS M&O 1997e	?	?	NA	NQ
Figure 10-67	Distribution of times for breach of waste packages	WAPDEG	?	?	?	NQ
Figure 10-68	CDF for waste-package failures from rockfall	WAPDEG ?	?	?	?	NQ
Figure 10-69	Comparison of waste-package failures for corrosion and rockfall	WAPDEG ?	?	?	?	NQ
Figure 10-70	CDFs for waste-package failures from corrosion and rockfall	WAPDEG ?	?	?	?	NQ
Figure 10-71	Comparison of patch failure from corrosion and rockfall	WAPDEG ?	?	?	?	NQ

Table 10-3. (continued).

Figure or Table	Subject	Code or Reference	Input filename	Output filename	Data Tracking or Record Accession Number	Q-Status
Figure 10-72	Dose-rate time histories for rockfall and base case	RIP Version 5.1901	?	?	SNT05072098001 .003MO9807MWD RIP00.000	NQ
Figure 10-73	Incremental heat output for 10000-year criticality	Data from Section 3 of this document	?	?	NA ?	NQ
Figure 10-74	Radionuclide inventory differences for 10000-year criticality	CRWMS M&O 1996c, Section 7.2.1	?	?	MOL.19970113.00 02	NQ
Figure 10-75	Dose rate time history for 10000-year criticality starting at 15000 years after emplacement	RIP Version 5.1901	RIP.IN	RIP.OUT	SNT05072098001 .004 MO9807MWDRIP 00.000	NQ
Figure 10-76	Difference in dose rates for criticality vs. base case	RIP Version 5.1901	RIP.IN	RIP.OUT	SNT05072098001 .004 MO9807MWDRIP 00.000	NQ
Figure 10-77	Dose rate time histories for the three largest contributors to dose	RIP Version 5.1901	RIP.IN	RIP.OUT	SNT05072098001 .004 MO9807MWDRIP 00.000	NQ
Figure 10-79	Range of waste-form dissolution rates in SZ waters	Gray et al. 1995	?	?	MOL.19960613.00 37	NQ
Figure 10-80	Range of waste-form fractional dissolution rates	Gray et al. 1995	?	?	MOL.19960613.00 37	NQ
Figure 10-81	Dose-rate time histories for individual radionuclides	RIP Version 5.1901	RIP.IN	RIP.OUT	SNT05072098001 .002	NQ
Figure 10-82	Dose-rate time histories for human intrusion	RIP Version 5.1901	RIP.IN	RIP.OUT	SNT05072098001 .002	NQ
Figure 10-83	Sensitivities of dose rates to model parameters	RIP Version 5.1901	RIP.IN	RIP.OUT	SNT05072098001 .002 MO9807MWDRIP 00.000	NQ

Table 10-3. (continued).

Figure or Table	Subject	Code or Reference	Input filename	Output filename	Data Tracking or Record Accession Number	Q-Status
Table 10-6	Eruptive Parameters for Analog Volcanoes	Jarzemba et al. 1997, Table 4-3, p. 4-5	NA	NA	SNT05072098002.001	NQ
p 10-49	Fragmentation Depth PDF	Wilson & Head 1981; Valentine & Perry 1998	NA	NA	MOL.19950111.0030 ?	NQ
Table 10-14	Magma Rise Velocity as a Function of Dike Width	Wilson & Head 1981, Table 5	NA	NA	MOL.19950111.0030	NQ
Table 10-8	Ascent Velocity as a Function of Conduit Diameter	Wilson & Head 1981, Table 3	NA	NA	MOL.19950111.0030	NQ
p 10-54	Intrusion Temperature	MacDonald 1972, Table 4.2	NA	NA	NNA.19940415.0006	NQ
Table 10-9	Number of Waste Packages per drift hit by a Dike	CRWMS M&O 1997k	NA	NA	MOL.19980408.0604	NQ
Table 10-10	Number of Waste Packages hit for circular conduits	?	NA	NA	?	NQ
Table 10-11	Waste Package Internal Pressure	CRWMS M&O 1997], Section 7.2.2.7	NA	NA	NA	NQ
p 10-64	Waste Package Internal Pressure vs. Temperature	?	NA	NA	?	NQ
Table 10-12	Fractional velocities for agglomerated pyroclast-waste particles	?	NA	NA	?	NQ
Table 10-13	Settling velocities (cm/s) for waste particles in Magma	After Carmichael et al 1977, eqn 58	NA	NA	NNA.19900306.0047	NQ
Table 10-14	Settling velocities (cm/s) for agglomerated waste-magma particles	After Carmichael et al 1977, eqn 58	NA	NA	NNA.19900306.0047	NQ

Table 10-3. (continued).

Figure or Table	Subject	Code or Reference	Input filename	Output filename	Data Tracking or Record Accession Number	Q-Status
p 10-74	Eruption volume	Jarzemba et al. 1997, Section 4.2.1.1	NA	NA	SNT05072098002 .001	NQ
p 10-74	Eruption power	Jarzemba et al. 1997, Section 4.2.1.1	NA	NA	SNT05072098002 .001	NQ
Table 10-15	Sample ashplume.in file	Jarzemba et al. 1997, App. A	NA	NA	SNT05072098002 .001	NQ
Table 10-16a	Selected examples of dike intrusions	Figs. 10.3-2 & 10.3-4	NA	NA	?	NQ
Table 10-16b	Selected example of dike intrusions	PDF on p 10-49	NA	NA	?	NQ
Table 10-16c	Numbers of packages hit by liquid-magma intrusions	Section 10.3.2.2	NA	NA	?	NQ
Table 10-16d	Numbers of packages hit by ash intrusions	Section 10.3.2.2	NA	NA	?	NQ
Table 10-16e	Waste-package breach simulations	Section 10.3.2.3.1	NA	NA	?	NQ
Table 10-16f	Waste-removal simulations	Figs. 10.3-16 & 10.3-17	NA	NA	?	NQ
Table 10-16g	Waste-entrainment simulations	Section 10.3.2.4	NA	NA	?	NQ
Table 10-16h	Amount of waste in eruptive source	?	NA	NA	?	NQ
Table 10-16i	Parameters for ASHPLUME simulations	Section 10.3.2.7	NA	NA	?	NQ
Table 10-17	Contributions of Intermediate Processes to Final Source Term	NA	NA	NA	NA	NQ

Table 10-3. (continued).

Figure or Table	Subject	Code or Reference	Input filename	Output filename	Data Tracking or Record Accession Number	Q-Status
Table 10-18	Waste Concentrations at Dose Receptor Points	ASHPLUME Version 1.3	RN14z1.in RN01z3.in RN12z.in RN17z.in RN11z1.in RN02z.in RN04z.in RN07z1.in RN13z.in RN15z.in RN06z1.in RN09z1.in RN03z2.in RN16z.in RN05z.in RN10z1.in RN08z2.in	RN14z1.out RN01z3.out RN12z.out RN17z.out RN11z1.out RN02z.out RN04z.out RN07z1.out RN13z.out RN15z.out RN06z1.out RN09z1.out RN03z2.out RN16z.out RN05z.out RN10z1.out RN08z2.out	SNT05072098002.001	NQ
p 10-98	Amount of UO ₂ dissolved	?	?	?	?	NQ
Table 10-19	Dissolution rates of uranium-bearing minerals	Bruno et al. 95, Table 1; Perez et al. 97	NA	NA	TIC Catalog No. 216341 MOL.19980505.0194	NQ
p 10-99	Overall dissolution rate; Basalt dissolution rate	?	?	?	?	NQ
Table 10-20	Waste elements susceptible to mobilization at magmatic temperatures	TSPA-VA base case; Hansen & Anderko 1958	NA	NA	MO9807MWD RIP 00.000 NNA.19891009.004	NQ

Table 10-3. (continued).

Figure or Table	Subject	Code or Reference	Input filename	Output filename	Data Tracking or Record Accession Number	Q-Status
Table 10-21a	Selected examples of dike intrusions	?	?	?	?	NQ
Table 10-21b	Calculation of total number of waste packages breached by magma intrusion	?	?	?	?	NQ
Table 10-21c	Calculation of UO ₂ dissolution	?	?	?	?	NQ
Table 10-21d	Calculation of basalt dissolution	?	?	?	?	NQ
Table 10-22	Rock Quality Ranges	CRWMS M&O 97d	NA	NA	MOL.19980219.01 04	NQ
Table 10-23	Thermal Spalling at Various Times after closure	EPRI 96, Ch 12	NA	NA	MOL.19980211.03 67	NQ
Table 10-24	Initial-Condition Factors for DL Calculation	Kaiser et al. 1992	NA	NA	NA	NQ
Table 10-25	PGV Values for various IC and DL Values	Kaiser et al. 1992	NA	NA	NA	NQ
Table 10-26	Frequencies of occurrence for various PGV values over different time periods	?	?	?	?	NQ
Table 10-27	DL values for various rock qualities	?	?	?	?	NQ
Table 10-28	Calculated Waste-Package Damages from Rockfall as a Function of Wall Thickness	CRWMS M&O 97c; CRWMS M&O 97b	NA	NA	MOL.19970813.05 31 MOL.19961217.03 18	NQ
Table 10-29a	Calculation of Damage Levels at Various Times	?	?	?	?	NQ
Table 10-29b	Calculation of Amounts of Waste-Package Degradation	?	?	?	?	NQ
Table 10-29c	Association of DL Values with Rock-Size Data	?	?	?	?	NQ

Table 10-3. (continued).

Figure or Table	Subject	Code or Reference	Input filename	Output filename	Data Tracking or Record Accession Number	Q-Status
Table 10-29d	Falling Rock Masses Resulting from Seismic Events	?	?	?	?	NQ
Table 10-30	Summary of Rockfall Grouped by time period	?	?	?	?	NQ
Table 10-31	Summary of In-Package Critical Configurations	CRWMS M&O 97f	?	?	MOL.19980204.02 81	NQ
Table 10-32	Summary of Near-Field Critical Configurations	CRWMS M&O 97f	?	?	MOL.19980204.02 81	NQ
Table 10-33	Summary of Far-Field Critical Configurations	CRWMS M&O 97f	?	?	MOL.19980204.02 81	NQ
p 10-171	Volume of waste dropped down borehole	Wilson et al. 1994	NA	NA	MOL.19940112.01 23	NQ
p 10-171	Temperature, Carbonate, Oxygen, pH, Burnup	Chapter 6 model	?	?	?	NQ
p 10-172	Temperature, Carbonate, Oxygen, pH	Chapter 6 model	?	?	?	NQ
p 10-173	Specific surface area of waste	Gray & Wilson 95, Table 2.2	NA	NA	MOL.19960613.00 35	NQ
Table 10-34	Contaminant masses available in saturated zone	Section 7.5, Section 10.3.2.10.1, Section 10.6.3.3	?	?	?	NQ
Table 10-35	Human-Intrusion Source Term for Disruption of 2.7 Metric Tons of Spent Fuel	?	?	?	?	NQ
Table 10-36	Human-Intrusion Source Term for Disruption of 0.55 Metric Tons of Spent Fuel	?	?	?	?	NQ

Table 10-4. Summary of TSPA-VA Screening for Selected NEA FEP Categories.

FEP No.	FEP Name	Screening Decision	Comment
1.0	EXTERNAL FACTORS	(see subcategories)	
1.1	Repository Issues	Most FEPs in this NEA category are included as EFEPs	FEPs included in this category relate to programmatic decisions regarding the waste inventory, site selection, and the design, operation, and closure of the repository. They are included in the YM TSPA through the design of the TSPA-VA base case modeling of the nominal scenario.
1.2	Geological Processes and Effects	(see subcategories)	
1.2.01	Tectonic movements and orogeny	Excluded, low consequence	Rates of tectonic movement are too slow to affect the disposal system significantly during the period of performance.
1.2.02	Deformation, elastic, plastic, or brittle	Excluded, low consequence	Rates of deformation are too slow to affect the disposal system significantly during the period of performance.
1.2.03	Seismicity	Included, DFEP	Earthquakes large enough to disrupt repository performance are treated as a potentially disruptive event with a probability less than 1.0, and are included in the analyses of disruptive scenarios (see Section 10.5 of this chapter).
1.2.04	Volcanic and magmatic activity	Included, DFEP	Basaltic volcanism is treated as a potentially disruptive event with a probability less than 1.0, and is included in the analyses of disruptive scenarios (see Section 10.4 of this chapter). Other forms of igneous activity are excluded based on low probability of occurrence during the period of performance.
1.3	Climatic processes and effects	(see subcategories)	
1.3.01	Climatic change, global	Included, EFEP	Global climatic change is expected to occur during the period of regulatory performance, and has been included in the nominal scenario. Uncertainty about the timing, magnitude, and consequences of global climatic change are incorporated in base case modeling (see Chapter 2).
1.3.02	Climatic change, regional and local	Included, EFEP	Regional and local climatic changes are expected to occur during the period of performance. Uncertainty about the timing, magnitude, and consequences of regional and local climatic change are included in the consideration of global climatic change (see Chapter 2).
1.3.03	Sea level changes	Excluded, low consequence	Yucca Mountain is sufficiently distant from oceans that changes in sea level will have no direct effects on performance during the period of performance. Indirect effects are incorporated in the nominal scenario through the treatment of climatic change.
1.3.04	Periglacial effects	Excluded, low probability	Periglacial effects (e.g., formation of permafrost) will not occur at Yucca Mountain in any reasonably foreseeable climate state during the period of performance.
1.3.05	Glacial and ice sheet effects, local	Excluded, low probability	Glaciers will not form at Yucca Mountain in any reasonably foreseeable climate state.

Table 10-4. (continued).

FEP No.	FEP Name	Screening Decision	Comment
1.3.06	Warm climate effects (tropical and desert)	Included, EFEP	A warm arid to semiarid climate is the expected state at Yucca Mountain.
1.3.07	Hydrological/hydrogeological response to climate changes	Included, EFEP	Hydrological changes in response to climatic changes are explicitly modeled in the TSPA-VA base case. See Chapters 2 and 8.
1.3.08	Ecological response to climate changes	Included, EFEP	Ecological changes in response to climatic changes are included in the nominal scenario implicitly through the treatment of changes in infiltration.
1.3.09	Human response to climatic change	Excluded, low consequence	Dose calculations for the TSPA-VA are based on the assumption that future human activities will be similar to those of the present. The major impact of cooler and wetter climates on exposure pathways will be to reduce the amount of irrigation used in agriculture, which would potentially reduce doses. Cooler and wetter climates could increase the number of people near the repository.
1.4	Future human actions	Included as a special case	The TSPA-VA includes a deterministic analysis of the consequences of an inadvertent drilling intrusion into the repository. See Section 10.6 of this chapter.
1.5.01	Meteorite Impact	Excluded, low probability	Impacts of meteorites large enough to disrupt the repository have occurred globally in the past with a frequency less than 10^{-8} /yr. (for comparable surface areas).
2.0	DISPOSAL SYSTEM DOMAIN: ENVIRONMENTAL FACTORS	(see subcategories)	
2.1	Wastes and Engineered Features	(see subcategories)	
2.1.01	Inventory, radionuclide and other material	Included, EFEP	The radionuclide inventory of the repository is included in TSPA-VA base case modeling. See Chapter 6.
2.1.02	Waste form materials and characteristics	Included, EFEP	Properties of the waste form are included in the TSPA-VA base case modeling. See Chapter 6.
2.1.03	Container materials and characteristics	Included, EFEP	Properties of the waste container are included in the TSPA-VA base case modeling. See Chapter 5.
2.1.04	Buffer/backfill materials and characteristics	Excluded, not relevant	The proposed repository design does not include buffers. Backfill is a design option being evaluated.
2.1.05	Seals, cavern/tunnel/shaft	Excluded, low consequence	The tunnel seals have no role in the long-term performance of the repository, beyond protecting the waste from disruption by humans or animals. Seals are not included in the TSPA-VA modeling.
2.1.06	Other engineered features, materials, and characteristics	Included, EFEP	Performance of the concrete liner, invert, and pedestal is included in the conceptual model for the disposal region. See Chapter 4.
2.1.07	Mechanical processes and conditions (in wastes and EBS)	Included, EFEP	Mechanical degradation of the EBS and waste packages is included in the conceptual model for the disposal region. See Chapter 5.

Table 10-4. (continued).

FEP No.	FEP Name	Screening Decision	Comment
2.1.08	Hydraulic/hydrogeological processes and conditions (in wastes and EBS)	Included, EFEP	Fluid flow and radionuclide mobilization and transport is included in the conceptual model for the disposal region. See Chapter 4.
2.1.09	Chemical/geochemical processes and conditions (in wastes and EBS)	Included, EFEP	Geochemical processes are included in the conceptual model for the disposal region. See Chapter 4.
2.1.10	Biological/biochemical processes and conditions (in wastes and EBS)	Included, EFEP	Biological processes within the disposal region will not significantly affect performance. Microbial induced corrosion can accelerate waste-package failure. See Chapter 5.
2.1.11	Thermal processes and conditions (in wastes and EBS)	Included, EFEP	Thermal processes are included in the conceptual model for the disposal region. See Chapter 3.
2.1.12	Gas sources and effects (in wastes and EBS)	Excluded, low consequence	Gas generated within the waste disposal region (e.g., by radiolysis) will vent through the unsaturated zone and will have no significant effect on performance.
2.1.13	Radiation effects (in wastes and EBS)	Excluded, low consequence	Direct effects of radiation (e.g., radiolysis) will have no significant effect on performance.
2.1.14	Nuclear criticality	Included, DFEP	Nuclear criticality is treated as a potentially disruptive event with a probability of occurrence during the period of performance less than 1.0, and is included in the analysis of disruptive scenarios. See Section 10.6 of this chapter.
2.2	Geological environment	Included, EFEP	FEPs in this category include features of the geologic system such as stratigraphy, and hydrologic properties of potential transport pathways. These FEPs are included in the conceptual model for the geologic system. See Chapter 2.
2.3	Surface environment	Included, EFEP	FEPs in this category include features of the surface environment such as topography, vegetation, and current meteorology. Most FEPs in this category are included implicitly in the analysis through the treatment of the infiltration and climate change. Some are excluded as being irrelevant to the Yucca Mountain site, such as those that relate to coastal environments.
2.4	Human behavior	Included, EFEP	FEPs in this category include aspects of human behavior such as dietary habits and land use that might affect exposure pathways. These FEPs are included in the assessment of doses through the assumption that future human behavior will be similar to that of the present.
3.0	DISPOSAL SYSTEM DOMAIN: RADIONUCLIDE/ CONTAMINANT FACTORS	(see subcategories)	
3.1	Contaminant characteristics	(see subcategories)	
3.1.01	Radioactive decay and ingrowth	Included, EFEP	Radioactive decay and ingrowth is included in TSPA-VA base case modeling. See Chapter 7.

Table 10-4. (continued).

FEP No.	FEP Name	Screening Decision	Comment
3.1.02	Chemical/organic toxin stability	Excluded, low consequence	Chemical contaminants in the waste form are not a significant factor in the long-term performance of the repository.
3.1.03	Inorganic solids/solutes	Included, EFEP	Inorganic chemistry of the disposal region environment is included in the conceptual model for radionuclide mobilization. See Chapter 4.
3.1.04	Volatiles and potential for volatility	Excluded, low consequence	Volatile compounds are not a significant factor in the long-term performance of the repository.
3.1.05	Organics and potential for organic forms	Excluded, low consequence	Organic materials are not a significant component of the waste package or the EBS.
3.1.06	Noble gases	Exclude, low consequence	Noble gases are not a significant factor in the long-term performance of the repository.
3.2	Contaminant Release/Migration Factors	(see subcategories)	
3.2.01	Dissolution, precipitation, and crystallization, contaminant	Included, EFEP	Effects of dissolution and precipitation reactions on aqueous concentrations of radionuclides are included in the conceptual model for radionuclide mobilization and transport. See Chapter 7.
3.2.02	Speciation and solubility, contaminant	Included, EFEP	Effects of speciation on radionuclide solubility are included in the conceptual model for radionuclide mobilization and transport. See Chapter 7.
3.2.03	Sorption/desorption processes, contaminant	Included, EFEP	Effects of sorption and desorption are included in the conceptual model for radionuclide transport. See Chapter 7.
3.2.04	Colloids, contaminant interactions and transport with	Included, EFEP	Effects of colloids on radionuclide transport are included in the conceptual model for radionuclide transport. See Chapter 7.
3.2.05	Chemical/complexing agents, effects on contaminant speciation/transport	Included, EFEP	Effects of complexing agents are included in the conceptual model for radionuclide transport. See Chapter 7.
3.2.06	Microbial/biological/plant-mediated processes, contaminant	Included, EFEP	Microbial processes that may contribute to colloidal transport are included in the conceptual model for radionuclide transport. See Chapter 4. Microbial induced corrosion can accelerate waste-package failure. See Chapter 4. Uptake of radionuclides in plants and livestock is considered in dose calculations. See Chapter 9.
3.2.07	Water-mediated transport of contaminants	Included, EFEP	Radionuclide transport in the unsaturated and saturated zones is included in the TSPA-VA base case modeling. See Chapter 8.
3.2.08	Solid-mediated transport of contaminants	Included only in volcanism and human intrusion analyses	Transport of solid waste excluded from the nominal scenario based on low probability. However, it is included as a relevant process in the modeling of volcanic disruption and human intrusion. See Sections and 10.6 of this chapter.

Table 10-4. (continued).

FEP No.	FEP Name	Screening Decision	Comment
3.2.09	Gas-mediated transport of contaminants	Excluded, low consequence	Some radionuclides will be transported from the repository in the gas phase (e.g., ¹⁴ C). Potential doses to humans will be insignificant, however, because of atmospheric dispersion.
3.3	Exposure Factors	Included, EFEP	FEPs in this category relate to exposure pathways, and most are included in the TSPA-VA dose calculations. See Chapter 9.

INTENTIONALLY LEFT BLANK

Table 10-5. Summary of PVHA Model Input Parameters (after CRWMS M&O 1996a).

Temporal Models	R. W. Carlson Volume Predictable [0.7] Homogeneous Poisson [0.3]	B. H. Crowe Observed Distribution [0.4] Structural [0.6]	W. A. Duffield Homogeneous Poisson [1.0]	R. V. Fisher Homogeneous Poisson [1.0]	W. R. Hackett Homogeneous Poisson [1.0]	M. A. Kuntz Homogeneous Poisson [0.8] Non-Homogeneous [0.2]	A. R. McElroy Homogeneous Poisson [1.0]	M. F. Sheridan Homogeneous Poisson [1.0]	G. A. Thompson Homogeneous Poisson [1.0]	G. P. L. Walker Homogeneous Poisson [1.0]
Time Period	Conditional on temporal model Post-1 Ma (vol. pred.) Post-1 Ma (homogeneous)	Conditional on zonation model and structural tectonic zone	Post-1 Ma [1.0]	Post-1 Ma [0.6] Post-5 Ma [0.3] Post-10 Ma [0.1]	Post-1 Ma [0.5] Post-5 Ma [0.5] Post-10 Ma [0.5]	Post-3 Ma [0.5] Post-5 Ma [0.5] Post-10 Ma [0.5]	Post-1 Ma [0.1] Post-5 Ma [0.9]	Post-5 Ma [1.0]	Post-1 Ma [0.3] Post-4 Ma [0.7]	Post-4.6 Ma [1.0]
Region of Interest	Conditional on temporal model: subdivided into regional models and YMR and YMRPO regions.	Southern Great Basin, subdivided into regional models and YMR and YMRPO regions.	40km radius [1.0]	Eastern Zone [0.8] 100-km radius [0.2]	10 Ma Zone [1.0]	Northern AVIP [1.0]	Northern AVIP [1.0]	200-km radius [0.25] 40km radius [0.25]	200-km radius [0.3] AVIP [0.7]	Node [1.0]
Spatial Models	Kernel Smoothing [0.6] Uniform [0.4]	Zonation [1.0]	Zonation [1.0]	Field Shape [0.7] Kernel Smoothing [0.2] Zonation [0.1]	Kernel Smoothing [0.6] Zonation [0.4]	Zonation [0.95] Kernel Smoothing [0.3] Uniform [0.2] Field Shape [0.15]	Zonation [0.9] Kernel Smoothing [0.1]	Zonation [1.0] Spatial Smoothing [0.5]	Zonation [1.0]	Field Shape [0.75] Zonation [0.25]
Type of Event	Small chondritic cone (small volume flows) (95%) P (Pinnac) 45% 3% of which might be near-type enclaves - includes hydromagmatic, Hydrovolcanic [0.05] 1% large volume tephritic, 1% rhyolite Ergusa silicic < 10 ¹⁰ yr	Alluvial Basins: Mixed strombolian/Hawaiian [0.9] Hydromagmatic [0.1] Basaltic dikes, cinder cones, small lava flows (expected) Hydromagmatic [0.1] Rhyolite intrusions: Mixed [0.95] Hydrovolcanic [0.05] Ergusa silicic < 10 ¹⁰ yr	Basaltic dikes, cinder cones, small lava flows (expected) Hydromagmatic P [1/1000] Slack volcanism No probability of rhyolite event	Basaltic enclaves (strombolian with lava flows and small volume dikes) Hydromagmatic P [1/1000] Large volume silicic P (insignificant)	Monogenic basaltic Scoria cones and lava flows [0.06] Single scoria cone [0.03] Hydrovolcanic turf cone [0.067] Small shield [0.033] Polygenetic tephra cone [0.033] Slack volcanism P (< 10 ⁻⁴ /yr)	Basaltic fissure enclaves forming under cones. Some significant ash Zones of deformation above an ascending dike Hydromagmatic P [2 to 4/100 events] Slack volcanism (negligible)	Small-volume basaltic eruption (expected) Hydromagmatic P [1/100 events] Slack volcanism P (rhyolite event) 0.025	Small scoria and lava (0.1 km) (most likely) large shield (1.0 km) [1 as likely] Hydromagmatic, and 0.1 km surrounding accidental material P [0.01-0.02 given an event] Ergusa large volume ash- flow event P [10 ⁻⁴ given an event]	Basaltic enclaves Similar to events that have occurred during past 4 Ma. Hydromagmatic P [1/100 events] Slack volcanism (very unlikely to reoccur) Slack volcanism P (rhyolite event) <0.05	Monogenic basaltic field (strombolian activity) 0.1 to 0.2 km ³ Hydromagmatic P [1 or 2/100 events] Slack volcanism P (rhyolite event) <0.05
Event Geometry										
Length	Cumulative distribution 1 [0.1] 3 [0.5] 5 [0.95] 12 [0.99] 20-30 [1.0] Maximum 20 [0.6] 25 [0.3] 30 [0.1]	Triangular distribution [0.6] 0.3, 3.5, 7.0 Normal distribution [0.4] Mean 3.5 - 3.0	Continuous distribution (1 to 7 km) (95%) 1 to max (98%) Maximum 20 [0.2] 30 [0.6] 40 [0.2]	Cumulative Distribution 0.5 [0.0] 1 [0.5] 5 [0.9] 10 [0.97] 20-25 [1.0] Maximum 20 [0.5] 25 [0.5]	<1 [0.2] 1-2 [0.3] 2-5 [0.3] 5-10 [0.1] 10-15 [0.05] >15 [0.05] Maximum 20 [0.3] 30 [0.4] 40 [0.3]	Cumulative distribution 1 [0.1] 3 [0.5] 8 [0.5] 10 [0.9] 10-18 [1.0] Maximum 10 [0.4] 12 [0.3] 18 [0.1]	3 [0.3] 5 [0.6] 15-20 [0.1] Maximum 15 [0.5] 20 [0.5]	Cumulative Distribution 1-3 [0.3] 10-12 [1.0] Maximum 10 [0.5] 12 [0.5]	Cumulative Distribution 2 [0.5] 3 [0.9] 12 [0.99] 15-20 [1.0] Maximum 15 [0.5] 20 [0.5]	Cumulative Distribution 2 [0.5] 3 [0.9] 12 [0.99] 15-20 [1.0] Maximum 15 [0.5] 20 [0.5]
Distribution	Event randomly placed relative to dike	Triangular distribution (centered)	Triangular Distribution (centered)	Triangular Distribution (centered)	Triangular Distribution (centered)	Semicircular Shape (centered)	Trapezoidal Distribution (75% density between 0.2 and 0.8 or dike length)	Triangular Distribution (centered)	Triangular Distribution (centered)	Triangular Distribution (centered)
Orientation	N25E 30 (90°) N45E 30 (90°) N40W, N20W, N05E	N10E 20 (90°) N15E 30 (2σ)	N10E 20 (90°) N25E 30 (2σ)	N30E 20 (95°)	N25E 30 (2σ)	N30E 30 (90°) [0.7] N15W 15 (90°) [0.3]	N30E 45 (80°)	N30E 15 (95°)	N40E 30 (2σ) [0.5] N20W 30 (2σ) [0.5]	N40E 30 (2σ) [0.5] N20W 30 (2σ) [0.5]

Table 10-5. (continued).

Width	0.5 to 1 m (2m ballooning)	No discussion	- 1 m	No discussion	0.5 to 2.0 m avg. 1m	1 to 2 m	No discussion	No discussion	1.1 m	L:W ~1,000/1 Ballooning near ground surface possible
Undetected Events	Multiplier 1.1 [1.0]	General assumption-there are no major undetected events.; considered in the assessment of maximum event models.	0 events / 1 Ma [0.99] 1 event / 1 Ma [0.01]	Multipliers 1.5 - 2.0 [0.5] 1.15-1.32 [0.5]	Included in estimate of maximum number of events	Multiplier 1.0 [0.25] 1.1 [0.5] 1.5 [0.2] 2.0 [0.05]	P (10 ⁻⁶) (includes cones that were subsequently buried and shallow dikes that did not erupt)	Multipliers 1.33 [0.185] 1.67 [0.83] 2.0 [0.185]	Multipliers Volcanic Domain 1 x counts [0.5] 2 x counts [0.5]	Cumulative 1 x counts [0.3] 2 x counts [0.5] 5 x counts [1.0]
Probability of no surface rupture assuming magma ascends to repository level	Low P (10 ⁻⁶)	Judged highly unlikely that magma would not erupt at surface at some point along dike.	No discussion	Undetected events in CFF would be about 300 m or more below repository	Basaltic magma that ascends to less than 1 km of the surface will have high probability of erupting.	In general, dikes ascending as shallow as repository (300 m) would be expected to vent at surface.	Even if dike extends from Crater Flat to Yucca Mountain, probability that it will rise to repository level is very low.	No discussion	Not discussed directly; may be potential for undetected surface or subsurface events at depths of less than 300 m but not represented at surface.	Not discussed directly.
Potential for Sill Formation	No discussion	No discussion	No discussion	No discussion	No discussion	No discussion	No discussion	No discussion	Due to the low magma volumes, formation of sills in the YMR is unlikely.	Large sill swarms generally are emplaced in non-lithified sediments just above basement rock, an area typically coincident with the level of neutral buoyancy (LNB).
Related Surface Deformation	No discussion	No discussion	No discussion	No discussion	Zone of magma-induced faulting and fissuring above a dike <0.5 km in width	Zones of deformation likely will form above ascending dike.	No discussion	No discussion	No discussion	No discussion

Table 10- 6. Eruptive Parameters for Analog Volcanoes.

	Total magmatic volume (V) (km ³)	Column Height (H) (km)	Eruption duration (T) (s)
Heimaey 1973	0.18	2	2.25 x 10 ⁶
Paricutín 1943	0.92	4-6	7.26 x 10 ⁶
Tolbachik Cone 1	0.52	6-10	1.21 x 10 ⁶
Tolbachik Cone 2	—	2-3	3.28 x 10 ⁶
Cerro Negro 1947	—	4-6.5	8.64 x 10 ⁵
Cerro Negro 1968	0.015	1-1.5	3.63 x 10 ⁶
Cerro Negro 1971	0.025	6	6.05 x 10 ⁵
Cerro Negro 1992	0.012	6.5	6.39 x 10 ⁴
Cerro Negro 1995	0.008	2	3.46 x 10 ⁵

Table 10- 7. Magma Rise Velocity as a Function of Dike Width (after Wilson and Head 1981, Table 5).

Width (m)	Velocity (m/s)
0.6	0.2
1.2	0.79
2	2.1
6	14.6

Table 10- 8. Ascent Velocity as a Function of Conduit Diameter (adapted from Wilson and Head 1981, Table 3).

Diameter (m)	Velocity (m/s)
1	0.2
2	0.8
6	6.9
20	38.5
60	86.2

Table 10- 9. Number of Waste Packages for each Waste Type (after CRWMS M&O 1997b, Key 04 Table 3-10).

Package Type	Number of Packages	Spacing (m)*	Waste Content (MTU)
21-PWR	4239	16.6	8.926
12-PWR	553	10.6	5.581
44-BWR	2826	13.3	7.742
24-BWR	49	5.7	—
Co-disposal	1663	—†	—
Direct-disposal	883	—†	—

Table 10- 10. Number of Waste Packages for each Waste Type (after CRWMS M&O 1997k, Key 04 Table 3-10)

Package Type	Number of Packages	Spacing (m)*	Waste Content (MTU)
21-PWR	4239	16.6	8.926
12-PWR	553	10.6	5.581
44-BWR	2826	13.3	7.742
24-BWR	49	5.7	—
Co-disposal	1663	—†	—
Direct-disposal	883	—†	—

* Includes the waste package length (5.5 m average) and the air gap between packages.

† These packages are placed in the gaps between the hot spent-fuel packages. They have lower inventories of heat-producing radionuclides.

Table 10- 11. Number of Waste Packages Hit for Circular Conduits.

Conduit Radius (m)	Distance to first drift (x ₁)	Distance to second drift (x ₂)	Distance to third drift (x ₃)	Number of pkgs hit in 1st drift	Number of pkgs hit in 2nd drift	Number of pkgs hit in 3rd drift	Total number of pkgs hit
6.7	4.4	0.0	0.0	1	0	0	1
2.4	14.0	0.0	0.0	0	0	0	0
58.9	14.2	14.4	42.8	8	8	6	22
20.5	11.4	17.2	0.0	2	2	0	4

Table 10- 12. Waste Package Internal Pressure.

Temperature (°C)	21 PWR / 44 BWR Pressure (Mpa)		
	10% Rods Burst	100% Rods Burst	100% Rods Burst *1.5
25	0.12 / 0.11	0.26 / 0.19	0.39 / 0.29
50	0.13 / 0.12	0.28 / 0.20	0.42 / 0.30
100	0.15 / 0.14	0.33 / 0.23	0.50 / 0.35
200	0.19 / 0.17	0.41 / 0.30	0.62 / 0.45
300	0.23 / 0.21	0.50 / 0.36	0.75 / 0.54
350	0.25 / 0.23	0.54 / 0.39	0.81 / 0.59
500	0.30 / 0.28	0.67 / 0.48	1.01 / 0.72

Table 10- 13. Fractional Velocities For Agglomerated Pyroclast-Waste Particles.

Waste Particle/ Magma Particle Ratio	Magma Density (g/cm ³)	
	1.5	2.65
0.01	1.0	1.0
0.1	1.0	1.0
0.2	0.9	.97
0.5	0.5	.66
0.7	0.3	.41
1	0.1	.19
10	1.4x10 ⁻⁴	2.4x10 ⁻⁴
100	1.4x10 ⁻⁷	2.4x10 ⁻⁷

Table 10- 14. Settling Velocities (cm/s) For Waste Particles in Magma.

Particle Diameter (cm)	Magma Density (g/cm ³)	
	2.65	1.5
0.1	11	15
.5	24	34
1	34	48
5	76	108
10	108	153
100	341	483

Table 10- 15. Settling Velocities (cm/s) For Agglomerated Waste-Magma Particles.

Particle Diameter (cm)	Magma Density (g/cm ³)	
	1.5	2.65
0.1	11	8
.5	24	17
1	34	24
5	76	54
10	108	76
100	341	241

Table 10- 16. Sample *ashplume.In* File.

1	Test RN01z4.	4/22/98 Deterministic Run	S
2	-0.1 0.1	! xmin, xmax in km	S
3	-0.1 0.1	! ymin, ymax in km	S
4	3	! numptsx	S
5	3	! numptsy	S
6	-2. 0	! vlogmin, vlogmax- logs of volume in km ³	D, M
7	9.41 11.55	! powlogmin, powlogmax- logs of P in W	D
8	-2.0 -0.3	! betalogmin, betalogmax-logs	D
9	-2.0 -1.0 1.0	! dmeanmin, dmeanmed, dmeanmax-logs of d in cm	D
10	0.1 1.0	! dsigmamin, dsigmamax	D
11	0.8 2.5	! ashdenmin, ashdenmax in g/cm ³	D, M
12	-2. -1.	! ashrhoLow, ashrhoHi	D
13	0.5	! fshape	S
14	0.001293 1.8E-04	! airden in g/cm ³ , airvis in g/cm-s	S
15	400.	! c in cm ² /s to the 5/2	S
16	10.	! dmax in cm	S
17	0.007943 0.07943 0.7943	! fdmin, fdmean, fdmax all in cm	S
18	0.001	! hmin in km	S
19	1.0E-10	! acutoff in g/cm ²	S
20	0.3	! rhocut-incorporation ratio	D
21	1.0E+08	! Uran- total mass of fuel in g	D

Table 10- 16a. Selected Examples of Dike Intrusions.

Realization Number	Northing (km from south end)	Orientation (degrees from north)	Length in Repository (km)	Number of Drifts Crossed	Number of Vents in Repository
3	2.866	37.5	0.993	12	1
8	1.816	32.5	0.375	11	2
9	0.535	37.5	1.525	42	0
10	2.468	37.5	0.325	9	0
11	1.281	12.5	1.825	62	1
13	2.774	62.5	1.092	16	2
14	0.029	122.5	0.192	1	2
22	2.850	32.5	0.923	13	1
26	1.733	147.5	0.040	1	1
27	0.683	22.5	1.225	40	1
33	3.108	162.5	0.000	0	1
34	0.776	27.5	0.225	7	0
35	1.851	22.5	1.425	46	1
36	0.601	22.5	0.475	15	1
53	1.150	22.5	1.675	54	1
57	0.223	157.5	0.502	8	0
58	1.926	57.5	0.175	3	0
59	2.627	37.5	0.175	5	0
60	2.729	12.5	0.616	17	2
67	2.424	32.5	0.425	13	1
80	1.299	37.500	1.525	42	1
84	1.023	17.5	2.333	77	1

Table 10- 16b. Selected Examples of Interaction Types.

Realization Number	Fragmentation Depth (m)	Interaction type
3	218	magma
8	397	ash
11	218	magma
13	180	magma
14	303	ash
22	317	ash
26	375	ash
27	354	ash
35	376	ash
36	310	ash
53	328	ash
60	357	ash
67	366	ash
80	337	ash
84	340	ash

Table 10- 16c. Numbers of Packages Hit By Liquid-Magma Intrusions.

Realization Number	Number of vents in Repository	Number of Drifts Crossed	Dike Width (m)	Number of Packages hit/drift	Total Packages Hit
3	1	12	0.5	1	12
11	1	62	0.9	1	62
13	2	16	4.7	2	32

Table 10- 16d. Numbers of Packages Hit by Ash Intrusions.

Realization Number	Number of vents in Repository	Conduit Diameter (m)	Total Packages Hit	Release Source
8	2	49.1	9	18
14	2	50.7	8	16
22	1	53.2	6	6
26	1	42.1	12	12
27	1	39.9	2	2
35	1	26.1	4	4
36	1	39.6	13	13
53	1	56.3	9	9
60	2	54.6	8	16
67	1	36.9	13	13
80	1	21.6	0	0
84	1	62.1	1	1

Table 10- 16e. Waste-Package Breach Simulations from corrosion.

Realization Number	Time of Occurrence (yrs)	Intrusion Temperature (°C)	Duration of Eruption (s)	Fraction of Original CRM Remaining	Breach?
3	401,921	1,080	2.44E+06	0.299	yes
8	701,922	1,181	2.58E+06	0.298	yes
11	700,648	1,004	6.54E+05	0.300	yes
13	516,696	949	1.15E+06	0.299	yes
14	52,452	803	4.27E+05	1.000	no
22	711,344	803	2.20E+06	0.299	yes
26	517,613	1,115	2.68E+06	0.298	yes
27	85,151	854	5.62E+05	1.000	no
35	977,155	1,061	3.53E+06	0.248	yes
36	250,738	955	7.07E+05	0.950	no
53	843,336	1,091	8.11E+05	0.300	yes
60	551,983	865	9.71E+05	0.300	yes
67	383,505	1,085	6.53E+05	0.500	yes
84	882,106	872	1.58E+06	0.299	yes

Table 10- 16f. Waste-Removal Simulations.

Realization Number	Magmatic particle size	Waste particle size	Elastic collision?	Inelastic collision?	Ascent velocity	Escape?
3	1.017	0.355	yes	yes	0.2	no
8	0.409	0.316	no	yes	68.3	yes
11	0.849	0.141	yes	yes	0.4	no
13	0.889	0.020	yes	yes	9.6	yes
22	0.616	0.501	no	yes	74.3	yes
26	0.214	0.398	no	no	62.4	no
35	0.563	0.089	yes	yes	45.7	yes
53	0.617	0.028	yes	yes	80.2	yes
60	1.064	0.141	yes	yes	74.3	yes
67	0.060	0.032	no	yes	56.4	yes
84	0.725	0.398	no	yes	86.2	yes

Table 10-16g. Waste-Entrainment Simulations.

Realization Number	Eruption type	Ascent velocity	Ash density	Settling velocity	Entrained?
8	ash	68.3	2.14	0.3	yes
13	magma	9.6	1.65	0.7	yes
22	ash	74.3	0.92	1.5	yes
35	ash	45.7	1.39	0.0	yes
53	ash	80.2	1.76	0.0	yes
60	ash	74.3	2.14	0.0	yes
67	ash	56.4	1.63	0.0	yes
84	ash	86.2	0.83	0.7	yes

Table 10-16h. Amount of Waste in Eruptive Source.

Realization Number	Number of pkgs hit	Fraction of waste entrained	Amount of waste in Source (g)
8	18	.46	6.82×10^7
13	32	.41	1.08×10^8
22	6	.55	2.72×10^7
35	4	.50	1.65×10^7
36	13	.48	5.14×10^7
53	9	.52	3.86×10^7
60	16	.45	5.93×10^7
67	13	.42	4.50×10^7
84	1	.50	4.12×10^6

Table 10-16i. Parameters for ASHPLUME Simulations.

Realization Number	Eruption Volume (km ³)	Eruption Height (km)	Eruption Power (W)	Ash Density (g/cm ³)	Exit ash velocity (m/s)	Wind Direction	Wind speed (cm/s)
8	0.367	5.05	1.32 x 10 ¹⁰	2.1	187.3	SW	1527
13	0.079	3.79	6.93 x 10 ¹⁰	1.7	63.6	SSW	684
22	0.272	4.77	1.57 x 10 ¹⁰	0.9	169.4	S	57
35	0.669	5.64	2.78 x 10 ¹⁰	1.4	158.4	N	1663
53	0.041	3.35	3.48 x 10 ¹⁰	1.8	178.7	SSE	235
60	0.058	3.57	1.82 x 10 ¹¹	2.1	181.5	S	70
67	0.027	3.11	2.89 x 10 ¹⁰	1.6	166.3	SW	1290
84	0.146	4.25	6.33 x 10 ¹⁰	0.8	188.2	NNE	159

Table 10- 17. Contributions of Intermediate Processes to Final Source Term.

Process/Reason for Elimination	Percentage of Realizations Eliminated	Cumulative Percentage Remaining
Dike Orientation/does not intersect repository	0.7%	99%
Dike Length/zero inside repository	2%	97%
Number of Vents/zero inside repository	60%	39%
Waste-Package Breach/insufficient time	20%	31%
Waste Removal from Package/particle-size difference	50%	16%
Waste Entrainment/insufficient ash velocity	70%	5%

Table 10- 18. Waste Concentrations at Dose Receptor Point.

Time of Occurrence (yr)	Compass Heading	Wind Speed (cm/s)	Mass of Waste Erupted (g)	Concentration at Dose Receptor Point (g/cm ²)
564326	S	231	8.72×10^7	4.914×10^{-11}
699212	SSW	631	1.66×10^8	1.727×10^{-11}
758425	S	1100	8.40×10^6	4.227×10^{-12}
473043	NE	158	2.27×10^7	3.197×10^{-12}
592074	SSW	684	8.40×10^6	2.740×10^{-14}
458491	N	592	5.14×10^7	5.612×10^{-16}
560800	NNW	231	2.77×10^7	1.701×10^{-16}
875269	NNE	164	1.09×10^8	1.233×10^{-17}
659526	WSW	106	5.88×10^7	5.144×10^{-20}
480606	SE	42	5.31×10^7	3.775×10^{-20}
437010	WNW	255	5.04×10^7	1.299×10^{-22}
808221	N	671	5.46×10^7	1.025×10^{-24}
660974	ESE	429	7.91×10^6	5.338×10^{-27}
653827	NE	268	4.55×10^7	3.405×10^{-30}
439589	NNE	640	3.78×10^7	5.448×10^{-39}
387644	N	478	4.20×10^6	5.476×10^{-59}
478081	N	1464	8.40×10^6	5.812×10^{-69}

Table 10- 19. Description Statistics for Dose Rate Results.

Statistic	Value
Arithmetic Mean	1.52×10^{-4}
Median	1.74×10^{-12}
Standard Deviation	4.36×10^{-4}
Skewness	3.53
Minimum	2.17×10^{-61}
Minimum	1.75×10^{-3}

Table 10- 20. Dissolution Rates of Uranium-Bearing Minerals.

Mineral	Stoichiometry	Rate (mg/m ² -day)	Reference
Schoepite	UO ₃ •2H ₂ O	19.3	Bruno et al. (1995)
Soddyite	(UO ₂) ₂ (SiO ₄)•2H ₂ O	40.7	Perez et al. (1997)
Uranophane	Ca(UO ₂) ₂ (SiO ₃) ₂ •(OH) ₂	0.083	Bruno et al. (1995)

Table 10- 21. Waste Elements Susceptible to Mobilization at Magmatic Temperatures.

Element/ Compound	Melting Point (°C)	Boiling Point (°C)	Eutectic (M. P.)	Amount* (moles/MTU)
Pu	639	—	Pu-Si (570)	32.2
PuCl ₃	760	—		
PuI ₃	777	—		
Cs	28	690		8.02
Cs ₂ O ₂	400	650		
Cs ₂ S ₃	217	—		
Sr	769	1150		3.54
Np	640	—		2.07
I	113	184		1.34
IO ₂	130	—		
Sn	232	2260		0.22
SnO	800	—		
SnS	882	—		
Se	217	685	Se-S (105)	0.08
SeO ₂	340	—		
SeS	118	—		
Ag	961	1950	Ag-S (805)	3.47 x 10 ⁻⁰⁶
Ag ₂ O	300	—		
Ag ₂ S	825	—		
Ra	700	1140		8.97 x 10 ⁻⁰⁹
Pb	327	1620		3.01 x 10 ⁻¹¹
Pb ₃ O ₄	500	—		
PbO	888	—		
PbO ₂	290	—		
PbS	1119	—		
PbI	402	954		

U	1132	—		
UI4	506	759		

* Assuming 25-year fuel and 30 GWd/MTU burnup

Table 10- 22a. Selected Examples of Dike Intrusions.

Realization Number	Northing (km from south end)	Orientation (degrees from north)	Length in Repository (km)	Number of Drifts crossed	Dike length fraction
1	0.754	22.5	2.025	65	0.185
2	1.196	12.5	1.025	35	0.185
3	1.603	37.5	1.425	40	0.185
4	2.615	22.5	0.700	21	0.140
33	0.983	17.5	0.000	0	0.000
34	1.168	22.5	0.125	4	0.185
35	0.040	27.5	1.125	35	0.185
36	2.566	12.5	0.675	23	0.161
37	3.178	47.5	1.294	1	0.128

Table 10-22b. Calculation of Total Number of Waste Packages Breached by Magma Intrusion.

Realization Number	Eruption Type	Number of Drifts crossed	Number of packages hit
1	ash	65	-
2	magma	35	70
3	magma	40	80
4	magma	21	42
33	ash	0	-
34	ash	4	-
35	magma	35	70
36	magma	23	46
37	magma	1	2

Table 10-22c. Calculation of UO₂ Dissolution.

Temperature (°C)	Spent fuel particle size (cm)	Specific surface area (m ² /mg)	UO ₂ dissolution rate (mg/m ² -day)	UO ₂ dissolved (/year)
1194	0.785	6.63 x 10 ⁻⁶	0.957	1.39 x 10 ⁻³
1085	0.010	9.07 x 10 ⁻⁵	0.603	1.50 x 10 ⁻²
1151	0.076	5.14 x 10 ⁻⁵	1.477	1.80 x 10 ⁻²
1167	0.115	4.33 x 10 ⁻⁵	6.794	6.98 x 10 ⁻²
1036	0.166	3.63 x 10 ⁻⁵	0.001	1.46 x 10 ⁻⁵
1109	0.270	2.70 x 10 ⁻⁵	0.001	4.24 x 10 ⁻⁶

Table 10-22d. Calculation of Basalt Dissolution.

Temperature (°C)	Basalt particle size (cm)	Specific surface area (m ² /mg)	Basalt dissolution rate (mg/m ² -day)	Basalt dissolved (/year)	Total dissolved (/year)
1194	1.48	1.78 x 10 ⁻⁶	0.0002	5.44 x 10 ⁻⁸	1.39 x 10 ⁻³
1085	1.97	1.62 x 10 ⁻⁶	0.0017	2.48 x 10 ⁻⁷	1.50 x 10 ⁻²
1151	1.90	1.64 x 10 ⁻⁶	0.0006	1.30 x 10 ⁻⁷	1.80 x 10 ⁻²
1167	1.64	1.73 x 10 ⁻⁶	0.0051	1.13 x 10 ⁻⁶	6.98 x 10 ⁻²
1036	0.91	2.05 x 10 ⁻⁶	0.0016	2.34 x 10 ⁻⁷	1.48 x 10 ⁻⁵
1109	1.20	1.90 x 10 ⁻⁶	0.0075	1.55 x 10 ⁻⁶	5.79 x 10 ⁻⁶

Total dissolved in Table 10.4-17d is the sum of the UO₂ and basalt dissolution.

Table 10- 23. Rock Quality Ranges.

Rock-Quality Descriptor	Block-Volume Range (m ³)	Percentile of Observed Joints	Probability of Occurrence in ESF
Strong	0.51 – 1.28	90 th – 100 th	0.10
Medium	0.01 – 0.51	20 th – 90 th	0.70
Weak	0.00035 – 0.01	4 th – 20 th	0.16
Very Weak	0.00012 – 0.00035	0 th – 4 th	0.04

Table 10- 24. Thermal Spalling at Various Times After Closure.

Rock-Quality Designation	100-Year Stability	10,000-yr Stability	1,000,000-yr Stability
Strong	2	1	1
Medium	3	2	2
Weak	4	3	3
Very Weak	5	5	5

Table 10- 25. Initial-Condition Factors for DL Calculation.

Rock-Quality Descriptor	IC
Strong	1.93
Medium	2.13
Weak	2.67
Very Weak	2.87

Table 10- 26. PGV Values that cause Various IC and DL Values.

DL Value	IC Value			
	1.93	2.13	2.67	2.87
1	8.5	7.1	4.3	3.6
2	17.0	14.1	8.6	7.1
3	33.9	28.2	17.2	14.3
4	67.9	56.5	34.3	28.5
5	135.8	112.9	68.6	57.1

Table 10- 27. Mean Frequencies of Occurrence for Various PGV Over Different Time Periods.

Time Period (years)	PGV (cm/s)				
	1	10	20	30	500
0 - 10 ³	2.85 x 10 ¹	1.74 x 10 ⁰	4.07 x 10 ⁻¹	1.55 x 10 ⁻¹	7.16 x 10 ⁻⁶
0 - 10 ⁴	2.85 x 10 ²	1.74 x 10 ¹	4.07 x 10 ⁰	1.55 x 10 ⁰	7.16 x 10 ⁻⁵
0 - 10 ⁵	2.85 x 10 ³	1.74 x 10 ²	4.07 x 10 ¹	1.55 x 10 ¹	7.16 x 10 ⁻⁴
0 - 10 ⁶	2.85 x 10 ⁴	1.74 x 10 ³	4.07 x 10 ²	1.55 x 10 ²	7.16 x 10 ⁻³

Table 10- 28. DL Values for Various Rock Qualities and PGV Levels.

Vertical PGV (cm/s)	IC			
	Strong	Medium	Weak	Very Weak
9	0.8	1.1	1.8	2.0
14	1.2	1.5	2.2	2.5
37	2.2	2.5	3.2	3.5
61	2.7	3.0	3.7	4.0
79	3.0	3.3	4.0	4.2
108	3.3	3.6	4.3	4.6

Table 10- 29. Calculated Waste-Package Damages from Rockfall as a Function of Wall Thickness.

CAM Wall Degradation	0%	50%	75%	100%	100%
CRM Wall Degradation	0%	0%	0%	0%	50%
Rock Mass to cause crack initiation (kg)	8,000	2,500	1,000	350	50
Rock Mass to cause a through crack (kg)	38,000	24,000	3,500	350*	50*

* These values are the same as the rock masses that cause crack initiation because the predicted margin of safety is so small that the analysis predicts essentially the same rock size for both initiation and a through crack.

Table 10- 30a. Calculation of Damage Levels at Various Times from Ground Shaking.

Time of Occurrence (yrs)	Sampled PGV (cm/s)	Strong-Rock DL	Medium-Rock DL
994	5.1	0.3	0.5
3148	13.7	1.2	1.5
49621	46.2	2.5	2.7
10660	23.7	1.8	2.1
95928	35.3	2.2	2.5
84917	49.8	2.5	2.8
35213	140.9	3.6	3.8
11719	12.5	1.2	1.4
84920	220.5	4.0	4.3
98921	22.2	1.7	2.0
730808	269.3	4.2	4.5
496645	161.3	3.7	4.0
536936	76.6	3.0	3.2

108556	41.1	2.3	2.6
488656	76.8	3.0	3.2
380511	89.1	3.1	3.4

Table 10-30b. Calculation of Amounts of Waste-Package Degradation.

Time of Occurrence (yrs)	CAM Thickness (%)	Adjusted time	CRM Thickness (%)
49621	0.05	24121	0.99
10660	0.50	0	1.00
95928	0.00	25928	0.99
84917	0.00	14917	0.99
35213	0.05	9713	0.99
11719	0.25	0	1.00
84920	0.00	14920	0.99
98921	0.00	28921	0.99
730808	0.00	660808	0.30
496645	0.00	426645	0.30
536936	0.00	466936	0.30
108556	0.00	38556	0.99
488656	0.00	418656	0.30
380511	0.00	310511	0.50

Table 10-30c. Association of DL Values with Rock-Size Data.

Damage Level	Rock Quality	Cumulative Fraction in Repository	Rock-Size CDF	Mass (kg)
0.0	Very Weak	0.04	0.000	10
2.0	Weak	0.20	0.270	50
3.0	Medium	0.90	0.513	350
3.5	Medium	0.90	0.823	1000
4.0	Strong	1.00	0.993	2500
4.2	Strong	1.00	0.999	3500
4.5	Strong	1.00	0.999	8000
4.7	Strong	1.00	1.000	24000
5.0	Strong	1.00	1.000	38000

Table 10-30d. Falling Rock Masses Resulting from Seismic Events.

Time of Occurrence (yrs)	Rock size for crack initiation	Rock size to breach	Strong Rock DL	Size of rock expected from DL	Size of rock from PDF	Rock avail. to fall?	Package damage?	Package Breach?
49621	320	350	2.5	142	327	yes	yes	0.238
10660	2500	24000	1.8	19	416	yes	no	-
95928	320	350	2.2	82	821	yes	yes	yes
84917	320	350	2.5	57	10	no	-	-
35213	320	350	3.6	1622	1908	yes	yes	yes
11719	1000	3500	1.2	32	10	no	-	-
84920	320	350	4.0	3298	127	no	-	-
98921	320	350	1.7	30	59	yes	no	-
730808	1	5	4.2	5190	565	yes	yes	yes
496645	1	5	3.7	1793	2333	yes	yes	yes
536936	1	5	3.0	33	146	yes	yes	yes
108556	320	350	2.3	216	322	yes	yes	0.062
488656	1	5	3.0	267	807	yes	yes	yes
380511	50	80	3.1	312	638	yes	yes	yes

Table 10- 31. Summary of Rockfall Grouped by Time Period.

Time Period (years)	Mean Time of Occurrence (years)	Mean PGV (cm/s)	Maximum PGV (cm/s)	Fraction of Packages Breached	Fraction of Packages Damaged
0 - 10 ³	507	1.81	61.96	0.0	0.001
0 - 10 ⁴	4800	1.81	33.85	0.0	0.001
0 - 10 ⁵	51580	2.00	93.49	0.146	0.009
0 - 10 ⁶	483100	1.70	42.01	0.279	0.009

Table 10- 32. Summary of In-Package Critical Configurations.

Config-uration	Waste Form	Neutron Absorber	Fuel	Failure Necessary for Criticality	Moderator/ Geometry	"Relative Probability"
IP-1a	Al-clad DOE SNF, & DHLW	Boride-loaded steel plates	HEU and MEU	Waste degradation only	Liquid water; homogeneous fuel and moderator with absorber nearby	2 – absorber should prevent criticality
IP-1b	Al-clad DOE SNF, & DHLW	Boride-loaded steel plates	HEU and MEU	Waste degradation; separation of fuel from absorber	Liquid water; homogeneous fuel and moderator	3 – fuel separated from absorber
IP-2a	Pu-glass/ceramic	Gd, Hf, (B)	^{239}Pu	Glass degradation; acidic conditions; absorbers flushed	Water & hydrated clay; homogeneous fuel/ moderator	2 – if Pu > 50 kg; absorbers dissolved and flushed
IP-2b	Pu-glass/ceramic	Gd, Hf, (B)	^{239}Pu	Glass degradation; WP bottom failure; acidic conditions; absorbers leached	Hydrated clays; homogeneous fuel and moderator	3 – if Pu > 50 kg; clay provides moderating water
IP-2c	Pu, U	B, Gd	^{239}Pu	Waste-form degradation in less than 50k years; absorber separation	Water and hydrated clays; homogeneous fuel and moderator	2 – rapid W. F. degradation required for there to be any Pu left
IP-3a	stainless-steel clad SNF	Boride-loaded steel plates	LEU (U & Pu)	Basket collapses, fuel assemblies collapse; absorber mobilized	Liquid water between fuel-pin assemblies, reduced fuel-pin spacing	2 – ^{238}U , and reduced reactivity of closer pins reduces reactivity
IP-3b	Zircaloy-clad SNF	Boride-loaded steel plates	LEU (U & Pu)	Basket partially collapses; absorbers mobilized	Liquid water between fuel-pin assemblies; some absorbers remain	3 – neutron absorption by ^{238}U , FeO, and B reduces reactivity
IP-3c	CSNF	Bor-Al wagon wheel (MPC)	LEU (U & Pu)	Absorber mobilized; "wagon wheel" later collapses; fuel assemblies collapse	Liquid water between fuel-pin assemblies, optimal fuel-pin spacing;	4 – neutron absorption by ^{238}U ; optimal spacing increases reactivity
IP-3d	CSNF	Bor-Al wagon wheel (MPC)	LEU (U & Pu)	Absorber mobilized	Liquid water between fuel-pin assemblies, non-collapsed pin spacing;	2 – neutron absorption by ^{238}U ; spacing decreases reactivity

Table 10-32. (continued).

Config-uration	Waste Form	Neutron Absorber	Fuel	Failure Necessary for Criticality	Moderator/ Geometry	"Relative Probablility"
IP-4a	Al-clad DOE SNF, & DHLW	Boride-loaded steel plates	HEU and MEU	Waste degradation only	Hydrated corrosion products; homogeneous fuel & moderator; absorber nearby	2 – absorber should prevent criticality; limited water
IP-4b	Al-clad DOE SNF, & DHLW	Boride-loaded steel plates	HEU and MEU	Waste degradation; separation of fuel and absorber	Hydrated corrosion products; homogeneous fuel & moderator	3 – fuel separated from absorber
IP-5a	Pu-glass/ceramic	Gd, Hf, (B)	^{239}Pu	Glass degradation; absorbers leached through WP bottom	Hydrated clays; homogeneous fuel and moderator	3 – if Pu > 50 kg; less moderating water
IP-6a	CSNF	Bor-Al wagon wheel (MPC)	LEU (U & Pu)	Wagon wheel degrades; absorbers flushed	Intact fuel assemblies; hydrated corrosion products	1 – optimal fuel-pin spacing; limited water

B00000000-01717-4600-00009 REV00B

F10-43

August 9, 1998

Table 10- 33. Summary of Near-Field Critical Configurations.

Config-uration	Fuel	Concentration Mechanism	Moderator/Geometry	"Relative Probability"
NF-1a	U	Sorption onto zeolites from altered cement, ferric oxides	Water, SiO ₂ ; variable geometry	1 – difficult to build up large uranium concentrations
NF-1b	U	Precipitation onto tuff	Water, SiO ₂ ; variable geometry	1 – difficult to build up large uranium concentrations
NF-2a	U, Pu	Acidic conditions leach absorbers from clayey mass	Hydrated corrosion products; planar geometry	1 – unfavorable geometry; acidic conditions unlikely
NF-3a	Pu	Filtration through corrosion products	Water, SiO ₂ ; variable geometry	1 – co-deposition of inert materials reduces fissile concentration
NF-3b	Pu	Sorptive separation of absorbers	Water, SiO ₂ ; variable geometry	1 – competitive sorption between fissile material and absorbers
NF-3c	Pu	Sorption onto finely divided concrete	Water, SiO ₂ ; variable geometry	1 – competitive sorption between fissile material and absorbers
NF-4a	U, Pu	Mechanical transport from WP	Water, SiO ₂ ; variable geometry	3 – like IP-3b, except outside of package
NF-4b	U, Pu	Stratification of FM; mixing with moderator by disturbance	Water, SiO ₂ ; planar -> toroidal geometry	1 – geometry must change to increase reactivity
NF-4c	U, Pu	Preferential dissolution of Uranium; filtration of Pu	Water, SiO ₂ ; variable geometry	1 – must happen soon enough that Pu has not decayed
NF-4d	Pu	Stratification of Pu; mixing with moderator by disturbance	Water, SiO ₂ ; variable geometry	1 – geometry must change to increase reactivity
NF-4e	Pu, U	fixed Pu decays to U	Water, SiO ₂ ; variable geometry	1 – rapid WP and WF degradation required

Table 10- 34. Summary of Far-Field Critical Configurations.

Config-uration	Fuel	Concentration Mechanism	Moderator/Geometry	"Relative Probability"
FF-1a	U	Precipitation from carrier plume due to pH change	Water, SiO ₂ ; cylindrical/spherical geometry	1 – low concentration of solute; low reactive potential of country rock
FF-1b	U	Sorption onto clays and zeolites in TSbv	Water, SiO ₂ ; variable geometry	1 – limited void space for accumulation of fissile
FF-1c	U	Accumulation in topographic lows; precipitation from chemical changes in perched water	Water, SiO ₂ ; planar geometry	1 – low concentration of solute; low reactive potential of country rock
FF-2a	Pu	Filtration of colloids in fractures	Water, SiO ₂ ; linear/parallel-plate geometry	1 – unlikely that significant number of colloids can travel to far field
FF-2b	Pu	Sorption onto clays and zeolites in TSbv	Water, SiO ₂ ; variable geometry	1 – unlikely that significant number of colloids can travel to far field
FF-2c	Pu	Accumulation in topographic lows; filtration by clays	Water, SiO ₂ ; planar geometry	1 – unlikely that significant number of colloids can travel to far field
FF-3a	U	Precipitation by reducing fluids from Pz carbonates into faults/ fractures	Water, SiO ₂ ; variable geometry	2 – no analyses or data to characterize source of reducing fluids
FF-3b	U	Precipitation by reducing front (groundwater resident in tufts)	Water, SiO ₂ ; variable geometry	2 – no identified analyses; may not have sufficient reducing potential
FF-3c	U	Precipitation by organic matter in alluvium	Water, SiO ₂ ; variable geometry	2 – need large concentration of organics to occur
FF-3d	U	Precipitation by organic material in restricted aquifer	Water, SiO ₂ ; variable geometry	2 – potentially higher concentrations by flow channeling
FF-3e	U	Precipitation by evaporation	SiO ₂ ; variable geometry	1 – requires vanadium; evaporation will concentrate U in soluble form; presence of boron

Table 10- 35. Contaminant Masses Available in Saturated Zone.

Radionuclide	Inventory (g/MTU)	Mass in waste in SZ (g)	Amount dissolved (g/yr)	Solubility limit (g/m ³)	Volume required to dissolve (m ³ /yr)	Solubility factor	Adjusted amount dissolved (g/yr)	Time to dissolve entire inventory (yr)
C-14	0.0845	0.047	0.0023	12000	1.95 x 10 ⁻⁷	1.00	0.0023	19.9
Se-79	5.27	2.91	0.146	38094	3.83 x 10 ⁻⁶	1.00	0.146	19.9
Tc-99	750.	414.1	20.764	12540	1.66 x 10 ⁻³	1.00	20.764	19.9
I-129	177.	97.96	4.912	127000	3.87 x 10 ⁻⁵	1.00	4.912	19.9
Pa-231	0.0804	0.044	0.0022	0.200	1.11 x 10 ⁻²	1.00	0.0022	19.9
U-234	332.	183.3	9.19	8.788	1.05	1.62 x 10 ⁻¹	1.485	123.5
Np-237	1760.	973.6	48.815	0.3408	144.	1.18 x 10 ⁻³	0.057	16946.
Pu-239	420.	2316.5	116.154	0.121	958.	1.76 x 10 ⁻⁴	0.020	113126.
Pu-242	436.	240.6	12.064	0.121	99.5	1.70 x 10 ⁻³	0.020	11749.

Notes: For this example, the mass of waste dropped down the borehole is 0.55 MTU. The fractional dissolution rate is 0.0501/year. The volumetric flux into the SZ is 24380 m³/year, and the flow rate into the borehole is 0.169 m³/year.

Table 10- 36. Human-Intrusion Source Term for Disruption of 2.7 Metric Tons of Spent Fuel.

Radionuclide	Mass (g)
C-14	0.755
Se-79	15.87
Tc-99	2101.26
I-129	481.37
Pa-231	1.53
U-234	926.48
Np-237	4799.27
Pu-239	14954.26
Pu-242	1202.79

Table 10- 37. Human-Intrusion Source Term for Disruption of 0.55 Metric Tons of Spent Fuel.

Radionuclide	Mass (g)
C-14	0.154
Se-79	3.23
Tc-99	427.61
I-129	97.96
Pa-231	0.312
U-234	188.54
Np-237	976.66
Pu-239	3043.21
Pu-242	244.77